Preprints.org

Article

Not peer-reviewed version

Information-Kinetic Theory: Unification of Gravity and the Standard Model on Discrete Quantum Walk Graphs

Andrey Starikovskiy *

Posted Date: 9 June 2026

doi: 10.20944/preprints202606.0589.v1

Keywords: information-kinetic theory; dynamic graphs; quantum walk; topological transition calculus; fundamental interactions; dark energy; macroscopic decoherence

Preprints.org is a free multidisciplinary platform providing preprint service that is dedicated to making early versions of research outputs permanently available and citable. Preprints posted at Preprints.org appear in Web of Science, Crossref, Google Scholar, Scilit, Europe PMC, OpenAlex.

Copyright: This open access article is published under a Creative Commons CC BY 4.0 license, which permit the free download, distribution, and reuse, provided that the author and preprint are cited in any reuse.

Preprints.org (www.preprints.org) | NOT PEER-REVIEWED | Posted: 9 June 2026 doi:10.20944/preprints202606.0589.v1

Disclaimer/Publisher's Note: The statements, opinions, and data contained in all publications are solely those of the individual author(s) and contributor(s) and not of MDPI and/or the editor(s). MDPI and/or the editor(s) disclaim responsibility for any injury to people or property resulting from any ideas, methods, instructions, or products referred to in the content.

Article

Information-Kinetic Theory: Unification of Gravity and the Standard Model on Discrete Quantum Walk Graphs

Andrey Starikovskiy

NEQLab, Plainsboro, New Jersey 08536, USA; astar@neqlab.com

Abstract

This paper proposes the Information-Kinetic Theory (IKT) – a background-independent graph-topological paradigm in which metric spacetime, fields, and particles are regarded as infrared interfaces of stochastic complex-phase routing on a dynamic graph. The fundamental microdynamics is formulated in terms of the local quantum-walk operator U_m acting on the oriented edges of the graph. Under prethermal coherent and statistically isotropic vacuum conditions, the effective Floquet dynamics yields the Weyl/wave envelope. The electromagnetic, strong, weak, and gravitational sectors are described as different macroscopic interfaces of a single graph microdynamics: the $U(1)$-link phase, $SU(3)_{\text{route}}$ color routing, the chiral weak gateway, and phase refraction χ_G. The Topological Transition Calculus (TTC) reformulates continuum UV integrations as finite sums over admissible graph transitions, while running and polarization corrections are treated as graph-computational matching and inference problems. Elementary particles are modeled as stable topological cycles of the graph, and rest mass is represented by the monodromic phase gap or by the integral algorithmic cost of maintaining a closed route. Within this framework, channel-topological anchors are formulated for a number of phenomenological quantities, including $\alpha_{\text{top}}^{-1} = 4\pi^3 + \pi^2 + \pi$, the parameter-rank interpretation of the minimal electronic skeleton $n_e^{(0)} = 10$, the reduction of G to the effective configuration volume of the electron route, the leading proton confinement anchor $m_p/m_e \simeq 6\pi^5$, and the logarithmic anchor for the neutron isospin splitting $\Delta m \simeq m_e \ln(4\pi)$. On cosmological scales, IKT formulates the dark-energy component as the two-component interface $\Lambda_{\text{DE},time}^{\text{IKT}} = \Lambda_{\text{par},time} + \Lambda_{\text{noise},time}^{\text{valve}}$. The dynamic parent-throughput background is proposed to drive the late acceleration, while the finite throughput of the parent valve limits the early insertion noise and leaves a small valve-limited t^{-2} tail in the late epoch. This dark-energy component is separated from the total expansion scalar $3H^2$, which also contains matter, radiation, neutrinos, the vortex/dark-matter sector, curvature, and coarse-graining corrections. Dark matter is modeled as a vortex topological sector, testable via CMB/LSS observables, BTFR, lensing, and cluster collisions. The theory also introduces TTC as a discrete calculus of topological transitions and formulates a set of falsifiable tests: DSR corrections to the propagation of high-energy massless packets, including photons; objective macroscopic decoherence; a cosmological birth-imprint scale for neutrino masses; constraints on stable fermion generations; and a statistical upper cutoff in the supermassive-black-hole mass function. IKT thus sets up a unified computational framework for reducing physical structures to the topology, spectrum, and routing of a dynamic graph. The material is organized in a three-level format: the introductory level gives a compact map of IKT and its main predictions; the technical corpus develops the mechanisms and derivations; and the audit and supplementary sections collect parameter classes, status labels, notation, and navigation aids.

Keywords: information-kinetic theory; dynamic graphs; quantum walk; topological transition calculus; fundamental interactions; dark energy; macroscopic decoherence

© 2026 by the author(s). Distributed under a Creative Commons CC BY license.

Preprints.org (www.preprints.org) | NOT PEER-REVIEWED | Posted: 9 June 2026 doi:10.20944/preprints202606.0589.v1

1. Introduction: The Crisis of the Continuum and the Need for a New Paradigm

1.1. Paradigm Shift and the Abolition of the Continuum

Historically, all of fundamental physics has been built around the concept of a "container." Newton postulated an absolute and rigid spatial container; Einstein, in the General Theory of Relativity, made this container flexible, transforming it into a dynamic metric tensor. However, both paradigms retained space and time as basic, pre-existing physical entities. Information-Kinetic Theory (IKT) takes the following radical ontological step: it does not postulate spacetime as a fundamental entity. In the architecture of IKT, empty space and physical time are treated as emergent infrared interfaces of graph dynamics rather than as primary ontological containers. What a macroscopic observer perceives as "geometric distance" is merely a measure of algorithmic complexity (the number of necessary logical steps) in the transfer of state between nodes of the basic quantum walk graph. What we call the "passage of time" is an emergent operational counter of completed microscopic computational cycles of this network. In the IKT paradigm, the Universe is not a geometric canvas upon which particle dynamics unfold; it is a stochastic graph process whose coarse-grained behavior gives rise to the spatial canvas used in macroscopic descriptions. Within the framework of Information-Kinetic Theory, the particle-field paradigm of the Standard Model is reformulated in graph-routing terms. Fundamental particles and interaction carriers–gauge bosons, the Higgs-channel scalar response, and hypothetical dark matter particles–are not postulated as primary, independent physical entities. In the proposed architecture, they are modeled as emergent macroscopic interfaces of an evolving discrete quantum-walk network. What traditional physics interprets as the exchange of virtual quanta or point-like field excitation is formalized in IKT as algorithmic graph processes: the formation of short-lived resonant gateways for node rewiring, the propagation of one-dimensional graph correction packets, the excitation of collective elastic modes of the vacuum phase bandwidth, and the dynamic self-focusing of topological routes, which contributes to route protection in the Nielsen–Ninomiya/doubler context. It is important to emphasize that this conceptual shift is merely a generalization of the accumulated empirical foundation of modern physics. In the low-energy limit, the topological dynamics of IKT is designed to reproduce the observed phenomenology of the Standard Model in the context of Effective Field Theory (EFT). Familiar wave equations, gauge symmetries, and mass vertices of couplings arise here not as free parameters, but as inevitable thermodynamic and spectral envelopes of the basic phase routing. Thus, quantum numbers (mass, spin, charge) are translated from the category of internal properties of unstructured point objects into the category of measurable geometric invariants of discrete topology. Methodologically, IKT is compared not with existing theories as ontological standards, but with experiment. The language of the Standard Model, GRT–STO, EFT, and phenomenological Lagrangians is used as an interface to measurable invariants, but not as a list of entities that graph microdynamics must accept.

1.2. Historical Context and Evolution of Discrete Topological Vacuum Models

The profound conceptual crisis in modern fundamental physics, manifested in the insurmountable gap between the continuous General Theory of Relativity (GTR) and the Standard Model of quantum field theory (QFT), has spurred the search for paradigms that go beyond the smooth continuum. One of the first conceptual attempts to abandon background space was the concept of spin networks, proposed by R. Penrose [1]. Subsequently, this graph formalism formed the basis of Loop Quantum Gravity (LQG) [2]. However, attempts to integrate macroscopic differential geometry and gauge symmetry groups into a discrete graph architecture led to mathematical divergences. In parallel, a topological approach to describing matter itself was developing. In the seminal work by S. Bilson-Thompson [3], a strict isomorphism was demonstrated between the fermion generations of the Standard Model and mathematical braids of three strands. Nevertheless, the Bilson-Thompson concept remained purely kinematic: topological knots were postulated in isolation from the global dynamics of the vacuum medium. The absence of a mathematical driver for graph evolution prevented this model from deriving an analytical hierarchy of particle masses and their interaction cross-sections. The

© 2026 by the author(s). Distributed under a Creative Commons CC BY license.

Preprints.org (www.preprints.org) | NOT PEER-REVIEWED | Posted: 9 June 2026 doi:10.20944/preprints202606.0589.v1

most radical rejection of continuous ontology was undertaken within the framework of the theory of evolving hypergraphs [4]. A fundamental limitation of this approach was its reliance on abstract combinatorial search in the absence of an internal physical or thermodynamic law determining the direction of the graph's evolution. The Information-Kinetic Theory (IKT), presented in this work, is constructed as a logical synthesis and resolution of the conceptual limitations of the aforementioned programs. Rejecting direct quantization of macroscopic fields (DQMF) and blind rule search (Wolfram), IKT introduces a single physical dynamics operator: the minimization of algorithmic phase delay in a stochastic quantum walk network [5].

1.3. The Current Crisis: Observational Anomalies and Modern Trends

In recent years, fundamental physics has been confronted with a growing stream of observational anomalies and experimental paradoxes requiring a radical reevaluation of the continuum paradigm [19]. The information-kinetic theory organically incorporates the latest trends in global research, offering a unified mechanism for resolving the following current problems:

- **Discreteness of space and the speed limit:** Modern attempts to quantize gravity are increasingly leading theorists to abandon continuous mathematics [20]. Recent studies of quantum speed limits and the minimum time for information mixing [21] require a new fundamental justification. In IKT, this limit is first formulated dimensionlessly as $c_{\text{graph}} = 1$: in a single causal layer, a state can traverse no more than one local edge. The bare adjacency of the graph defines the hardware rate $c_* = a_0/\tau_0$, whereas the observed c_0 is the speed of the coherent massless branch and the SI-projection of the metric cone; $l_0 = c_0\tau_0$ and τ_0 are related metrization scales.
- **Destruction of temporality:** Quantum optics experiments, interpreted as the phenomenon of "negative time" in photon scattering [22], and philosophical debates on the superposition of time arrows [23] motivate a reevaluation of the status of physical time. In IKT, time is not introduced as a fundamental axis but arises as a local counter of adjacency matrix update cycles; in this framework, such effects receive a kinematic interpretation as features of phase routing and the selection of the observed envelope [24].
- **Hubble Tension:** The observational discrepancy in the expansion rates of the early and modern Universe forces cosmologists to reconsider the postulate of metric homogeneity [25]. In Appendix E.4.4 (Methods), we will show that this tension can be interpreted as a consequence of the two-component nature of the expansion of the Multiverse (the transition from endogenous damped noise to a quasi-stationary external phase influx).
- **The Dark Matter Crisis:** A series of recent publications reflects astrophysicists' growing skepticism regarding hypothetical weakly interacting massive particles (WIMPs), stimulating the search for structural gravitational vacuum anomalies [26,27]. This work proposes a topological mechanism without introducing a new particle: the excess gravity of galaxies is interpreted as a macroscopic vortex entanglement of the graph. The mechanism is refined as an asymptotic 2D waveguide reduction with finite vertical leakage and predicts a flattened vortex halo correlated with the baryon angular momentum.
- **The black hole information paradox:** An insurmountable contradiction within the framework of GR and semi-classical QFT between Hawking radiation and the unitarity of quantum mechanics. In IKT, the black-hole boundary is described as a finite graph-accessibility neck with a small Cheeger parameter, not as a fundamental Schwarzschild event horizon. In the B3 branch this neck is coupled to an exponential exterior phase metric and gives a discrete route to the scaling $S \propto A_{\text{gate}}$ and to a Page-curve-compatible toy model for information unwinding through correlated 1D routes.
- **Neutrino mass and the scale of dark energy:** The striking coincidence of the energy scales of the neutrino mass and the cosmological vacuum ($\sim 10^{-3}$ eV) remains unexplained within the Standard Model. IKT offers a purely geometric solution: the neutrino mass arises as a 1D/3D

© 2026 by the author(s). Distributed under a Creative Commons CC BY license.

Preprints.org (www.preprints.org) | NOT PEER-REVIEWED | Posted: 9 June 2026 doi:10.20944/preprints202606.0589.v1

projection of the graph's total generation rate, linking the birth mass of a 1D packet to the Dark Energy density and predicting the cosmological drift of the masses of relic populations.

- **The problem of primordial supermassive black holes (SMBHs):** Recent data from the JWST (e.g., the quasar Abell2744-QSO1) show that giant black holes existed as early as 700 million years after the Big Bang and formed before their host galaxies [28,29]. Within the framework of classical accretion, limited by the Eddington limit, their ultra-rapid growth is inexplicable. In IKT, this paradox is resolved naturally: SMBHs are not the final product of stellar evolution, but rather primary "gateways" (nodes of the Topological Archipelago) from which the inflationary generation of the graph began. Baryonic galaxies condense around them as a secondary process.

1.4. Objectives of the Work

Thus, modern fundamental physics relies on two extremely successful but difficult-to-reconcile paradigms: quantum field theory on a fixed background and the geometry of spacetime in general relativity. Divergences of continuous field integrals, gravitational singularities, the problem of the nature of constants, the dark sector, and the absence of a unified microscopic description of mass motivate the search for a level where the field, the metric, and the particle are not fundamental entities. IKT proposes such a level: a dynamic stochastic graph on which the complex phase is locally routed by a unitary micro-operator. Continuum space, fields, particles, and interactions are regarded as operational interfaces arising after coarse-graining. The overall architecture of the transition from the fundamental microdynamics of the graph to observable macroscopic physics is schematically illustrated in Figure 1.

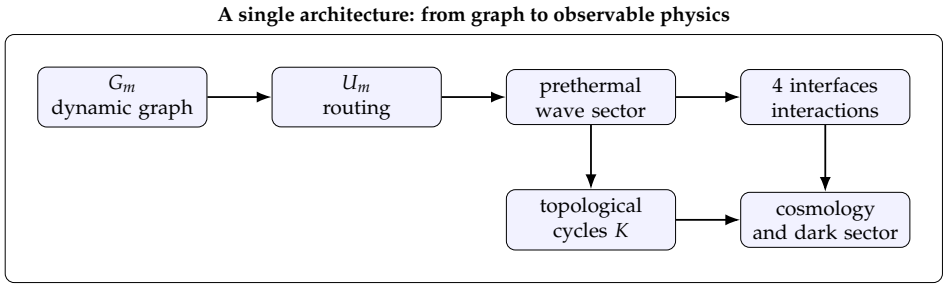

Figure 1. The unified architecture of IKT. A single graph routing micro-operator generates a wave sector, interactions, particles, and cosmological interfaces.

This research aims to construct a self-consistent mathematical language of IKT: graph quantum walk, local phase delay, node insertion rules, continuum limits, and topological particle models. The central goal is not to postulate a new set of fields over an already existing spacetime, but to show under what conditions the coordinates themselves, wave equations, gauge degrees of freedom, and effective metric coefficients emerge as large-scale envelopes of discrete phase routing. Particular attention is paid to dimensionless ratios. The electron mass m_e remains the base scale for mass ratios, whereas the elementary charge e is derived not as an independent axiom, but as a dimensional projection of the channel-normalized electromagnetic coupling α_{top}. The mass ratios of leptons and baryons, the neutron isospin splitting $m_n - m_p$, the fine-structure constant α, the confinement anchor of the strong interaction $\alpha_{s,\text{top}}$, the minimal charge channel g_{em}, the configuration normalization G, and the parameters of the observable scalar channel are expressed in terms of the measures of the corresponding phase spaces, discrete frame configurations, and elastic susceptibilities of the graph. Therefore, the following formulas should be understood in the strict logical context specified in the text: some of them are definitions, some are consequences of graph kinematics, and some are testable topological hypotheses about the measure. In addition to the static derivation of the mass spectrum and constants, the aim of this work is to formulate the Topological Transition Calculus (TTC)—a computational framework that replaces continuum Feynman integrals with their UV divergences by finite discrete sums over classes of graph surgery.

© 2026 by the author(s). Distributed under a Creative Commons CC BY license.

Preprints.org (www.preprints.org) | NOT PEER-REVIEWED | Posted: 9 June 2026 doi:10.20944/preprints202606.0589.v1

2. Microkinetics and Wave Emergence

2.1. Base Graph and Hilbert Space

The fundamental object of the theory at a discrete causal step m is a stochastic causal graph:

$$G_m = (V_m, E_m). \tag{1}$$

The graph has no global axes and is not embedded in a predefined Euclidean space. Unlike classical models on cubic lattices, the fundamental kinematic Hilbert space of IKT is defined not on vertices, but on directed edges (half-edges):

$$\mathcal{H}_m^{\text{edge}} = \ell^2(\vec{E}_m) \otimes \mathbb{C}^2_{\text{spin}}. \tag{2}$$

The spinor structure $\mathbb{C}^2_{\text{spin}}$ is not introduced as an artificial quantum spin of particles, but arises as the minimal complex representation of the Clifford algebra Cl_3, necessary for the isotropic conservation of routing in the effective three-dimensional limit. The unitary translation micro-operator U_m acts precisely on this edge space. The usual knot fields ($\ell^2(V_m) \otimes \mathbb{C}^2_{\text{env}}$) are merely coarse-grained envelopes. For a stable closed path K, an effective particle space $\mathcal{H}_K^{\text{eff}}$ emerges. This hierarchy of Hilbert spaces and their corresponding dynamical regimes (from edge unitarity to the effective Weyl and Dirac equations) is shown in Figure 2.

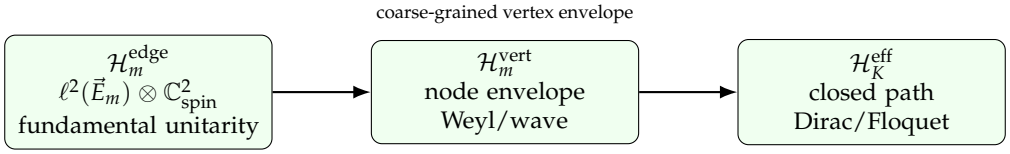

Figure 2. Hierarchy of Hilbert spaces. The old node labels refer to the infrared envelope, and the fundamental operator U_m acts on the edge space.

2.2. The Prethermal Phase and the Weyl Equation

The free wave sector cannot be obtained by simple averaging over random graphs (which would lead to diffusion and Anderson localization). In IKT, the random vacuum graph is in the *prethermal coherent phase*. Under the condition $\epsilon_{\text{pt}} = J_{\text{loc}}/\Omega_{\text{graph}} \ll 1$, the fast microdynamics of local link updates forms an effective Floquet Hamiltonian:

$$U_{\text{cyc}} \simeq \exp[-iH_{\text{pre}}T_{\text{cyc}}/\hbar]. \tag{3}$$

In the long-wavelength limit, the coherent branch of directed translation acquires a Weyl-like principal symbol. The infrared envelope of the stochastic graph is described, in the coherent prethermal sector, by the Weyl equation (see Appendix A.2.4 for the derivation from the prethermal Floquet Hamiltonian):

$$i\hbar\partial_t\psi = -i\hbar c_0\,\vec{\sigma}\cdot\nabla\psi. \tag{4}$$

The reversible second order of this branch forms the free wave kinematics $\partial_t^2\psi = c_0^2\nabla^2\psi$ for transverse $U(1)$ traffic. The discreteness of the stochastic network breaks strict Lorentz invariance only at ultra-high energies, forming an isotropic DSR-like dispersion for massless packets:

$$\omega^2 = c_0^2k^2 - c_0^2a_0^2A_4k^4 + \cdots \quad \text{(see (A2) for the derivation of the dispersion)}, \tag{5}$$

where $A_4 = \eta_4 - \lambda_{\text{wave}}/12$ is the spectral excess of the vacuum ensemble, and a_0 is the graph step. This opens up the possibility of experimentally verifying the theory through time-of-flight tests of gamma-ray bursts. The mechanism for the formation of a smooth wave sector from the prethermal phase of a stochastic graph is clearly illustrated in Figure 3.

© 2026 by the author(s). Distributed under a Creative Commons CC BY license.

Preprints.org (www.preprints.org) | NOT PEER-REVIEWED | Posted: 9 June 2026 doi:10.20944/preprints202606.0589.v1

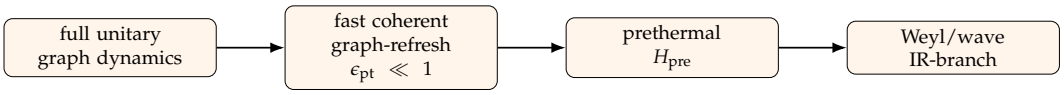

The coherent prethermal phase replaces the incorrect idea of the unitarity of the simple annealed average. Decoherence appears as a small reduced leakage from the coherent branch.

Figure 3. Prethermal vacuum branch. The ballistic Weyl limit is a spectral property of the physical vacuum phase, not of an arbitrary random graph.

(The mathematical formalism of graph kinematics and the derivation of the ballistic branch from the stochastic ensemble are presented in Appendices A.1 and A.2 of Methods).

3. Origin of Mass and Topological Constants

(The detailed mathematical apparatus for the transition to the Dirac equation from Floquet monodromy is given in Appendix A.3 Methods).

A particle in IKT is a stable closed path of phase translation. What is detected as a particle is a stable closed phase-translation route (a quantum 4π-cycle K). Generations of leptons and quarks are decomposed into classes of knots of increasing topological complexity. For a clear visualization of the lepton hierarchy, Figure 4 shows schematic projections of the basic topological routes: the trivial electron knot (0_1), the toric trefoil of the muon (3_1), and the hyperbolic figure-eight of the tau lepton (4_1). The complexity of a knot (the number of crossings) directly determines its phase capacity.

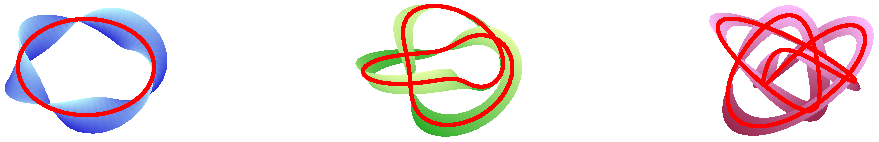

(a) Electron (0_1) **(b) Muon** (3_1) **(c) Tau lepton** (4_1)

Figure 4. Three-dimensional isometric projections of framed lepton topological routes in the IKT framework. **(a) Electron** (trivial knot, $C_K = 0$). The red line represents the base central curve p. The blue polygonal ribbon visualizes the transverse discrete frame ν, which undergoes exactly two full twists along the route, corresponding to the fermionic topological invariant $Lk(p, p + \nu) = \pm 2$. **(b) Muon** (trefoil torus knot, $C_K = 3$). Each crossing increases the local phase capacity of the knot, leading to exponential mass growth ($m_\mu \propto 6^3 m_e$). The green discrete frame remains fully exposed to external $U(1)$-traffic ($f_{3_1} = 1$). **(c) Tau lepton** (hyperbolic figure-eight knot, $C_K = 4$). Unlike the toric muon, this route possesses a volumetric hyperbolic core contributing to the mass factor H_{4_1}. The purple discrete frame is partially screened by self-intersections, manifesting as a reduced electromagnetic susceptibility ($f_{4_1} \simeq 0.20$).

3.1. Mass as a Monodromic Phase Gap

The micro-operator U_m does not contain "bare" mass in the form of a scalar parameter. A massive Dirac sector arises only for those topological cycles that connect two chiral branches (left and right). The inertial mass is defined as the integral algorithmic delay—the Floquet monodromy spectral gap of a closed route:

$$M_K c_0^2 = \frac{\hbar}{T_K} |\Theta_K| \quad \text{(see (A4) for the derivation)}, \tag{6}$$

where Θ_K is the effective phase of the rest monodromy. This formula serves as a general principle: electrons, leptons, nucleons, and composite topological knots differ in their spectrum of allowed paths, their holonomies, and their channel capacities. Correlations between channels are accounted for by the factor Ξ_e. The general logic of the emergence of inertial mass as a monodromic phase gap of a closed route is illustrated in Figure 5.

The properties of the simplest charged path (the electron) are determined by its parametric manifold. For a single chiral directed step, the choice of the translation beam (S^2_{dir}), the spin-frame carrier (S^2_{spin}), and the relative $U(1)$-holonomy (S^1_{hol}) together yield a dimension of 5. Due to the

© 2026 by the author(s). Distributed under a Creative Commons CC BY license.

Preprints.org (www.preprints.org) | NOT PEER-REVIEWED | Posted: 9 June 2026 doi:10.20944/preprints202606.0589.v1

Dirac/Floquet doubling of the L/R branches, the minimal 4π-spinor skeleton has a factored parametric rank of $n_e^{(0)} = 10$ (see Proposition A2).

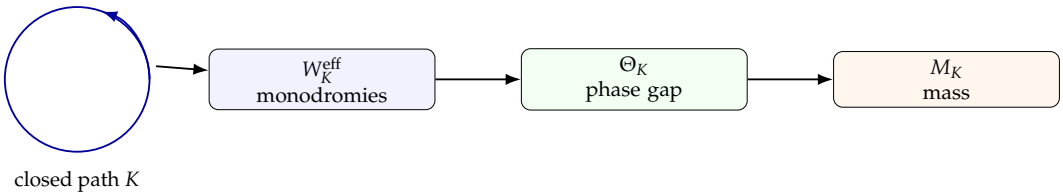

Figure 5. Mass as a spectral invariant. A massive Dirac envelope appears after the Floquet/homogenization projection of a closed topological path.

4. The Four Interactions as Interfaces

4.1. The Emergence of the Four Forces

The four interactions are described not as four independent ontologies, but as four modes of access to a single graph routing. Historically, physics introduced various continuous fields and independent carriers for each of the fundamental forces. In IKT, the four interactions are formalized as different macroscopic interfaces for accessing the same graph microdynamics U_m:

1. **Electromagnetism:** Free translation of the transverse Abelian $U(1)$-link phase of the edge transporter. After coarse-graining, it generates a covariant Dirac current $j^\mu = \bar{\Psi}\gamma^\mu\Psi$, and the channel anchor of the fine structure takes the form $\alpha_{\text{top}}^{-1} = 4\pi^3 + \pi^2 + \pi$. 2. **Strong interaction:** It is considered as a color-routing interface—an internal color $SU(3)_{\text{route}}$ routing with a rigid topological singlet constraint $Q_A^{\text{col}}|\Psi_{\text{phys}}\rangle = 0$. The topological coupling anchor at the confinement scale is given by the lattice geometry: $\alpha_{s,\text{top}} = \mu_{\text{col}}^{\text{ch}}/\mu_{\text{arc}} = \pi^2/\pi^3 = 1/\pi$. 3. **Weak interaction:** It is not a long-range phase, but rather a local resonant algorithmic gate ($\mathcal{G}_W$) that performs a topological frame remapping. The gateway acts exclusively on the levorotatory sector (P_L) due to the spontaneous macroscopic vacuum helicity $\Xi_{\text{vac}} \neq 0$, fixed during the cosmological percolation epoch. 4. **Gravity:** The macroscopic phase refraction χ_G (see Appendix B.4 for the microscopic derivation) arises as phase refraction with the effective metric

$$ds^2 = -e^{-2\chi_G} c_0^2 dt^2 + e^{2\chi_G} d\mathbf{R}^2. \tag{7}$$

The conceptual division of the four fundamental interactions as macroscopic interfaces providing access to the same edge routing U_m is visualized in Figure 6.

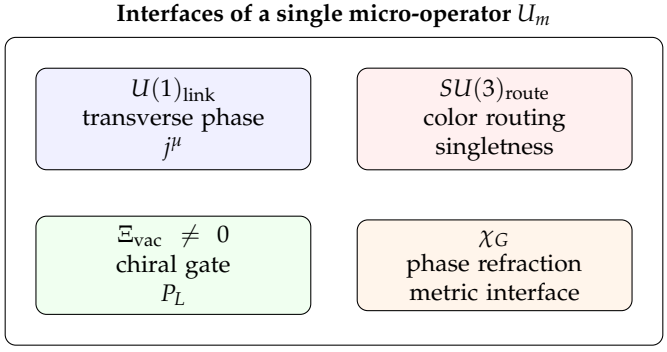

Figure 6. Four interactions as macroscopic interfaces of graph microdynamics.

For a clear systematization of the results, Table 1 presents a summary matrix of all fundamental physical theories. It demonstrates the conceptual unity of IKT: familiar macroscopic equations (the low-energy limit) emergently arise from a single basic translation operator. At the same time, the table shows how these classical equations are inevitably modified upon transition to Planck scales. The expansion of the effective graph update in terms of network quanta (τ_0, l_0) defines a testable class of high-energy corrections—ranging from DSR kinematics and objective decoherence to proposed graph mechanisms of strong interaction.

© 2026 by the author(s). Distributed under a Creative Commons CC BY license.

Preprints.org (www.preprints.org) | NOT PEER-REVIEWED | Posted: 9 June 2026 doi:10.20944/preprints202606.0589.v1

Table 1. Comparison matrix of fundamental theories: direct comparison of macroscopic limits and graph equations of IKT.

Interaction (fundamental theory)	**Macroscopic limit (Standard Model / GRT)**	**QFT equation (Topological reduction)**	**Sources of QFT corrections**	**Emergent physical effect**	**Connection to the text**
Continuum kinematics(Einstein's SRT)	Strict dispersion: $\omega^2 = c^2k^2$	Stochastic dispersion: $\omega^2 = c_0^2k^2\left[1 - a_0^2\left(\eta_4 - \frac{\lambda_{\text{wave}}}{12}\right)k^2 + \dots\right]$	a_0 — graph step, η_4 — vacuum spectral excess.	DSR kinematics. The velocity of rigid gamma quanta decreases proportionally to the square of the energy.	Appendix A.2.8
Quantum dynamics(Schrödinger / Dirac)	Unitary evolution: $i\hbar\frac{\partial\rho}{\partial t} = [\hat{H}, \rho]$	Reduced dynamics: $\frac{d\rho}{dt} = -\frac{i}{\hbar}[\hat{H}, \rho] - \frac{\tau_0}{2\hbar^2}[\hat{H}, [\hat{H}, \rho]]$	τ_0 — the metric cycle of the graph (insertion $\mathcal{I}_m$).	Objective decoherence of superpositions. Lifetime of a 1D bridge: $t \propto M^{-4}$.	Appendices A.3.1 (Dirac envelope) and A.3.5 (Decoherence)
Electro-magnetism(Maxwell)	Field and current equations: $\Box\mathbf{A} = \mu_0\mathbf{j}$ $\mathcal{L}_{\text{int}} = eA_\mu j^\mu$	Symmetric graph update: $\mathbf{A}(t+\tau_0) - 2\mathbf{A}(t) + \mathbf{A}(t-\tau_0) = \lambda_{\text{wave}}L_G\mathbf{A}(t)$ TTC (emergent current from $\delta\mathcal{U}_{ij}^{(A)}$): $\mathcal{M}_{\text{em}}^{\text{TTC}} = g_{\text{em}}\int d^4x\, A_\mu j^\mu$	UV corrections from the discrete Laplacian L_G. The charge is determined by the measure of phase strata: $\alpha_{\text{top}}^{-1} = 4\pi^3 + \pi^2 + \pi$	The EM field is the macro-envelope of $U(1)$-link phases. The Dirac current j^μ arises from the annealed averaging of local transitions.	Appendix B.1 (see Appendices B.1.3 and B.1.4)
Gravity(General Relativity / Newton)	PPN metric (β, γ): $g_{00} \approx -1 + 2\Phi - 2\beta\Phi^2$ $g_{ii} \approx 1 + 2\gamma\Phi$	Refractive metric: $g_{00} = -e^{-2\chi_G} \approx -1 + 2\chi_G - 2(1)\chi_G^2$ $g_{ii} = e^{2\chi_G} \approx 1 + 2(1)\chi_G$	χ_G — phase delay. $\gamma = 1$ from the inverse phase impedance.	A natural conclusion is $\beta = 1, \gamma = 1$. The curvature of spacetime is graph refraction.	Appendix B.4
Interaction(basic theory)	**Macro-limit (Standard Model / GRT)**	**EQM (Topological reduction)**	**Sources of EQM corrections**	**Emergent physical effect**	**Connection to the text**
Strong interaction(QCD)	String potential: $V(r) = \sigma_{\text{str}}r$	Dimensionless algorithmic cost: $V(r) = \left(\hat{\sigma}_{\text{QCD}}\frac{m_e^2c_0^3}{\hbar}\right)r$	$\hat{\sigma}_{\text{QCD}}$ — the cost of 1 color tube step.	The linearity of confinement follows from the one-dimensional routing of the color current.	Appendix B.2
Weak interaction(Electroweak Theory)	Left-handed current: $J_L^\mu = \Psi\gamma^\mu\frac{1-\gamma^5}{2}\Psi$	Response to graph chirality: $\mathcal{M}_{\text{weak}}^{\text{TTC}} \approx g_W\int d^4x\, W_\mu\Psi\gamma^\mu P_\Xi\Psi$ $\left(\text{where } P_\Xi = \frac{1-\text{sgn}(\Xi_{\text{vac}})\gamma^5}{2}\right)$	Ξ_{vac} — global spirality of vacuum percolation.	The violation of P-parity is due not to the Lagrangian, but to the asymmetry of the initial graph injection.	Appendix B.3

© 2026 by the author(s). Distributed under a Creative Commons CC BY license.

Preprints.org (www.preprints.org) | NOT PEER-REVIEWED | Posted: 9 June 2026 doi:10.20944/preprints202606.0589.v1

5. Microscopic Limit: Topological Particle Spectrum

The fundamental constants of the Standard Model in IKT acquire a rigorous geometric meaning. IKT aims to derive these constants via information measures and spectral capacities of phase channels. The three most important anchors:

$$\alpha_{\text{top}}^{-1} = 4\pi^3 + \pi^2 + \pi \quad \text{(see Proposition A1)}, \tag{8}$$

$$G_{\text{IKT}} = \frac{\hbar c_0}{M_{K_e}^2 \left(\Gamma_e \mathcal{N}_\alpha^{10} \Xi_e\right)^2} \quad \text{(see Appendix B.4.3)}, \tag{9}$$

$$\Delta m_{np}^{\text{top}} = M_{K_e} \ln(4\pi) \quad \text{(see (A29))}. \tag{10}$$

Their status currently differs: α_{top} is a no-fit channel anchor under spectral equipartition; G reduces to the calculation of M_{K_e}, Γ_e, and Ξ_e; the neutron-proton gap receives a logarithmic anchor of the internal $U(1)$ compactification. The logical chain of reduction of the gravitational constant G_{IKT} to dimensionless information measures and the mass of the electron route is illustrated in the dependence graph (Figure 7).

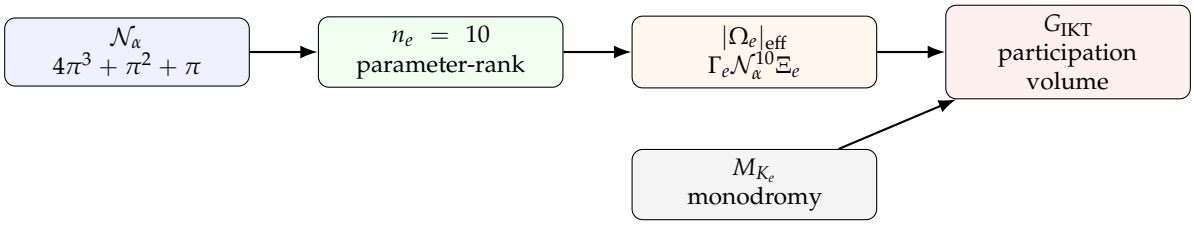

Figure 7. Example of a dependency chain for gravitational normalization: G is reduced to the mass of the electron path, the channel capacitance, the frame factor, and the correlation factor.

Fine-structure constant (α): In IKT, α is defined as the ratio of one quantized action channel ($\mu_{\text{ch}} = 1$ in h-units) to the total information capacity of the electromagnetic block U_m. The stratified space of electromagnetic recombination consists of a regular stratum ($\mathcal{C}_4 \simeq U(1) \times SU(2)$), a reduced Cartan stratum ($\mathcal{C}_2$), and a phase-locked line ($\mathcal{C}_1$). Under the postulate of spectral equipartition of orthogonal strata, we obtain the leading (no-fit) topological anchor:

$$\alpha_{\text{top}}^{-1} = \mu(\mathcal{C}_4) + \mu(\mathcal{C}_2) + \mu(\mathcal{C}_1) = 4\pi^3 + \pi^2 + \pi. \tag{11}$$

Numerically, $\alpha_{\text{top}}^{-1} \approx 137.0363$. The deviation from the laboratory value $\alpha(0)^{-1} \simeq 137.0360$ (~ 2.2 ppm) is attributed to infrared polarization corrections of the graph (Π_{IR}), calculated via the graph renormalization group. **Proton mass and confinement:** In QCT, confinement is not a force potential; it is a topological requirement for the closure of the color current. The proton is modeled as a singlet coupling of three open fermionic arcs. The channel measure of this minimal baryon cell $\mathcal{C}_p$ is calculated as the product of three Dirichlet modes of the arcs (π^3) and two neutral Cartan holonomies $SU(3)$ of the singlet coupling (π^2). Under the condition of marginal rigidity of the 3D lattice (external routing specifies $k_{\text{ext}} = 6$ isostatic channels), the topological confinement mass of the proton is derived as:

$$\left(\frac{m_p}{m_e}\right)_{\text{top}} = k_{\text{ext}} \mu_p(\mathcal{C}_p) = 6\pi^5 \quad \text{(see Lemma A8)}. \tag{12}$$

This gives $m_p^{\text{top}} \approx 1836.12 m_e$. The relative discrepancy with the physical mass ($\sim 1.9 \times 10^{-5}$) is explained by small radiation corrections and the current masses of quarks. The energy of free beta decay, accordingly, is given by $Q_\beta \simeq m_e[\ln(4\pi) - 1]$. The topological structure of nucleons, which explains this mass difference as the entropy cost of compactifying an open $U(1)$-flux, is shown in Figure 8.

© 2026 by the author(s). Distributed under a Creative Commons CC BY license.

Preprints.org (www.preprints.org) | NOT PEER-REVIEWED | Posted: 9 June 2026 doi:10.20944/preprints202606.0589.v1

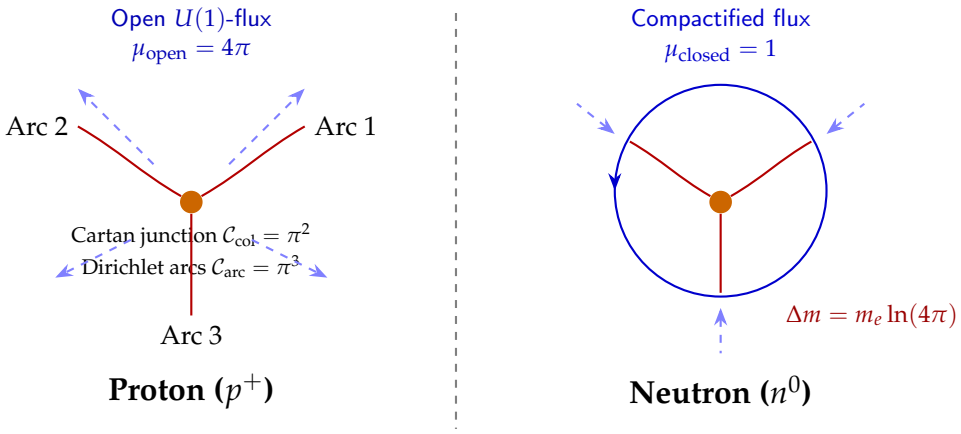

Figure 8. Topological structure of nucleons in IKT and the nature of isospin splitting. **Left:** The proton is an open baryon framework (three fermion arcs connected by a neutral Cartan holonomy). The $U(1)$-flux freely escapes into the external 3D network (angular measure $\mu_{\text{open}} = 4\pi$). **Right:** The neutron possesses the same internal framework, but its $U(1)$-flux is forcibly compactified into an internal loop ($C_K = 0$). The mass difference $m_n - m_p$ arises as the entropic cost of this topological compactification, equal to $m_e \ln(4\pi)$ (up to small Rydberg deformations).

Neutron and isospin splitting (Δm): The neutron possesses the same basic baryonic framework as the proton. The difference in their masses arises exclusively from the algorithmic work of internally compactifying the $U(1)$ charge flux. For the proton, the external angular measure of the routing is open ($\mu_{\text{open}} = 4\pi$). For the neutron, the current is forcibly confined to a closed channel ($\mu_{\text{closed}} = 1$). The integral of the phase-compression work yields an exact logarithmic anchor for isospin splitting:

$$\Delta\theta_{\text{closure}} = \int_1^{4\pi} \frac{d\mu}{\mu} = \ln(4\pi) \quad \text{(see (A29))}, \tag{13}$$

which, when projected onto the reference mass of the electron compensator, leads to the relation $m_n - m_p \simeq m_e \ln(4\pi)$.

For a comprehensive understanding of the microscopic paradigm, Table 2 presents the topological reduction of quantum numbers and fundamental phenomenological structures. This table establishes the interpretive layer; the exact numerical coefficients, masses, lifetimes, and coupling constants have the statuses indicated in the summary of results below.

Table 2. Topological reduction of the Standard Model in terms of IKT. The table records updated interpretations, including the dynamic stability of the graph and a bypass of the Nielsen–Ninomiya theorem; a rigorous derivation of exact numerical coefficients requires the specification of normed measures for the corresponding configuration spaces.

Observed phenomenon	Standard Model	Information-kinetic interpretation
Mass and stability	Intrinsic property of the particle (Higgs). Particles are absolutely stable if there are no allowed decays.	Integral phase delay of a closed loop: $M_K/m_e = \mathcal{M}(K)$. The loop dynamically shields itself from breaking by stochastic vacuum noise ($\gamma_{\text{surg}}(e)$), ensuring the cosmological stability of matter.
Fermion chirality	Left and right Weyl spinors are introduced axiomatically.	On a protected quasi-one-dimensional path, 1D duplicates inevitably arise. In IKT, they are not parasitic but form the conjugate left and right chiral branches of the Dirac bispinor (a solution to the Nielsen–Ninomiya problem).
Generations of fermions	Three families of particles without an explanation for the hierarchy.	Classes of topological knot complexity: $C_K = 0$ (electron), $C_K = 3$ (muon), $C_K = 4$ (tau); the absence of $C_K = 1, 2$ is due to the topological triviality of such closed structures.

© 2026 by the author(s). Distributed under a Creative Commons CC BY license.

Preprints.org (www.preprints.org) | NOT PEER-REVIEWED | Posted: 9 June 2026 doi:10.20944/preprints202606.0589.v1

Table 2. *Cont.*

Observed phenomenon	Standard Model	Information-kinetic interpretation
Spin and statistics	Postulated quantum spin and the Pauli principle.	Path orientation: a fermionic Möbius-like cycle closes over 4π. The exchange of two identical cycles has the Finkelstein–Rubinstein sign -1, which gives $\Psi(2,1) = -\Psi(1,2)$ (topological Pauli principle).
Electric charge	Internal $U(1)$ charge, normalized empirically via e.	Dimensionless minimal channel $g_{\text{em}}^2 = 4\pi\alpha_{\text{top}}$; the dimensional charge e_{top} is the SI projection of the topologically derived information capacity of the routing channels.
Color and confinement	$SU(3)$ charge and the absence of free quarks in the vacuum.	Confinement is a geometric requirement for the closure of the color current. A baryon is formed by the neutral singlet coupling of three open color channels (arcs).
Electroweak structure	Left $SU(2)_L$ doublets, right singlets, $U(1)_Y$ hypercharge, mixing.	The charged-current gate (surgical gluing) acts only on the left-handed sector: $\mathcal{G}_W P_R = 0$. The photon and Z arise as orthogonal combinations of B_μ and W_μ^3, and the CKM/PMNS matrices — as matrix elements of the gluing.
Neutrinos	Light neutral fermions participating only in the weak interaction.	One-dimensional graph correction packets. They arise as "byproducts" (discharge of excess phase and momentum) during the surgical untangling and gluing of topological knots in the weak gauge group $\mathcal{G}_W$.

(Topological calculations of node measures, derivation of the baryon spectrum, and isospin splitting are presented in Appendices C.2 and C.3 of the Methods).

5.1. Summary Table of the Audit of Fundamental Parameters

© 2026 by the author(s). Distributed under a Creative Commons CC BY license.

Preprints.org (www.preprints.org) | NOT PEER-REVIEWED | Posted: 9 June 2026
doi:10.20944/preprints202606.0589.v1

Table 3. Audit of Fundamental Parameters: Direct Comparison of SM Phenomenology and IKT Numerical Topological Predictions.

Physical Quantity / Phenomenon	**Value in SM / ΛCDM**	**Dimensional-free IKT invariant (Micro-level)**	**Dimensional projection (Quantitative IKT prediction)**	**Status/Comment**
Speed of light in a vacuum (c)	299 792 458 m/s (STO constant)	$c_{\text{graph}} = 1$ (1 edge per 1 cycle)	$c_0 \equiv \mathbf{299\,792\,458}$ m/s (SI calibration anchor)	c_0 — macro-limit of the coherent branch; a_0/τ_0 — hardware rate (see Section A.1.3.1).
UV resolution (Planck scales)	$t_{\text{Pl}} \approx 5.39 \times 10^{-44}$ s $l_{\text{Pl}} \approx 1.61 \times 10^{-35}$ m	$\epsilon_0 = 1/\lvert\Omega_e\rvert_{\text{eff}}$ (fraction of the electron path)	$\tau_0 = \epsilon_0 \tau_e \simeq \mathbf{5.39 \times 10^{-44}}$ s $l_0 = c_0 \tau_0 \simeq \mathbf{1.61 \times 10^{-35}}$ m	Planck scales are SI projections of the electron's configurational density (see Section F.1.2).
Newton's constant (G)	6.674×10^{-11} m^3/(kg·s^2) (fundamental constant)	$\alpha_G^{(e)} = \frac{1}{\lvert\Omega_e\rvert_{\text{eff}}^2} = \frac{1}{(\Gamma_e \mathcal{N}_\alpha^{10} \Xi_e)^2}$	$G_{\text{IKT}} = \mathbf{6.674 \times 10^{-11}}$ m^3/(kg · s^2) (with rank factor $n_e^{(0)} = 10$)	Reduction of gravity to the electron mass, $U(1)$ gauge, and rank parameter 10 (see Section B.4.3).
Fine-structure constant (α)	$\approx 1/137.035999$ (as $Q^2 \to 0$)	$\alpha_{\text{top}}^{-1} = 4\pi^3 + \pi^2 + \pi$ (measures of the U_m stratum)	$\alpha_{\text{top}}^{-1} = \mathbf{137.0363038}$ (Residual IR polarization: $\Pi_{\text{IR}} \simeq 2.2 \times 10^{-6}$)	α_{top} — pure topological anchor (see Proposition A1); the running coupling requires consideration of the graph polarization.
Elementary charge (e)	1.602×10^{-19} C (external parameter)	$g_{\text{em}} = \sqrt{4\pi\alpha_{\text{top}}}$ (dimensionless $U(1)$ channel)	$e_{\text{top}} = \sqrt{4\pi\varepsilon_0 \hbar c_0 \alpha_{\text{top}}} \simeq \mathbf{1.602 \times 10^{-19}}$ C	The charge is the laboratory SI projection of the graph's topological connection (see Section B.1.4.1).
Proton mass (m_p)	938.2721 MeV (empirical value)	$(m_p/m_e)_{\text{top}} = 6 \cdot (\pi^3 \cdot \pi^2) = 6\pi^5$	$m_p^{\text{top}} = m_e 6\pi^5 \approx \mathbf{938.2544}$ MeV (Deviation $\sim 1.9 \times 10^{-5}$)	The baryon mass follows from the spectral-channel measure of the confinement cell (see Lemma A8).
Isospin splitting ($m_n - m_p$)	$\Delta m \approx 1.29333$ MeV ($Q_\beta \approx 0.78233$ MeV)	$\Delta\theta_{\text{closure}} = \int_1^{4\pi} \frac{d\mu}{\mu} = \ln(4\pi)$ (value of $U(1)$ contraction)	$\Delta m_{\text{top}} = m_e \ln(4\pi) \approx \mathbf{1.29335}$ MeV $Q_\beta^{\text{top}} \approx \mathbf{0.78235}$ MeV (Residual $\delta_{np}^{\text{IR}} \approx -18$ eV)	Good agreement between the topological work of charge compactification and the physical splitting of nucleons (see Section C.3.4).
Strong coupling constant (α_s)	$\alpha_s(M_Z) \simeq 0.118$ (running parameter of the QCD)	$\alpha_{s,\text{top}}(\mathcal{Q}_{\text{conf}}) = \frac{\mu_{\text{col}}^{\text{ch}}}{\mu_{\text{arc}}} = \frac{1}{\pi}$	Anchor: $\alpha_{s,\text{top}} \approx \mathbf{0.318}$ (at $Q \sim 1$ GeV). RG shift to M_Z: $\alpha_s^{\text{eff}}(M_Z) \sim \mathbf{0.12}$	Ratio of color gate and arc measures (see Section C.3.3); the shift to M_Z requires the IKT color β-function.
Lepton masses (m_μ, m_τ)	$m_\mu \approx 105.66$ MeV $m_\tau \approx 1776.8$ MeV	$m_K/m_e = 6^{c(K)} H_K \cdot$ $\cdot(1 - 6\alpha_{\text{top}} f_K)$	Muon ($c = 3$): $m_\mu^{\text{top}} \approx 206.54 m_e \approx \mathbf{105.54}$ MeV. Tau ($c = 4$): $m_\tau^{\text{top}} \sim \mathbf{1790}$ MeV (for $\kappa_{\text{emb}} \approx 4/3$)	The hierarchy is controlled by the knot complexity $c(K)$ and the EM shielding f_K (see Section C.2.2).
125 GeV scalar channel (Higgs)	$m_H \simeq 125$ GeV VEV: $v_{\text{EW}} \approx 246$ GeV $m_f = y_f v_{\text{EW}}/\sqrt{2}$	$\lambda_K \simeq 1$ (universal susceptibility)	$F_h \simeq v_{\text{EW}} \approx \mathbf{246}$ GeV $g_{hKK}^{\text{obs}} = \lambda_K M_K / F_h$	125 GeV — the elastic longitudinal mode of the graph (see Section C.4); 246 GeV — its stiffness. The amplitudes are mass-dependent ($g_{hKK} \propto M_K$).

© 2026 by the author(s). Distributed under a Creative Commons CC BY license.

Preprints.org (www.preprints.org) | NOT PEER-REVIEWED | Posted: 9 June 2026 doi:10.20944/preprints202606.0589.v1

Table 3. *Cont.*

Physical Quantity / Phenomenon	**Value in SM / ΛCDM**	**Dimensional-free IKT invariant (Micro-level)**	**Dimensional projection (Quantitative IKT prediction)**	**Status/Comment**
Dark energy (Late acceleration Λ)	$\Lambda \sim 10^{-52}$ m^{-2} Equation of state $w \simeq -1$	$\Lambda^{\mathrm{IKT}}_{\mathrm{DE,time}} = \Lambda_{\mathrm{par},time} + \Lambda^{\mathrm{valve}}_{\mathrm{noise},time}$ (DE component; not total $3H^2$)	$\Lambda_{\mathrm{par}} \simeq$ **const** (the $\mathcal{F}_{\mathrm{par}}$ window gives $w \simeq -\mathbf{1}$) $\Lambda^{\mathrm{valve}}_{\mathrm{noise}} \propto \mathbf{t^{-2}}$ (late tail; the early cap sets Λ_{valve})	Two-component interface (see Section E.2): the background of the parent branch yields a ΛCDM-like regime, and the valve-limited t^{-2} noise has a finite plateau Λ_{valve}; $d_0^2 = \lambda_{\max}/\lambda_{\mathrm{valve}}$ is its dimensionless projection.
Dark matter and halos	WIMP mass $\sim 10^2$ GeV Spherical halo	Vortex potential of the waveguide: $v_f^4 = GM_{\mathrm{bar}}a_{\mathrm{vort}}$	$a_{\mathrm{vort}} = \frac{c_0 H_{\mathrm{bg}}}{2\pi} \approx \mathbf{1.04 \times 10^{-10}}$ m/s^2 (empirical MOND threshold $\sim 1.2 \times 10^{-10}$)	The halo is a quasi-2D waveguide (see Section E.3.3); a_{vort} is the physical limit of vortical acceleration.
Bridge decoherence time	No objective collapse in the SM	$\Gamma_{\mathrm{IKT}} t = \frac{(\Delta\varepsilon_G)^2}{2\lvert\Omega_e\rvert_{\mathrm{eff}}} \tilde{t}$	Macro-object (1 kg, $\Delta x = 0.1$ m): $t^{\mathrm{oom}}_{\mathrm{IKT}} \approx \mathbf{9.3 \times 10^{-7}}$ s Micro-object (e^-): $t^{\mathrm{oom}}_{\mathrm{IKT}} \sim \mathbf{10^{98}}$ s	Lifetime filter $t_{\mathrm{IKT}} \propto M^{-4}$, equivalently $\Gamma_{\mathrm{IKT}} \propto M^4$ at fixed geometry (see Section A.3.5); for the microworld, coherence is stable, while macro-superpositions collapse instantaneously.

© 2026 by the author(s). Distributed under a Creative Commons CC BY license.

Preprints.org (www.preprints.org) | NOT PEER-REVIEWED | Posted: 9 June 2026 doi:10.20944/preprints202606.0589.v1

6. Topological Transition Calculus (TTC)

6.1. Elimination of UV Divergences via Graph Cobordisms

One of the main problems of the continuum QFT is the appearance of ultraviolet divergences (infinities) when calculating Feynman diagrams. In TTC, the continuum UV source of this problem is replaced by finite graph-transition sums.

The Topological Transition Calculus (TTC) replaces continuous path integrals with a finite discrete sum over admissible graph cobordisms (adjacency matrix permutations). Local graph cobordisms are transformed into amplitudes, cross sections, and decay widths:

$$\text{graph cobordism} \Rightarrow \mathcal{M} \Rightarrow \sigma, \Gamma, \tau. \tag{14}$$

Instead of continuous UV integrals, finite sums over admissible topological transitions are used. Check conditions include the unitarity of the full S-matrix, the optical theorem, graph Ward identities, FR statistics, and the separation of UV finiteness from IR-inclusive procedures.

(The formal apparatus of graph cobordisms and the properties of unitarity are given in Appendices D.1 and D.3 of Methods).

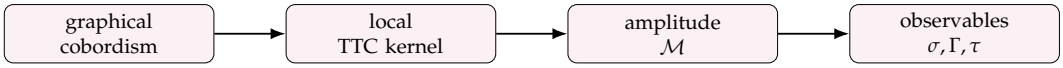

Figure 9. TTC as a discrete computational chain from graph re-linking to phenomenological quantities.

The observed transition amplitude is calculated as:

$$\mathcal{M}^{\mathrm{TTC}}_{\beta\alpha} = \sum_{\mathfrak{C}} \mathcal{N}[\mathfrak{C}] e^{iS_{\mathrm{top}}[\mathfrak{C}]} \mathcal{K}_{\mathrm{loc}} \prod F_K(q^2) \quad \text{(see (A31))}. \tag{15}$$

Here, $\mathcal{K}_{\mathrm{loc}}$ is the local gluing kernel, and $F_K(q^2)$ is the topological form factor of stable cycles. The discrete step of the graph a_0 and the form factors act as a natural physical UV cut-off of the spectrum.

6.2. Topological Surgery in Practice: Weak and Electromagnetic Vertices

For example, the weak interaction in the TTC formalism is described as a local resonant re-gating (surgery) of a fermion's topological path with the emission of a 1D neutrino packet, as illustrated in Figure 10.

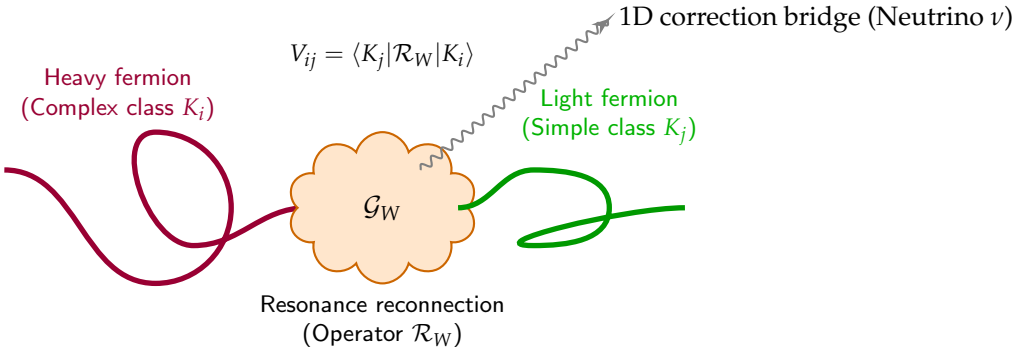

Figure 10. Topological mechanics of weak interaction (charged-current gateway). In IKT, weak bosons are not carrier particles in the traditional sense. They are short-lived overstressed graph regions — resonance gateways $\mathcal{G}_W$ where algorithmic reconnection of the fermion topological class occurs. A heavy (topologically complex) cycle enters the gateway, loses a fraction of its crossings, and exits as a simpler (lighter) fermion. The released algorithmic phase and momentum are discarded as a 1D graph error correction wavepacket — a neutrino. The transition probabilities are determined, in the effective interface, by the matrix elements of the topological reconnection operator $\mathcal{R}_W$ (emergent CKM and PMNS matrices).

© 2026 by the author(s). Distributed under a Creative Commons CC BY license.

Preprints.org (www.preprints.org) | NOT PEER-REVIEWED | Posted: 9 June 2026 doi:10.20944/preprints202606.0589.v1

In turn, the electromagnetic interaction (e.g., Møller scattering) is formalized as an exchange via a phase bypass route on the background graph, taking into account the Finkelstein–Rubinstein sign in the spatial exchange of fermionic cycles (Figure 11).

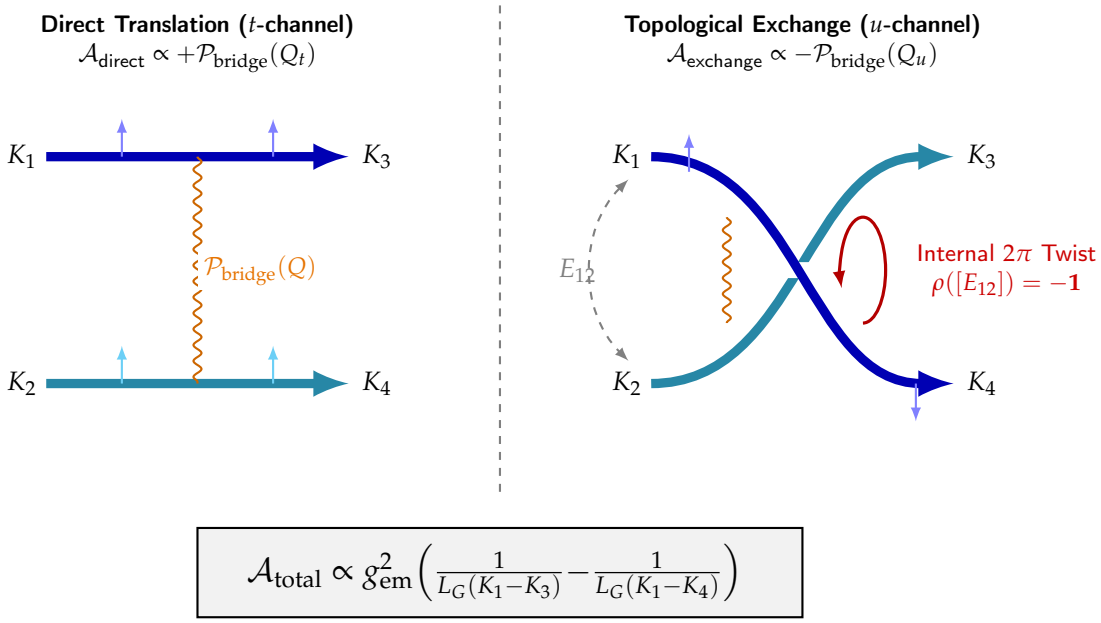

$$\mathcal{A}_{\text{total}} \propto g_{\text{em}}^2 \left(\frac{1}{L_G(K_1 - K_3)} - \frac{1}{L_G(K_1 - K_4)} \right)$$

Figure 11. Topological Transition Calculus (TTC) for Møller scattering. In IKT, interaction is not an exchange of point-like particles, but an algorithmic reconnection of framed topological routes. **Left:** The direct t-channel, where two 4π-spinor routes (electrons) exchange a phase detour $\mathcal{P}_{\text{bridge}}$ over the background graph. **Right:** The exchange u-channel. Because electrons are Möbius-like topological defects, the spatial swap of their incoming graph paths (an operation denoted as the exchange loop E_{12}, which swaps K_1 and K_2) is topologically equivalent to a 2π rotation of their internal discrete frames (indicated by the red circular arrow). According to the Finkelstein-Rubinstein condition on the graph, this generates a phase factor of -1. Thus, the Pauli exclusion principle and antisymmetric amplitudes emerge purely from graph topology, without postulating ad-hoc anticommutation relations.

7. Cosmological Limit

In cosmology, IKT uses the same mechanism of graph insertion and phase routing. Algorithmic inflation is interpreted as avalanche-like graph generation; dark energy—as a two-component interface between the parent throughput background and the valve-limited tail of residual insertion; dark matter—as a vortex topological sector with an early, nearly cold regime and a late galactic waveguide.

$$\chi_{\text{lens}} = \chi_G + \chi_{\text{vort}}^{\text{prim}} + \chi_{\text{vort}}^{\text{gal}} \quad \text{(see Appendix E.3.5.1 for the derivation of the eikonal).} \tag{16}$$

This formula defines a unified lensing potential that combines the baryonic phase delay and the vortex components. The dark sector becomes testable via the CMB/LSS, BTFR, halo shapes, lensing offsets, and cluster collisions. The cascading evolution of the multiverse is illustrated in detail in Figure 12. The scenario covers the initiation of a daughter universe via the Topological Archipelago, inflationary geometrization, the two-component dark energy epoch, and the final topological drain.

Remark 1 (Empirical confirmation: SMCHDs prior to galaxy formation). *A consequence of the Topological Archipelago model is the inversion of the classical scenario of galaxy formation. Since the initial state of the daughter graph is determined by distributed over-stressed clusters ($p_{\text{stay}} \to 1$), primordial supermassive black holes (SMBHs) are born together with the very geometry of space, bypassing the phase of stellar collapse. Baryonic matter subsequently condenses around these pre-existing gravitational anchors. This topological prediction of IKT is motivated by recent observations from the James Webb Space Telescope (JWST), which detected giant*

© 2026 by the author(s). Distributed under a Creative Commons CC BY license.

Preprints.org (www.preprints.org) | NOT PEER-REVIEWED | Posted: 9 June 2026 doi:10.20944/preprints202606.0589.v1

SMHBs in the early Universe whose mass constitutes the overwhelming majority of the mass of their tiny host galaxies, making their gradual growth from stellar remnants impossible.

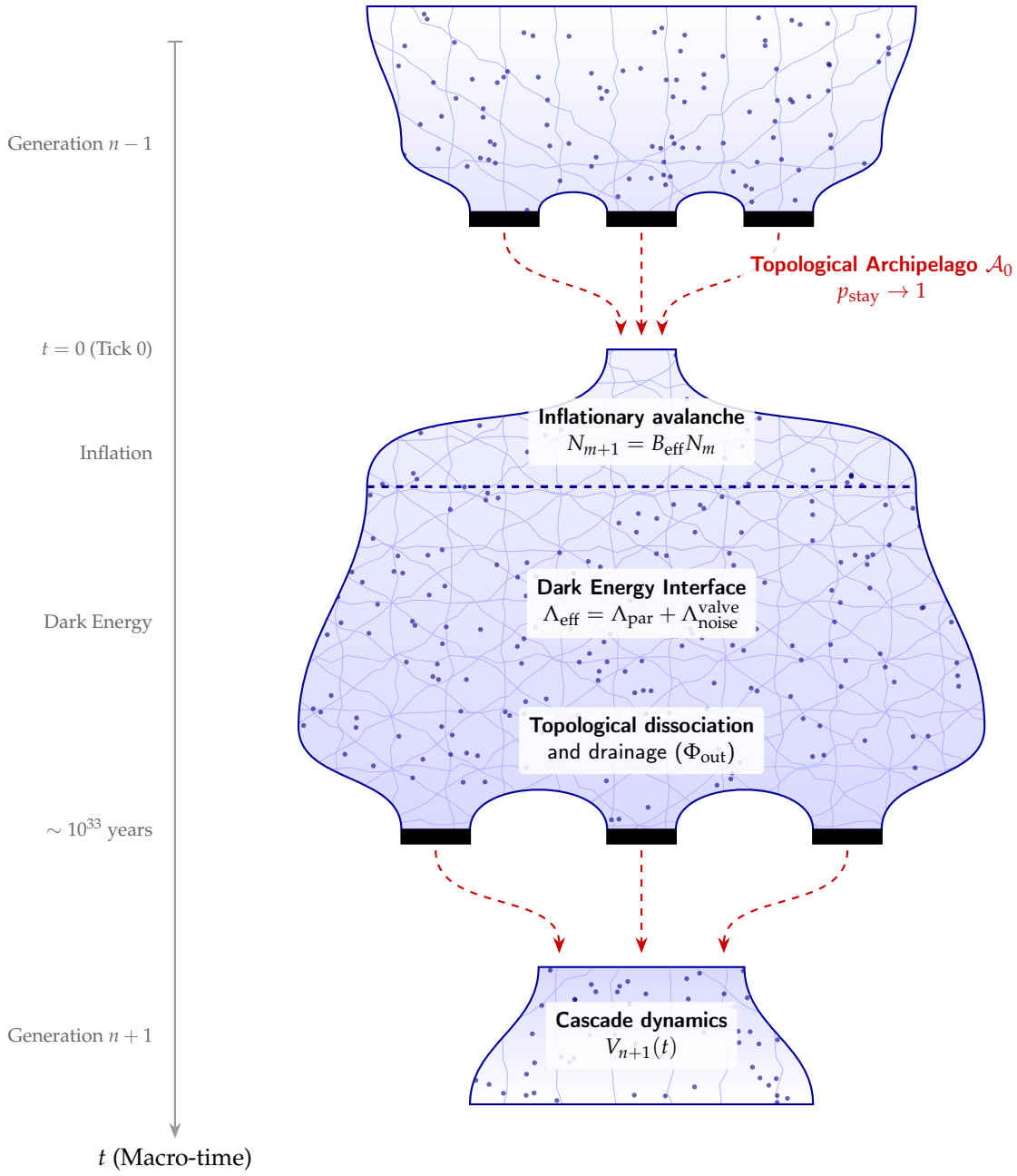

Figure 12. Cascade evolution of the Multiverse in IKT. The discrete nature of space is illustrated by the background edge network (base graph). (1) **Archipelago:** The daughter universe is initiated by a distributed phase flow through multiple SMBHs of the parent graph, united into a single equivalence class S_∞. (2) **Inflation:** Rapid binary growth of the address space of the supersaturated graph. (3) **Dark Energy:** Two-component expansion phase driven by quasi-stationary parent throughput (Λ_{par}) yielding $w \simeq -1$, and a small valve-limited residual insertion tail ($\Lambda_{\text{noise}}^{\text{valve}} \propto 1/t^2$ at late times). (4) **Drainage:** Upon reaching the limit of $\sim 10^{33}$ years, the macroscopic graph undergoes topological dissociation, draining the phase flow Φ_{out} into generation $n+1$.

7.1. Algorithmic Refraction and Reduction of G

In IKT, metric space is not curved (as in GR) and gravitons do not exist. Massive nodes create a local algorithmic delay χ_G, which reduces the graph's phase bandwidth. To an external observer, this appears as a slowing of local clocks ($d\tau = e^{-\chi_G} dt$) and an increase in phase impedance. The physical

© 2026 by the author(s). Distributed under a Creative Commons CC BY license.

Preprints.org (www.preprints.org) | NOT PEER-REVIEWED | Posted: 9 June 2026 doi:10.20944/preprints202606.0589.v1

mechanism of gravity as macroscopic algorithmic refraction (the slowing down of local clocks and the refraction of phase paths) is clearly demonstrated in Figure 13.

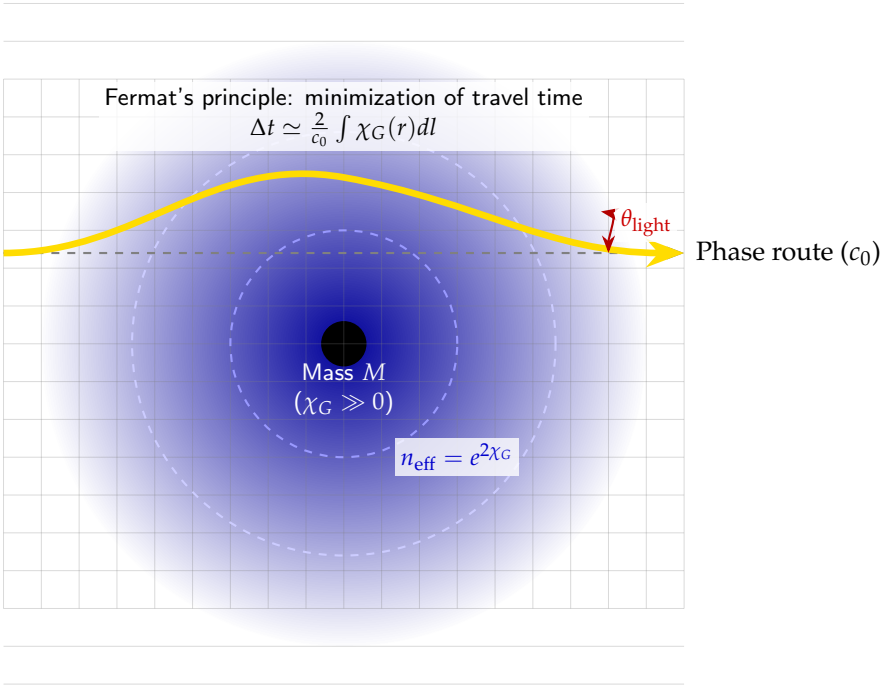

Figure 13. Gravity as macroscopic algorithmic refraction (weak-field PPN limit). In IKT, space is not a curved smooth manifold. A massive body (center) generates a distributed field of phase delay χ_G. This locally reduces the vacuum graph's throughput, which to an external observer is equivalent to an increase in the effective refractive index: $n_{\text{eff}}(\mathbf{r}) = e^{2\chi_G(\mathbf{r})}$. A coherent massless phase packet (light) bypasses the zone of high algorithmic cost, obeying the graph analogue of Fermat's principle. This opto-kinetic dynamics automatically reproduces gravitational lensing (θ_{light}) and Shapiro radar delay effects without invoking the metric tensor of General Relativity.

This opto-kinetic refraction is macroscopically projected as an effective PPN metric ($\beta = \gamma = 1$), reproducing the weak-field effects of General Relativity in a weak field (perihelion precession, Shapiro delay, and gravitational lensing):

$$ds^2 = -e^{-2\chi_G} c_0^2 dt^2 + e^{2\chi_G} d\mathbf{R}^2. \tag{17}$$

The Newtonian constant G in IKT loses its status as an independent axiom. It is reduced to the mass of the minimal electronic path M_{K_e} and its configurational sparsity $|\Omega_e|_{\text{eff}}$. Recalling the parametric rank of the electron ($n_e^{(0)} = 10$), we obtain a analytical relationship between gravity, electromagnetism ($\mathcal{N}_\alpha$), and topology:

$$G_{\text{IKT}} = \frac{\hbar c_0}{M_{K_e}^2 (\Gamma_e \mathcal{N}_\alpha^{10} \Xi_e)^2}, \tag{18}$$

where Γ_e is the Möbius-closure frame factor, and Ξ_e is the correlation factor (see Appendix B.4.3 for a rigorous derivation).

7.2. Two-Component Dark Energy

IKT rejects the concept of a vacuum continuum energy, which introduces an error of 120 orders of magnitude. The observed late acceleration is described by a two-component dark-energy source, $\Lambda_{\text{DE,time}}^{\text{IKT}} = \Lambda_{\text{par},time} + \Lambda_{\text{noise},time}^{\text{valve}}$, which is compared to the residual expansion term after subtracting matter, radiation, neutrinos, the vortex/dark-matter sector, curvature, and coarse-graining corrections from $3H^2$.

© 2026 by the author(s). Distributed under a Creative Commons CC BY license.

Preprints.org (www.preprints.org) | NOT PEER-REVIEWED | Posted: 9 June 2026 doi:10.20944/preprints202606.0589.v1

The main contribution Λ_{par} comes from the quasi-stationary parent phase influx, which ensures the observed equation of state $w \simeq -1$. The second component is the local valve-limited noise of residual insertion. Its early limit is physically constrained by the finite bandwidth of the parent valve Λ_{valve}, and in the late epoch it leaves only a small dynamic tail $\Lambda_{\text{noise}}^{\text{valve}} \propto t^{-2}$.

7.3. Dark Matter without WIMPs (Topological Vortex)

Excess gravitational attraction is explained without introducing hypothetical non-collisional particles. Dark matter is deconstructed into a macroscopic topological vortex χ_{vort}, which integrates into a single eikonal lensing potential:

$$\chi_{\text{lens}} = \chi_G + \chi_{\text{vort}}^{\text{prim}} + \chi_{\text{vort}}^{\text{gal}}. \tag{19}$$

The primary component ($\chi_{\text{vort}}^{\text{prim}}$) is responsible for the nearly cold (CDM) limit on the formation of acoustic peaks in the cosmic microwave background (CMB) and large-scale structure (LSS). In the galactic epoch, the rotation of the baryonic disk reorients the graph, forming a quasi-2D refractive waveguide ($\chi_{\text{vort}}^{\text{gal}}$). Asymptotic waveguide reduction predicts the formation of a flattened halo (whose height depends on the vertical phase leakage ϵ_z) and gives a testable explanation for the flat rotation curves of galaxies. The geometry of this macroscopic vortex waveguide, which forms a flattened dark matter halo, is shown in Figure 14. In the saturated limit, IKT mathematically derives the Tull-Fisher baryon ratio (BTFR):

$$v_f^4 = GM_{\text{bar}} a_{\text{vort}} \quad \text{(see (A52))}. \tag{20}$$

In this case, the waveguide acceleration scale a_{vort} is not adjusted manually, but is rigidly calibrated by the cosmological vacuum dephasing background H_{bg}:

$$a_{\text{vort}} = \frac{c_0 H_{\text{bg}}}{2\pi} \quad \text{(for geometric calibration, see (A55))}. \tag{21}$$

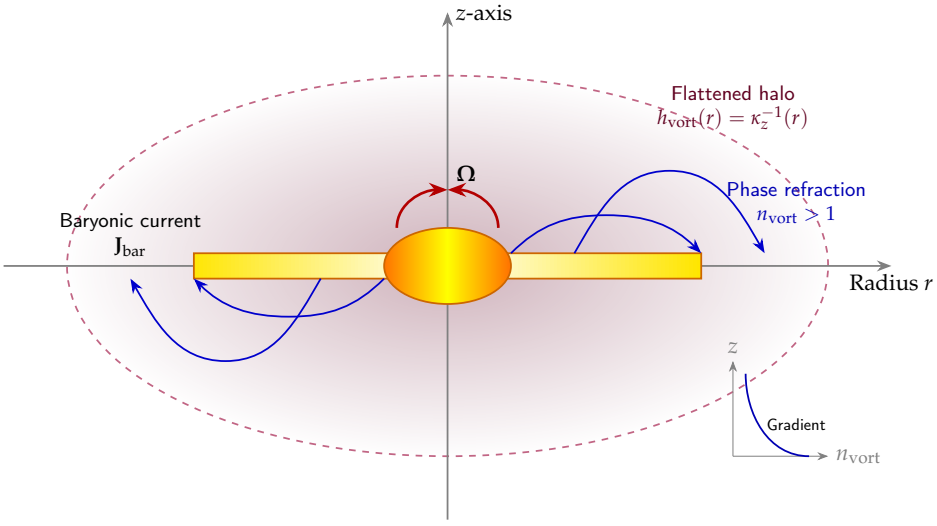

Figure 14. Formation of the galactic dark matter halo as a macroscopic vortex waveguide (cross-section). The rotating baryonic disk ($\mathbf{J}_{\text{bar}}$) generates a vorticity field $\boldsymbol{\Omega}$ and a gradient of the vortex refractive index n_{vort}. Phase trajectories (blue arrows) attempting to escape along the vertical z-axis undergo refraction and return to the equatorial plane. As a result of this quasi-2D reduction ($\epsilon_z \ll 1$), an evanescent flattened halo of algorithmic delay with a finite height $h_{\text{vort}}(r)$ is formed, rather than a spherical cloud of hypothetical particles.

In a high-energy cluster collision (e.g., the Bullet Cluster 1E 0657-56), the vortex phase soliton kinetically detaches from the decelerating X-ray gas. Since the topological vortex has no electric charge and experiences no electromagnetic drag, it continues to move by inertia. This fully explains the observed shift of gravitational lensing peaks without invoking hypothetical WIMP particles

© 2026 by the author(s). Distributed under a Creative Commons CC BY license.

Preprints.org (www.preprints.org) | NOT PEER-REVIEWED | Posted: 9 June 2026 doi:10.20944/preprints202606.0589.v1

(see Appendix E.3.5 for the analytical derivation of the soliton detachment). The kinematics of this separation of a phantom vortex soliton from the baryonic gas is illustrated in detail in Figure 15.

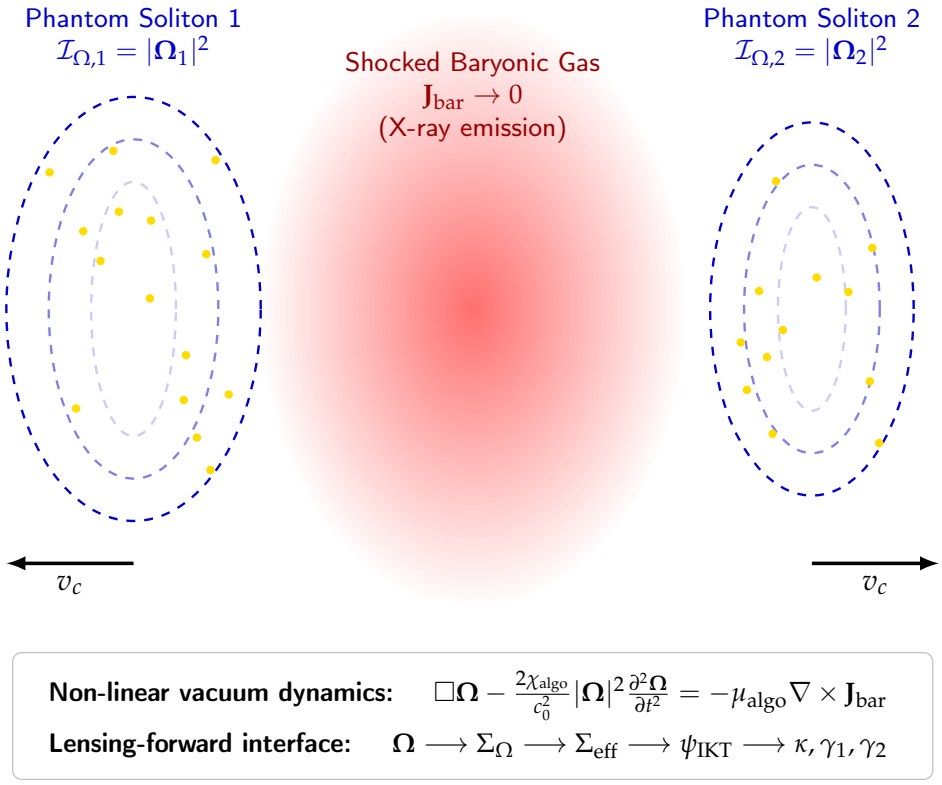

Figure 15. Kinematic detachment of the topological vortex in the IKT framework (Bullet Cluster phenomenon). During a high-energy collision of two galaxy clusters, the hot baryonic gas (red region) experiences electromagnetic friction and shock deceleration, causing the macroscopic baryonic current $\mathbf{J}_{\rm bar}$ to abruptly stall. However, the topological vorticity field $\mathbf{\Omega}$ of the graph connections lacks electric charge. Obeying the non-linear wave equation, the macroscopic vortices detach from the stalled gas and continue propagating by inertia as weakly dissipative phantom solitons (blue contours) with velocity v_c. Following the lensing-forward ansatz, the observable weak lensing maps (convergence κ and shear γ) are computed directly from the invariant amplitude $\mathcal{I}_\Omega = |\mathbf{\Omega}|^2$. This gives a testable account of the observed displacement between X-ray emission and gravitational lensing centers without introducing fundamental collisionless dark-matter particles.

7.4. Neutrinos and the Information Balance of Black Holes

Dark-energy scale of neutrinos: A neutrino is modeled as a 1D packet of graph phase error corrections. Lacking its own $3D$ volume, such a packet acquires mass as a birth-imprint of the graph generation density at the moment of birth. The minimum self-consistent scale is given by the quarter-root projection

$$m_{\nu,i}^{\rm birth}(t_b)c_0^2 = \beta_i\left[\rho_{\rm gen}(t_b)(\hbar c_0)^3\right]^{1/4}, \qquad \rho_{\rm gen} = \rho_{\rm par} + \rho_{\rm noise}^{\rm valve}.$$

For the current dark energy density

$$E_{\Lambda,0} = [\rho_{\Lambda,0}(\hbar c_0)^3]^{1/4} \simeq 2.3\,{\rm meV},$$

which naturally falls within the neutrino range; generation differences are encoded by moderate flavor/topology factors β_i.

Black-hole information balance: The black-hole boundary is formalized as a finite graph-accessibility neck with small Cheeger connectivity. In the B3 branch, topological dissociation of the neck is modeled as unitary unwinding of correlated 1D routes. The combinatorics of this process

© 2026 by the author(s). Distributed under a Creative Commons CC BY license.

Preprints.org (www.preprints.org) | NOT PEER-REVIEWED | Posted: 9 June 2026 doi:10.20944/preprints202606.0589.v1

provides a discrete explanation of the scaling $S \propto A_{\text{gate}}$ and a Page-curve-compatible toy model (see Appendix E.4.3) for preserving correlations in the full graph algebra without postulating "firewalls".

(Solutions to graph equations for dark energy, vortex halos, and black hole thermodynamics are detailed in Appendices E.1–E.4 Methods).

8. Decoherence and the Macroscopic Limit

8.1. Objective Collapse of Macro-Superpositions

The resolution of the "Schrödinger-cat" paradox and the emergence of a local arrow of time in IKT follow from the objective loss of information (partial trace) during the insertion growth of the network. When attempting to create a spatial superposition of a macroscopic object, the graph forms 1D bridges between distant branches.

*(A numerical derivation of the rate of objective collapse from the CP insertion channel is given in Appendix **??** Methods).*

8.2. Hard Coherence Filter

The lifetime of such bridge coherence is strictly suppressed by the square of the energy (gravitational) conflict of mass distributions (ΔE_G). The damping exponent and the lifetime must be kept distinct:

$$\Gamma_{\text{IKT}} t = \frac{1}{2|\Omega_e|_{\text{eff}}} (\Delta\varepsilon_G)^2 \tilde{t}, \qquad \Gamma_{\text{IKT}} \propto M^4, \qquad t_{\text{IKT}} = \Gamma_{\text{IKT}}^{-1} \propto M^{-4} \quad \text{(one-scale fixed-geometry limit; see Appendix ??).} \tag{22}$$

For a single electron, the microscopic bridge is stable (its lifetime exceeds 10^{90} years). However, for a kilogram-mass macro-object, the lifetime filter $t_{\text{IKT}} \propto M^{-4}$ causes coherence to irreversibly collapse within microseconds ($\sim 10^{-6}$ s). This provides an objective, physically grounded collapse of the wave function without any mystical appeal to the "observer's consciousness."

9. Conclusions, Predictions, and Research Directions

The Information-Kinetic Theory (IKT) formulates a background-independent graph-topological program in which the metric, wave sector, masses, interactions, and cosmological dynamics are not postulated as independent entities, but are reduced to structural properties of a single process — the routing of the complex phase on a discrete stochastic graph. Below, the main results are grouped by level: established graph kernel constructions, phenomenological interfaces, testable predictions, and open computational problems.

9.1. Main Results of Theoretical Synthesis

1. **Graph kernel and prethermal vacuum.** The fundamental microdynamics is defined on the space of oriented edges $\mathcal{H}_m^{\text{edge}}$. The smooth wave envelope (Weyl/wave envelope) arises not from arbitrary averaging, but as a consequence of the nearly unitary prethermal Floquet branch of the stochastic graph vacuum.
2. **A bypass of the Nielsen–Ninomiya theorem.** The problem of chiral fermions on a lattice is solved via a dynamic protection mechanism. Irreversible graph surgery acts selectively:

$$\gamma_{\text{surg}}(e) = \gamma_0 \Pi_{\text{UV}}(e) e^{-\theta_e},$$

where Π_{UV} isolates unbound short-wavelength or incoherent components. Therefore, surgery suppresses UV-doublerr-like sectors but does not destroy the prethermal IR branch and stable topological routes. UV-doublerr-like sectors do not become observable asymptotic states. In spectral terms, they go not into the peripheral but into the non-peripheral decaying sector of the reduced prethermal/annealed superoperator:

$$|\lambda_{\text{UV}}| \le e^{-\gamma_{\text{UV}} \Delta t}, \qquad \gamma_{\text{UV}} > 0.$$

© 2026 by the author(s). Distributed under a Creative Commons CC BY license.

Preprints.org (www.preprints.org) | NOT PEER-REVIEWED | Posted: 9 June 2026 doi:10.20944/preprints202606.0589.v1

The physical infrared Weyl/Dirac branch, on the other hand, corresponds to an almost unitary peripheral spectrum:

$$|\lambda_{\mathrm{IR}}(k)| \simeq 1, \qquad ka_0 \ll 1.$$

Thus, the absence of independent light doublers is formulated not as an automatic consequence of the stochasticity of the graph, but as a spectral condition: the IR branch remains peripheral and coherent, while UV-doublerr-like modes decay rapidly.

3. **Topological mass and scalar response.** The rest mass of particles is decomposed into the integral phase cost (monodromic gap Θ_K) of maintaining a closed path. The observed 125 GeV resonance is interpreted not as an excitation of the fundamental scalar field, but as an elastic longitudinal mode of the graph phase capacitance, which naturally explains the mass-proportional response amplitudes ($g_{hKK} \propto M_K$).
4. **Interaction interfaces and TTC.** Electromagnetism, confinement, weak P-parity violation, and gravity are constructed as different macroscopic interfaces (modes) of a single graph routing. The Topological Transition Calculus (TTC) replaces continuous Feynman diagrams with discrete sums over graph cobordisms. Continuous UV integrals are replaced by finite TTC graph sums, while running and polarization corrections become graph-computational matching problems.
5. **Channel and spectral anchors.** The theory analytically derives the basic dimensionless relations: the topological anchor of the fine structure $\alpha_{\mathrm{top}}^{-1} = 4\pi^3 + \pi^2 + \pi$, the proton confinement anchor $m_p/m_e \simeq 6\pi^5$, the neutron charge compactification work $\Delta m \simeq m_e \ln(4\pi)$ and the reduction of the gravitational constant to the effective configuration volume of the electron $G_{\mathrm{IKT}} \propto |\Omega_e|_{\mathrm{eff}}^{-2}$.
6. **Deconstruction of the Dark Sector.** Dark matter is formalized as a macroscopic topological vortex, whose asymptotic 2D waveguide reduction naturally generates flat rotation curves and flattened halos. Dark energy is described as a two-component interface: a quasi-stationary parent throughput background gives rise to late acceleration ($w \simeq -1$), while the valve-limited tail of residual insertion ($\Lambda_{\mathrm{noise}}^{\mathrm{valve}} \propto t^{-2}$ in the late epoch) provides a finite early noise plateau through Λ_{valve}.
7. **Black-hole information balance.** Black holes in IKT are graph bottlenecks with a small Cheeger parameter. Topological dissociation of the graph neck is modeled as unitary unwinding of correlated 1D routes. In the B3 branch this provides the scalings $S \propto A_{\mathrm{gate}}$ and $T \propto 1/M$ via finite edge combinatorics, while the exact coefficients remain a TTC neck-spectrum problem. The Page-curve-compatible toy model preserves information balance in the reduced algebra of observables without introducing "firewalls".

9.2. Testable Predictions of IKT

IKT is a falsifiable theory that offers a number of testable distinctions from the standard continuous paradigm:

- **Kinematics and coherence:** DSR kinematics predicts a statistically isotropic velocity decay of rigid gamma quanta ($\omega^2 = c_0^2k^2 - c_0^2a_0^2A_4k^4 + \cdots$). Macroscopic quantum superpositions undergo objective graph decoherence with a rigid scale filter ($t_{\mathrm{decoh}} \propto M^{-4}$).
- **Fermion spectrum:** The topological hierarchy of routes constrains the number of stable generations; a stable fourth generation of leptons and quarks (for $C_K \geq 5$) must be absent due to local routing saturation.
- **Neutrino sector:** IKT predicts cosmological memory of neutrino birth masses as birth-imprints of the graph-generation density:

$$m_{\nu,i}^{\mathrm{birth}}(t_b)c_0^2 = \beta_i \left[\rho_{\mathrm{gen}}(t_b)(\hbar c_0)^3\right]^{1/4}.$$

After birth, this imprint is practically preserved,

$$m_{\nu,i}^{\mathrm{eff}}(t_{\mathrm{obs}}; t_b) \simeq m_{\nu,i}^{\mathrm{birth}}(t_b),$$

© 2026 by the author(s). Distributed under a Creative Commons CC BY license.

Preprints.org (www.preprints.org) | NOT PEER-REVIEWED | Posted: 9 June 2026 doi:10.20944/preprints202606.0589.v1

therefore, relic $C\nu B$ neutrinos may have an effective propagation mass different from that of modern solar or laboratory neutrinos:

$$\frac{m_{\nu,i}^{C\nu B}}{m_{\nu,i}^{\mathrm{now}}} = \left[\frac{\rho_{\mathrm{gen}}(t_{\mathrm{dec}})}{\rho_{\mathrm{gen}}(t_0)}\right]^{1/4}.$$

- **Astrophysics of halos and black holes:** The morphology of the dark halo of galaxies must be flattened and correlated with the macroscopic vorticity field of the baryonic disk. The mass function of supermassive black holes (quasars) must have a statistical upper cutoff ($M_{\mathrm{crit}} \sim 10^{12} M_{\odot}$), associated with the loss of topological coherence of the accretion vortex.
- **Ultra-high-energy astrophysics:** The detection of ultra-high-energy neutrinos (of the order of hundreds of PeV) [30] from active black holes is interpreted in IKT not as a result of classical shock acceleration, but as a product of the topological unwinding of complex matter in the graph-accessibility B3 neck ($p_{\mathrm{stay}} \to 1$). Such ultra-stiff 1D correction packets are ideal candidates for testing the DSR vacuum dispersion: IKT predicts an accumulated time delay in their arrival compared to low-energy photons, proportional to $(E/E_{\mathrm{Pl}})^2$ in the leading DSR term, which opens the way to a direct measurement of the graph's discrete step a_0.

9.3. Directions for Further Research

This work establishes the boundary between the already established topological framework and the IKT computational program. Unresolved problems requiring a mathematically rigorous calculation from the microdynamics U_m include:

1. deriving spectral equipartition $\rho_s = 1$ for exact confirmation of α_{top};
2. calculation of the monodromic mass M_{K_e}, the frame factor Γ_e, and the correlation factor Ξ_e to complete the first-principles prediction of the gravitational constant G;
3. proof of the automorphism theorem $SU(3)_{\mathrm{route}}$ and derivation of the graph β-function of the strong interaction;
4. construction of the 1D/3D projection operator and weak/flavor factors β_i for the exact derivation of the neutrino birth-imprint formula

$$m_{\nu,i}^{\mathrm{birth}} c_0^2 = \beta_i [\rho_{\mathrm{gen}} (\hbar c_0)^3]^{1/4};$$

5. derivation of the PMNS and CKM mixing matrices as matrix elements of the weak-gateway surgery;
6. a full joint CMB/LSS/BAO/SN fit of two-component dark energy and the primary vortex dark sector.

IKT can be refuted by the failure of the channel anchor α_{top} when polarizations are accurately accounted for, by an incorrect sign of the DSR correction, by the detection of spherically symmetric non-rotating dark halos, the absence of the predicted bridge-lifetime scaling $t_{\mathrm{decoh}} \propto M^{-4}$, equivalently the rate scaling $\Gamma_{\mathrm{IKT}} \propto M^4$, or the impossibility of obtaining the spectral gap $\mathcal{E}_{\mathrm{ann}}$ to circumvent the Nielsen–Ninomiya theorem. Thus, IKT opens a new, mathematically rigorous, and testable path to the unification of fundamental physics outside the continuum paradigm.

Appendix A. Axiomatics, Vacuum, and Topological Defects

Appendix A.1. Mathematical Foundation and Axioms of IKT

Appendix A.1.1. Basic Graph and Hilbert Space Hierarchy

To avoid ambiguity, working definitions are established below. The fundamental edge space of microdynamics, the nodal infrared envelope, and the effective space of a closed route differ fundamentally.

© 2026 by the author(s). Distributed under a Creative Commons CC BY license.

Preprints.org (www.preprints.org) | NOT PEER-REVIEWED | Posted: 9 June 2026 doi:10.20944/preprints202606.0589.v1

Definition A1 (Basic graph). *The fundamental object of IKT at update step m is a directed graph*

$$G_m = (V_m, E_m, A_m),$$

where V_m is the set of topological dipoles, E_m is the set of directed edges, and A_m is the adjacency matrix. The indices $i, j \in V_m$ are not spatial coordinates; they denote only elements of discrete connectivity.

Definition A2 (Effective embedding). *The coordinates $\mathbf{r}_i$, the distance $|\mathbf{r}_i - \mathbf{r}_j|$, the integrals $d^3\mathbf{r}$, and the Laplacian ∇^2 are used only after the coarse-graining transition*

$$\iota_m : V_m \longrightarrow M_{\text{eff}},$$

when the large subgraph admits a stable spectral or thermodynamic embedding into the effective manifold M_{eff}.

Definition A3 (Fundamental edge space). *For a fixed causal graph*

$$G_m = (V_m, E_m)$$

the fundamental kinematic space of the minimal micro-operator is defined on the oriented edges:

$$\boxed{\mathcal{H}_m^{\text{edge}} = \ell^2(\vec{E}_m) \otimes \mathbb{C}^2_{\text{spin}}}.$$

Here, $\vec{E}_m$ is the set of oriented edges, and $\mathbb{C}^2_{\text{spin}}$ is the minimal complex representation of Cl_3 required for an isotropic first-order Weyl-like operator.

The fundamental local routing operator

$$U_m^{(0)} = S_m C_m$$

is unitary precisely on $\mathcal{H}_m^{\text{edge}}$:

$$(U_m^{(0)})^\dagger U_m^{(0)} = I_{\mathcal{H}_m^{\text{edge}}}.$$

Definition A4 (Vertex Envelope). *The space*

$$\boxed{\mathcal{H}_m^{\text{vert}} = \ell^2(V_m) \otimes \mathbb{C}^2_{\text{env}}}$$

is not a fundamental space of microdynamics. It arises as a coarse-grained vertex envelope after summing or tracing the half-edge degrees of freedom.

Schematically, the mapping from the fundamental edge space to the vertex envelope is given by

$$\mathcal{P}_{\text{vert}} : \mathcal{H}_m^{\text{edge}} \longrightarrow \mathcal{H}_m^{\text{vert}},$$

$$\psi_i^{\text{vert}} = \sum_{j \sim i} w_{ij}^{1/2}\, \Gamma_{ji}\, \psi_{j\to i}^{\text{edge}},$$

where Γ_{ji} maps the spinor from the coordinate system of the adjacent edge to the local coordinate system of vertex i, and w_{ij} are the coarse-graining weights.

Therefore, any expression of the form

$$\ell^2(V_m) \otimes \mathbb{C}^2$$

should be understood as a description of the infrared envelope, rather than as the fundamental domain of action of U_m.

© 2026 by the author(s). Distributed under a Creative Commons CC BY license.

Preprints.org (www.preprints.org) | NOT PEER-REVIEWED | Posted: 9 June 2026 doi:10.20944/preprints202606.0589.v1

Definition A5 (Effective Hilbert Space of a Closed Route)**.** *For a stable closed topological route K, we introduce a spectral-topological projector*

$$P_K : \mathcal{H}_m^{\text{edge}} \longrightarrow \mathcal{H}_K^{\text{eff}}.$$

The effective low-energy space of the massive Dirac-envelope particle takes the form

$$\boxed{\mathcal{H}_K^{\text{eff}} \simeq \mathcal{H}_K^{\text{chir}} \otimes \mathbb{C}^2_{\text{spin}}}$$

with

$$\mathcal{H}_K^{\text{chir}} = \text{span}\{|L_K\rangle, |R_K\rangle\}.$$

At this level, an effective bispinor arises

$$\Psi_K = \begin{pmatrix} \psi_L \\ \psi_R \end{pmatrix} \in \mathbb{C}^4,$$

and only after the Floquet/homogenization projection does the local Dirac-envelope operator appear.

Postulate A1 (Notation convention for $\mathcal{H}_m$)**.** *If the symbol $\mathcal{H}_m$ is used without an additional index in a microdynamic context, the fundamental edge space is meant by default*

$$\mathcal{H}_m \equiv \mathcal{H}_m^{\text{edge}}.$$

If we are referring to the continuous Weyl/wave limit, one should use the notation $\mathcal{H}_m^{\text{vert}}$ or explicitly refer to the vertex-envelope. If we are referring to a particle as a stable closed route, one should use $\mathcal{H}_K^{\text{eff}}$.

Lemma A1 (Consistency of the Three Levels of Description)**.** *In IKT, the following hierarchy holds:*

$$\mathcal{H}_m^{\text{edge}} \xrightarrow{\mathcal{P}_{\text{vert}}} \mathcal{H}_m^{\text{vert}} \xrightarrow{P_K} \mathcal{H}_K^{\text{eff}}.$$

Fundamental unitarity applies to the operator $U_m^{(0)}$ on $\mathcal{H}_m^{\text{edge}}$. The Weyl equations and the wave limit refer to the coherent infrared envelope in $\mathcal{H}_m^{\text{vert}}$. The Dirac equation refers to the Floquet/homogenized sector $\mathcal{H}_K^{\text{eff}}$ of the closed path K.

Consequently, the notation $\ell^2(V_m) \otimes \mathbb{C}^2$ should not be used as the fundamental space of U_m; it is only an infrared vertex-envelope description.

Appendix A.1.2. Fundamental Postulates

The minimal version of IKT uses four postulates. They are formulated so as not to introduce either global time or background Euclidean geometry in advance.

Postulate A2 (Background Independence)**.** *The fundamental graph G_m is not embedded in a predefined space. Its adjacency matrix defines only the reachability relation between topological dipoles. Effective coordinates, dimension, and metric arise only after thermodynamic averaging over a large number of nodes.*

Postulate A3 (Local Causal Kinematics)**.** *State updates are local: the amplitude at node i in the next causal layer depends only on the finite neighborhood of the node in the graph metric $d_G(i, j)$. The fundamental form of the postulate is dimensionless:*

$$c_{\text{graph}} = 1,$$

that is, over one causal layer, the state cannot traverse more than one local edge. After effective embedding, one must distinguish between the bare-step graph adjacency a_0 and the metric UF-step l_0.

© 2026 by the author(s). Distributed under a Creative Commons CC BY license.

Preprints.org (www.preprints.org) | NOT PEER-REVIEWED | Posted: 9 June 2026 doi:10.20944/preprints202606.0589.v1

The bare-rate of local adjacency is equal to

$$c_* = \frac{a_0}{\tau_0}.$$

This quantity is not the directly observable propagation speed of a physical signal: a coherent massless mode must maintain a transverse frame and propagates through the channels of a 3D network. The observed speed of light is given by the wave branch:

$$c_0 = \sqrt{\lambda_{\mathrm{wave}}}\,\frac{a_0}{\tau_0}, \qquad l_0 \equiv c_0\tau_0 = \sqrt{\lambda_{\mathrm{wave}}}\,a_0.$$

In electron units, the metric scales take the form

$$l_0 = \epsilon_0\frac{\hbar}{m_e c_0}, \qquad \tau_0 = \epsilon_0\frac{\hbar}{m_e c_0^2}, \qquad a_0 = \frac{l_0}{\sqrt{\lambda_{\mathrm{wave}}}}.$$

Thus, a_0/τ_0 is the hardware adjacency rate of the graph, and c_0 is the physical speed of the coherent massless branch.

Postulate A4 (Quantum Translation)**.** *On a fixed graph, the microscopic evolution of the phase state is given by a unitary quantum walk operator. Classical transition probabilities appear only after taking the squares of the moduli and performing coarse-graining averaging.*

Postulate A5 (Graph Growth)**.** *The graph allows local operations of inserting new vacuum dipoles. Deletion is not introduced as a fundamental inverse operation: its implementation would require global memory of how to reconnect the removed links. Therefore, irreversibility applies not to the unitary translation on a fixed graph, but to the growth of the state space itself.*

Appendix A.1.3. Dimensionless Metrization and Scale Calibration

Definition A6 (Dimensionless Metrization of a Graph)**.** *Until an effective embedding is introduced, a graph does not carry meters, seconds, or kilograms. A convenient natural normalization is given by three dimensionless conditions*

$$c_{\mathrm{graph}} = 1, \qquad \hbar_{\mathrm{graph}} = 1, \qquad m_e^{\mathrm{graph}} = 1.$$

Dimensional physics arises when these three units are projected onto laboratory standards:

$$c_{\mathrm{graph}} = 1 \mapsto c_0, \qquad \hbar_{\mathrm{graph}} = 1 \mapsto \hbar, \qquad m_e^{\mathrm{graph}} = 1 \mapsto m_e.$$

All predictive statements of IKT must be formulated as dimensionless relations; l_0, τ_0, G, and other dimensional quantities are the results of metricization or dimensional projection conditions.

Matching of Metric Scales c_0, a_0, τ_0, and λ_{Wave}

In the stochastic Weyl limit, the speed of the coherent branch is determined by the second moment of the edge distribution:

$$c_0^{\mathrm{Weyl}} = \frac{a_0\kappa_2}{\Delta t}.$$

In the reversible wave sector, the same observed velocity is written as

$$c_0^{\mathrm{wave}} = \sqrt{\lambda_{\mathrm{wave}}}\,\frac{a_0}{\tau_0}.$$

Physical consistency requires that these two velocities be identified:

$$\boxed{\frac{\kappa_2}{\Delta t} = \frac{\sqrt{\lambda_{\mathrm{wave}}}}{\tau_0}} \qquad \Longleftrightarrow \qquad \lambda_{\mathrm{wave}} = \kappa_2^2\left(\frac{\tau_0}{\Delta t}\right)^2.$$

© 2026 by the author(s). Distributed under a Creative Commons CC BY license.

Preprints.org (www.preprints.org) | NOT PEER-REVIEWED | Posted: 9 June 2026 doi:10.20944/preprints202606.0589.v1

Therefore, a_0, τ_0, Δt, and λ_{wave} are not independent physical constants. The independent observable is the speed of the coherent massless branch c_0, while the remaining parameters determine the choice of discrete metric calibration.

It is precisely l_0, and not the bare step a_0, that enters the electronic metric $l_0 = \epsilon_0 \lambda_e$ and the weak-field macroscopic metrics. Under these conditions, the standard massless wave equation takes the form

$$\left(\nabla^2 - \frac{1}{c_0^2}\partial_t^2\right)\Psi = 0.$$

Appendix A.1.4. Notation Conventions

Definition A7 (Gravitational and Vortical Potentials)**.** *The weak-field gravitational response is denoted by a separate quantity χ_G, and the macroscopic galactic vortex delay by χ_{vort}. They are not self-loop probabilities and therefore need not lie in the interval $[0,1]$. The convention*

$$\Phi_N = -\frac{GM}{r}, \qquad \chi_G = -\frac{\Phi_N}{c_0^2} > 0.$$

Therefore, the observed Newtonian acceleration is written as

$$\mathbf{g} = c_0^2 \nabla(\chi_G + \chi_{\text{vort}}).$$

For an isolated mass, this gives $\mathbf{g} = -GM\hat{\mathbf{r}}/r^2$.

To avoid symbol overload, the following conventions are used hereafter. C_m denotes the local quantum walk coin, $\mathcal{C}_{ij}$ denotes the color-routing transporter, $\mathfrak{C}_\alpha$ denotes the stratified space of electromagnetic phase channels, and $\mathcal{C}_2(K)$ denotes the configuration space of two identical routes. Similarly, χ_G denotes the gravitational delay, χ_{vort} denotes the vortex delay, and χ_{lens} denotes the total delay entering the lensing interface.

- **Emergence:** the emergence of macroscopic fields, dimensions, and metrics as stable statistical envelopes of discrete graph kinetics.
- **Topological dipole:** the minimal quantum of connectivity, characterized by the orientation of state transfer and internal chirality.
- **Phase translation:** a local unitary or isometric update of the complex phase state on a graph.
- **Insertion:** a graph extension operation $G_m \mapsto G_{m+1}$, described by an isometry or a quantum channel, rather than a unitary operator within a fixed-dimensional space.
- **Status of statements:** hereinafter, formulas not derived from the initial definitions are explicitly marked as postulates or hypotheses. This separates the mathematical core of the model from the testable topological assumptions.

Appendix A.2. Vacuum Kinematics: Prethermal Phase and Wave Emergence

In this section, the free stochastic sector of the IKT micro-operator is fixed. Unlike regular lattice models, the fundamental graph of the IKT is not a $\mathbb{Z}^3$-type crystal lattice. It is a dynamic, locally finite, stochastic graph whose macroscopic geometry emerges only after coarse-graining. The purpose of this section is to show that ballistic wave kinematics, spinor structure, the isotropic continuum limit, and the free transverse $U(1)$ sector can be understood as infrared properties of prethermal stochastic routing, rather than as a consequence of a pre-specified rigid background.

Appendix A.2.1. Stochastic Graph and Conditions for Emergent Three-Dimensionality

The IKT vacuum graph has no global x, y, z axes and does not possess exact translational invariance on the microscopic scale. It belongs to the stochastic vacuum ensemble $\mathfrak{G}_{\text{vac}}$, which satisfies local finiteness and macroscopic three-dimensionality. The average connectivity may be of the order $\langle k \rangle \simeq 6$,

© 2026 by the author(s). Distributed under a Creative Commons CC BY license.

Preprints.org (www.preprints.org) | NOT PEER-REVIEWED | Posted: 9 June 2026 doi:10.20944/preprints202606.0589.v1

but by itself does not define a three-dimensional continuum. Therefore, additional conditions on the volumetric and spectral dimensions are required

$$\langle |B_R(i)| \rangle_{\mathfrak{G}} \sim R^3, \qquad d_H = 3,$$

and

$$P_{\mathrm{ret}}(s) \sim s^{-d_s/2}, \qquad d_s = 3.$$

Here, $B_R(i)$ denotes a ball of radius R in the graph metric, and $P_{\mathrm{ret}}(s)$ denotes the probability of return of the graph thermal kernel after s steps.

For each vertex i, a local orthonormal basis is introduced. It is not an embedding of the graph into a predefined Euclidean space. It is an internal graph frame, reconstructed from the spectral geometry of the local neighborhood. Operationally, it can be defined as a three-dimensional low-frequency subspace of the graph Laplacian on the sphere $B_R(i)$:

$$\mathcal{F}_i = \mathrm{span}\{\varphi_i^1, \varphi_i^2, \varphi_i^3\} \subset \mathrm{Eig}_{\mathrm{low}}\Big(L_{B_R(i)}\Big),$$

where $\varphi_i^a : B_R(i) \to \mathbb{R}$ are three stable low-lying modes of the local graph Laplacian, chosen after removing the constant mode and orthonormalized with respect to the local measure π_i:

$$\sum_{v \in B_R(i)} \pi_i(v)\, \varphi_i^a(v) \varphi_i^b(v) = \delta^{ab}.$$

A directed edge $i \to j$ obtains its internal spectral coordinates as the difference between the values of these modes:

$$\tilde{n}_{ij}^a = \varphi_i^a(j) - \varphi_i^a(i), \qquad a = 1, 2, 3.$$

If $\tilde{n}_{ij} \neq 0$, the normalized direction is defined as

$$\boxed{\hat{n}_{ij}^a = \frac{\tilde{n}_{ij}^a}{\left(\sum_{b=1}^3 (\tilde{n}_{ij}^b)^2\right)^{1/2}}}.$$

In the degenerate case, when local low modes do not distinguish between edges at a chosen radius R, the coarse-graining radius is increased to the first stable value $R' = R + \Delta R$ for which $\tilde{n}_{ij} \neq 0$ and the orientation becomes stable. Thus, $\hat{n}_{ij}$ is a graph-internal quantity defined in terms of the spectral coordinates of the graph itself, rather than a hidden embedding vector or a relic of the etheric medium.

For normalized routing weights

$$w_{ij} \geq 0, \qquad \sum_{j \sim i} w_{ij} = 1,$$

statistical isotropy is given by the conditions

$$\left\langle \sum_{j \sim i} w_{ij} \hat{n}_{ij}^a \right\rangle_{\mathfrak{G}} = 0, \qquad \left\langle \sum_{j \sim i} w_{ij} \hat{n}_{ij}^a \hat{n}_{ij}^b \right\rangle_{\mathfrak{G}} = \kappa_2 \delta^{ab}.$$

For an ideally isotropic ensemble, $\kappa_2 = 1/3$. To restore the isotropy of the first dispersion corrections, isotropy of the fourth moment is also required:

$$\left\langle \sum_{j \sim i} w_{ij} \hat{n}_{ij}^a \hat{n}_{ij}^b \hat{n}_{ij}^c \hat{n}_{ij}^d \right\rangle_{\mathfrak{G}} = \kappa_4 (\delta^{ab}\delta^{cd} + \delta^{ac}\delta^{bd} + \delta^{ad}\delta^{bc}),$$

© 2026 by the author(s). Distributed under a Creative Commons CC BY license.

Preprints.org (www.preprints.org) | NOT PEER-REVIEWED | Posted: 9 June 2026 doi:10.20944/preprints202606.0589.v1

where, for an ideally isotropic ensemble, $\kappa_4 = 1/15$. Thus, the cubic invariant $\sum_a k_a^4$ is not a fundamental object of IKT; it arises only in an artificial regular map and is replaced by the isotropic k^4-term after ensemble coarse-graining.

Hypothesis A1 (Marginal topological rigidity and external baryon routing capacity)**.** *In the random graph paradigm, the effective spectral dimension $D_{\text{eff}} = 3$ does not impose a strict kinematic constraint on the degree of an individual node, as is the case in a cubic lattice, where $k \equiv 2D = 6$. However, the formation of a stable macroscopic vacuum requires a condition of marginal topological rigidity, which is the graph-theoretic analogue of Maxwell's criterion for isostatic networks.*

If the average external connectivity of the vacuum ensemble $\langle k \rangle$ is less than the critical value, the stochastic 3D network is locally soft and unable to stably support spinor frames and closed routes. If $\langle k \rangle$ is significantly greater than the critical value, the network becomes overstressed; the excess of constraints triggers local insertions, connectivity rearrangement, and, in the cosmological regime, algorithmic expansion.

Consequently, the stable IKT IR vacuum self-organizes to a critical point of marginal stiffness

$$k_{\text{ext}} \equiv \langle k \rangle_c = 2D_{\text{eff}} = 6.$$

This number is not the number of Cartesian axes and does not correspond to the fundamental lattice $\mathbb{Z}^3$. It defines the average external algorithmic capacity of the interaction between the internal topological core and the marginally rigid stochastic vacuum.

In particular, leading-order baryon routing uses $k_{\text{ext}} = 6$ as the number of external isostatic channels connecting the internal confinement capacity C_p to the background vacuum. Therefore, the appearance of the factor 6 in baryonic and leptonic leading anchors should be interpreted as a consequence of the marginal rigidity of the stochastic network, rather than as a consequence of a cubic coordinate structure. From a mathematical point of view, this statement is not a proven theorem, but rather the goal of a future constraint-counting derivation: it must be shown that the local stability of spectral frames, the minimality of routing constraints, and the absence of floppy modes indeed lead to the criterion $\langle k \rangle_c = 2D_{\text{eff}}$. Until such a conclusion is reached, $k_{\text{ext}} = 6$ has the status of a marginal stiffness hypothesis, rather than a relic of a cubic lattice.

Appendix A.2.2. Unitary Operator on Edges and Edge Transporter

The fundamental IKT operator is not a non-unitary sum over neighbors. Unitarity is defined on the space of directed edges:

$$\mathcal{H}_m = \ell^2(\vec{E}_m) \otimes \mathbb{C}^2_{\text{spin}},$$

where $\vec{E}_m$ is the set of oriented edges of the graph. The minimal massless routing operator is defined as

$$U_m^{(0)} = S_m C_m.$$

Here $C_m = \bigoplus_{i \in V_m} C_i$ is a local unitary coin that redistributes the amplitude among the half-edge degrees of freedom of node i, and S_m is a flip-flop shift along the oriented edges. If the edge $i \to j$ transfers a spinor from the basis i to the basis j, then

$$S_m : |i \to j\rangle \otimes \psi_i \longmapsto |j \to i\rangle \otimes \mathcal{U}_{ij}\psi_i.$$

The unitarity of S_m is ensured by the condition $\mathcal{U}_{ji} = \mathcal{U}_{ij}^\dagger$. Since C_m and S_m are unitary, $U_m^{(0)}$ is unitary.

On each oriented edge, a minimal transporter is introduced

$$\mathcal{U}_{ij} = L_{ij}\Gamma_{ij}R_{ij}.$$

Here

$$L_{ij} = e^{-i\phi_{ij}} \in U(1), \qquad \Gamma_{ij} \in SU(2),$$

© 2026 by the author(s). Distributed under a Creative Commons CC BY license.

Preprints.org (www.preprints.org) | NOT PEER-REVIEWED | Posted: 9 June 2026 doi:10.20944/preprints202606.0589.v1

and

$$R_{ij} = \exp[-i\theta_0(\vec{\sigma}\cdot\hat{n}_{ij})]$$

— is the elementary directed spinor routing operator along the edge. The quantity θ_0 is the universal elementary routing phase, not the particle mass.

Under a local $U(1)$ transformation $\psi_i \to e^{i\lambda_i}\psi_i$, the link phase transforms as

$$L_{ij} \to e^{i\lambda_j} L_{ij} e^{-i\lambda_i}, \qquad \phi_{ij} \to \phi_{ij} + \lambda_i - \lambda_j.$$

Under a local frame rotation $\psi_i \to G_i\psi_i$, where $G_i \in SU(2)$, the spin coupling transforms as

$$\Gamma_{ij} \to G_j \Gamma_{ij} G_i^{\dagger}.$$

Then the total translation along the edge is covariant:

$$\mathcal{U}_{ij}\psi_i \to e^{i\lambda_j} G_j \mathcal{U}_{ij}\psi_i.$$

If the directed decomposition is used

$$P_{ij}^{(\pm)} = \frac{1}{2}(I \pm \vec{\sigma}\cdot\hat{n}_{ij}),$$

then the Abelian link phase does not conflict with the projectors, since L_{ij} acts as a scalar in spin space:

$$[L_{ij}, P_{ij}^{(\pm)}] = 0.$$

Appendix A.2.3. Emergence of $\mathbb{C}^2$ and Clifford algebras

Let the first-order infrared have the form

$$\partial_t \psi = -c_0 A_a \partial_a \psi,$$

where A_a are Hermitian matrices of the inner space. The requirement that the invertible second-order operator yield an isotropic Laplacian,

$$(A_a\partial_a)^2 = \nabla^2 I,$$

is equivalent to the Clifford relations

$$\{A_a, A_b\} = 2\delta_{ab} I.$$

The minimal complex representation of this algebra in three spatial dimensions has dimension 2 and is realized by the Pauli matrices $A_a = \sigma_a$. Therefore,

$$\text{3D locality} + \text{unitarity} + \text{isotropic first-order limit} \Rightarrow Cl_3 \Rightarrow \mathbb{C}^2_{\text{spin}}.$$

The spinor structure emerges as the minimal algebraic capacity for isotropic phase routing on a stochastic graph.

Appendix A.2.4. Prethermal Coherent Vacuum and the Weyl Ballistic Limit

The random graph vacuum should not be understood as a static quenched medium. In such a medium, a wave packet would generally experience Anderson-like localization or transition to a diffusion regime. Nor can the Weyl infrared equation be obtained by simply averaging unitarity operators

$$\left\langle U_G^{(0)} \right\rangle_{G\sim\mathfrak{G}_{\text{vac}}},$$

since the average of unitary operators is generally not a unitary operator.

© 2026 by the author(s). Distributed under a Creative Commons CC BY license.

Preprints.org (www.preprints.org) | NOT PEER-REVIEWED | Posted: 9 June 2026 doi:10.20944/preprints202606.0589.v1

In IKT, a stronger regime is assumed: the vacuum graph is in a prethermal coherent phase. On the extended space

$$\mathcal{H}_{\text{full}} = \mathcal{H}_{\text{packet}} \otimes \mathcal{H}_{\text{graph}}$$

the fast microdynamics of local link updates remain unitary. A single cycle of fast graph refresh is given by the product of local unitary steps

$$U_{\text{cyc}} = U_N U_{N-1} \cdots U_1.$$

Here we are talking about coherent updating of local routing, not about the reduced insertion $\mathcal{I}_m$, which extends the Hilbert space and is responsible for the arrow of time.

Let

$$\Omega_{\text{graph}} = \frac{2\pi}{T_{\text{cyc}}}$$

— the fast graph update frequency, and J_{loc} — the characteristic local scattering frequency or the router's spectral width. The prethermal regime is defined by the condition

$$\epsilon_{\text{pt}} = \frac{J_{\text{loc}}}{\Omega_{\text{graph}}} \ll 1.$$

Then, for times

$$t \ll t_{\text{pre}}, \qquad t_{\text{pre}} \sim T_{\text{cyc}} \exp\left(c \frac{\Omega_{\text{graph}}}{J_{\text{loc}}}\right),$$

where $c = O(1)$, there exists an effective prethermal Floquet-Hamiltonian

$$U_{\text{cyc}} = \exp\left[-\frac{i}{\hbar} H_{\text{pre}} T_{\text{cyc}}\right] + O\left(e^{-c\Omega_{\text{graph}}/J_{\text{loc}}}\right).$$

The reduced description of an observer who does not track the graph degrees of freedom is a CPTP channel

$$\mathcal{E}_{\text{ann}}(\rho) = \text{Tr}_{\text{graph}}\left[U_{\text{full}}(\rho \otimes \sigma_{\text{graph}})U_{\text{full}}^{\dagger}\right].$$

In the prethermal phase, this channel has a nearly unitary coherent sector:

$$\mathcal{E}_{\text{ann}}\big|_{\mathcal{H}_{\text{coh}}} = \mathcal{U}_{\text{pre}} + O\left(e^{-c\Omega_{\text{graph}}/J_{\text{loc}}}\right) + O(\Gamma_{\text{leak}} T_{\text{cyc}}).$$

It is precisely this sector, and not the average $\langle U_G \rangle$, that is responsible for the observed ballistic branch.

In the infrared coherent sector, the principal symbol of the prethermal Hamiltonian has Weyl form. For a directed conditional translation along the edge $i \to j$:

$$\mathcal{T}_{ij}\psi(\mathbf{R}) = \psi(\mathbf{R}) - a_0(\vec{\sigma} \cdot \hat{n}_{ij})(\hat{n}_{ij} \cdot \nabla)\psi(\mathbf{R}) + O(a_0^2).$$

Using second-moment statistical isotropy,

$$\left\langle \sum_{j \sim i} w_{ij} \hat{n}_{ij}^a \hat{n}_{ij}^b \right\rangle_{\mathfrak{G}} = \kappa_2 \delta^{ab},$$

we obtain

$$H_{\text{pre}}^{\text{IR}} = -i\hbar c_0 \vec{\sigma} \cdot \nabla + O(a_0^2 \nabla^3) + O(J_{\text{loc}}^2/\Omega_{\text{graph}}),$$

where

$$c_0 = \frac{a_0 \kappa_2}{\Delta t}.$$

Consequently, at prethermal times

$$\boxed{i\hbar \partial_t \psi = -i\hbar c_0 \vec{\sigma} \cdot \nabla \psi}$$

© 2026 by the author(s). Distributed under a Creative Commons CC BY license.

Preprints.org (www.preprints.org) | NOT PEER-REVIEWED | Posted: 9 June 2026 doi:10.20944/preprints202606.0589.v1

with residual decoherence

$$\Gamma_{\mathrm{decoh}} \lesssim T_{\mathrm{cyc}}^{-1} e^{-c\Omega_{\mathrm{graph}}/J_{\mathrm{loc}}} + \Gamma_{\mathrm{leak}}.$$

Thus, IKT does not claim that arbitrary annealed averaging of random unitary operators remains unitary. The claim is that the physical vacuum ensemble realizes a prethermal coherent phase in which the effective Weyl branch is described by a nearly unitary Floquet Hamiltonian at times $t \ll t_{\mathrm{pre}}$.

Appendix A.2.5. Dynamic Protection of Topological Paths and the Status of the Nielsen–Ninomiya Theorem

The classical Nielsen–Ninomiya theorem applies to local lattice theories of chiral fermions on a regular translation-invariant lattice with a compact Brillouin zone. The IKT fundamental vacuum is not such a lattice: it is defined by a dynamic stochastic graph with a prethermal coherent sector. Therefore, the standard lattice formulation of the no-go theorem does not apply directly.

However, the absence of a Brillouin torus does not in itself guarantee the existence of observable fermions. Instead of the lattice doubling problem, a spectral condition arises for the reduced prethermal/annealed channel: the physical infrared sector must have a coherent peripheral branch, whereas the unbound ultraviolet sectors must fade into a non-peripheral damping spectrum:

$$\lambda_{\mathrm{IR},\pm}(k) = e^{-\Gamma_{\mathrm{IR}}(k)\Delta t} e^{\mp i c_0 |k| \Delta t + O(k^2 a_0 \Delta t)},$$

$$|\lambda_{\mathrm{UV}}| \le e^{-\gamma_{\mathrm{UV}}\Delta t}, \qquad \gamma_{\mathrm{UV}} > 0.$$

In a prethermal vacuum

$$\Gamma_{\mathrm{IR}}(k) = O(e^{-c\Omega_{\mathrm{graph}}/J_{\mathrm{loc}}}) + O((ka_0)^p), \qquad p > 0,$$

therefore, smooth infrared wave packets retain ballistic coherence for times $t \ll t_{\mathrm{pre}}$. In contrast, UV modes lacking topological protection rapidly transition into the incoherent noise sector.

Stochastic graph surgery in IKT is not uniform classical noise on all edges. Its effective rate depends on the local phase load. For an edge e, let us introduce a local delay

$$\theta_e = \frac{S_{\mathrm{top}}(e)}{\hbar_{\mathrm{graph}}}.$$

Then the rate of irreversible topological re-linking takes a selective form

$$\gamma_{\mathrm{surg}}(e) = \gamma_0 \, \Pi_{\mathrm{UV}}(e) \, e^{-\theta_e},$$

where Π_{UV} denotes the projection onto unbound short-wavelength or incoherent local components. Such surgery suppresses UV-doublerr-like sectors but does not act as uniform decoherence on the prethermal IR branch.

For a stable fermionic route K, the phase load is large:

$$\theta_e \gg 1, \qquad e \in K.$$

Therefore, the rate of random path breakage is limited:

$$\gamma_{\mathrm{break}}(K) \lesssim \sum_{e \in K} \gamma_0 e^{-\theta_e}.$$

The cosmological stability of an electronic path requires

$$\gamma_{\mathrm{break}}(K_e) T_{\mathrm{obs}} \ll 1.$$

© 2026 by the author(s). Distributed under a Creative Commons CC BY license.

Preprints.org (www.preprints.org) | NOT PEER-REVIEWED | Posted: 9 June 2026 doi:10.20944/preprints202606.0589.v1

In this sense, a stable 4π-fermion cycle dynamically shields itself with its own topological phase charge.

The protected path K is a quasi-one-dimensional coherent channel within a stochastic $3D$ vacuum. The two directed low-energy branches of such a channel are not interpreted as parasitic lattice doublers. They form the necessary chiral space of the massive Dirac/Floquet sector:

$$\mathcal{H}_K^{\mathrm{chir}} = \mathrm{span}\{|L_K\rangle, |R_K\rangle\}.$$

It is precisely the monodromic mixing of these branches that generates the mass gap

$$M_K c_0^2 = \frac{\hbar}{T_K}|\Theta_K|.$$

Weak chirality does not require an isolated single Weyl fermion as an asymptotic state; it is realized as the action of the weak-gateway projector P_Ξ on the Dirac/Floquet sector.

Remark A1 (Status of the Nielsen–Ninomiya theorem)**.** *IKT does not claim that the Nielsen–Ninomiya theorem is violated. The standard prerequisites of the theorem are absent on the fundamental stochastic graph, and the lattice doubling problem is replaced by the spectral problem of a prethermal/annealed superoperator. The necessary conditions are: the existence of a nearly unitary IR-peripheral branch, the damping of UV sectors, and exponential protection of stable closed routes. The rigorous derivation of the spectral gap for a fully nonlinear channel with feedback*

$$\gamma_{\mathrm{surg}}(e) \propto e^{-\theta_e}$$

remains a problem in mathematical physics.

Appendix A.2.6. Nonlinear Self-Focusing as Additional Protection for Coherent Paths

Even after the transition from a regular lattice to a stochastic graph, an important problem remains: in general, an arbitrary wave packet in an unstructured medium must undergo scattering, diffusion, or localization. Therefore, the stochasticity of the graph alone is insufficient to explain the stability of the observed fermionic states.

In IKT, this problem is solved not by fundamental nonlinearity of the wave function, but by the graph's self-consistent response to local phase traffic. The complete graph-packet microdynamics remains unitary or isometric on the extended state space. Nonlinearity appears only in the coarse-grained description after excluding fast graph degrees of freedom.

Let

$$\rho_e = \langle\psi|\Pi_e|\psi\rangle$$

— the local phase density on the oriented edge e, where Π_e is the projector onto the corresponding edge channel. The local phase delay receives a self-consistent contribution:

$$\boxed{\theta_e = \theta_{\mathrm{vac}} + \theta_{\mathrm{top}}(e) + g_{\mathrm{sf}}\frac{\rho_e}{\rho_* + \rho_e}}.$$

Saturation at $\rho_e \gg \rho_*$ prevents the unlimited collapse of the packet and transitions the self-focusing into a regime of local topological rigidity.

The rate of irreversible graph surgery is then given by

$$\gamma_{\mathrm{surg}}(e) = \gamma_0 \Pi_{\mathrm{UV}}(e) e^{-\theta_e}.$$

Here, Π_{UV} highlights the unbound short-wavelength or incoherent components. Therefore, incoherent UV modes remain subject to rapid attenuation, whereas edges carrying a stable coherent path receive exponential protection.

© 2026 by the author(s). Distributed under a Creative Commons CC BY license.

Preprints.org (www.preprints.org) | NOT PEER-REVIEWED | Posted: 9 June 2026 doi:10.20944/preprints202606.0589.v1

For a closed fermionic path K, we have

$$\gamma_{\text{break}}(K) \lesssim \sum_{e \in K} \gamma_0 e^{-\theta_e}.$$

The cosmological stability of the electron path requires

$$\gamma_{\text{break}}(K_e) T_{\text{obs}} \ll 1.$$

In this sense, a massive particle in IKT is not a passive packet on a random graph, but a self-consistent topological routing soliton that locally increases the stiffness of its own channel.

Self-focusing should not alter the principal Weyl symbol of the infrared dynamics. It enters as an internal binding/mass contribution, whereas the coefficient in front of the kinetic term remains universal. At the effective massive-envelope level, defined in subsection A.3.1, this can be written schematically as:

$$H_{\text{eff}} = -i\hbar c_0 \vec{\alpha} \cdot \nabla + M_K c_0^2 \beta_K + V_{\text{sf}}[\rho],$$

where

$$\partial_k V_{\text{sf}} = O((k a_0)^2).$$

This condition ensures infrared Lorentz invariance, allowing deviations only in the DSR order.

Finally, for route mobility, the pinning energy of the self-focused channel must be small compared to its monodromic energy:

$$E_{\text{pin}}(K) \ll M_K c_0^2.$$

Thus, the prethermal coherent phase ensures mobility, while nonlinear self-focusing ensures the stability of the topological route. This mechanism serves as an additional safeguard for massive routes: it does not replace the prethermal Weyl sector and is not an independent bypass of the Nielsen–Ninomiya theorem, but it reinforces the separation between unbound UV modes and stable topological fermionic loops.

Appendix A.2.7. Reversible Second Order and Free Wave Kinematics

Reversible second order follows from the Weyl equation. Using $(\vec{\sigma} \cdot \nabla)^2 = \nabla^2 I$, we obtain

$$\boxed{\partial_t^2 \psi = c_0^2 \nabla^2 \psi} \tag{A1}$$

in the infrared limit. This equation is a universal vacuum-wave kinematics statement for coherent massless envelopes. It is not yet an electromagnetic statement: the electromagnetic interface is obtained only after projecting the universal wave branch onto the transverse $U(1)$-link sector.

The leading high-energy correction is likewise controlled by the stochastic graph-vacuum ensemble rather than by any specific interaction channel. The detailed annealed-graph derivation and the DSR-like coefficient controlled by the fourth spectral moment are given in the next subsection.

Appendix A.2.8. High-energy Stochastic-Vacuum Dispersion and DSR-like Correction

Since the fundamental IKT vacuum is not an ideal crystal lattice but a dynamic stochastic graph, the exact dispersion of macroscopic wave packets cannot be described by separable trigonometric functions of the form $\sum_a \sin^2(k_a a_0/2)$, characteristic of cubic geometry. Such a formula is admissible only as a verification proxy for a regular chart approximation, but not as the fundamental kinematics of IKT.

© 2026 by the author(s). Distributed under a Creative Commons CC BY license.

Preprints.org (www.preprints.org) | NOT PEER-REVIEWED | Posted: 9 June 2026 doi:10.20944/preprints202606.0589.v1

The dispersion relation for the macroscopic envelope is derived from the spectral decomposition of the annealed-graph Laplacian. On an isotropic stochastic vacuum, the eigenvalues of the averaged Laplacian depend on the magnitude of the macroscopic wave vector

$$k = |\mathbf{k}|,$$

rather than on its projections onto the global coordinate axes, which do not exist in the fundamental graph.

The fundamental wave update is written for a generic coherent massless envelope $\mathcal{W}_m$, rather than for an electromagnetic potential:

$$\mathcal{W}_{m+1} - 2\mathcal{W}_m + \mathcal{W}_{m-1} = \lambda_{\text{wave}} \langle L_G \rangle_{\mathfrak{G}} \mathcal{W}_m.$$

Only after projection to the transverse $U(1)$-link sector may this envelope be identified with the photon field, schematically $\mathcal{W}_m \to \mathbf{A}_m^{\perp}$. Passing to continuous time $t = m\tau_0$ and using the isotropic expansion of the annealed Laplacian in terms of the small parameter ka_0, we obtain

$$-\omega^2\tau_0^2 + \frac{\tau_0^4}{12}\omega^4 + O(\omega^6\tau_0^6) = \lambda_{\text{wave}}\Big(-k^2a_0^2 + \eta_4 k^4 a_0^4 + O(k^6 a_0^6)\Big).$$

Here, η_4 is a dimensionless coefficient determined by the fourth moment of the stochastic distribution of the graph's links, i.e., the excess of the vacuum ensemble $\mathfrak{G}_{\text{vac}}$. Unlike in a cubic lattice, where anisotropic terms $\sum_a k_a^4$ arise, in the stochastic vacuum the leading fourth-order correction has a rotationally symmetric form $\eta_4 k^4$.

Calibrating the speed of the coherent massless branch as

$$c_0 = \sqrt{\lambda_{\text{wave}}}\,\frac{a_0}{\tau_0},$$

we obtain a DSR-like dispersion relation

$$\omega^2 = c_0^2 k^2 - c_0^2 a_0^2 \left(\eta_4 - \frac{\lambda_{\text{wave}}}{12}\right) k^4 + O(k^6 a_0^4). \tag{A2}$$

In the dispersion (A2) under central normalization $\lambda_{\text{wave}} = 1$, the coefficient reduces to $\eta_4 - 1/12$. Therefore, the violation of Lorentz invariance on scales of the order of a_0 is not cubic-anisotropic but statistically isotropic.

Possible residual anisotropies are not electromagnetic parameters; they measure incomplete isotropization of the annealed vacuum ensemble. For a coarse-graining scale L they are expected to decay as

$$\eta_{\text{aniso}}(L) \sim \left(\frac{a_0}{L}\right)^p, \qquad p > 0.$$

The phase velocity of high-energy packets is given by

$$v_{\text{phase}}(k) = \frac{\omega}{k} \simeq c_0\left[1 - \frac{1}{2}\left(\eta_4 - \frac{\lambda_{\text{wave}}}{12}\right)(ka_0)^2\right].$$

For observational time-of-flight tests, the group velocity is relevant

$$v_{\text{group}}(k) = \frac{d\omega}{dk} \simeq c_0\left[1 - \frac{3}{2}\left(\eta_4 - \frac{\lambda_{\text{wave}}}{12}\right)(ka_0)^2\right].$$

Thus, the search for DSR-like effects in IKT is transformed from fitting arbitrary parameters into the problem of calculating the spectral excess η_4 for a specific class of stochastic vacuum graphs.

© 2026 by the author(s). Distributed under a Creative Commons CC BY license.

Preprints.org (www.preprints.org) | NOT PEER-REVIEWED | Posted: 9 June 2026 doi:10.20944/preprints202606.0589.v1

Appendix A.2.9. Transverse $U(1)$-sector and Free Maxwell Limit

Equation (A1) is in itself a free wave equation, not a complete Maxwell system. To obtain the electromagnetic interface, it is necessary to isolate the transverse $U(1)$-link-sector of the graph. The Abel phase $L_{ij} = e^{-i\phi_{ij}}$ is already included in the edge transporter $\mathcal{U}_{ij}$. In the continuous interface, after selecting the topological charge sector, we can identify

$$\phi_{ij} = \frac{q_{\text{top}}}{\hbar} \int_i^j A_\mu dx^\mu,$$

where q_{top} is not a parameter of the minimal operator, but a topological access index to the $U(1)$ channel. Then the standard covariant derivative arises: $\partial_a \to D_a = \partial_a + iq_{\text{top}} A_a/\hbar$.

Free photon modes correspond to transverse excitations of the link phase. In terms of the Riemann–Silberstein vector $\mathbf{F} = \mathbf{E} + ic_0\mathbf{B}$, the free Maxwell sector is given by the conditions

$$i\partial_t \mathbf{F} = c_0 \nabla \times \mathbf{F}, \qquad \nabla \cdot \mathbf{F} = 0.$$

From these, it follows that $\partial_t^2 \mathbf{F} = c_0^2 \nabla^2 \mathbf{F}$.

Appendix A.3. Dynamics of the Local Phase: Mass, Spin, and the Arrow of Time

The free vacuum sector contains coherent Weyl/wave envelopes. Particles, mass, and the observable arrow of time appear only after the emergence of stable topological defects, closed routes, and insertion operations.

Appendix A.3.1. From Monodromy to Mass: the Emergence of the Dirac Equation

The minimal vacuum operator of IKT does not contain a fundamental bare mass: $U_m^{(0)} = S_m C_m$. A massive Dirac sector arises only for a stable closed topological route K, when the inner loop has two low-energy coarse-grained branches

$$\mathcal{H}_K^{\text{chir}} = \text{span}\{|L_K\rangle, |R_K\rangle\}.$$

The effective low-energy space of the path takes the form

$$\mathcal{H}_K^{\text{eff}} \simeq \mathcal{H}_K^{\text{chir}} \otimes \mathbb{C}^2_{\text{spin}},$$

and the macroscopic envelope

$$\Psi_K = |L_K\rangle \otimes \psi_L + |R_K\rangle \otimes \psi_R \in \mathbb{C}^4.$$

Let $K = (e_1, e_2, \ldots, e_{N_K})$ consist of oriented edges, and $T_K = N_K \tau_{\text{step}}$ be the time of one internal loop. The rest monodromy operator is defined as the ordered product of edge transporters

$$W_K(0) = \mathcal{P}_{\text{ord}} \prod_{j=1}^{N_K} \mathcal{U}_{e_j}.$$

If P_K is the projection onto the low-energy subspace $\mathcal{H}_K^{\text{eff}}$ and $\|[P_K, W_K(0)]\| \ll 1$, then the effective rest monodromy is defined as the unitary part of the contracted operator:

$$W_K^{\text{eff}}(0) = \text{polar}(P_K W_K(0) P_K)\Big|_{\mathcal{H}_K^{\text{eff}}}.$$

Let its eigenchiral phases be of the form

$$\lambda_\pm(W_K^{\text{eff}}(0)) = e^{-i(\bar{\Theta}_K \pm \Theta_K)}.$$

© 2026 by the author(s). Distributed under a Creative Commons CC BY license.

Preprints.org (www.preprints.org) | NOT PEER-REVIEWED | Posted: 9 June 2026 doi:10.20944/preprints202606.0589.v1

Then

$$\boxed{\Theta_K = \frac{1}{2}\,\mathrm{Arg}_{\mathrm{lift}}\left(\frac{\lambda_-(W_K^{\mathrm{eff}}(0))}{\lambda_+(W_K^{\mathrm{eff}}(0))}\right)} \tag{A3}$$

and

$$\boxed{M_K c_0^2 = \frac{\hbar}{T_K}|\Theta_K|.} \tag{A4}$$

The phase gap (A3) and the mass normalization (A4) define the monodromic mass-anchor of the route. For the macroscopic envelope, we introduce $\alpha_a = \tau_z \otimes \sigma_a$ and $\beta_K = \tau_x \otimes I_2$, which satisfy the Dirac algebra. The Dirac equation in IKT is not a microscopic equation at every vertex of the graph. This is a homogenized equation for the slow envelope of the center of a composite topological excitation. In the regime

$$L \gg \ell_K, \qquad T \gg T_K, \qquad q\ell_K \ll 1, \qquad \epsilon_{\mathrm{leak}} \ll 1,$$

the quasi-impulse effective monodromy

$$W_K^{\mathrm{eff}}(\mathbf{q}) = \mathrm{polar}(P_K W_K(\mathbf{q}) P_K)\Big|_{\mathcal{H}_K^{\mathrm{eff}}}$$

and the Floquet-Hamiltonian

$$H_K^{\mathrm{eff}}(\mathbf{q}) = \frac{i\hbar}{T_K}\,\mathrm{Log}_{\mathrm{lift}}\, W_K^{\mathrm{eff}}(\mathbf{q}).$$

In the limit as $\mathbf{q}$ approaches zero

$$H_K^{\mathrm{eff}}(\mathbf{q}) = E_K^{(0)} I_4 + M_K c_0^2 \beta_K + \hbar c_0 \vec{\alpha}\cdot\mathbf{q} + O(q^2\ell_K^2, \epsilon_{\mathrm{leak}}, a_0/\ell_K).$$

After substituting $\mathbf{q} \to -i\nabla_{\mathbf{R}}$, we obtain the effective Dirac equation

$$\boxed{i\hbar\partial_t \Psi_K(\mathbf{R},t) = \left(-i\hbar c_0 \vec{\alpha}\cdot\nabla_{\mathbf{R}} + M_K c_0^2 \beta_K\right)\Psi_K(\mathbf{R},t)} \tag{A5}$$

with corrections determined by the leakage from the physical sector, the finite size of the cycle, and the discreteness of the graph. Equation (A5) is an effective Dirac-envelope limit, not a microscopic equation at a single vertex of the graph. The mass term is local only with respect to the coarse-grained cell carrying the entire K route.

Appendix A.3.2. Topological Source of Fermionic Sign

The local internal frame is lifted from $SO(3)$ to $SU(2)$:

$$R(\hat{n},\phi) = \exp[-\frac{i}{2}\phi\hat{n}\cdot\vec{\sigma}].$$

For a rotation by 2π, we have $R(\hat{n},2\pi) = -I$, and for 4π, $+I$. For two identical closed paths, the exchange is a loop $\gamma_{\mathrm{exch}} \in \pi_1(\mathcal{C}_2(K))$. The fermionic sector is given by a Finkelstein–Rubinstein-type representation

$$\rho_{\mathrm{FR}} : \pi_1(\mathcal{C}_2(K)) \to \{\pm 1\}.$$

If $\rho_{\mathrm{FR}}(\gamma_{\mathrm{exch}}) = -1$, then $\Psi(1,2) = -\Psi(2,1)$ and $\Psi(1,1) = 0$. This argument does not claim to replace the full relativistic spin-statistics theorem; its role is to show the topological origin of the required fermionic sign.

© 2026 by the author(s). Distributed under a Creative Commons CC BY license.

Preprints.org (www.preprints.org) | NOT PEER-REVIEWED | Posted: 9 June 2026 doi:10.20944/preprints202606.0589.v1

Appendix A.3.3. Local Phase Delay and Retention Probability

Definition A8 (Dimensionless phase delay and self-loop probability)**.** *The fundamental delay is a phase, not a dimensional energy. In electron projection units, let us introduce*

$$\tau_e = \frac{\hbar}{m_e c_0^2}, \qquad \lambda_e = \frac{\hbar}{m_e c_0},$$

and the dimensionless UV resolution of the graph

$$\epsilon_0 = \frac{\tau_0}{\tau_e} = \frac{l_0}{\lambda_e}.$$

Then, for a local node with dimensionless energy

$$\varepsilon_j = \frac{E_j}{m_e c_0^2}$$

the phase delay is equal to

$$\theta_j = \varepsilon_j \epsilon_0.$$

For the local effective mass-energy concentrated in a single elementary graph cell, a local phase load is introduced

$$\theta_{\mathrm{loc}} = \epsilon_0 \frac{M_{\mathrm{loc}}}{m_e} = \frac{M_{\mathrm{loc}}}{M_0}, \qquad M_0 = \frac{m_e}{\epsilon_0} = \frac{\hbar}{c_0^2 \tau_0}.$$

For a single compact topological loop, one can write $\theta_M = \theta_{\mathrm{loc}}$, but for composite macroscopic bodies, the saturation is determined by the distribution $M_{\mathrm{loc}}(v)$, rather than the total mass of the object. Topological normalization of the gravitational sector introduces a configuration index for the electron path

$$N_e^{\mathrm{top}} = |\Omega_e|_{\mathrm{eff}}.$$

Then

$$\epsilon_0 = \frac{1}{|\Omega_e|_{\mathrm{eff}}}, \qquad M_0 = m_e |\Omega_e|_{\mathrm{eff}}, \qquad \alpha_G^{(e)} = \frac{1}{|\Omega_e|_{\mathrm{eff}}^2}.$$

The observed delay probability is given by the restricted function

$$p_j = 1 - e^{-\theta_j}, \qquad 0 \le p_j < 1.$$

In the weak regime $\theta_j \ll 1$, $p_j \simeq \theta_j$ holds, which reproduces the linear approximation of the delay.

The massless operator $U_m^{(0)}$ describes the free unitary dynamics of the coherent branch. In the general case, a local subgraph or closed path K can create a topological barrier to phase emergence. This barrier is characterized by a non-negative topological action $S_{\mathrm{top}}(K) \ge 0$. The dimensionless local delay is defined as

$$\boxed{\theta_{\mathrm{loc}}(K) = \frac{S_{\mathrm{top}}(K)}{\hbar_{\mathrm{graph}}}}$$

and

$$\boxed{p_{\mathrm{stay}}(K) = 1 - \exp[-S_{\mathrm{top}}(K)/\hbar_{\mathrm{graph}}] = 1 - e^{-\theta_{\mathrm{loc}}(K)}.}$$

In the limit $S_{\mathrm{top}} \ll \hbar_{\mathrm{graph}}$, we have $p_{\mathrm{stay}} \approx S_{\mathrm{top}}/\hbar_{\mathrm{graph}}$, and when $S_{\mathrm{top}} \gg \hbar_{\mathrm{graph}}$, we obtain $p_{\mathrm{stay}} \to 1$.

© 2026 by the author(s). Distributed under a Creative Commons CC BY license.

Preprints.org (www.preprints.org) | NOT PEER-REVIEWED | Posted: 9 June 2026 doi:10.20944/preprints202606.0589.v1

Appendix A.3.4. Insertion Rule and Reduced Arrow of Time

When $p_{\text{stay}} \to 1$, free phase translation through a subgraph is blocked. To prevent local computational paralysis, the graph allows insertion: an extension of the available Hilbert space. At the level of pure states, a single selected channel is defined by the isometry

$$V_{m,\ell} : \mathcal{H}_m \to \mathcal{H}_{m+1}, \qquad V_{m,\ell}^{\dagger} V_{m,\ell} = I_{\mathcal{H}_m}.$$

If a macroscopic observer does not distinguish between alternative local insertions, the reduced dynamics are described by Kraus operators $R_{m,\ell}$:

$$\mathcal{E}_m(\rho) = \sum_{\ell} R_{m,\ell} U_m \rho U_m^{\dagger} R_{m,\ell}^{\dagger}, \qquad \sum_{\ell} R_{m,\ell}^{\dagger} R_{m,\ell} = I_{\mathcal{H}_m}.$$

A convenient choice: $R_{m,\ell} = \sqrt{p_\ell}\, V_{m,\ell}$, $p_\ell \geq 0$, $\sum_\ell p_\ell = 1$. The isometry itself does not destroy information on the entire Hilbert space; irreversibility arises for a macroscopic observer after coarse-graining and tracing the hidden new degrees of freedom:

$$\rho_{\text{obs}} = \text{Tr}_{\text{hidden}}(|\Psi_{m+1}\rangle\langle\Psi_{m+1}|).$$

Appendix A.3.5. Macroscopic Superposition and Decoherence Time

The qualitative statement regarding the breakdown of macroscopic 1D bridges can be formalized numerically, but this must be done in the dimensionless IKT metric. At the microscopic level, G and t_{Pl} cannot be considered independent ontological constants: both quantities are SI-projections of the topological sparsity of the electronic path. Therefore, let us start with the CP-version of the anti-Hermitian correction. At the amplitude level, it takes the form

$$i\hbar\partial_t \Psi = \hat{H}\Psi - i\frac{\tau_0}{2\hbar}\hat{H}^2\Psi + \mathcal{O}(\tau_0^2),$$

but physically it should be understood not as an independent non-Hermitian evolution of the normalized wave function, but as the effective trace of a completely positive coarse-graining channel of graph insertion. In density-matrix form, the minimal model is written as

$$\frac{d\rho}{dt} = -\frac{i}{\hbar}[\hat{H}, \rho] - \frac{\tau_0}{2\hbar^2}[\hat{H}, [\hat{H}, \rho]].$$

For two superposition branches with an energy splitting of ΔE, this gives

$$\rho_{12}(t) = \rho_{12}(0)\exp[-\Gamma_{\text{IKT}} t], \qquad \Gamma_{\text{IKT}} = \frac{\tau_0}{2\hbar^2}(\Delta E)^2.$$

To eliminate implicit circularity, we rewrite this result in electron-dimensionless units:

$$\tilde{t} = \frac{t}{\tau_e}, \qquad \Delta\varepsilon_G = \frac{\Delta E_G}{m_e c_0^2}, \qquad \tau_e = \frac{\hbar}{m_e c_0^2}.$$

Then the damping coefficient of the off-diagonal element is given by

$$\Gamma_{\text{IKT}} t = \frac{\epsilon_0}{2}(\Delta\varepsilon_G)^2 \tilde{t}.$$

Using the topological normalization

$$\epsilon_0 = \frac{1}{|\Omega_e|_{\text{eff}}},$$

© 2026 by the author(s). Distributed under a Creative Commons CC BY license.

Preprints.org (www.preprints.org) | NOT PEER-REVIEWED | Posted: 9 June 2026 doi:10.20944/preprints202606.0589.v1

we obtain a closed dimensionless form

$$\boxed{\Gamma_{\mathrm{IKT}} t = \frac{1}{2|\Omega_e|_{\mathrm{eff}}} (\Delta\varepsilon_G)^2 \tilde{t}}.$$

Physically, this means that the destruction of a macroscopically conflicting 1D bridge is suppressed by the large "empty" capacity of the vacuum graph: the larger $|\Omega_e|_{\mathrm{eff}}$ is, the smaller the elementary UV resolution ϵ_0 is, and the longer the microscopic bridge coherences live.

For the spatial superposition of a massive object, the energy conflict is given by the gravitational self-energy of the difference between the two mass distributions:

$$\Delta E_G = \frac{G}{2} \int d^3\mathbf{r}\, d^3\mathbf{r}' \frac{[\rho_1(\mathbf{r}) - \rho_2(\mathbf{r})][\rho_1(\mathbf{r}') - \rho_2(\mathbf{r}')]}{|\mathbf{r} - \mathbf{r}'|}.$$

It is precisely this integral form that is fundamental. The one-scale estimate

$$\Delta E_G \sim \mathcal{S}_G \frac{GM^2}{R_{\mathrm{eff}}} \tag{A6}$$

is merely an order-of-magnitude estimate. Here, $\mathcal{S}_G$ denotes a dimensionless geometric coefficient that depends on the object's shape, density distribution, relative branch separation, and the chosen coarse-graining scale. Therefore, all numerical estimates below should be interpreted as order-of-magnitude estimates, not as exact universal collapse times. If the branch separation Δx is comparable to this scale, one can set $R_{\mathrm{eff}} \sim \Delta x$; a more general single-scale audit is written as

$$\Delta E_G(M, \Delta x, R_{\mathrm{eff}}) \sim \mathcal{S}_G \frac{GM^2}{R_{\mathrm{eff}}} F\!\left(\frac{\Delta x}{R_{\mathrm{eff}}}\right), \qquad F(y) \sim y^2 \ (y \ll 1), \quad F(y) \to 1 \ (y \gg 1).$$

This dispels the false conclusion that an arbitrary increase in the distance between the branches must always prolong coherence. At large separations, the conflict energy is saturated by the intrinsic gravitational scale of the mass distribution.

Rate–lifetime convention.

The M^{-4} law refers to the lifetime of the coherent bridge, not to the instantaneous damping rate and not to the dimensionless damping exponent at fixed laboratory time. The observable damping exponent is

$$\mathcal{D}_{\mathrm{IKT}}(t) \equiv \Gamma_{\mathrm{IKT}} t = \frac{\tau_0}{2\hbar^2} (\Delta E_G)^2 t = \frac{1}{2|\Omega_e|_{\mathrm{eff}}} (\Delta\varepsilon_G)^2 \tilde{t}. \tag{A7}$$

For a one-scale family of superpositions with fixed shape factor and fixed relative branch geometry,

$$\Delta E_G \sim \mathcal{S}_G \frac{GM^2}{R_{\mathrm{eff}}}. \tag{A8}$$

Hence

$$\Gamma_{\mathrm{IKT}}^{\mathrm{oom}} \sim \frac{\tau_0 \mathcal{S}_G^2 G^2}{2\hbar^2} \frac{M^4}{R_{\mathrm{eff}}^2}, \qquad \mathcal{D}_{\mathrm{IKT}}(t) \propto \frac{M^4}{R_{\mathrm{eff}}^2}\, t. \tag{A9}$$

The bridge lifetime is the inverse rate,

$$t_{\mathrm{IKT}}^{\mathrm{oom}} = \Gamma_{\mathrm{IKT}}^{-1} \propto R_{\mathrm{eff}}^2 M^{-4}. \tag{A10}$$

Thus the hard macroscopic filter is equivalently

$$\boxed{\Gamma_{\mathrm{IKT}}^{\mathrm{oom}} \propto M^4 R_{\mathrm{eff}}^{-2}, \qquad t_{\mathrm{IKT}}^{\mathrm{oom}} \propto R_{\mathrm{eff}}^2 M^{-4}}. \tag{A11}$$

© 2026 by the author(s). Distributed under a Creative Commons CC BY license.

Preprints.org (www.preprints.org) | NOT PEER-REVIEWED | Posted: 9 June 2026 doi:10.20944/preprints202606.0589.v1

Therefore any wording of the form "$\Gamma_{\mathrm{IKT}} t \propto M^{-4}$" is incorrect unless t is already being identified with the lifetime $t_{\mathrm{IKT}} = \Gamma_{\mathrm{IKT}}^{-1}$. At fixed observation time, larger masses produce a larger damping exponent; the M^{-4} dependence belongs only to the survival time of the coherent bridge.

For a completely dimensionless notation, let us introduce the electron length

$$\lambda_e = \frac{\hbar}{m_e c_0},$$

the coordinates

$$\tilde{\mathbf{r}} = \frac{\mathbf{r}}{\lambda_e},$$

and dimensionless densities

$$\tilde{\rho}_a(\tilde{\mathbf{r}}) = \frac{\lambda_e^3}{m_e}\rho_a(\mathbf{r}), \qquad a = 1, 2.$$

Then

$$\mathcal{J}_{12} = \int d^3\tilde{\mathbf{r}}\, d^3\tilde{\mathbf{r}}' \frac{[\tilde{\rho}_1(\tilde{\mathbf{r}}) - \tilde{\rho}_2(\tilde{\mathbf{r}})][\tilde{\rho}_1(\tilde{\mathbf{r}}') - \tilde{\rho}_2(\tilde{\mathbf{r}}')]}{|\tilde{\mathbf{r}} - \tilde{\mathbf{r}}'|}$$

is a purely geometric functional of the two branches. Using

$$G_{\mathrm{IKT}} = \frac{\hbar c_0}{m_e^2 |\Omega_e|_{\mathrm{eff}}^2},$$

we obtain

$$\Delta\varepsilon_G = \frac{\Delta E_G}{m_e c_0^2} = \frac{1}{2|\Omega_e|_{\mathrm{eff}}^2}\mathcal{J}_{12}.$$

Therefore,

$$\boxed{\Gamma_{\mathrm{IKT}} t = \frac{\mathcal{J}_{12}^2}{8|\Omega_e|_{\mathrm{eff}}^5}\tilde{t}}.$$

This is the most self-contained form of the estimate: it uses neither the empirical t_{Pl} nor the independent Newtonian constant G.

For the laboratory SI frame, one can return to the one-scale estimate (A6). Then the lifetime of the bridge coherence

$$t_{\mathrm{IKT}} = \frac{1}{\Gamma_{\mathrm{IKT}}}$$

takes the form

$$t_{\mathrm{IKT}}^{\mathrm{oom}} \sim \frac{2|\Omega_e|_{\mathrm{eff}}^5 m_e^5 R_{\mathrm{eff}}^2}{\hbar\, \mathcal{S}_G^2 M^4}.$$

There is no c_0^2 factor here: it cancels out in the transition from $\tau_e = \hbar/(m_e c_0^2)$ and $\lambda_e = \hbar/(m_e c_0)$ to SI time. The equivalent expression in terms of τ_0 and G is valid only as a derivative of the SI projection after substitution

$$\tau_0 = \frac{\tau_e}{|\Omega_e|_{\mathrm{eff}}}, \qquad G = \frac{\hbar c_0}{m_e^2 |\Omega_e|_{\mathrm{eff}}^2}.$$

For $\mathcal{S}_G = 1$ and $|\Omega_e|_{\mathrm{eff}} \simeq 2.39 \times 10^{22}$, we obtain

$$t_{\mathrm{IKT}}^{\mathrm{oom}} \approx 9.26 \times 10^{-5}\,\mathrm{s}\left(\frac{R_{\mathrm{eff}}}{1\,\mathrm{m}}\right)^2\left(\frac{1\,\mathrm{kg}}{M}\right)^4 \mathcal{S}_G^{-2}.$$

This numerical scale reproduces the sharp macroscopic filter

$$t_{\mathrm{IKT}}^{\mathrm{oom}} \propto R_{\mathrm{eff}}^2 M^{-4},$$

© 2026 by the author(s). Distributed under a Creative Commons CC BY license.

Preprints.org (www.preprints.org) | NOT PEER-REVIEWED | Posted: 9 June 2026 doi:10.20944/preprints202606.0589.v1

but its absolute values depend on the geometric functional $\mathcal{J}_{12}$, that is, on the shape of the object and the configuration of the two branches.

The equivalent light lifetime is given by

$$L_{\text{life}}^{(3D)} = c_0 t_{\text{IKT}}^{\text{oom}}.$$

This quantity is not the topological length of the 1D bridge itself: in the base graph, the bridge may remain a single edge, whereas $L_{\text{life}}^{(3D)}$ only indicates the distance light would travel during the lifetime of coherence.

For an electron with $M = 9.11 \times 10^{-31}$ kg and $R_{\text{eff}} \sim 10^{-9}$ m, a single-scale audit yields

$$t_{\text{IKT}}^{\text{oom}} \sim 10^{98}\,\text{s} \sim 10^{90}\,\text{years},$$

that is, microscopic quantum coherence is practically stable. For a dust particle with $M \sim 10^{-9}$ kg and $R_{\text{eff}} \sim 10^{-6}$ m, we obtain

$$t_{\text{IKT}}^{\text{oom}} \sim 10^{20}\,\text{s} \sim 10^{12}\,\text{years}.$$

For a macroscopic object with $M = 1$ kg and $R_{\text{eff}} = 0.1$ m at $\mathcal{S}_G = 1$:

$$t_{\text{IKT}}^{\text{oom}} \approx 9.3 \times 10^{-7}\,\text{s}, \qquad L_{\text{life}}^{(3D)} \approx 2.8 \times 10^{2}\,\text{m}.$$

The fundamental difference from the Diossi–Penrose gravitational estimate [11,12] lies in the quadratic dependence of the decay rate on the energy conflict:

$$t_{\text{DP}} \sim \frac{\hbar}{\Delta E_G}, \qquad t_{\text{IKT}} \sim \frac{2\hbar^2}{\tau_0 \Delta E_G^2}.$$

For small ΔE_G, IKT yields much longer-lived coherence than the linear DP law, while for truly macroscopic objects with large M, the strict M^{-4} law applies. Therefore, the Schrödinger-cat scenario receives a numerical resolution in the form of a conditional mechanism: microscopic and mesoscopic 1D bridges can survive for extremely long times, whereas bridges of kilogram-scale objects collapse in microseconds or even shorter times without involving the observer's consciousness.

Remark A2 (Status of Numerical Estimates)**.** *The formulas in this subsection do not constitute a complete theorem on the fundamental collapse of the wave function. They provide a conditional numerical consequence of the CP-version of the anti-Hermitian correction. A rigorous verification requires deriving the corresponding Lindblad/CP operator directly from the stochastic insertion of the graph, computing the geometric functional $\mathcal{J}_{12}$ for specific experimental masses and forms, construct the spectrum of possible IKT spontaneous emission, and compare it with experimental constraints on the DP/CSL scenarios [13].*

Appendix A.4. Summary of the Fundamental Basis

Appendix A.4.1. Status of the Fundamental Basis Results

The minimal stochastic sector yields the following hierarchy of results:

- $d_H = d_s = 3$ and statistical isotropy $\Rightarrow$ an emergent 3D continuum.
- Local unitarity on $\ell^2(\vec{E}_m)$ and edge transporters $\Rightarrow U_m^{(0)} = S_m C_m$.
- 3D locality, unitarity, and isotropic first order $\Rightarrow Cl_3 \Rightarrow \mathbb{C}^2_{\text{spin}}$.
- Prethermal coherent vacuum phase, $\epsilon_{\text{pt}} \ll 1$, statistical isotropy, and $U_m^{(0)} \Rightarrow$ Weyl IR-envelope.
- Absence of Brillouin torus, prethermal peripheral spectrum, dynamic protection, and nonlinear self-focusing of routes $\Rightarrow$ absence of light independent doublers and suppression of diffusion of massive routes.
- Isotropy of the fourth moment $\Rightarrow$ isotropic k^4-correction instead of a cubic invariant.

© 2026 by the author(s). Distributed under a Creative Commons CC BY license.

Preprints.org (www.preprints.org) | NOT PEER-REVIEWED | Posted: 9 June 2026 doi:10.20944/preprints202606.0589.v1

- Transverse $U(1)^{\perp}_{\text{link}}$-sector and wave envelope $\Rightarrow$ free Maxwell sector.
- Closed route K and $W_K^{\text{eff}}(0) \Rightarrow \Theta_K \Rightarrow M_K$.
- $H_K^{\text{eff}}(\mathbf{q}) = \frac{i\hbar}{T_K} \operatorname{Log}_{\text{lift}} W_K^{\text{eff}}(\mathbf{q}) \Rightarrow$ local Dirac envelope.
- $SU(2)$-holonomy of the frame and $\rho_{\text{FR}} \Rightarrow$ fermionic sign.
- $\theta_{\text{loc}}(K) = S_{\text{top}}(K)/\hbar_{\text{graph}} \Rightarrow p_{\text{stay}}(K)$.
- $p_{\text{stay}} \to 1, \mathcal{I}_m$ and $\text{Tr}_{\text{hidden}} \Rightarrow$ effective arrow of time.

This ansatz does not contain any prior assumptions regarding generation masses, the fine-structure constant, the strong constant, the gravitational constant, the CKM/PMNS matrices, or the cosmological constant. Its goal is to define a minimal stochastic kinematic kernel upon which further topological, gauge, gravitational, and cosmological sectors of IKT can be built as extensions rather than as independent postulates.

Appendix A.4.2. Scope Limits of Part I

Part I establishes the minimal fundamental basis of IKT: graph kinematics, a unitary micro-operator on oriented edges, a prethermal coherent Weyl branch, a free wave limit, a monodromic origin of mass, a topological fermion sign, a local phase delay, and isometric insertion. It does not claim to provide a complete derivation of all gauge, flavor, RG, and cosmological structures.

Subsequent sections use this basis as input. Part II constructs four macroscopic interaction interfaces—electromagnetic, strong, weak, and gravitational. The sections on constants, particle spectra, the dark sector, and cosmological extensions use additional channel, automorphism, and spectral hypotheses, the status of which is indicated separately in the dependency map.

Appendix B. Macroscopic Limit: Fields and Interactions

Appendix B.1. Electromagnetic Interaction: $U(1)$-Link Phase and Maxwell Interface

In IKT, the electromagnetic field is not an independent entity. It is the macroscopic transverse component of the $U(1)$ phases on the edges of the graph.

Remark A3 (Four levels of the electromagnetic interface)**.** *In the electromagnetic sector, four levels must be distinguished: (i) the local $U(1)$-link-covariance of the edge transporter; (ii) the free transverse link-wave sector, giving the Maxwell envelope; (iii) the TTC-vertex matter-current, from which the current j^μ arises; (iv) the information channel normalization α_{top}, which determines the dimensionless weight g_{em} and the SI projection e_{top}. These levels do not duplicate one another but form a chain*

$$U(1)_{\text{link}} \Rightarrow D_\mu, \qquad U(1)^{\perp}_{\text{link}} \Rightarrow Maxwell, \qquad \delta L_{ij} \Rightarrow j^\mu, \qquad \mathcal{C}_\alpha \Rightarrow g_{\text{em}}, e_{\text{top}}.$$

Appendix B.1.1. Step-by-step Derivation of the Wave Equation from the Symmetric Update

Let the smoothed transverse component of the graph state be denoted by $\mathbf{A}(\mathbf{r}, t)$. On a fixed graph, its reversible low-energy branch satisfies

$$\mathbf{A}(t + \tau_0, \mathbf{r}) - 2\mathbf{A}(t, \mathbf{r}) + \mathbf{A}(t - \tau_0, \mathbf{r}) = \lambda_{\text{wave}} L_G \mathbf{A}(t, \mathbf{r}).$$

After effective integration and expansion of L_G, the left-hand side yields $\tau_0^2 \partial_t^2 \mathbf{A}$, and the leading bare-space term yields $a_0^2 \nabla^2 \mathbf{A}$. Therefore

$$\partial_t^2 \mathbf{A} = c_{\text{em}}^2 \nabla^2 \mathbf{A}, \qquad c_{\text{em}}^2 = \lambda_{\text{wave}} \frac{a_0^2}{\tau_0^2}.$$

© 2026 by the author(s). Distributed under a Creative Commons CC BY license.

Preprints.org (www.preprints.org) | NOT PEER-REVIEWED | Posted: 9 June 2026 doi:10.20944/preprints202606.0589.v1

The observed speed of light fixes the calibration of the transverse electromagnetic branch $c_{\mathrm{em}} = c_0$, so that the metric step is equal to $l_0 = c_0\tau_0 = \sqrt{\lambda_{\mathrm{wave}}}a_0$. In the Coulomb transverse sector, this is equivalent to the free Maxwell wave equation

$$\nabla^2\mathbf{A} - \frac{1}{c_0^2}\frac{\partial^2\mathbf{A}}{\partial t^2} = 0.$$

Appendix B.1.2. Local $U(1)$-gauge Freedom and the Transverse Sector

Gauge invariance is not determined by the condition $\nabla \cdot \mathbf{A} = 0$ itself, but by the local freedom of phase choice at the nodes. On the edge $j \to i$, we introduce the phase factor

$$U_{ij}^{(q_{\mathrm{em}})} = e^{iq_{\mathrm{em}}\theta_{ij}}.$$

The local transformation

$$\psi_i \to e^{iq_{\mathrm{em}}\chi_i}\psi_i, \qquad U_{ij}^{(q_{\mathrm{em}})} \to e^{iq_{\mathrm{em}}\chi_i}U_{ij}^{(q_{\mathrm{em}})}e^{-iq_{\mathrm{em}}\chi_j}$$

does not change the observed loop phases

$$W(\mathcal{C}_{\mathrm{loop}}) = \prod_{(ij)\in\mathcal{C}_{\mathrm{loop}}} U_{ij}^{(q_{\mathrm{em}})} = \exp\left(iq_{\mathrm{em}}\oint_{\mathcal{C}_{\mathrm{loop}}} A_\mu dx^\mu\right).$$

In the continuous limit, this yields the standard transformation $A_\mu \to A_\mu + \partial_\mu\chi$. The transverse projector $P_{ab} = \delta_{ab} - n_a n_b$ selects the physical transverse sector and, in coordinate notation, corresponds to the Coulomb gauge $\nabla \cdot \mathbf{A} = 0$, but does not exhaust all gauge freedom.

Appendix B.1.3. From Microoperator to Macroscopic Current: The TTC Vertex of Electromagnetic Interaction

A fundamental test of a background-independent theory is the ability to derive continuous interaction vertices and corresponding currents directly from microdynamics, without postulating a phenomenological Lagrangian of the form $\mathcal{L}_{\mathrm{int}} = J^\mu A_\mu$. This subsection shows how the macroscopic Dirac current and the electromagnetic TTC vertex arise from a small $U(1)$-link fluctuation of the complete edge transporter of a stochastic graph.

The electromagnetic sector is used at four distinct but consistent levels:

1. **Link covariance:** The $U(1)$ phase L_{ij} defines the covariant transport and leads to D_μ.
2. **Transverse wave sector:** transverse $U(1)$-link fluctuations yield the free Maxwell limit.
3. **TTC-current vertex:** a small fluctuation L_{ij} on path K after annealed averaging yields the current j^μ.
4. **Channel normalization:** the information measure $\mathcal{C}_\alpha$ determines α_{top}, g_{em}, and the SI projection e_{top}.

These four levels are not a repetition of the same statement; they form a chain from the local edge transporter to the observed coupling constant.

The complete edge transporter and a small $U(1)$ perturbation

On an oriented edge $i \to j$, the minimal transporter of a stochastic graph is given by

$$\mathcal{U}_{ij} = L_{ij}\Gamma_{ij}R_{ij}.$$

Here

$$L_{ij} = e^{-i\phi_{ij}} \in U(1)$$

© 2026 by the author(s). Distributed under a Creative Commons CC BY license.

Preprints.org (www.preprints.org) | NOT PEER-REVIEWED | Posted: 9 June 2026 doi:10.20944/preprints202606.0589.v1

— the Abelian link phase,

$$\Gamma_{ij} \in SU(2)$$

— the spin coupling between local representatives, and

$$R_{ij} = \exp\left[-i\theta_0(\vec{\sigma}\cdot\hat{n}_{ij})\right]$$

— the universal directed routing operator along the edge. The quantity θ_0 is the elementary routing phase, not the particle mass.

In the absence of electromagnetic perturbation

$$\mathcal{U}_{ij}^{(0)} = \Gamma_{ij}R_{ij}.$$

A small $U(1)$ perturbation of the link phase yields

$$L_{ij} = e^{-i\phi_{ij}} = 1 - i\phi_{ij} + O(\phi_{ij}^2),$$

and, consequently,

$$\delta\mathcal{U}_{ij}^{(A)} = -i\phi_{ij}\mathcal{U}_{ij}^{(0)} + O(\phi_{ij}^2).$$

Under a local $U(1)$ transformation

$$\psi_i \longrightarrow e^{i\lambda_i}\psi_i$$

the link phase is transformed as

$$L_{ij} \longrightarrow e^{i\lambda_j}L_{ij}e^{-i\lambda_i},$$

or

$$\phi_{ij} \longrightarrow \phi_{ij} + \lambda_i - \lambda_j.$$

Therefore, $\mathcal{U}_{ij}\psi_i$ transforms covariantly at the end vertex j.

At a continuous interface, the link phase is the Wilson phase along the edge:

$$\phi_{ij} = \frac{q_{\text{top}}}{\hbar}\int_i^j A_\mu dx^\mu.$$

For a short spatial edge with direction $\hat{n}_{ij}$:

$$\phi_{ij} = \frac{q_{\text{top}}a_0}{\hbar}\hat{n}_{ij}\cdot\mathbf{A}(\mathbf{R}) + O(a_0^2\nabla A),$$

and the temporal link similarly generates the A_0-part of the gauge interface.

Local TTC vertex and transit amplitude

Consider a stable 4π-spinor cycle K with a slow Dirac-envelope $\Psi_K(\mathbf{R},t)$. In TTC, the emission or absorption of a photon is described by the local cobordism operation $\mathfrak{C}_{\text{em}}$, in which the graph path changes the link phase without changing the topological class of K.

The first-order matrix element for the link phase on the edge $i \to j$ is given by

$$\delta\mathcal{M}_{i\to j}^{(A)} = -i\phi_{ij}\left\langle\Psi_{\text{out}}(j),\mathcal{U}_{ij}^{(0)}\Psi_{\text{in}}(i)\right\rangle + O(\phi_{ij}^2).$$

In the long-wavelength limit, the directional component $\mathcal{U}_{ij}^{(0)}$ generates the local symbol

$$\vec{\alpha}\cdot\hat{n}_{ij},$$

© 2026 by the author(s). Distributed under a Creative Commons CC BY license.

Preprints.org (www.preprints.org) | NOT PEER-REVIEWED | Posted: 9 June 2026 doi:10.20944/preprints202606.0589.v1

where $\vec{\alpha} = \gamma^0\vec{\gamma}$ acts in the effective Dirac-envelope space $\mathcal{H}_K^{\text{eff}} \simeq \mathbb{C}^4$. Therefore, the spatial part of the transit amplitude takes the form

$$\delta\mathcal{M}_{i\to j}^{(A)} \propto \frac{q_{\text{top}} a_0}{\hbar}(\hat{n}_{ij}\cdot\mathbf{A})\Psi_{\text{out}}^\dagger(\vec{\alpha}\cdot\hat{n}_{ij})\Psi_{\text{in}}.$$

Annealed averaging and the total Dirac current

A single edge is not an observable continuous object. The observable TTC vertex arises after annealed averaging over the IR cell of the stochastic vacuum. Using the second-order moment isotropy

$$\left\langle \sum_{j\sim i} w_{ij}\hat{n}_{ij}^a\hat{n}_{ij}^b \right\rangle_{\mathfrak{G}} = \kappa_2\delta^{ab},$$

we obtain

$$\left\langle (\vec{\alpha}\cdot\hat{n}_{ij})(\hat{n}_{ij}\cdot\mathbf{A})\right\rangle_{\mathfrak{G}} = \kappa_2\vec{\alpha}\cdot\mathbf{A}.$$

After renormalizing the fields and absorbing $\kappa_2 a_0/\hbar$ into the definition of the continuous interface, the spatial part of the vertex becomes

$$\mathcal{V}_{\text{em}}^{\text{spatial}} = g_{\text{em}}\int d^4x\,\mathbf{A}(x)\cdot\left[\Psi_{\text{out}}^\dagger(x)\vec{\alpha}\Psi_{\text{in}}(x)\right].$$

The time link gives the density

$$j^0(x) = \Psi^\dagger(x)\Psi(x),$$

and the spatial part of the current is equal to

$$\mathbf{j}(x) = \Psi^\dagger(x)\vec{\alpha}\Psi(x).$$

Together, they form the full gauge-covariant Dirac current

$$\boxed{j^\mu(x) = \bar{\Psi}(x)\gamma^\mu\Psi(x)}.$$

Consequently, the TTC vertex of the electromagnetic interaction takes the standard covariant form

$$\boxed{\mathcal{M}_{\text{em}}^{\text{TTC}} = g_{\text{em}}\int d^4x\,A_\mu(x)j^\mu(x)} \tag{A12}$$

up to corrections related to the finite size of the coarse-grained cell, leakage from the Dirac-envelope sector, and residual non-ideality of the annealed isotropy.

Lemma A2 (Ward identity)**.** *The local $U(1)$-covariance of the edge transporter and the unitarity of U_m in the coherent sector imply discrete conservation of the graph current:*

$$\Delta_\mu j_G^\mu = 0.$$

After taking the annealed/coarse-grained limit, this yields

$$\partial_\mu j^\mu = 0.$$

Consequently, under the gauge transformation $A_\mu \to A_\mu + \partial_\mu\Lambda$, the amplitude in (A12) remains unchanged:

$$\delta_\Lambda\mathcal{M}_{\text{em}}^{\text{TTC}} = g_{\text{em}}\int d^4x\,\partial_\mu\Lambda\,j^\mu = -g_{\text{em}}\int d^4x\,\Lambda\,\partial_\mu j^\mu = 0,$$

up to boundary terms.

© 2026 by the author(s). Distributed under a Creative Commons CC BY license.

Preprints.org (www.preprints.org) | NOT PEER-REVIEWED | Posted: 9 June 2026 doi:10.20944/preprints202606.0589.v1

Thus, the current j^μ is not introduced as an independent Lagrangian entity. It arises as the continuous mathematical expectation of a directed spinor routing symbol when a topological cycle traverses a small $U(1)$-link fluctuation.

Appendix B.1.4. Channel Normalization of the Fine-Structure Constant from the Strata of the Micro-Operator U_m

The fine-structure constant in IKT is related not to an arbitrary numerical fit, but to the ratio of one elementary action channel to the total number of phase-topological channels available to the minimal act of electromagnetic recombination. In this section, the stratified space $\mathcal{C}_\alpha$ is constructed as a channel model of the compact part of the electromagnetic block of the microscopic operator U_m; its normalization is fixed by the quantization of the action, and then the status of the resulting quantity is separately formulated as an infrared channel anchor α_{top} and a source of scale dependence $\alpha_{\text{eff}}(\mathcal{Q}^2)$.

The key difference is as follows. In the amplitude of the quantum transition, the action appears as $\exp(iS/\hbar)$, so in the dimensionless graph normalization, the primary expression is

$$\hbar_{\text{graph}} = 1.$$

One complete closed phase cycle corresponds to a change in action

$$\Delta S = 2\pi\hbar = h, \qquad h_{\text{graph}} = 2\pi.$$

It is precisely this complete cycle, and not an infinitesimally small phase angle, that defines a single minimal allowed channel of electromagnetic translation. Therefore, the subsequent measure of phase channels is understood as a channel phase measure in units of a complete 2π-cycle of action.

Definition A9 (Electromagnetic block of the microstep operator)**.** *On an oriented edge $j \to i$, the transverse electromagnetic sector of the operator U_m takes the form*

$$U^{\text{em}}_{ij,m} = S_{ij}\big(P_\perp(\vec{n}_{ij}) \otimes \mathfrak{u}_{ij}\big), \qquad \mathfrak{u}_{ij} = e^{i\varphi_{ij}} R_{ij},$$

where S_{ij} is the state shift along the oriented edge, $P_\perp$ is the transverse projector, $\varphi_{ij} = q_{\text{em}}\theta_{ij}$ is— the local $U(1)$ phase of the edge, and $R_{ij} \in SU(2)$ — the spinor transport of the internal transverse frame. After isolating the graph shift and the projector, the entire compact phase freedom of the electromagnetic channel is given by the pair

$$(e^{i\varphi}, R) \in U(1)_\varphi \times SU(2)_R.$$

Here, the spinor cover is used, rather than the factorization $(U(1) \times SU(2))/\mathbb{Z}_2$. This is essential: the sign $R = -I$ is not identified until fermionic recombination is complete, since the spinor cycle distinguishes between 2π- and 4π-closures.

The local gauge freedom at the nodes acts on $\mathfrak{u}_{ij}$ via conjugations and phase shifts. Therefore, physically distinguishable recombination channels are classified not by individual matrix elements U_m, but by orbits of the compact part of $U(1)_\varphi \times SU(2)_R$. This action has three natural orbital types.

Definition A10 (Strata of the electromagnetic recombination phase space)**.** *The stratified space of electromagnetic recombination is defined as the disjoint union of orbital types*

$$\mathcal{C}_\alpha = \mathcal{C}_4 \sqcup \mathcal{C}_2 \sqcup \mathcal{C}_1.$$

They are defined as follows.

1. ***Regular four-dimensional sector:***

$$\mathcal{C}_4 = U(1)_\varphi \times SU(2)_R.$$

© 2026 by the author(s). Distributed under a Creative Commons CC BY license.

Preprints.org (www.preprints.org) | NOT PEER-REVIEWED | Posted: 9 June 2026 doi:10.20944/preprints202606.0589.v1

This is the general case in which the edge $U(1)$ phase and the spinor $SU(2)$ transport are independent, and the channel stabilizer is discrete.

2. ***Reduced two-dimensional sector:***

$$\mathcal{C}_2 = \big([0,\pi]_\varphi \times [0,\pi]_\vartheta\big)_{\mathrm{red}}.$$

It arises when the $SU(2)$ transport falls into the maximal torus $T \subset SU(2)$,

$$R(\vartheta) = \exp(i\vartheta\sigma_z),$$

and therefore has an additional Abelian stabilizer. The range $[0,\pi]$ arises from two independent involutions: the charge conjugation $\varphi \sim -\varphi$ in the $U(1)$-phase and the Weyl identity $\vartheta \sim -\vartheta$ in the Cartan torus $SU(2)$.

3. ***One-dimensional phase-locked sector:***

$$\mathcal{C}_1 = \{(\eta,\eta) : 0 \le \eta \le \pi\}_{\mathrm{lock}}.$$

This is a fixed line of intersection between the charge and spinor reductions, where the $U(1)$ phase and the Cartan angle $SU(2)$ cease to be independent. Physically, it describes the limiting channel in which the same phase parameter simultaneously determines the charge loop phase and the spinor rotation of the transverse frame.

Definition A11 (Information Channel Measure)**.** *Let $\mathcal{C}_\alpha$ be the stratified space of phase channels of electromagnetic recombination:*

$$\mathcal{C}_\alpha = \mathcal{C}_4 \sqcup \mathcal{C}_2 \sqcup \mathcal{C}_1, \qquad \mathcal{S}_\alpha = \{4,2,1\}.$$

Each stratum $\mathcal{C}_s$ is an independent phase-topological channel of internal dimension

$$d_s = s$$

and is equipped with an induced canonical measure $d\omega_s$.

Let $\delta\varphi$ be the universal fundamental phase resolution of the graph translator. The number of hardware phase microstates in the stratum $\mathcal{C}_s$ has the asymptotic form

$$N_s(\delta\varphi) = \frac{1}{(\delta\varphi)^{d_s}} \int_{\mathcal{C}_s} d\omega_s + o\Big((\delta\varphi)^{-d_s}\Big).$$

The information channel measure of the stratum is defined as the dimension-normalized capacity:

$$\boxed{\mu_s(\mathcal{C}_s) = \lim_{\delta\varphi\to 0} N_s(\delta\varphi)(\delta\varphi)^{d_s} = \int_{\mathcal{C}_s} d\omega_s}.$$

Axiom 1 (Orthogonality of Phase Channels)**.** *Each stratum $\mathcal{C}_s$ defines an orthogonal subchannel of the phase routing Hilbert space:*

$$\mathcal{H}_\alpha = \bigoplus_{s\in\mathcal{S}_\alpha} \mathcal{H}_s, \qquad P_s P_t = \delta_{st} P_s.$$

The microrouting operator U_m can route a phase packet through any of these channels, but the channels themselves are independent alternative transport branches.

Axiom 2 (Channel Dimension Normalization)**.** *The raw counts of hardware phase cells $N_s(\delta\varphi)$ are not physically comparable between strata of different dimensions. The only comparable quantity is the specific channel capacity*

$$\mu_s = \lim_{\delta\varphi\to 0} N_s(\delta\varphi)(\delta\varphi)^{d_s}.$$

© 2026 by the author(s). Distributed under a Creative Commons CC BY license.

Preprints.org (www.preprints.org) | NOT PEER-REVIEWED | Posted: 9 June 2026 doi:10.20944/preprints202606.0589.v1

This eliminates the artificial dominance of the raw 4D count $N_4 \sim (\delta\varphi)^{-4}$ over the lower strata: each channel is normalized by its own phase resolution.

Axiom 3 (Additivity of the direct sum of channels)**.** *If the channels are orthogonal, then the total information capacity of phase recombination is equal to the direct sum of the channels:*

$$\mu(\mathcal{C}_\alpha) = \mathrm{Tr}_{\mathrm{ch}}\,\mu = \sum_{s\in\mathcal{S}_\alpha} \mu_s(\mathcal{C}_s).$$

This sum is not the volume of a single manifold of mixed dimension; it is the sum of the capacities of independent phase channels.

Definition A12 (Canonical quotient normalization)**.** *Let the physical channel $\mathcal{C}_s$ be obtained from the parameterizing space $\widetilde{\mathcal{C}}_s$ by factorization with respect to the group of redundant descriptions $\mathcal{G}_s$:*

$$\mathcal{C}_s = \widetilde{\mathcal{C}}_s/\mathcal{G}_s.$$

Then the canonical channel measure is given by the quotient volume:

$$\mu_s(\mathcal{C}_s) = \int_{\widetilde{\mathcal{C}}_s/\mathcal{G}_s} d\omega_s.$$

For a finite discrete group $\mathcal{G}_s$, this is equivalent to

$$\mu_s(\mathcal{C}_s) = \frac{1}{|\mathcal{G}_s|}\int_{\widetilde{\mathcal{C}}_s} d\widetilde{\omega}_s.$$

Two points in the parameterizing space connected by a gauge reparameterization, indistinguishable orientation, frame stabilizer, or phase locking are not considered different information microchannels.

Definition A13 (Admissible electromagnetic recombination channel)**.** *A stratum $\mathcal{C}_s$ is part of $\mathcal{C}_\alpha$ if and only if the following conditions are satisfied:*

$$\begin{aligned} P_s U_m P_{\mathrm{in}} &\neq 0,\\ P_{\mathrm{out}} U_m P_s &\neq 0,\\ [P_s, Q_{\mathrm{top}}] &= 0,\\ \mu_s(\mathcal{C}_s) &< \infty. \end{aligned}$$

Here, P_{in} and P_{out} denote the input and output phase sectors of recombination, Q_{top} denotes the topological charge index of access to the $U(1)$ channel, and P_s denotes the projector onto the corresponding channel.

Lemma A3 (Canonical Volumes of the Three Phase Strata)**.** *In the minimal normalization of the phase action $\hbar_{\mathrm{graph}} = 1$, the three admissible channels have the following quotient volumes:*

$$\begin{aligned} &\mathcal{C}_4 \simeq S^1_{\mathrm{phase}} \times S^3_{\mathrm{frame}}, && \mu_4 = (2\pi)(2\pi^2) = 4\pi^3,\\ &\mathcal{C}_2 \simeq (S^1 \times S^1)/(\mathbb{Z}_2 \times \mathbb{Z}_2), && \mu_2 = \frac{(2\pi)^2}{4} = \pi^2,\\ &\mathcal{C}_1 \simeq S^1/\mathbb{Z}_2, && \mu_1 = \frac{2\pi}{2} = \pi. \end{aligned}$$

Proof. For a regular sector, we use the product of the standard measure on $U(1)$ and the Haar measure on $SU(2) \simeq S^3$:

$$\mu_4(\mathcal{C}_4) = \mathrm{Vol}(U(1))\,\mathrm{Vol}(SU(2)) = (2\pi)(2\pi^2) = 4\pi^3.$$

© 2026 by the author(s). Distributed under a Creative Commons CC BY license.

Preprints.org (www.preprints.org) | NOT PEER-REVIEWED | Posted: 9 June 2026 doi:10.20944/preprints202606.0589.v1

The reduced sector is obtained from the two-torus parametrization after factorizing out the charge conjugation and the Weyl reflection:

$$\mu_2(\mathcal{C}_2) = \frac{(2\pi)^2}{|\mathbb{Z}_2 \times \mathbb{Z}_2|} = \pi^2.$$

In the phase-locked sector, a single independent parameter of the total S^1 remains after identifying opposite phases:

$$\mu_1(\mathcal{C}_1) = \frac{2\pi}{2} = \pi.$$

Singular strata have zero measure with respect to the four-dimensional Haar measure, but in stratified phase counting they are distinct orbital types of the electromagnetic block U_m and are therefore accounted for by their own internal information measures. □

Postulate A6 (Normalization of a unit channel by the action h)**.** *One elementary channel of electromagnetic translation corresponds to one complete closed phase cycle of the electromagnetic block U_m:*

$$\exp(iS/\hbar) \mapsto \exp(i(S+h)/\hbar) = \exp(iS/\hbar).$$

Consequently,

$$\Delta S = h = 2\pi\hbar,$$

and the measure of a single minimal allowed channel in units of h is

$$\mu_{\text{ch}} = 1.$$

Postulate A7 (Spectral equipartition of orthogonal channels)**.** *The routing micro-operator U_m acts on the direct sum of orthogonal phase channels*

$$\mathcal{H}_\alpha = \bigoplus_{s \in \mathcal{S}_\alpha} \mathcal{H}_s.$$

In the general case, the total channel capacity is given by

$$\alpha_{\text{ch}}^{-1} = \sum_{s \in \mathcal{S}_\alpha} \rho_s \, \mu_s(\mathcal{C}_s),$$

where ρ_s is the spectral access density of the micro-operator U_m to the stratum $\mathcal{C}_s$. The postulate of information equipartition states that in the canonical normalization $\hbar_{\text{graph}} = 1$ and in the zero-infrared approximation, the allowed orthogonal channels have equal spectral weights:

$$\rho_4 = \rho_2 = \rho_1 = 1.$$

A possible violation of strict equipartition is described by a small infrared polarization correction

$$\rho_s = 1 + \delta\rho_s^{\text{IR}}, \qquad |\delta\rho_s^{\text{IR}}| \ll 1.$$

This correction is not identical to the total running polarization $\Pi_{\text{IKT}}(\mathcal{Q}^2)$; it describes only the low-energy deviation from the equality of channel spectral weights.

Proposition A1 (Channel count of topological fine structure)**.** *Under spectral equipartition $\rho_4 = \rho_2 = \rho_1 = 1$, the total information capacity of the electromagnetic recombination channel is equal to*

$$\mu(\mathcal{C}_\alpha) = \rho_4\mu_4 + \rho_2\mu_2 + \rho_1\mu_1 = 4\pi^3 + \pi^2 + \pi.$$

© 2026 by the author(s). Distributed under a Creative Commons CC BY license.

Preprints.org (www.preprints.org) | NOT PEER-REVIEWED | Posted: 9 June 2026 doi:10.20944/preprints202606.0589.v1

In the normalization $\hbar_{\mathrm{graph}} = 1$, the topological constant of the fine structure is defined as the weight of a single elementary h-channel relative to the total channel capacity:

$$\boxed{\alpha_{\mathrm{top}} = \frac{\mu_{\mathrm{ch}}}{\mu(\mathcal{C}_\alpha)} = \frac{1}{4\pi^3 + \pi^2 + \pi}}.$$

Equivalently,

$$\boxed{\alpha_{\mathrm{top}}^{-1} = 4\pi^3 + \pi^2 + \pi}.$$

Proof. By definition of the information channel measure, each stratum $\mathcal{C}_s$ contributes not a raw number of hardware microstates $N_s(\delta\varphi)$, but a dimension-normalized capacity

$$\mu_s = \lim_{\delta\varphi \to 0} N_s(\delta\varphi)(\delta\varphi)^{d_s}.$$

By the orthogonality axiom, the channels $\mathcal{C}_4$, $\mathcal{C}_2$, and $\mathcal{C}_1$ correspond to mutually orthogonal subspaces $\mathcal{H}_4$, $\mathcal{H}_2$, and $\mathcal{H}_1$. Consequently, the total capacity is the trace of the direct sum of the channels with weights ρ_s:

$$\mu(\mathcal{C}_\alpha) = \sum_s \rho_s \mu_s.$$

At the spectral equipartition point $\rho_s = 1$, substituting the canonical quotient volumes gives

$$\mu(\mathcal{C}_\alpha) = 4\pi^3 + \pi^2 + \pi.$$

Since one elementary channel is normalized as $\mu_{\mathrm{ch}} = 1$, the formula for α_{top} follows from the previous expression. □

Remark A4 (Status of the information-channel formula)**.** *The formula for α_{top} is not a theorem about the standard Haar measure and is not an unconditional consequence of a single topology. It is a conditional no-fit channel anchor, following from three independent elements: the admissibility of the strata $\mathcal{C}_4, \mathcal{C}_2, \mathcal{C}_1$, the canonical quotient norm, and the spectral equipartition postulate $\rho_s = 1$.*

Strata of different internal dimensions do not add up as geometric volumes of a single space. What add up are the dimension-normalized information capacities of orthogonal transport channels. Therefore, the paradoxical dominance of the raw 4D number of microstates over the lower strata does not arise: each capacity is first normalized to its own phase quantum $(\delta\varphi)^{d_s}$, and then enters the trace via the direct sum of channels.

A rigorous derivation of α_{top} from the microdynamics U_m requires, in the future, a proof of equipartition $\rho_s = 1$ as a spectral property of the electromagnetic routing block. Until such a proof is provided,

$$\alpha_{\mathrm{top}}^{-1} = 4\pi^3 + \pi^2 + \pi$$

has the status of a conditional topological prediction, rather than an absolute geometric theorem.

Two-Step Derivation of the Elementary Charge

In the rationalized SI notation, the fine-structure constant, the elementary charge, Planck's constant, and the speed of light are related by the equation

$$\alpha = \frac{e^2}{4\pi\varepsilon_0 \hbar c_0}.$$

Therefore, in IKT, one cannot simultaneously treat e as an independent, irreducible parameter and use α_{top} as the channel anchor of the electromagnetic block U_m. This would amount to double-counting the same calibration normalization.

© 2026 by the author(s). Distributed under a Creative Commons CC BY license.

Preprints.org (www.preprints.org) | NOT PEER-REVIEWED | Posted: 9 June 2026 doi:10.20944/preprints202606.0589.v1

The solution consists of a two-step transition from dimensionless topology to dimensional macrophysics. In the first step, the fundamental object is not the SI charge in coulombs, but the minimal dimensionless electromagnetic gauge channel

$$g_{\mathrm{em}}.$$

Since α_{top} is defined as the channel weight of a single quantized h-action channel relative to all available phase-topological channels of the electromagnetic block,

$$\alpha_{\mathrm{top}} = \frac{\mu_{\mathrm{ch}}}{\mu(\mathcal{C}_\alpha)},$$

the minimal dimensionless $U(1)$ coupling is given by the formula

$$\boxed{g_{\mathrm{em}}^2 = 4\pi\alpha_{\mathrm{top}}}, \qquad g_{\mathrm{em}} = \sqrt{4\pi\alpha_{\mathrm{top}}}.$$

It is precisely g_{em}, and not the dimensional quantity e, that is the primary gauge normalization of the IKT electromagnetic sector.

In the second step, a macroscopic system of electromagnetic units is chosen. In the rationalized SI normalization, the dimensional projection of the minimal channel is equal to

$$\boxed{e_{\mathrm{top}} = \sqrt{4\pi\varepsilon_0\hbar c_0\,\alpha_{\mathrm{top}}}}.$$

Here, ε_0 is not introduced as a new microscopic entity of the graph. It is a coefficient of the macroscopic electromagnetic normalization that converts the dimensionless coupling g_{em} into the SI unit of the coulomb. In Heaviside–Lorentz units or natural units, this second step simply vanishes, and the fundamental information remains in the dimensionless number $g_{\mathrm{em}}^2 = 4\pi\alpha_{\mathrm{top}}$.

Thus, the elementary charge ceases to be an external dimensional parameter of the Standard Model. It becomes the SI projection of a conventionally normalized dimensionless electromagnetic coupling:

$$e_{\mathrm{top}} \longleftrightarrow \alpha_{\mathrm{top}} \longleftrightarrow \mathcal{C}_\alpha = \mathcal{C}_4 \sqcup \mathcal{C}_2 \sqcup \mathcal{C}_1.$$

At a finite resolution scale, it is not the topological anchor that changes, but the effective polarization coupling. Therefore, the running charge is defined via the running constant

$$e_{\mathrm{eff}}(\mathcal{Q}^2) = \sqrt{4\pi\varepsilon_0\hbar c_0\,\alpha_{\mathrm{eff}}(\mathcal{Q}^2)}.$$

Low-Energy Renormalization and the Scale Dependence of $\alpha(\mathcal{Q}^2)$

The resulting quantity should not be interpreted as the value of the electromagnetic coupling at all energy scales and should not be automatically identified with the experimental number $\alpha(0)$. The formula

$$\alpha_{\mathrm{top}}^{-1} = 4\pi^3 + \pi^2 + \pi$$

defines the *infrared channel anchor*: the conditional trace of the chosen stratified measure of the electromagnetic sector after the massive and topologically non-trivial virtual excitations of the graph are contracted into a compact orbital-type capacity $\mathcal{C}_\alpha$. In the idealized limit with no residual infrared polarization, we can write

$$\alpha_{\mathrm{anchor}} \equiv \alpha_{\mathrm{top}}.$$

The physically measurable low-energy constant admits a small correction

$$\alpha_{\mathrm{obs}}(0) = \frac{\alpha_{\mathrm{top}}}{1 - \Pi_{\mathrm{IR}}}, \qquad |\Pi_{\mathrm{IR}}| \ll 1.$$

© 2026 by the author(s). Distributed under a Creative Commons CC BY license.

Preprints.org (www.preprints.org) | NOT PEER-REVIEWED | Posted: 9 June 2026 doi:10.20944/preprints202606.0589.v1

For the values $\alpha_{\mathrm{top}}^{-1} = 137.0363038$ and $\alpha_{\mathrm{obs}}(0)^{-1} \simeq 137.035999$, this corresponds to $\Pi_{\mathrm{IR}} \simeq 2.2 \times 10^{-6}$. Hereinafter, the notation α_{top} refers to the pure topological anchor, rather than to a running constant at an arbitrary momentum resolution.

Here, $\mathcal{Q}^2$ denotes the external resolution scale of the probe. For space-like exchange, one can consider $\mathcal{Q}^2 > 0$ to be the Euclidean momentum scale; time-like processes are obtained by analytical continuation, taking into account the thresholds for the emergence of the corresponding topological resonances. When $\mathcal{Q}^2 = 0$, an ideal probe observes the convolved channel count, but a specific experimental setup may retain a residual polarization correction Π_{IR}. Therefore

$$\lim_{\mathcal{Q}^2 \to 0} \alpha_{\mathrm{eff}}^{\mathrm{ideal}}(\mathcal{Q}^2) = \alpha_{\mathrm{top}}, \qquad \alpha_{\mathrm{eff}}(0) = \frac{\alpha_{\mathrm{top}}}{1 - \Pi_{\mathrm{IR}}}.$$

At finite resolution, the electromagnetic block U_m is no longer a rigid compact cell $U(1)_\varphi \times SU(2)_R$. An external probe is capable of virtually exciting additional local channels of the graph: polarization loops, charge-anticharge node pairs, short-lived edge inserts, and resonant deformations of the transverse frame. These channels do not change the basic topological measure $\mu(\mathcal{C}_\alpha)$; they alter the effective channel conductance/impedance, that is, they renormalize the coupling observed by the probe.

In IKT, this is conveniently written as

$$\alpha_{\mathrm{eff}}(\mathcal{Q}^2) = \frac{\alpha_{\mathrm{top}}}{1 - \Pi_{\mathrm{IKT}}(\mathcal{Q}^2)}, \qquad \Pi_{\mathrm{IKT}}(0) = \Pi_{\mathrm{IR}},$$

or, equivalently, in terms of the inverse channel capacitance

$$\alpha_{\mathrm{eff}}^{-1}(\mathcal{Q}^2) = \mu(\mathcal{C}_\alpha)\,[1 - \Pi_{\mathrm{IKT}}(\mathcal{Q}^2)] = \mu(\mathcal{C}_\alpha) - \Delta\mu_{\mathrm{pol}}(\mathcal{Q}^2),$$

where

$$\Delta\mu_{\mathrm{pol}}(\mathcal{Q}^2) = \mu(\mathcal{C}_\alpha)\Pi_{\mathrm{IKT}}(\mathcal{Q}^2).$$

The minus sign in front of $\Delta\mu_{\mathrm{pol}}$ has a simple meaning: virtually excited channels do not add to the static number of final microstates, but rather reduce the effective inverse stiffness of the electromagnetic channel. As a result, as the resolution increases, the coupling may strengthen, even though the initial topological count $\mu(\mathcal{C}_\alpha)$ remains unchanged.

The function Π_{IKT} is the graph-theoretic analogue of vacuum polarization. Its spectral structure should be determined not by external phenomenological constants, but by the complete set of charged topological excitations of the graph:

$$\Pi_{\mathrm{IKT}}(\mathcal{Q}^2) = \sum_{\lambda \in \mathcal{S}_{\mathrm{ch}}} \Pi_\lambda\left(\frac{\mathcal{Q}^2}{M_\lambda^2}, C_\lambda, \mu_\lambda\right),$$

where $\mathcal{S}_{\mathrm{ch}}$ is the spectrum of charged graph resonances, M_λ are their topological masses, C_λ are the complexities of the node class, and μ_λ are the internal phase measures of the corresponding channels. When $\mathcal{Q}^2 \ll M_\lambda^2$, the contribution of this resonance is suppressed; upon reaching the threshold, it begins to participate in the polarization renormalization.

Thus, the formula $\alpha_{\mathrm{top}}^{-1} = 4\pi^3 + \pi^2 + \pi$ does not compete with the scale dependence of the electromagnetic coupling. It defines a pure infrared topological anchor, whereas the running $\alpha_{\mathrm{eff}}(\mathcal{Q}^2)$ arises as a dynamic response of the graph to finite resolution. In the current renormalization, the channel sum gives $\alpha_{\mathrm{top}}^{-1} = 137.0363038$; its difference from the physical $\alpha_{\mathrm{obs}}(0)^{-1} \simeq 137.035999$ is determined by a small value of Π_{IR} and remains a task of microscopic inference from the spectrum of low-energy polarization modes. This separates three tasks: the channel sum of the compact block U_m, the infrared polarization correction, and the actual renormalization group of the IKT at $\mathcal{Q}^2 > 0$.

© 2026 by the author(s). Distributed under a Creative Commons CC BY license.

Preprints.org (www.preprints.org) | NOT PEER-REVIEWED | Posted: 9 June 2026 doi:10.20944/preprints202606.0589.v1

Thus, the three terms in the formula for α_{top}^{-1} acquire different microscopic meanings: $4\pi^3$ — the volume of the regular spinor-phase sector $U(1) \times SU(2)$, π^2 — the measure of the Abelianized Cartan sector with discrete identities, and π — the measure of the fully phase-locked line. The numerator of the formula is no longer an arbitrary unit: it is fixed by the quantization of the action, since one complete phase cycle has a dimensionless measure $h_{\text{graph}} = 2\pi$. Therefore, the low-energy anchor of the fine-structure constant acquires a channel interpretation

$$\boxed{\alpha_{\text{top}} = \frac{\mu_{\text{ch}}}{\mu(\mathcal{C}_\alpha)}}.$$

In other words, the numerator contains a single action quantum, while the denominator contains all available phase channels of the electromagnetic block U_m. Equivalently, α_{top} is the ratio of a single quantized h-channel of action to the total phase-topological capacity of the electromagnetic block. In this form, the formula ceases to be a simple numerical fit and becomes a conditional statement about the phase count of orbital types in the compact part of the micro-operator U_m.

Appendix B.1.5. Photon Dispersion as a Projection of Vacuum Kinematics

The high-energy dispersion of photon packets is not an independent electromagnetic-channel effect. It is the projection of the universal stochastic-vacuum dispersion derived in subsection A.2.8 onto the transverse $U(1)$-link sector. Therefore the coefficient

$$\eta_4 - \frac{\lambda_{\text{wave}}}{12}$$

belongs to the vacuum graph ensemble, not to the fine-structure normalization and not to electromagnetic vacuum polarization. Electromagnetic running and polarization are encoded in the charged-channel response of $\alpha_{\text{eff}}(\mathcal{Q}^2)$, whereas the DSR-like correction is a universal property of the coherent massless branch of the stochastic graph vacuum.

In this language the generic coherent massless envelope $\mathcal{W}_m$ of subsection A.2.8 is projected as

$$\mathcal{W}_m \longrightarrow \mathbf{A}_m^{\perp}$$

for the transverse photon branch. This keeps the hierarchy explicit:

$$\text{stochastic vacuum kinematics} \longrightarrow \text{transverse } U(1) \text{ projection} \longrightarrow \text{Maxwell interface.}$$

Appendix B.1.6. Topological Symmetry and the Nature of the Magnetic Monopole

In IKT, the concept of charge is transformed from the category of "internal properties of particles" to the category of "graph topology." Electric charge (q_e) is a kinetic algorithmic phenomenon—a local phase delay during translation. Magnetic charge (q_m) is a topological defect of the adjacency matrix of the graph itself.

In this subsection, the Heaviside–Lorentz normalization is used. In natural units $\hbar = c_0 = 1$, the Dirac condition takes the form

$$q_e q_m = 2\pi n, \qquad n \in \mathbb{Z}.$$

Upon restoring dimensions:

$$\boxed{\frac{q_e q_m}{2\pi\hbar c_0} \in \mathbb{Z}}.$$

This condition is interpreted as a requirement for the uniqueness of the compact $U(1)$ phase on the graph in the presence of a non-trivial topological defect.

In a macroscopic "hedgehog" defect, the phase vectors $\vec{n}_{ij}$ point radially outward. The surface integral of the magnetic induction around the defect does not vanish but yields a topological invariant,

© 2026 by the author(s). Distributed under a Creative Commons CC BY license.

Preprints.org (www.preprints.org) | NOT PEER-REVIEWED | Posted: 9 June 2026 doi:10.20944/preprints202606.0589.v1

the normalization of which depends on the chosen unit system. In the Heaviside–Lorentz notation, the minimal monopole charge satisfies the Dirac condition given above. IKT does not require the creation of such defects in modern colliders: their creation implies a global topological rearrangement of the adjacency matrix, rather than a local excitation of the field on a fixed graph.

Appendix B.2. Strong Interaction: Color Routing, Singletness, and Confinement

The electromagnetic sector arises from an Abelian $U(1)$-link phase, which changes the phase of the route without altering its internal topological stitching. The strong interaction has a different status. It is associated not with a single scalar phase on an edge, but with a non-Abelian permutation of the internal color routes of a closed topological cycle. Therefore, the strong sector in the present bridge has the status of a color-routing interface: it specifies the form of the color current and the condition of confinement singletness, but does not claim to provide a complete derivation of running QCD, Λ_{QCD}, and the hadron spectrum.

In the minimal stochastic ansatz, the edge transporter takes the form

$$\mathcal{U}_{ij} = L_{ij}\Gamma_{ij}R_{ij}.$$

For the color sector, this transporter is extended by an internal routing factor:

$$\boxed{\mathcal{U}_{ij}^{\mathrm{col}} = L_{ij}\Gamma_{ij}R_{ij}\,\mathcal{C}_{ij}}$$

where

$$\mathcal{C}_{ij} \in SU(3)_{\mathrm{route}}$$

acts on the three-dimensional internal space of color routes

$$\mathcal{H}_{\mathrm{col}} = \mathrm{span}\{|r\rangle, |g\rangle, |b\rangle\}.$$

Here, $SU(3)_{\mathrm{route}}$ is not postulated as an external gauge group over spacetime. In IKT, it is interpreted as the group of automorphisms of the three-equivalent internal routing capacity of a closed cycle. The complete derivation of this group as the unique automorphism group of the color route is a separate task; in the present framework, it is fixed as the minimal non-Abelian color structure compatible with baryonic singlet coupling.

Appendix B.2.1. Non-Abelian Link Phase and Color Current

Let the small color perturbation of an edge be given by

$$\mathcal{C}_{ij} = \exp\left[-i\theta_{ij}^{A}T_{A}\right], \qquad A = 1,\ldots,8,$$

where T_A are the generators of $su(3)$ in the fundamental representation. In the continuous interface

$$\theta_{ij}^{A} = g_s\int_i^j G_\mu^A dx^\mu.$$

Expansion in terms of the small θ_{ij}^{A} gives the first non-Abelian contribution to the TTC amplitude:

$$\delta\mathcal{M}_{i\to j}^{(G)} \propto -i\theta_{ij}^{A}\left\langle \Psi_{\mathrm{out}}(j), \mathcal{U}_{ij}^{(0)}T_A\Psi_{\mathrm{in}}(i)\right\rangle.$$

After annealed averaging over the local stochastic cell and taking the Dirac-envelope limit, a color current arises

$$\boxed{J_A^\mu(x) = \bar{\Psi}(x)\gamma^\mu T_A\Psi(x)}.$$

© 2026 by the author(s). Distributed under a Creative Commons CC BY license.

Preprints.org (www.preprints.org) | NOT PEER-REVIEWED | Posted: 9 June 2026 doi:10.20944/preprints202606.0589.v1

The corresponding TTC vertex of the strong interface has the standard non-Abelian form

$$\boxed{\mathcal{M}^{\mathrm{TTC}}_{\mathrm{strong}} = g_s \int d^4x\, G^A_\mu(x) J^\mu_A(x)}$$

with corrections related to the finite size of the topological cycle, leakage from the color-routing sector, and non-Abelian self-routing terms.

Appendix B.2.2. Confinement as a Singlet-Routing Constraint

Unlike the electromagnetic $U(1)$ channel, the color routing factor does not specify a free long-range charge. Physical asymptotic states in IKT must be closed topological routes. This leads to the singlet-routing constraint:

$$\boxed{Q^{\mathrm{col}}_A |\Psi_{\mathrm{phys}}\rangle = 0, \qquad A = 1, \ldots, 8.} \tag{A13}$$

For a meson route, this corresponds to the $\bar{q}q$ singlet,

$$|\Psi_{\mathrm{meson}}\rangle \propto \delta^a_b |q_a \bar{q}^b\rangle,$$

and for the baryon route —

$$|\Psi_{\mathrm{baryon}}\rangle \propto \epsilon_{abc} |q^a q^b q^c\rangle.$$

An open color end is not a valid asymptotic state, since it requires an open routing suture. Its amplitude is suppressed by the topological action of the color string:

$$\mathcal{A}_{\mathrm{nonsinglet}}(R) \sim \exp\left[-\frac{S_{\mathrm{conf}}(R)}{\hbar_{\mathrm{graph}}}\right],$$

where, in the long route,

$$S_{\mathrm{conf}}(R) \sim \sigma_{\mathrm{top}} RT.$$

Thus, confinement in IKT is not a supplementary potential, but rather a condition of topological closure of admissible routes.

Singlet Screening of Macroscopic Vacuum Chirality

A critical test is the question: why does the global chirality of the vacuum graph

$$\Xi_{\mathrm{vac}} \neq 0,$$

which defines a left-chiral weak-gateway, does not lead to large P- and CP-violations in the strong sector. In IKT, the answer is related to the singlet-routing constraint (A13).

Background chirality can be transferred to the color routing sector only via an adjoint deformation of the form

$$\delta H^{\mathrm{col}}_\Xi = \Xi_{\mathrm{vac}}\, \xi^A T_A,$$

where T_A are the generators of $su(3)_{\mathrm{route}}$, and ξ^A is the local coefficient of chiral skew transfer to the color sector. For a physical meson or baryon singlet

$$\langle \Psi_{\mathrm{singlet}} | T_A | \Psi_{\mathrm{singlet}} \rangle = 0,$$

therefore

$$\langle \Psi_{\mathrm{singlet}} | \delta H^{\mathrm{col}}_\Xi | \Psi_{\mathrm{singlet}} \rangle = 0.$$

The global chirality of the vacuum can manifest in open or surgically broken frames of the weak-gateway sector, but is screened in closed color singlets.

© 2026 by the author(s). Distributed under a Creative Commons CC BY license.

Preprints.org (www.preprints.org) | NOT PEER-REVIEWED | Posted: 9 June 2026 doi:10.20944/preprints202606.0589.v1

This mechanism eliminates the direct transfer of cosmological chirality into observable strong singlet amplitudes. The complete elimination of the strong θ-angle analogue requires an additional topological condition

$$\theta_{\text{col}}^{\text{top}} = 0 \mod 2\pi,$$

or its derivation from the future automorphism theorem of $SU(3)_{\text{route}}$. Therefore, this section serves as a protective lemma for color singlets, rather than a complete solution to all strong-CP questions.

Appendix B.2.3. Topological Entanglement and Hadronic Consequences of the Color-Routing Interface

After fixing the interface level $SU(3)_{\text{route}} \Rightarrow J_A^\mu$ and the singlet-routing constraint, we can consider the hadronic consequences of this same strong sector: the confinement tube, the baryon spectral-channel cell, the proton and neutron anchors, as well as the roadmap running-couplings.

The strong interaction is a contact, non-perturbative effect. It arises where the local topology of the graph and the routing operator U_m form a complex closed color loop.

The Confinement Mechanism and the Dimensionless String Tension

A quark in IKT is not an independent, topologically closed particle. It is an incomplete cyclic subgraph with an open color channel. Such a channel cannot be freely emitted into three-dimensional vacuum: due to destructive interference of transverse phases, Gauss's law on the graph degenerates into one-dimensional routing. The color current forms a linear phase tube.

The topological conclusion of confinement lies primarily in the linearity of the potential. If the length of the tube contains N_{col} coarse-grained color steps, then its dimensionless energy takes the form

$$\mathcal{E}_{\text{str}}^{\text{graph}}(N_{\text{col}}) = \hat{\sigma}_{\text{col}} N_{\text{col}},$$

where

$$\hat{\sigma}_{\text{col}} = \frac{\Delta \mathcal{E}_{\text{col}}}{\Delta N_{\text{col}}}$$

— the dimensionless cost of extending the color tube by one coarse-grained color step.

After dimensional projection, the linear potential is written as

$$V(r) = \sigma_{\text{str}} r.$$

However, the absolute normalization of σ_{str} should not be directly identified with the bare value of a single fundamental vacuum node. If we use the electronic metric, then

$$\boxed{\sigma_{\text{str}} = \hat{\sigma}_{\text{QCD}} \frac{m_e^2 c_0^3}{\hbar}}.$$

Equivalently, using the bare scale of the graph, one can write

$$\sigma_{\text{str}} = \eta_{\text{col}} \frac{M_0 c_0^2}{l_0},$$

where η_{col} is the color coarse-graining and polarization factor. Without this factor, the expression $M_0 c_0^2 / l_0$ corresponds to the Planckian bare tension, rather than the observed QCD string. Consequently, IKT topologically explains the linearity of confinement, but the absolute hadronic normalization σ_{str} remains a problem for the color graph renormalization group.

When the energy threshold is exceeded, the color tube breaks, generating new closed topological pairs. A single quark does not appear in isolation because an open color channel is not a valid asymptotic state of the graph.

© 2026 by the author(s). Distributed under a Creative Commons CC BY license.

Preprints.org (www.preprints.org) | NOT PEER-REVIEWED | Posted: 9 June 2026 doi:10.20944/preprints202606.0589.v1

Effective Nonlinear Color Tube Equation and Asymptotic Freedom

The probability of translation delay in the color tube increases with the phase flux density. In the weakly nonlinear approximation, we can write

$$p_{\text{str}}(\mathbf{A}) \simeq 1 - e^{-\kappa_{\text{str}}|\mathbf{A}|^2}.$$

Substituting the saturable delay into the wave equation yields a self-focusing nonlinear term:

$$\Box\mathbf{A} + g^2|\mathbf{A}|^2\mathbf{A} = \mathbf{J}_{\text{quarks}}.$$

The minimal condition for color neutrality of the three open phase channels is given by

$$1 + e^{2\pi i/3} + e^{4\pi i/3} = 0.$$

By itself, this condition specifies the discrete symmetry C_3, not the entire group $SU(3)$. The continuous color group arises after introducing the inner product of the three channels

$$\mathcal{H}_{\text{col}} \simeq \mathbb{C}^3, \qquad \mathbf{q}_c \to G_c\mathbf{q}_c, \quad G_c \in SU(3),$$

and the requirements for baryon singlet conservation

$$\frac{1}{\sqrt{6}}\epsilon_{abc}q_1^a q_2^b q_3^c.$$

The eight gluon directions correspond to the generators $T_a = \lambda_a/2$, $a = 1, \ldots, 8$. Thus, the three-phase condition explains the minimal color neutrality, and $SU(3)$ arises as a continuous freedom of local mixing of the three color channels while preserving the norm and the singlet node.

At high energies, the dispersion term ∇^4 prevents the string from collapsing into a singularity. In the regime $\kappa_{\text{str}}|\mathbf{A}|^2 \gg 1$, the delay becomes saturated, $p_{\text{str}} \to 1$, and a further increase in flux density hardly increases the effective coupling. This provides a qualitative picture of asymptotic freedom. A quantitative confinement anchor for the strong interaction is introduced below in Section C.3.3 via the splitting of the measures of the minimal baryon cell.

Appendix B.2.4. Status of the Strong Constant

At the level of the minimal IKT bridge, the strong interface fixes the non-Abelian form of the color current and the singlet-routing constraint:

$$U_m \Rightarrow SU(3)_{\text{route}} \Rightarrow J_A^\mu \Rightarrow \text{color singlets}.$$

If a topological anchor is used

$$\alpha_s^{\text{top}} = \frac{g_s^2}{4\pi},$$

then it must be understood as a bare/topological routing value on the graph matching scale, rather than as a directly measurable running constant $\alpha_s(\mu)$. The connection to observed QCD requires a separate RG bridge:

$$\alpha_s^{\text{top}} \Rightarrow \alpha_s(\mu) \Rightarrow \Lambda_{\text{QCD}} \Rightarrow \text{hadron spectrum}.$$

In this section, this bridge is treated as an open problem rather than a completed conclusion.

The complete derivation of the $SU(3)_{\text{route}}$ group itself also remains a separate automorphism problem. The minimal goal of the strong sector of IKT is to prove a theorem of the form

$$\text{Aut}_{\text{route}}\left(\mathcal{R}_{\text{min}}^{\text{baryon}}\right) \simeq SU(3),$$

© 2026 by the author(s). Distributed under a Creative Commons CC BY license.

Preprints.org (www.preprints.org) | NOT PEER-REVIEWED | Posted: 9 June 2026 doi:10.20944/preprints202606.0589.v1

where $\mathcal{R}_{\min}^{\text{baryon}}$ is the minimal internal routing capacity of the baryonic singlet coupling. Until this theorem is established, $SU(3)_{\text{route}}$ has the status of a conditional non-Abelian color-routing interface, compatible with QCD-like singletness, but not a complete microdynamic derivation of QCD.

Appendix B.3. Weak Interaction: Cosmological Chirality, Weak Gateway, and Electroweak Interface

Appendix B.3.1. Cosmological Chirality as a Source of Parity Violation

The electromagnetic and gravitational interfaces depend on the parity-even statistics of the stochastic vacuum: the second moment of orientation gives an isotropic Laplacian, and the scalar phase delay χ_G determines refraction. Therefore, they do not require a choice between left- or right-handed chirality.

The weak charged-current interaction has a different status. In IKT, it describes not a small phase link fluctuation, but a profound graph-surgery operation: the tearing and re-gluing of a 4π-spinor frame. Such an operation is sensitive not only to local isotropy, but also to the global chirality of the vacuum graph.

This section identifies only the source of the violation of spatial parity, namely the chiral filter of the weak gate. The complete electroweak interface—$SU(2)_L$, hypercharge, the Weinberg angle, g_W, CKM/PMNS, and the low-energy Fermi limit—remains a separate matching layer and is not considered to be derived solely from cosmological chirality.

The spectral local reference frame $\mathcal{F}_i$ is in itself defined up to the choice of an orthonormal basis. For parity-even quantities, the $O(3)$ class suffices, but to define the chiral pseudoscalar, the orientation structure must be fixed. Therefore, an orientation double-cover of the local frame bundle and a discrete orientation field are introduced

$$\epsilon_i \in \{+1, -1\}.$$

Upon local reparameterization of the spectral basis

$$\hat{n}_{ij} \longrightarrow O_i \hat{n}_{ij}, \qquad O_i \in O(3),$$

the orientation field is transformed as

$$\epsilon_i \longrightarrow \operatorname{sgn}(\det O_i)\, \epsilon_i.$$

Consequently, the combination

$$\epsilon_i \det(\hat{n}_{ij}, \hat{n}_{ik}, \hat{n}_{i\ell})$$

does not depend on the arbitrary choice of a local spectral basis. After the spontaneous selection of a global orientation branch of the early graph, the admissible spin-frame transformations are $SO(3)/SU(2)$-covariant, and the global spatial reflection P changes the sign of the entire orientation section.

The pseudoscalar vacuum spin invariant is defined as the gauge-invariant density of oriented local frame triples of the stochastic graph:

$$\Xi_i = \epsilon_i \sum_{(j,k,\ell)} w_{ijk\ell} \det\big(\hat{n}_{ij}, \hat{n}_{ik}, \hat{n}_{i\ell}\big),$$

$$\boxed{\Xi_{\text{vac}} = \lim_{R\to\infty} \frac{1}{|B_R|} \sum_{i\in B_R} \Xi_i}.$$

Here, $\hat{n}_{ij}$ are the internal directions in the spectral graph coordinate system, not embedding vectors; the factor ϵ_i eliminates the dependence of the definition on the local choice of frame orientation. In IKT, a nonzero average Ξ_{vac} arises upon the spontaneous choice of one of the two CP-conjugate percolation

© 2026 by the author(s). Distributed under a Creative Commons CC BY license.

Preprints.org (www.preprints.org) | NOT PEER-REVIEWED | Posted: 9 June 2026 doi:10.20944/preprints202606.0589.v1

branches of the early graph, which is equivalent to choosing the matter branch instead of the antimatter branch. Under spatial parity

$$P: \quad \Xi_{\text{vac}} \longrightarrow -\Xi_{\text{vac}},$$

therefore, a non-zero Ξ_{vac} defines the global chiral background for weak graph surgery operations.

In the effective Dirac-envelope space, this manifests as a topological chirality filter:

$$P_\Xi = \frac{1}{2}(1 - s_\Xi \gamma^5), \qquad s_\Xi = \operatorname{sgn} \Xi_{\text{vac}}.$$

For the branch $s_\Xi = +1$ chosen in our universe, this filter coincides with the left-chiral projector

$$P_\Xi = P_L = \frac{1}{2}(1 - \gamma^5),$$

up to the sign of γ^5.

For the branch $s_\Xi = +1$ chosen in our universe, this filter coincides with the left-chiral projector

$$P_\Xi = P_L = \frac{1}{2}(1 - \gamma^5),$$

up to the sign of γ^5.

By analogy with the electromagnetic and color sectors, directed graph surgery generates an effective macroscopic current of the weak gauge:

$$\boxed{J^\mu_{\text{weak}}(x) = \bar{\Psi}(x)\gamma^\mu P_\Xi \Psi(x)}.$$

Then the amplitude of the weak gate takes the covariant form

$$\mathcal{M}^{\text{TTC}}_{\text{weak}} = g_W \int d^4x\, W_\mu(x) J^\mu_{\text{weak}}(x) + O(\varepsilon_R).$$

Here, ε_R is the amplitude of the chirally incompatible gluing operation. In the minimal topological model, it is exponentially suppressed:

$$\varepsilon_R \sim \exp\left[-\frac{\Delta S_{\text{chiral}}}{\hbar_{\text{graph}}}\right],$$

where ΔS_{chiral} is the topological cost of local inversion of the graph's background chirality. In the limit

$$\Delta S_{\text{chiral}} \gg \hbar_{\text{graph}}$$

we obtain the standard $(V - A)$-structure:

$$\mathcal{M}^{\text{TTC}}_{\text{weak}} \approx g_W \int d^4x\, W_\mu \bar{\Psi}_{\text{out}} \gamma^\mu P_L \Psi_{\text{in}}.$$

Thus, the violation of spatial parity in the weak sector is not postulated as a separate property of the local Lagrangian. It is a consequence of the global chirality of the stochastic vacuum, fixed during early cosmological percolation. In this picture, CKM/PMNS complex phases must arise from the residual complex holonomies of non-ideal gluings; their complete derivation pertains to a separate theorem of the weak/flavor interface and is not considered a completed result of this minimal bridge.

Appendix B.3.2. Electroweak Structure and Flavour Topology

The weak interaction in IKT is not a long-range free phase translation in the same sense as electromagnetism. It arises as a local algorithmic process: a short-lived resonant graph gateway in which the internal frame of a fermionic route can be remapped. In the low-energy laboratory projection,

© 2026 by the author(s). Distributed under a Creative Commons CC BY license.

Preprints.org (www.preprints.org) | NOT PEER-REVIEWED | Posted: 9 June 2026 doi:10.20944/preprints202606.0589.v1

this process should yield observable weak amplitudes, which in modern phenomenological language are encoded by the structure

$$SU(2)_L \times U(1)_Y.$$

In this section, the electroweak structure of the Standard Model is used as a *phenomenological interface*, rather than as a microscopic ontology of IKT. The group $SU(2)_L \times U(1)_Y$, hypercharges, the Weinberg angle, and CKM and PMNS mixing are not declared here to be fundamental entities and are not considered to be strictly derived from the micro-operator U_m. They serve as coordinates for describing the observed low-energy amplitudes. The task of IKT is not to accept the electroweak Lagrangian as the starting theory, but to derive from U_m those experimental invariants that this Lagrangian successfully parametrizes: left-handed weak currents, hypercharge compensation, charge ratios, and the structure of weak mixing.

Left Doublets, Right Singlets, and the Charged Weak Gate

Let P_L and P_R denote the chiral projectors. The charged weak gauge $W^{\pm}$ acts only on the left-chiral sector:

$$\mathcal{G}_W P_L = \mathcal{G}_W, \qquad \mathcal{G}_W P_R = 0.$$

Topologically, this means that left-chiral Möbius cycles have an internal frame orientation compatible with the resonant gluing of the graph, whereas right-chiral cycles do not enter the charged-current gauge.

For leptons, this yields weak doublets

$$L_{\ell L} = \begin{pmatrix} \nu_\ell \\ \ell^- \end{pmatrix}_L, \qquad \ell = e, \mu, \tau,$$

and for quarks

$$Q_{iL} = \begin{pmatrix} u_i \\ d_i \end{pmatrix}_L.$$

Right-handed fermions are an $SU(2)_L$ singlets:

$$\ell_R, \qquad u_R, \qquad d_R.$$

In the minimal version, the neutrino has no right-handed weak partner; if a sterile ν_R is introduced, it is a complete weak singlet.

It is important that right-handed charged fermions do not disappear from the entire electroweak structure. They do not participate in the charged $W^{\pm}$ gate, but carry hypercharge and therefore enter the neutral sector after Weinberg mixing:

$$T_a^{(L)} P_R = 0, \qquad Y P_R \neq 0.$$

The continuous group $SU(2)_L$ arises not as a discrete permutation of two states, but as a local freedom of unitary mixing of the two-component left-chiral space while preserving the norm:

$$\Psi_L \to G_L \Psi_L, \qquad G_L \in SU(2)_L.$$

Charged transitions are generated by the operators

$$T_{\pm}^{(L)} = T_1^{(L)} \pm i T_2^{(L)},$$

which map the upper component of the doublet to the lower one and vice versa.

© 2026 by the author(s). Distributed under a Creative Commons CC BY license.

Preprints.org (www.preprints.org) | NOT PEER-REVIEWED | Posted: 9 June 2026 doi:10.20944/preprints202606.0589.v1

Hypercharge and Electroweak Mixing

In addition to the $SU(2)_L$ node gluing, the electroweak sector contains a neutral edge phase channel $U(1)_Y$, which defines the weak hypercharge. In the effective matching layer, the covariant operator of the electroweak translation is written in the standard form

$$D_\mu = \partial_\mu + ig_L T_a^{(L)} W_\mu^a + ig_Y \frac{Y}{2} B_\mu.$$

In IKT, the fields W_μ^a and B_μ should be understood as macroscopic names for two types of graph operations:

$$W_\mu^a : \quad \text{node exchange of a left-chiral doublet,}$$

$$B_\mu : \quad \text{hypercharge phase shift of an edge channel.}$$

In the standard electroweak matching language, the electric charge is given by the sum of the internal orientation of the weak isospin and the background hypercharge flux:

$$\boxed{Q_{\text{em}} = T_3^{(L)} + \frac{Y}{2}}. \tag{A14}$$

For the left lepton doublet

$$Y(L_{\ell L}) = -1,$$

therefore

$$Q_{\text{em}}(\nu_\ell) = +\frac{1}{2} - \frac{1}{2} = 0, \qquad Q_{\text{em}}(\ell^-) = -\frac{1}{2} - \frac{1}{2} = -1.$$

For the right-handed charged lepton

$$T_3^{(L)} = 0, \qquad Y(\ell_R) = -2,$$

and again

$$Q_{\text{em}}(\ell_R) = -1.$$

Similarly for quarks:

$$Y(Q_L) = \frac{1}{3}, \qquad Y(u_R) = \frac{4}{3}, \qquad Y(d_R) = -\frac{2}{3}.$$

At this point, these values serve as electroweak matching data. Their topological reconstruction is given below, in subsection C.1.4: The fractional nature of quark charges is associated not with a mechanical division of the electromagnetic flux, but with color tripletness, hypercharge compensation within a single generation, and the shunting of right-handed singlet states into the edge $U(1)_Y$ channel.

The neutral sector contains two Q_{em}-conserving operations: the isospin-neutral W^3 channel and the hypercharge B channel. Due to the finite algorithmic rigidity of the vacuum graph, these channels are not diagonal eigenmodes of the observable translation. The eigenmodes are given by the Weinberg rotation:

$$A_\mu = B_\mu \cos\theta_W + W_\mu^3 \sin\theta_W,$$

$$Z_\mu = W_\mu^3 \cos\theta_W - B_\mu \sin\theta_W.$$

The relations satisfy

$$\tan\theta_W = \frac{g_Y}{g_L}, \qquad g_{\text{em}} = g_L \sin\theta_W = g_Y \cos\theta_W.$$

Since a channel anchor is distinguished in the electromagnetic sector of IKT

$$g_{\text{em}}^2 = 4\pi\alpha_{\text{top}},$$

© 2026 by the author(s). Distributed under a Creative Commons CC BY license.

Preprints.org (www.preprints.org) | NOT PEER-REVIEWED | Posted: 9 June 2026 doi:10.20944/preprints202606.0589.v1

the Weinberg angle becomes the geometric angle between the two neutral channels W^3 and B. Its numerical value must be derived from the ratio of the algorithmic capacities of the node gluing and the edge hypercharge translation.

Masses of W, Z, and the Masslessness of the Photon

The massiveness of weak gates in IKT is related to the finite integral delay of the resonant gluing:

$$\Theta_{\text{knot}} = \int_{\text{resonance}} \Gamma_{\text{dwell}}\, dt, \qquad p_{\text{res}} = 1 - e^{-\Theta_{\text{knot}}}.$$

In the phenomenological electroweak interface, it is convenient to use the same elastic scale F_h that normalizes the collective scalar graph mode. In the laboratory projection, this scale is expected to coincide with the measurable electroweak scale:

$$F_h \simeq v_{\text{EW}}.$$

To express the masses of weak bosons, we introduce a half-scale

$$\boxed{M_{\text{EW}} \equiv \frac{F_h}{2}}.$$

Then the charged-current gate has a mass

$$M_W = g_L M_{\text{EW}} = \frac{g_L F_h}{2},$$

and the neutral mass matrix takes the standard matching form

$$\mathcal{M}_0^2 = M_{\text{EW}}^2 \begin{pmatrix} g_L^2 & -g_L g_Y \\ -g_L g_Y & g_Y^2 \end{pmatrix}.$$

Its eigenstates are the massless photon and the massive Z boson:

$$M_A = 0, \qquad M_Z = M_{\text{EW}} \sqrt{g_L^2 + g_Y^2} = \frac{F_h}{2} \sqrt{g_L^2 + g_Y^2}.$$

Therefore,

$$\boxed{M_Z = \frac{M_W}{\cos\theta_W}}.$$

The Weinberg angle is given by the standard matching relations

$$\sin\theta_W = \frac{g_Y}{\sqrt{g_L^2 + g_Y^2}}, \qquad g_{\text{em}} = g_L \sin\theta_W = g_Y \cos\theta_W.$$

The masslessness of the photon implies that the electromagnetic $U(1)$ phase is an orthogonal, unlocked mode that does not require a left-chiral frame shift. The microdynamic derivation of the quantities measured in the laboratory frame as F_h, g_L, g_Y, and θ_W remains a key task in reconciling IKT with experiment, rather than a commitment to electroweak theory as an ontology.

Fermion Low-Energy Limit

At energies much below the mass of the W-gate, the resonance occurs only virtually, and the charged-current process reduces to a local four-fermion operator. In units of $\hbar = c_0 = 1$

$$\frac{G_F}{\sqrt{2}} = \frac{g_L^2}{8 M_W^2}.$$

© 2026 by the author(s). Distributed under a Creative Commons CC BY license.

Preprints.org (www.preprints.org) | NOT PEER-REVIEWED | Posted: 9 June 2026 doi:10.20944/preprints202606.0589.v1

In dimensional notation, the factors $\hbar$ and c_0 are restored in the usual way. In IKT, this formula implies that the weakness of the low-energy interaction is determined not by the smallness of the topological switch, but by the high energy cost of the virtual resonance gate.

CKM and PMNS as Projected Weak Re-Gluing Blocks

The CKM and PMNS matrices in this subsection are used as an effective matching parameterization of the weak renormalization. Their unitarity, hierarchy, and CP phases must be derived from the spectrum of the charged weak re-gluing operator $\mathcal{R}_W$ on the spaces of knot classes and one-dimensional correction packages, rather than being introduced as already proven microscopic results.

Fermion generations in IKT are interpreted as classes of topological complexity of a closed path. The charged-current W gate not only changes weak isospin; it also performs a local knot-class re-gluing. Therefore flavor mixing is determined not by external angles, but by matrix elements of the weak re-gluing operator.

For quarks, the relevant microscopic object is the quark charged weak re-gluing operator $\mathcal{R}_W^{(q)}$, not the color-gluon sector. The full weak re-gluing map is assumed to be an isometry on the complete quark topological Hilbert space,

$$(\mathcal{R}_W^{(q)})^\dagger \mathcal{R}_W^{(q)} = I_{\mathcal{H}_d}.$$

However, the observed CKM matrix is not the full operator $\mathcal{R}_W^{(q)}$. It is the compression of this operator to the physical three-generation up- and down-type quark subspaces:

$$V_{ij}^{\mathrm{CKM}} = \left\langle \widetilde{K}_{u_i} \middle| P_u \, \mathcal{R}_W^{(q)} \, P_d \middle| \widetilde{K}_{d_j} \right\rangle.$$

Here P_u and P_d project onto the observed three-generation mass-eigenstate sectors, and $|\widetilde{K}_{u_i}\rangle$, $|\widetilde{K}_{d_j}\rangle$ denote orthonormalized physical knot states. The probability of the corresponding charged-current transition is therefore

$$P(d_j \to u_i W^-) = |V_{ij}^{\mathrm{CKM}}|^2.$$

Exact CKM unitarity is not a consequence of an arbitrary isometry alone. It follows only under the three-generation flavour-closure condition

$$(1 - P_u)\mathcal{R}_W^{(q)} P_d = 0, \qquad \mathcal{R}_W^{(q)} \mathcal{H}_d^{(3)} = \mathcal{H}_u^{(3)}.$$

In this closed weak-flavour block one obtains

$$(V^{\mathrm{CKM}})^\dagger V^{\mathrm{CKM}} = I_3, \qquad V^{\mathrm{CKM}} (V^{\mathrm{CKM}})^\dagger = I_3.$$

If the weak re-gluing map has leakage into hidden, sterile, heavy, or non-observed topological sectors, the observed CKM block is a contraction:

$$(V^{\mathrm{CKM}})^\dagger V^{\mathrm{CKM}} = I_3 - \Delta_d,$$

with the positive semidefinite leakage operator

$$\Delta_d = P_d (\mathcal{R}_W^{(q)})^\dagger (1 - P_u) \mathcal{R}_W^{(q)} P_d \geq 0.$$

Thus CKM unitarity in IKT is a conditional consequence of weak-gateway isometry plus three-generation flavour closure, not a result of the color routing sector.

The hierarchical structure of CKM arises because preserving the topological class requires less algorithmic restructuring than a radical change in knot complexity. The exponential distance law

© 2026 by the author(s). Distributed under a Creative Commons CC BY license.

Preprints.org (www.preprints.org) | NOT PEER-REVIEWED | Posted: 9 June 2026 doi:10.20944/preprints202606.0589.v1

should be interpreted as the envelope of a raw topological overlap kernel, not as an already unitary matrix. In a leading approximation one may write

$$A_{ij}^{(q)} = \mathcal{N}_{ij} \exp\left[-\frac{\lambda_q}{2} d_{\text{knot}}(K_{u_i}, K_{d_j})\right] e^{i\phi_{ij}^{\text{topo}}}.$$

Here d_{knot} is the topological distance between knot classes, and λ_q is the stiffness of the quark knot. In the closed three-generation approximation, the physical CKM matrix is the unitary part of this overlap kernel,

$$V^{\text{CKM}} = A^{(q)} \left[(A^{(q)})^\dagger A^{(q)}\right]^{-1/2}.$$

This keeps the topological hierarchy while enforcing probability conservation inside the observed weak-flavour block. If the closed-block condition fails, the same raw kernel defines a non-unitary compressed mixing block with leakage measured by Δ_d.

For neutrinos, mixing is described analogously, but the corresponding states are not rigid three-dimensional knots, but rather softer correction packets of the graph:

$$\nu_{\alpha L} = \sum_i U_{\alpha i}^{\text{PMNS}} \nu_{iL}.$$

At the weak-gluing level,

$$U_{\alpha i}^{\text{PMNS}} = \left\langle \widetilde{L}_\alpha \middle| P_\ell \, \mathcal{R}_W^{(\ell)} \, P_\nu | \widetilde{\nu}_i \right\rangle.$$

If the active three-neutrino block is closed, U_{PMNS} is unitary in the same projected sense as CKM. If sterile or hidden graph-packet sectors are present, the observed active block becomes

$$U_{\text{PMNS}}^\dagger U_{\text{PMNS}} = I_3 - \Delta_\nu, \qquad \Delta_\nu \geq 0.$$

The effective topological stiffness of neutrino packets is significantly smaller,

$$\lambda_\nu \ll \lambda_q.$$

Therefore the off-diagonal elements of PMNS can be large, whereas CKM remains nearly diagonal.

The complex CP phases in CKM and PMNS correspond to irreducible holonomies of the weak re-gluing operator:

$$V_{ij} = |V_{ij}| e^{i\phi_{ij}^{\text{topo}}}.$$

Their numerical derivation requires the definition of a phase measure on the spaces of node reconfigurations.

Selection Rules

The following selection rules correspond to the electroweak structure of IKT:

$$W^\pm: \qquad \Delta T_3^{(L)} = \pm 1, \qquad \Delta Q_{\text{em}} = \pm 1, \qquad \Delta Y = 0,$$

$$Z, A: \qquad \Delta Q_{\text{em}} = 0, \qquad \Delta Y = 0.$$

At the tree level, neutral currents do not alter the flavor, since the eigenstates are orthogonal, and mixing occurs via the charged-current coupling through the CKM/PMNS matrices.

Appendix B.4. Gravity as Algorithmic Refraction of a Stochastic Graph Network

In IKT, gravity is described not by the self-loop probability p_j, but by the low-field optokinetic potential χ_G. The probability p_j characterizes the local delay of a defect, whereas $\chi_G(\mathbf{r})$ describes the macroscopic change in phase routing around a mass distribution. The fundamental graph is not

© 2026 by the author(s). Distributed under a Creative Commons CC BY license.

Preprints.org (www.preprints.org) | NOT PEER-REVIEWED | Posted: 9 June 2026 doi:10.20944/preprints202606.0589.v1

embedded in a predefined pseudoriemannian manifold; the metric interface emerges as the effective refraction matrix of phase packets in a non-uniformly loaded stochastic network.

Appendix B.4.1. Phase Throughput, Coordinate Velocity, and Effective Metric

Let a massive graph configuration generate a dimensionless delay $\chi_G(\mathbf{R})$. We define the local phase throughput

$$\Pi_G(\mathbf{R}) = e^{-\chi_G(\mathbf{R})}.$$

In the absence of delay, $\Pi_G = 1$, and the massless coherent branch propagates at a speed of c_0.

It is important to distinguish between three quantities. First, Π_G defines the clock-throughput factor:

$$d\tau = \Pi_G dt = e^{-\chi_G} dt.$$

This means that the local phase clock-rate is slowed down relative to coordinate time t. Second, the average number of elementary graph attempts required to traverse a fixed coordinate interval increases inversely proportional to the throughput. Therefore, the phase length of the coordinate interval scales as

$$d\ell_{\text{ph}} = \Pi_G^{-1} d\ell = e^{\chi_G} d\ell.$$

Third, the coordinate velocity of the null ray is not equal to $c_0\Pi_G$. The quantity $c_0\Pi_G$ describes only the local slowing down of the clock-throughput. The coordinate velocity of light is determined by the effective metric and is equal to

$$c_{\text{coord}} = \frac{d\ell}{dt} = c_0\Pi_G^2 = c_0 e^{-2\chi_G}.$$

The quadratic form of the measurement interface is given by

$$\boxed{ds^2 = -c_0^2 e^{-2\chi_G} dt^2 + e^{2\chi_G} d\mathbf{R}^2} \tag{A15}$$

The metric (A15) is equivalent to the expression

$$g_{00} = -e^{-2\chi_G}, \qquad g_{ij} = e^{2\chi_G}\delta_{ij}.$$

For a null ray $ds^2 = 0$, we obtain

$$\frac{d\ell}{dt} = c_0 e^{-2\chi_G},$$

and the corresponding coordinate refractive index:

$$n_{\text{opt}} = \frac{c_0}{c_{\text{coord}}} = e^{2\chi_G} = \Pi_G^{-2}.$$

In this case, the locally measured velocity through physical phase intervals remains equal to c_0:

$$\frac{d\ell_{\text{ph}}}{d\tau} = c_0.$$

Appendix B.4.2. Reciprocal-impedance Rule

The relation

$$d\tau = \Pi_G dt, \qquad d\ell_{\text{ph}} = \Pi_G^{-1} d\ell$$

is an additional interface condition, but not an arbitrary fit. It expresses the rate-waiting-time reciprocity of stochastic graph routing.

© 2026 by the author(s). Distributed under a Creative Commons CC BY license.

Preprints.org (www.preprints.org) | NOT PEER-REVIEWED | Posted: 9 June 2026 doi:10.20944/preprints202606.0589.v1

If the local probability of successful phase translation per unit of coordinate time decreases by a factor of Π_G, then the average number of elementary attempts required to traverse a fixed coordinate interval increases as Π_G^{-1}. Therefore, clock-rate and phase-length scaling are inversely proportional:

$$\text{clock throughput} \sim \Pi_G, \qquad \text{phase path length} \sim \Pi_G^{-1}.$$

In this sense, the reciprocal-impedance rule is the graph-theoretic analogue of the conservation of local phase action: the attenuation of throughput over time is compensated by an increase in phase length at the spatial interface.

A more general ansatz takes the form

$$d\tau = \Pi_G dt, \qquad d\ell_{\text{ph}} = \Pi_G^{-a} d\ell.$$

Then the weak-field spatial component of the metric yields the PPN parameter

$$\gamma = a.$$

The reciprocal-impedance rule fixes $a = 1$ and thus leads to $\gamma = 1$. Consequently, $\gamma = 1$ in IKT does not follow from the delay χ_G alone; it follows from the delay together with the reciprocal-impedance condition:

$$\text{phase throughput} + \text{reciprocal impedance} \Rightarrow \gamma = 1.$$

Appendix B.4.3. The Mechanism of Gravitational Refraction and the Topological Normalization of G

The initial microscopic scale is not the Planck mass, which depends on the already known G, but the dimensionless configuration volume of the electron path. The electron is interpreted as a minimal stable 1D phase cycle, but not as a single rigid thread: it is an ergodic class of microroutes that preserve the same macroscopic topology of the 4π-spinor frame. The effective size of this class is denoted by

$$N_e^{\text{top}} = |\Omega_e|_{\text{eff}}.$$

In a single local act of gravitational contact, the electron occupies a fraction

$$\mathcal{S}_e = \frac{1}{|\Omega_e|_{\text{eff}}}$$

of the saturated three-dimensional hardware capacity of the graph. Therefore,

$$\epsilon_0 = \mathcal{S}_e = \frac{1}{|\Omega_e|_{\text{eff}}}, \qquad M_0 = m_e |\Omega_e|_{\text{eff}}.$$

The local phase delay is determined by the local phase mass, not the total mass of the composite object:

$$\theta_{\text{loc}}(v) = \epsilon_0 \frac{M_{\text{loc}}(v)}{m_e} = \frac{M_{\text{loc}}(v)}{M_0},$$

$$p_{\text{stay}}(v) = 1 - e^{-\theta_{\text{loc}}(v)}.$$

For a distributed system $M = \sum_v M_{\text{loc}}(v)$, the saturation $p_{\text{stay}} \to 1$ is determined by the local concentration of the delay, rather than by the total mass itself.

The gravitational charge of an electron in apparatus units is equal to its average dilute fraction:

$$q_G(e) = \mathcal{S}_e = \frac{1}{|\Omega_e|_{\text{eff}}}.$$

© 2026 by the author(s). Distributed under a Creative Commons CC BY license.

Preprints.org (www.preprints.org) | NOT PEER-REVIEWED | Posted: 9 June 2026 doi:10.20944/preprints202606.0589.v1

For two unentangled electrons, the connected-correlator of instrumental fluctuations vanishes at distances exceeding the correlation length of micropaths, so the two-point normalization of the source factors into:

$$\alpha_G^{(e)} = q_G(e)^2 = \frac{1}{|\Omega_e|_{\text{eff}}^2}$$

in the minimal apparatus normalization. This quantity is not the probability of a literal contact coincidence of two electrons at any node; it defines the dimensionless strength of the gravitational source. The long-range form arises separately from the Green's function of the 3D graph Laplacian.

In the weak-field continuous limit, $L_G^{-1}(r) \to 1/(4\pi r)$ up to the normalization of the Poisson equation, and the potential of two electrons is written as

$$V_{ee}(r) = -\frac{\hbar c_0}{r}\frac{1}{|\Omega_e|_{\text{eff}}^2}.$$

Comparison with $V_{ee}(r) = -Gm_e^2/r$ yields

$$\boxed{G_{\text{IKT}} = \frac{\hbar c_0}{m_e^2 |\Omega_e|_{\text{eff}}^2}}.$$

The internal logic of IKT requires that m_e in this formula be not an external empirical input, but the previously obtained monodromic mass of the electron path:

$$m_e = M_{K_e} = \frac{\hbar}{c_0^2 T_{K_e}} |\Theta_{K_e}|.$$

Therefore, the gravitational normalization has the following structure of dependencies

$$K_e \Rightarrow \Theta_e \Rightarrow m_e, \qquad K_e \Rightarrow |\Omega_e|_{\text{eff}}, \qquad (m_e, |\Omega_e|_{\text{eff}}) \Rightarrow G_{\text{IKT}}.$$

Prior to the independent calculation of M_{K_e} and $|\Omega_e|_{\text{eff}}$, this formula is a reduction of G to the electronic spectral-topological sector; after such a calculation, it becomes a full-fledged prediction. Equivalently,

$$G_{\text{IKT}} = \frac{\hbar c_0}{M_0^2}, \qquad l_0 = \frac{\lambda_e}{|\Omega_e|_{\text{eff}}}, \qquad \tau_0 = \frac{\tau_e}{|\Omega_e|_{\text{eff}}}.$$

The configuration estimate of this volume uses the electromagnetic phase volume of a single independent routing channel,

$$\mathcal{N}_\alpha = \alpha_{\text{top}}^{-1} = 4\pi^3 + \pi^2 + \pi.$$

If the minimal electronic 4π-spinor skeleton has a factorized rank parameter $n_e^{(0)}$ of independent phase coordinates, then

$$|\Omega_e|_{\text{eff}} = \Gamma_e \mathcal{N}_\alpha^{n_e^{(0)}} \Xi_e, \qquad n_e^{(0)} \in \mathbb{Z},$$

where Γ_e accounts for the finite frame factor of Möbius closure and embedding constraints, and Ξ_e is the correlation factor between phase channels. The observed gravitational normalization indicates

$$\frac{\ln |\Omega_e|_{\text{eff}}^{\text{obs}}}{\ln \mathcal{N}_\alpha} \approx 10.47,$$

that is, a minimum skeleton of about ten independent phase channels. In integer notation, the natural configuration target takes the form

$$n_e^{(0)} = 10, \qquad \Gamma_e \approx 10.23, \qquad \Xi_e \approx 1 \quad \text{(in the factored limit)}.$$

© 2026 by the author(s). Distributed under a Creative Commons CC BY license.

Preprints.org (www.preprints.org) | NOT PEER-REVIEWED | Posted: 9 June 2026 doi:10.20944/preprints202606.0589.v1

These numbers are not introduced as a new dimensional constant; they fix the open topological problem of constructing a minimal electronic frame.

The macroscopic gravitational potential χ_G is determined via the graph Poisson equation

$$\Delta_G \chi_G = -\kappa_G \rho_\theta,$$

where ρ_θ is the phase delay density. After the continuous transition

$$\nabla^2 \chi_G = -\frac{4\pi G_{\mathrm{IKT}}}{c_0^2}\rho.$$

Thus, weak-field gravity is normalized by the configuration volume of the electronic path, rather than by the circular introduction of the Planck mass.

Appendix B.4.4. Principle of Equivalence

The inertial mass and the gravitational source in IKT must be consistent without the introduction of a separate phenomenological postulate. The inertia of a stable path K is determined by its Floquet monodromy, whereas the long-range weakness of gravity is determined by the path's hardware sparsity in the stochastic vacuum graph. These two roles should be distinguished: monodromy specifies a local phase source, while the participation volume specifies the probability of hardware overlap between sources.

Theorem A1 (Phase Action and the Weak Equivalence Principle)**.** *In the weak-field static limit, the inertial mass and the gravitational source of a stable topological path K are two variations of the same phase action.*

Proof. The inertial mass of the path is determined by the spectral gap of monodromy:

$$M_K c_0^2 = \frac{\hbar}{T_K}|\Theta_K|.$$

In the phase-bandwidth field χ_G, the path's eigenphase time scales as

$$d\tau = e^{-\chi_G} dt.$$

Therefore, the action of the cycle is given by

$$S_K[\chi_G] = -\int M_K c_0^2 \, d\tau = -\int M_K c_0^2 e^{-\chi_G} dt.$$

Variation with respect to χ_G gives

$$\frac{\delta S_K}{\delta \chi_G} = M_K c_0^2 e^{-\chi_G}.$$

Therefore, the positive density of the delay source is defined as

$$\boxed{\rho_G^{(K)} = \frac{1}{c_0^2}\frac{\delta S_K}{\delta \chi_G} = M_K e^{-\chi_G}}. \tag{A16}$$

From the definition of the source in (A16) in a weak field $\chi_G \ll 1$, we obtain

$$\rho_G^{(K)} \simeq M_K.$$

Consequently, the equality of inertial and gravitational masses in the weak-field sense follows from the universal scaling of the proper phase time of all closed paths. It does not require a separate introduction of gravitational mass. □

© 2026 by the author(s). Distributed under a Creative Commons CC BY license.

Preprints.org (www.preprints.org) | NOT PEER-REVIEWED | Posted: 9 June 2026 doi:10.20944/preprints202606.0589.v1

The participation volume $|\Omega_K|_{\text{eff}}$ is responsible not for the equality of inertial and gravitational masses itself, but for the spatial sparsity of the source:

$$\mathcal{S}_K = |\Omega_K|_{\text{eff}}^{-1}.$$

It is precisely this sparsity that determines the magnitude of the long-range route overlap and the normalization of G, whereas M_K specifies the local phase source.

Lemma A4 (Ergodic Route Sparseness). *For an ergodic closed route K, the average hardware visit density of node v is equal to the stationary measure of quantum walk:*

$$\bar{\rho}_K(v) = \pi_K(v).$$

If K uniformly explores the accessible configuration space Ω_K, then

$$\bar{\rho}_K(v) \simeq |\Omega_K|_{\text{eff}}^{-1}.$$

Thus, the graph-theoretic analogue of the return lemma justifies the sparsity of $\mathcal{S}_K$, but does not replace the definition of inertial mass via Floquet monodromy.

The full strong form of the equivalence principle requires a further derivation of the universal coupling of all components of the energy-momentum. In this section, its weak-field static limit is used.

Appendix B.4.5. Weak-field PPN Limit: Kinematic Derivation of $\beta = 1$ and Conditional Lemma for $\gamma = 1$

In a spherically symmetric weak field, the solution to the Poisson equation is normalized as

$$\chi_G(r) = -\frac{\Phi_N(r)}{c_0^2} + \mathcal{O}(r^{-2}) = \frac{GM}{c_0^2 r} + \mathcal{O}(r^{-2}), \qquad \chi_G \ll 1.$$

It is important to note that χ_G is not a probability. The probability of local gravitational delay can be written as a saturated function

$$p_G = 1 - e^{-\chi_G},$$

but for PPN inference, it is more convenient to use not a probability but an impedance quantity—the local phase throughput

$$\Pi_G = e^{-\chi_G}.$$

Here, Π_G should not be understood as the literal probability of a photon jumping to a neighboring edge. It is the local phase-throughput coefficient, which determines what fraction of the graph's clock cycle is available for the successful phase evolution of the local process.

Lemma A5 (Time component and parameter β). *The proper time of the local oscillator is proportional to the number of successful local phase evolution acts. Therefore*

$$d\tau = \Pi_G dt = e^{-\chi_G} dt.$$

Consequently,

$$g_{00} = -\left(\frac{d\tau}{dt}\right)^2 = -e^{-2\chi_G}.$$

In a weak field

$$g_{00} = -1 + 2\chi_G - 2\chi_G^2 + \mathcal{O}(\chi_G^3).$$

© 2026 by the author(s). Distributed under a Creative Commons CC BY license.

Preprints.org (www.preprints.org) | NOT PEER-REVIEWED | Posted: 9 June 2026 doi:10.20944/preprints202606.0589.v1

Comparison with the PPN form

$$g_{00}^{\mathrm{PPN}} = -1 + 2\chi_G - 2\beta\chi_G^2 + \cdots$$

yields in a single-scalar weak-field matching

$$\boxed{\beta = 1}.$$

An additional kinematic statement is required for the spatial part. The physical distance in IKT is measured by the phase transfer value, not by the number of edges.

Lemma A6 (Inverse phase impedance and the parameter γ)**.** *In an isotropic 3D coarse-grained graph, the phase current through a coordinate interval is conserved. If the local phase capacity is Π_G, then the phase impedance length of the coordinate interval scales inversely with this capacity:*

$$d\ell_{\mathrm{ph}} = \Pi_G^{-1} d\ell.$$

When $\Pi_G = e^{-\chi_G}$, we obtain

$$d\ell_{\mathrm{ph}} = e^{\chi_G} d\ell.$$

Consequently,

$$d\ell_{\mathrm{ph}}^2 = e^{2\chi_G} d\mathbf{r}^2,$$

and the spatial part of the effective metric takes the form

$$g_{ij} = e^{2\chi_G}\delta_{ij} = \left(1 + 2\chi_G + \mathcal{O}(\chi_G^2)\right)\delta_{ij}.$$

Comparison with the PPN form

$$g_{ij}^{\mathrm{PPN}} = (1 + 2\gamma\chi_G)\delta_{ij}$$

gives

$$\boxed{\gamma = 1}.$$

Thus, the weak-field static metric limit of IKT is written as

$$ds^2 = -e^{-2\chi_G} c_0^2 dt^2 + e^{2\chi_G} d\mathbf{r}^2, \tag{A17}$$

and its post-Newtonian expansion yields

$$\beta = \gamma = 1.$$

Lemma A6 is a conditional kinematic lemma: in a more general setting

$$d\ell_{\mathrm{ph}} = \Pi_G^{-a} d\ell$$

we would obtain $\gamma = a$. Therefore, the microderivation of the index $a = 1$ directly from the spectrum of the local operator U_m, the phase current conservation law, and isotropic coarse-graining remains a key test for the gravitational sector. At the level of weak-field tests, the exponential form (A17) is the PPN interface. The B3 branch is retained as the strong-field continuation of this same phase-capacity law rather than replacing it by a Schwarzschild/Kerr completion.

Appendix B.4.6. B3 Strong-Field Exponential Exterior and Finite Graph Neck

The preceding PPN argument fixes only the weak-field interface. In the B3 branch of IKT we choose the minimal strong-field continuation that preserves the original throughput ontology:

$$\boxed{\Pi_G = e^{-\chi_G}} \tag{A18}$$

© 2026 by the author(s). Distributed under a Creative Commons CC BY license.

Preprints.org (www.preprints.org) | NOT PEER-REVIEWED | Posted: 9 June 2026 doi:10.20944/preprints202606.0589.v1

remains the exact static exterior phase-capacity law of the graph. The corresponding exterior optical metric is

$$\boxed{ds^2 = -e^{-2\chi_G} c_0^2 dt^2 + e^{2\chi_G}\left(dr^2 + r^2 d\Omega^2\right)} \tag{A19}$$

with

$$\chi_G(r) = \frac{M_g}{r}, \qquad M_g = \frac{GM}{c_0^2}, \tag{A20}$$

for the exterior embedding domain of an isolated non-rotating overloaded cluster.

Hypothesis A2 (B3 exterior, not Schwarzschild completion)**.** *The metric* (A19) *is not an ansatz for a Schwarzschild event horizon. It is the macroscopic optical interface of the exterior graph-routing field. The black-hole condition in IKT is not* $g_{00} = 0$ *at a finite continuum radius, but the formation of a graph-accessibility neck with small Cheeger connectivity.*

The B3 continuation must not be read as a smooth continuum extension to a mathematical point $r = 0$. IKT has no physical point of zero radius. The fundamental lower object is an edge, or a finite layer of edges, and the exterior embedding terminates when the graph-neck algebra becomes the correct description. Let

$$n = d_G(\Sigma_{\text{ext}}, B_{\text{neck}})$$

be the graph-layer distance from the last exterior shell to the saturated neck. Then there is a finite cutoff layer

$$n \geq n_{\min}, \qquad \chi_{\text{neck}} = \chi_G(n_{\min}) < \infty, \qquad \Pi_{\text{neck}} = e^{-\chi_{\text{neck}}} \ll 1,$$

while the continuum symbol $r \to 0$ is only a formal limit of the exterior parametrization.

The relevant B3 surfaces are therefore distinct:

$$\begin{aligned} r_{\text{ph}} &= 2M_g, & b_{\text{ph}} &= 2eM_g, \\ r_{\text{gate}} &= M_g, & R_{\text{gate}} &= eM_g, \\ r_{\text{ISCO}} &= (3+\sqrt{5})M_g, & R_{\text{ISCO}} &= (3+\sqrt{5})e^{1/(3+\sqrt{5})}M_g. \end{aligned}$$

Here r_{ph} is the photon-capture shell of the exterior optical metric, r_{gate} is the minimal areal throat of the exponential interface, and the finite graph-accessibility neck is a discrete layer rather than the continuum point $r = 0$. The gate area is

$$\boxed{A_{\text{gate}} = 4\pi R_{\text{gate}}^2 = 4\pi e^2 M_g^2 = \pi b_{\text{ph}}^2} \tag{A21}$$

which gives the natural B3 area to be used in graph-neck counting. This area replaces the Schwarzschild horizon area in the B3 branch unless an independent TTC computation shows otherwise.

Conditional Corollary 1 (B3 optical observables)**.** *For the static B3 exterior, the capture impact parameter differs from the Schwarzschild value* $\sqrt{27}M_g$ *by*

$$\frac{2e - \sqrt{27}}{\sqrt{27}} \simeq 4.6\%,$$

and the areal ISCO scale differs from $6M_g$ *by a few percent. These numbers are not imposed as fits to GR; they are consequences of the exponential exterior* (A19) *and should be treated as B3 observational predictions, subject to ray-tracing and perturbation analysis.*

© 2026 by the author(s). Distributed under a Creative Commons CC BY license.

Preprints.org (www.preprints.org) | NOT PEER-REVIEWED | Posted: 9 June 2026 doi:10.20944/preprints202606.0589.v1

Appendix B.4.7. Compact-Holonomy Graph Dragging and Rotating B3 Exteriors

Angular momentum is introduced in IKT by the same non-commutative routing mechanism that produces galactic graph dragging, but its compact-object limit is different. A galaxy produces an extended weak-field quasi-2D waveguide; a collapsed B3 neck produces a stationary axial shift of the exterior phase-routing interface.

At the edge level the rotating transporter is written as

$$\mathcal{U}_{ij}^{B3,J} = \mathcal{U}_{ij}^{B3} \exp\left[i\,\theta_{ij}^{(J)}\right], \qquad \theta_{ij}^{(J)} = \eta_J W_\chi(i,j) \frac{\mathbf{\Omega}_{\rm neck} \cdot (\mathbf{r}_i \times \mathbf{r}_j)}{c_0 |\mathbf{r}_i - \mathbf{r}_j|}. \tag{A22}$$

Here W_χ is a strong-field weight determined by the delay profile. The constant η_J must be identified with, or derived from, the same microscopic non-commutative routing coefficient that appears in the galactic vortex sector; it is not an independent Kerr-fitting parameter.

After coarse-graining, the minimal rotating B3 interface has the form

$$ds^2 = -e^{-2\chi} c_0^2 dt^2 + e^{2\chi}\left[dr^2 + r^2 d\theta^2 + r^2 \sin^2\theta (d\phi - \omega_{\rm IKT}(r,\theta) dt)^2\right] + O(J_{\rm scalar}^2), \tag{A23}$$

where $\omega_{\rm IKT}$ is the angular graph-dragging shift. In the weak-holonomy regime it must reproduce a Lense–Thirring-type falloff, while its strong-field behavior is controlled by compact holonomy rather than by an unbounded linear velocity field.

Lemma A7 (Compact-holonomy saturation)**.** *Let rotational graph dragging be represented by compact edge transporters $U_e^{(J)} \in U(1)$, or more generally by a compact routing group. Then every gauge-invariant plaquette holonomy*

$$H_p = \prod_{e \in \partial p} U_e^{(J)}$$

lives in a compact group, and the local phase curvature is represented by

$$F_p = \mathrm{Arg}\, H_p \in (-\pi, \pi].$$

Consequently, the edge current

$$J_{ij} \propto \mathrm{Im}\left(\psi_i^* U_{ij}^{(J)} \psi_j\right) \sim \sin\theta_{ij}^{(J)}$$

is bounded. The linear dragging law is only the small-holonomy expansion $\sin\theta \simeq \theta$; in the strong-field regime the local dragging current saturates and the excess angular momentum is stored in winding and phase-slip sectors of the finite neck layer.

This lemma replaces any empirical saturation rule for compact rotation. The finite number of gate channels gives a topological spin-capacity scale. If each gate edge carries a finite maximum angular phase current, then

$$J_{\max} \propto N_{\rm gate} \propto A_{\rm gate} \propto M^2,$$

which yields an IKT extremality principle of the form

$$a_*^{\rm IKT} = \frac{c_0 J}{G M^2} \leq C_{\rm spin},$$

with $C_{\rm spin}$ to be computed from the compact-holonomy spectrum of the neck rather than imported from the Kerr solution.

© 2026 by the author(s). Distributed under a Creative Commons CC BY license.

Preprints.org (www.preprints.org) | NOT PEER-REVIEWED | Posted: 9 June 2026 doi:10.20944/preprints202606.0589.v1

Appendix B.4.8. Gravitational Refraction, Shapiro, and Lensing

A locally massless phase packet propagates along the phase metric at a speed of c_0:

$$\frac{d\ell_{\mathrm{ph}}}{d\tau} = c_0.$$

Substituting

$$d\ell_{\mathrm{ph}} = e^{\chi_G} d\ell, \qquad d\tau = e^{-\chi_G} dt,$$

we obtain the coordinate velocity

$$\frac{d\ell}{dt} = c_0 e^{-2\chi_G} = c_0\Big(1 - 2\chi_G + \mathcal{O}(\chi_G^2)\Big).$$

It is precisely this first post-Newtonian structure, equivalent to $\gamma = 1$, that determines the leading effects of light deflection and the Shapiro delay. The effective refractive index of vacuum is given by

$$n_{\mathrm{eff}}(\mathbf{r}) = \frac{c_0}{d\ell/dt} = e^{2\chi_G(\mathbf{r})} = 1 + 2\chi_G(\mathbf{r}) + \mathcal{O}(\chi_G^2), \qquad v_{\mathrm{eff}} = \frac{c_0}{n_{\mathrm{eff}}}. \tag{A24}$$

The quantity in (A24) defines the optical interface; the trajectory of a light packet follows Fermat's principle: graph routing minimizes the total phase time.

At short distances, the singularity is regularized not by the probability p_j, but by the potential. To preserve the PPN normalization $\chi_G \to GM/(c_0^2 r)$ at long distances, it is convenient to write

$$\chi_G(r) = \frac{r_s}{2r}\Big(1 - e^{-r/\lambda_0}\Big), \qquad r_s = \frac{2GM}{c_0^2}.$$

The physical probability of delay associated with this potential is equal to $p_G(r) = 1 - e^{-\chi_G(r)}$ and therefore always remains less than one.

For a weak field

$$\Delta t = \frac{1}{c_0}\int (n_{\mathrm{eff}} - 1) dl \simeq \frac{2}{c_0}\int \chi_G(r)\, dl.$$

The logarithmic integral along the ray reproduces the Shapiro effect. The angle of light deflection in the post-Newtonian form is given by

$$\theta_{\mathrm{light}} = (1+\gamma)\frac{2GM}{c_0^2 b}.$$

Since the lemma on inverse phase impedance implies $\gamma = 1$, we obtain the standard leading result of GR

$$\theta_{\mathrm{light}} = \frac{4GM}{c_0^2 b}.$$

Appendix B.4.9. Perihelion Precession

Orbital dynamics depend on both post-Newtonian coefficients. Since the exponential delay gives $\beta = 1$ and the inverse phase impedance under isotropic coarse-graining gives $\gamma = 1$, the Binet equation takes the standard weak-field form

$$\frac{d^2u}{d\phi^2} + u = \frac{GM}{\ell_{\mathrm{orb}}^2} + 3\frac{GM}{c_0^2}u^2,$$

and yields

$$\Delta\phi = \frac{6\pi GM}{c_0^2 a_{\mathrm{orb}}(1 - e_{\mathrm{orb}}^2)}.$$

© 2026 by the author(s). Distributed under a Creative Commons CC BY license.

Preprints.org (www.preprints.org) | NOT PEER-REVIEWED | Posted: 9 June 2026 doi:10.20944/preprints202606.0589.v1

Thus, the Shapiro effect, lensing, and perihelion precession follow in IKT from a single weak-field mechanism: the exponential delay of local clocks and the inverse phase impedance of the spatial metric.

Appendix B.4.10. Gravitational Waves

The dynamic tensor fluctuation of the gravitational potential is denoted by $\delta\chi_{ij}^{TT}$. Its free sector obeys the same symmetric graph update:

$$\delta\chi_{ij}^{TT}(t+\tau_0) - 2\delta\chi_{ij}^{TT}(t) + \delta\chi_{ij}^{TT}(t-\tau_0) = l_0^2\nabla^2\delta\chi_{ij}^{TT}(t).$$

In the continuous limit

$$\left(\nabla^2 - \frac{1}{c_0^2}\partial_t^2\right)\delta\chi_{ij}^{TT} = 0.$$

The TT projector leaves two transverse trace-free polarizations, which corresponds to a spin-2 gravitational wave.

Appendix B.5. Unified Summary of IKT Field Modes

Appendix B.5.1. Summary of the Interaction Interface Chain

Taking into account the electromagnetic, color, weak, and gravitational blocks, the minimal unification chain takes the form

$$U_m \Rightarrow \text{Weyl/wave envelope} \Rightarrow \begin{cases} U(1)_{\text{link}} & \Rightarrow j^\mu,\ \alpha_{\text{top}},\ e_{\text{top}}, \\ SU(3)_{\text{route}} & \Rightarrow J_A^\mu,\ \text{color singlets}, \\ \Xi_{\text{vac}} \neq 0 & \Rightarrow P_L\ \text{weak gateway}, \\ \chi_G & \Rightarrow g_{\mu\nu},\ G_{\text{eff}}. \end{cases}$$

The strong sector in this chain serves as a color-routing interface. It derives the non-Abelian form of the color current and the confinement constraint, but does not claim to provide a complete derivation of running QCD, Λ_{QCD}, and the hadron spectrum.

Appendix B.5.2. Summary of Translation Modes (EM, Strong, Weak, Gravity)

In the IKT concept, there is no need for different "carriers" of interactions. The entire diversity of physics is simply four mathematical operating modes of the same graph:

1. Electromagnetism: $\Box\mathbf{A} = \mu_0\mathbf{J}_{phase}$
2. Gravity: $\Box(\delta\chi_G^{TT}) = \kappa \cdot \mathbf{D}_{algo}^{quadrupole}$
3. Strong interaction: $\Box\mathbf{A} + g^2|\mathbf{A}|^2\mathbf{A} = \mathbf{J}$
4. Weak interaction: $SU(2)_L \times U(1)_Y$, charged-current gauge $\mathcal{G}_W P_R = 0$ and Fermi limit $G_F/\sqrt{2} = g_L^2/(8M_W^2)$.

Appendix B.5.3. Ontological Status of Carriers: From Objects to Graph Processes

This subsection concludes the unified summary of field modes and establishes a general ontological conclusion from the four interfaces. The key conceptual difference between IKT and the Standard Model is the complete rejection of the corpuscular interpretation of interaction carriers. What is classified as carrier particles in modern physics are, in IKT, merely macroscopic labels for various algorithmic modes of transmission: A photon is a pure algorithmic act: a directed relay of a phase state. A graviton is propagating information about a change in bandwidth. A gluon is the very topological edge of the base graph in a state of extreme tension. W/Z bosons are short-lived algorithmic "gates."

© 2026 by the author(s). Distributed under a Creative Commons CC BY license.

Preprints.org (www.preprints.org) | NOT PEER-REVIEWED | Posted: 9 June 2026 doi:10.20944/preprints202606.0589.v1

Appendix C. Microscopic Limit: Topological Spectrum of Particles

Appendix C.1. Basic Principles of Topological Reduction: Mass, Charge, Color, and Spin

Appendix C.1.1. Particles as Stable Quantum Cycles of a Graph

Despite its unprecedented predictive accuracy, the Standard Model (SM) remains conceptually a phenomenological construct. It postulates the existence of fundamental particles and gauge symmetries, leaving open the question of their ultimate origin. Masses and charges are introduced into the theory as free parameters determined empirically.

In Information-Kinetic Theory (IKT), fundamental particles are not postulated as primary point-like entities. The vacuum is a 3D phase-translation network. What we call a "particle" is simply a stable closed path, a local algorithm failure that has looped back on itself. In classical quantum field theory, particles are postulated as point excitations of fundamental fields. Within the framework of IKT, what the observer interprets as a "particle" is a local, topologically protected closed phase-translation route (a quantum topological cycle) possessing its own algorithmic support value. The quantum numbers SM (mass, charge, spin, flavor) are given a graph interpretation through the geometric and matrix properties of this cycle; a rigorous derivation of the complete set of numbers remains a task for further formalization.

Appendix C.1.2. Algorithmic Mass as a Phase Integral

In IKT, rest mass is the integral phase cost of maintaining a closed topological cycle. For a node K, we introduce a dimensionless delay

$$\Theta_K = \oint_K \theta(s)\,\frac{dl}{l_0}.$$

The absolute mass scale is fixed by the electronic invariant m_e; the theory further aims primarily at deriving mass relations, rather than eliminating the most basic scale m_e itself.

For the electron, interpreted as a trivial Möbius loop, the following normalization is adopted

$$\Theta_e \equiv 1, \qquad M_K = m_e\,\mathcal{M}(K),$$

where $\mathcal{M}(K)$ is the dimensionless topological measure of the corresponding knot. This approach clarifies the logical status of the subsequent formulas: they are statements about the topological measure $\mathcal{M}$, rather than an independent derivation of m_e from zero parameters.

Appendix C.1.3. Minimum Parameter Rank of the Electron Phase Skeleton and $N_e = 10$

In the electromagnetic sector of IKT, a single independent phase channel has an effective information capacity

$$\mathcal{N}_\alpha \equiv \alpha_{\text{top}}^{-1} = 4\pi^3 + \pi^2 + \pi.$$

This quantity is not a literal integer number of microstates. It is a dimension-normalized channel measure of the phase strata of $U(1)$-routing.

The number n_e should not be understood as the usual dimension of a Hilbert space and should not be derived by summing heterogeneous quantities, such as the spatial dimension and the complex rank of the spinor carrier. In the present formulation, n_e is interpreted as the parametric rank indicator of the minimal charged 4π-route: the number of independent phase coordinates required to specify a single factorized electronic routing skeleton before accounting for correlations between channels.

The parametric manifold of a single chiral branch.

The infrared Weyl symbol of a coherent branch describes the directed translation of a spinor carrier state. In the minimal local description, a single directed routing step is specified by three parametric components.

© 2026 by the author(s). Distributed under a Creative Commons CC BY license.

Preprints.org (www.preprints.org) | NOT PEER-REVIEWED | Posted: 9 June 2026 doi:10.20944/preprints202606.0589.v1

1. **Edge direction.** In the emergent $3D$ interface, the choice of the translation beam corresponds to a point on the sphere of directions
$$S^2_{\text{dir}},$$
which gives
$$r_{\text{dir}} = 2.$$
2. **Spin-frame carrier.** The minimal spinor carrier is given by $\mathbb{C}^2_{\text{spin}}$. A normalized pure state, up to a global phase, belongs to
$$\mathbb{CP}^1 \simeq S^2_{\text{spin}}.$$
This gives
$$r_{\text{spin}} = 2.$$
Here, S^2_{spin} denotes the internal spin-frame carrier of the local router prior to helicity-locking and monodromic closure. Possible correlations between direction and spin-frame are accounted for by the factor Ξ_e.
3. **Relative $U(1)$-holonomy phase.** The local link transport contains a phase factor
$$L_{ij} = e^{-i\phi_{ij}} \in U(1).$$
After factorizing the local gauge reparameterizations, the physical channel is the relative link-holonomy phase
$$S^1_{\text{hol}}.$$
It yields
$$r_{\text{phase}} = 1.$$

Consequently, the factorized parametric manifold of a single chiral branch takes the form

$$\mathcal{M}^{(1)}_{\text{route}} = S^2_{\text{dir}} \times S^2_{\text{spin}} \times S^1_{\text{hol}}.$$

Its real dimension is equal to

$$r_{\text{route}} = \dim_{\mathbb{R}} \mathcal{M}^{(1)}_{\text{route}} = 2 + 2 + 1 = 5.$$

In this formulation, we are not talking about the sum of the dimensions of Hilbert spaces, but about the dimension of the parametric manifold of a single directed routing step.

Dirac/Floquet doubling and nonzero mass gap.

A single Weyl branch can be massless. A nonzero Dirac/Floquet mass gap for a closed route K requires two low-energy chiral branches:

$$\mathcal{H}^{\text{chir}}_K = \text{span}\{|L_K\rangle, |R_K\rangle\}.$$

In the factorized minimal approximation, these branches are described by two conjugate directed routing skeletons:

$$r^{(L)}_{\text{route}} = r^{(R)}_{\text{route}} = 5.$$

Proposition A2 (Minimal parameter rank of the electron skeleton)**.** *Under the conditions:*

1. *the directed routing direction is given by S^2_{dir};*
2. *the internal spin-frame carrier is given by $\mathbb{CP}^1$;*
3. *the $U(1)$ component is considered as the relative link-holonomy after the gauge quotient;*
4. *the massive Dirac/Floquet route contains two conjugate chiral branches;*

© 2026 by the author(s). Distributed under a Creative Commons CC BY license.

Preprints.org (www.preprints.org) | NOT PEER-REVIEWED | Posted: 9 June 2026 doi:10.20944/preprints202606.0589.v1

the factorized rank parameter of the minimal electronic 4π-route is equal to

$$\boxed{n_e^{(0)} = r_{\text{route}}^{(L)} + r_{\text{route}}^{(R)} = 5 + 5 = 10.}$$

Connection to the configuration volume and G_{IKT}.

The transition from the parametric rank $n_e^{(0)}$ to the configuration volume relies on the hypothesis of equal channel normalization of the electronic phase skeleton: each independent phase coordinate of the minimal charged 4π-path carries the same information capacity as an elementary $U(1)$ channel. Then

$$|\Omega_e|_{\text{eff}} = \Gamma_e \mathcal{N}_\alpha^{n_e^{(0)}} \Xi_e.$$

Here, Γ_e is the Möbius closure and embedding constraint factor, and Ξ_e is the correlation factor between phase channels. In the ideal factored limit

$$\Xi_e = 1,$$

and then

$$|\Omega_e|_{\text{eff}} = \Gamma_e \mathcal{N}_\alpha^{10}.$$

The gravitational normalization takes the form

$$\boxed{G_{\text{IKT}} = \frac{\hbar c_0}{M_{K_e}^2 \left(\Gamma_e \mathcal{N}_\alpha^{10} \Xi_e\right)^2}.}$$

Consequently, the degree 10 is no longer a free phenomenological fit. It acquires the status of a conditional parameter-rank result for the factorized electron routing skeleton. A complete prediction of G requires an independent calculation of

$$M_{K_e}, \qquad \Gamma_e, \qquad \Xi_e,$$

as well as verification of the assumption of equal channel normalization of all ten phase coordinates.

Appendix C.1.4. The Topological Nature of Charge, Color, and Fractional Quantum Numbers

In the previous sections, the electroweak structure $SU(2)_L \times U(1)_Y$ was introduced as the effective matching language of the low-energy graph dynamics of IKT. Now we will clarify the topological meaning of charge, color, and fractional quantum numbers within this matching layer.

First of all, we must correct the naive formulation of the edge flux. For a complex unitary translation kernel, the directed phase flux cannot be identified with the simple difference $\mathcal{U}_{ij}^{\text{eff}} - \mathcal{U}_{ji}^{\text{eff}}$. Such a formulation is correct only for a real or pre-symmetrized effective kernel. In the general case, the physically observable directed quantity must be constructed from the anti-Hermitian part of the operator, i.e., taking into account the Hermitian conjugate of the opposite block.

Definition A14 (Edge phase flux)**.** *Let $\mathcal{U}^{\text{eff}}$ denote the effective edge kernel obtained after coarse-graining the micro-operator U_m, and $\mathcal{U}_{ij}^{\text{eff}}$ denote its block that maps internal states from the neighborhood j to the neighborhood i. For an Abelian channel X, let P_X denote the projection onto the corresponding internal subspace. The anti-Hermitian part of the kernel in this channel is given by*

$$\mathfrak{J}_{ij}^{(X)} = \frac{1}{2}\left[P_X \mathcal{U}_{ij}^{\text{eff}} P_X - \left(P_X \mathcal{U}_{ji}^{\text{eff}} P_X\right)^\dagger\right],$$

and the Hermitian observable phase flux is defined as

$$F_{ij}^{(X)} = \frac{1}{i}\mathfrak{J}_{ij}^{(X)} = \frac{1}{2i}\left[P_X \mathcal{U}_{ij}^{\text{eff}} P_X - \left(P_X \mathcal{U}_{ji}^{\text{eff}} P_X\right)^\dagger\right].$$

© 2026 by the author(s). Distributed under a Creative Commons CC BY license.

Preprints.org (www.preprints.org) | NOT PEER-REVIEWED | Posted: 9 June 2026 doi:10.20944/preprints202606.0589.v1

In the scalar $U(1)$ limit, this quantity reduces to the directed phase difference of the edge path. In the continuous limit, the field tensor arises not from a single edge, but from the coarse-grained circulation or plate-like holonomy of such edge flows.

The topological charge of a region V is defined as the normalized outflow of the corresponding channel through the boundary of the region:

$$Q_X(V) = \mathcal{N}_X \sum_{i\in V,\, j\notin V} \mathrm{Tr}_{\mathrm{int}}\, F_{ij}^{(X)},$$

where $\mathcal{N}_X$ fixes the choice of the unit of charge. For the electromagnetic channel, the physical SI projection is then given by $q_{\mathrm{phys}} = e_{\mathrm{top}} Q_{\mathrm{em}}$, whereas the dimensionless channel anchor satisfies $g_{\mathrm{em}}^2 = 4\pi\alpha_{\mathrm{top}}$.

In the electroweak matching layer, the electromagnetic charge is not a primary independent number. Repeating the rule in (A14), it is decomposed into two graph channels:

$$Q_{\mathrm{em}} = T_3^{(L)} + \frac{Y}{2}.$$

Here, $T_3^{(L)}$ describes the orientation of the left-chiral $SU(2)_L$ node, and Y describes the edge hypercharge phase shift of the $U(1)_Y$ channel.

Conditional Corollary 2 (Color triplet and hypercharge of the left-handed quark doublet)**.** *Let the minimal quark sector of a single generation be a color triplet,*

$$Q_L = \begin{pmatrix} u \\ d \end{pmatrix}_L \otimes \mathbb{C}^3_{\mathrm{col}},$$

and the color singlet configuration of the baryon node is given by the invariant combination

$$|B\rangle_{\mathrm{col}} = \frac{1}{\sqrt{6}} \epsilon_{abc} |q^a q^b q^c\rangle.$$

The requirement of local $SU(3)_c$-invariance implies that the hypercharge generator must commute with color mixing. Therefore, on the color triplet, it acts with a weight of one:

$$Y_Q = y_Q\, \mathbf{1}_3.$$

In other words, the three colors are not three different hypercharges, but three degenerate copies of the same hypercharge channel.

For a complete topological generation cell, compensation of the macroscopic hypercharge divergence of the left-chiral $SU(2)_L$ sector is required:

$$Y(L_L) + \mathrm{Tr}_{\mathrm{col}}\, Y_Q = 0.$$

Since neutrino neutrality and the electron charge give

$$Y(L_L) = -1,$$

and $\mathrm{Tr}_{\mathrm{col}}\, Y_Q = 3y_Q$, we obtain

$$-1 + 3y_Q = 0, \qquad y_Q = \frac{1}{3}.$$

Therefore,

$$Y(Q_L) = \frac{1}{3}.$$

© 2026 by the author(s). Distributed under a Creative Commons CC BY license.

Preprints.org (www.preprints.org) | NOT PEER-REVIEWED | Posted: 9 June 2026 doi:10.20944/preprints202606.0589.v1

Now, the fractional quark charges arise not as a consequence of the division of the electromagnetic flux, but from the combined action of the weak isospin and the hypercharge channel:

$$Q_{\mathrm{em}}(u_L) = +\frac{1}{2} + \frac{1}{2}\frac{1}{3} = +\frac{2}{3},$$
$$Q_{\mathrm{em}}(d_L) = -\frac{1}{2} + \frac{1}{2}\frac{1}{3} = -\frac{1}{3}.$$

Thus, the fractions $2/3$ and $-1/3$ do not arise as an independent postulate or as a mechanical splitting of a unit electromagnetic charge across three arcs. They are a consequence of color tripletness, hypercharge compensation of generation, and the electroweak rule (A14).

Conditional Corollary 3 (Topological shunting of right-handed singlets)**.** *Right-handed fermions do not enter the charged-current gate:*

$$\mathcal{G}_W P_R = 0, \qquad T_3^{(L)} P_R = 0.$$

However, the electromagnetic charge is a topological invariant of the fermionic path and should not depend on whether the state is described by the left or right electroweak matching component. Therefore, for right-handed quark singlets, the entire electromagnetic charge is projected into the edge hypercharge channel:

$$Q_{\mathrm{em}}(u_R) = +\frac{2}{3}, \qquad T_3^{(L)}(u_R) = 0 \quad \Rightarrow \quad Y(u_R) = \frac{4}{3},$$
$$Q_{\mathrm{em}}(d_R) = -\frac{1}{3}, \qquad T_3^{(L)}(d_R) = 0 \quad \Rightarrow \quad Y(d_R) = -\frac{2}{3}.$$

Similarly, for the right-handed charged lepton:

$$Q_{\mathrm{em}}(\ell_R) = -1, \qquad T_3^{(L)}(\ell_R) = 0 \quad \Rightarrow \quad Y(\ell_R) = -2.$$

If a sterile right-handed neutrino singlet is introduced, then

$$Q_{\mathrm{em}}(\nu_R) = 0, \qquad Y(\nu_R) = 0.$$

The resulting structure is consistent with the standard conditions for compensating chiral anomalies of a single generation. In terms of right-handed fermion fields, they take the form

$$\begin{aligned} 3Y(Q_L) + Y(L_L) &= 0, \\ 2Y(Q_L) - Y(u_R) - Y(d_R) &= 0, \\ 6Y(Q_L) + 2Y(L_L) - 3Y(u_R) - 3Y(d_R) - Y(e_R) &= 0, \\ 6Y(Q_L)^3 + 2Y(L_L)^3 - 3Y(u_R)^3 - 3Y(d_R)^3 - Y(e_R)^3 &= 0. \end{aligned}$$

In IKT, these equations are interpreted as conditions for the absence of uncompensated algorithmic divergence of the hypercharge current during the insertion of a complete generation. If this condition is violated, the coarse-grained graph does not admit a stable macroscopic electroweak matching layer.

The open color ends of quark routes are still not asymptotic states. Their phase flux must close into a color singlet: either in the $q\bar{q}$ meson channel or in the $\epsilon_{abc} q^a q^b q^c$ baryon channel. Therefore, confinement in IKT remains a geometric requirement for the closure of the color current, whereas fractional electromagnetic charges are a consequence of the hypercharge structure of the complete generation.

Remark A5 (Mass, chirality, and the observable scalar channel)**.** *In IKT, the microscopic source of inertial mass is associated not with a fundamental scalar field or with a mandatory mechanism of continuous $L \leftrightarrow R$-jump, but with the integral algorithmic delay Θ_K of a stable topological route. The left and right electroweak*

© 2026 by the author(s). Distributed under a Creative Commons CC BY license.

Preprints.org (www.preprints.org) | NOT PEER-REVIEWED | Posted: 9 June 2026 doi:10.20944/preprints202606.0589.v1

components are different low-energy projections of a single topological carrier, rather than two states between which a particle must continuously oscillate in order to possess inertia.

Consequently, IKT is not required to reproduce the Higgs mechanism, the Yukawa sector, or the electroweak Lagrangian as a microscopic ontology. It must reproduce the observed content: the mass spectrum, weak mass scales, a scalar resonance channel near 125 GeV *with quantum numbers* 0^{++}*, measured branching ratios, production cross sections, and the unitarization of longitudinal WW scattering. The variables* $h(x)$*,* F_h*,* g_{hff}*,* g_{hVV}*, and* λ_K *should be understood as coordinates of a phenomenological projection, rather than as fundamental objects of the graph's microdynamics.*

Appendix C.1.5. Spin 1/2, Exchange Phase, and the Pauli Topological Principle

Spin in IKT is formalized via the orientability of a closed phase route. Bosonic modes correspond to orientable cycles: the local frame returns to its initial state after one complete loop, that is, after a rotation of 2π. Fermionic modes correspond to cycles with a Möbius-like half-twist of the internal frame. Such a cycle realizes spinor holonomy:

$$\psi(\theta + 2\pi) = -\psi(\theta), \qquad \psi(\theta + 4\pi) = \psi(\theta).$$

In other words, the fermionic cycle distinguishes between 2π- and 4π-closures. This property alone determines the spinor nature of a single excitation, but does not yet prove the Pauli principle. To derive fermionic statistics, it is necessary to relate the local 2π-rotation of the internal frame to the spatial exchange of two identical cycles.

Definition A15 (Configuration space of two fermionic cycles)**.** *Let* $\mathcal{Q}_{\mathrm{F}}^{(2)}$ *denote the configuration space of two identical fermionic Möbius-like cycles embedded in the emergent three-dimensional manifold* M_{eff}*, with the diagonal of coinciding complete states excluded and with factorization by permutation of identical objects:*

$$\mathcal{Q}_{\mathrm{F}}^{(2)} = \frac{(\mathcal{Q}_{\mathrm{F}} \times \mathcal{Q}_{\mathrm{F}}) \setminus \Delta}{S_2}.$$

Here, Δ *denotes the coincidence of all quantum-topological labels of a cycle: spatial support, internal frame, spin, charge, and knot class.*

Postulate A8 (Finkelstein–Rubinstein condition for IKT fermionic cycles)**.** *In the configuration space* $\mathcal{Q}_{\mathrm{F}}^{(2)}$*, a loop corresponding to the continuous exchange of two identical fermionic cycles belongs to the same non-trivial class* $\pi_1(\mathcal{Q}_{\mathrm{F}}^{(2)})$ *as the local* 2π*-rotation of the internal frame of one of the cycles:*

$$[E_{12}] = [R(2\pi)].$$

The quantization of a fermionic loop defines a one-dimensional representation of this non-trivial class:

$$\rho([R(2\pi)]) = -1, \qquad \rho([R(4\pi)]) = +1.$$

This condition is the topological analogue of the Finkelstein–Rubinstein constraint for soliton excitations: the exchange loop in configuration space takes on the same sign as the corresponding 2π-rotation of the frame [9,10].

Theorem A2 (Exchange antisymmetry of two fermionic cycles)**.** *If condition A8 is satisfied, the joint amplitude of two identical fermionic cycles is antisymmetric under exchange:*

$$\Psi(2,1) = -\Psi(1,2).$$

© 2026 by the author(s). Distributed under a Creative Commons CC BY license.

Preprints.org (www.preprints.org) | NOT PEER-REVIEWED | Posted: 9 June 2026 doi:10.20944/preprints202606.0589.v1

Proof. The exchange operator $\hat{E}_{12}$ acts on the two-particle amplitude as a transposition of the arguments:

$$(\hat{E}_{12}\Psi)(1,2) = \Psi(2,1).$$

According to condition A8, the exchange loop $[E_{12}]$ has the same topological class as the local 2π-rotation of the fermionic frame. Therefore, the action of this loop on the raised wave function is given by the sign

$$\rho([E_{12}]) = \rho([R(2\pi)]) = -1.$$

Consequently,

$$\hat{E}_{12}\Psi = -\Psi,$$

or, in coordinate notation,

$$\Psi(2,1) = -\Psi(1,2).$$

In the Fock representation, this corresponds to the anti-commutation sign for the creation operators of identical fermionic loops. □

Corollary A1 (Pauli's topological principle)**.** *If two identical fermionic loops attempt to occupy the same complete quantum-topological state a, then*

$$\Psi(a,a) = -\Psi(a,a),$$

hence

$$\Psi(a,a) = 0.$$

Consequently, the symmetric state of two identical fermionic cycles with completely coinciding quantum-topological labels is forbidden.

Remark A6 (Microdynamic interpretation of the prohibition)**.** *The amplitude proof above does not require reference to local graph overloading. However, at the level of IKT microdynamics, the same prohibition has a structural interpretation: an attempt to route two identical Möbius routes through the same complete local subgraph leads to competition for the same edge channels. In the limit of critical connectivity $k_{\mathrm{crit}} = 6$, this corresponds to local saturation of the delay $p_{\mathrm{stay}} \to 1$. Therefore, the Pauli principle manifests itself not only as amplitude antisymmetry, but also as the limiting capacity of a fermionic route in the vacuum network.*

Appendix C.2. Lepton Hierarchy and the Neutrino Sector

Appendix C.2.1. The Electron as a Minimal 4π-Route and a Normalizing Lepton Node

The electron in IKT is the minimal charged 4π-spinor route. In the microscopic spectrum, it plays a dual role: on the one hand, it is the first stable closed fermionic cycle K_e, whose monodromic mass must be obtained as

$$M_{K_e}c_0^2 = \frac{\hbar}{T_{K_e}}|\Theta_{K_e}|;$$

on the other hand, in the laboratory projection, m_e is used as the normalizing lepton scale for the relative mass anchors of heavier charged leptons and baryons.

Appendix C.2.2. Generation Hierarchy as Classes of Nodes: Topological Capacity and Electromagnetic Cancellation

In IKT, generations of charged leptons are interpreted as classes of closed fermionic paths of increasing topological complexity. A natural discrete measure of such complexity is the minimum number of crossings in a regular planar knot diagram:

$$C_K \equiv c(K).$$

© 2026 by the author(s). Distributed under a Creative Commons CC BY license.

Preprints.org (www.preprints.org) | NOT PEER-REVIEWED | Posted: 9 June 2026 doi:10.20944/preprints202606.0589.v1

It is important to distinguish between two types of configuration volume. In the gravitational sector, $|\Omega_e|_{\text{eff}}$ measures the sparsity of the electronic path relative to the hardware 3D capacity. In the lepton hierarchy, the mass of a generation is determined by another quantity: the local phase capacity of the minimal topological framework. Each independent topological intersection opens a set of local phase delay channels.

Hypothesis A3 (Channel capacity of topological crossings)**.** *In a three-dimensional network, the basic external routing multiplicity is equal to*

$$k_{\text{crit}} = 2D = 6.$$

In the leading approximation, each independent topological intersection increases the local phase capacity of a node by a factor of k_{crit}. Therefore, the basic inertial delay of a node class K is given by

$$\frac{M_K^{(0)}}{m_e} = 6^{c(K)} H_K. \tag{A25}$$

Here, H_K is an additional internal topological factor. For a toric trefoil, $H_{3_1} = 1$. For a hyperbolic figure-eight, H_{4_1} is determined by the hyperbolic core of the knot.

Hypothesis A4 (Electromagnetic phase capacity subtraction)**.** *The longitudinal phase delay, interpreted as inertial mass, and the transverse electromagnetic $U(1)$ traffic, interpreted as electric charge, share a common local resource of the quantum walk operator U_m. If a charged cycle supports an external electromagnetic channel, part of its phase capacitance transfers from the longitudinal inertial sector to the transverse channel.*

The leading low-energy correction is given by the channel weight $6\alpha_{\text{top}}$:

$$\rho_K = 1 - 6\alpha_{\text{top}} f_K + \delta_K^{\text{pol}}.$$

Here $0 \le f_K \le 1$ — the topological electromagnetic susceptibility of the node, measuring the fraction of the phase capacity geometrically open to the external $U(1)$ channel, and δ_K^{pol} — a small graph/IR polarization correction.

The resulting leading formula for a charged lepton takes the form

$$\boxed{\frac{m_K}{m_e} = 6^{c(K)} H_K \left(1 - 6\alpha_{\text{top}} f_K + \delta_K^{\text{pol}}\right)}. \tag{A26}$$

The electron is used as the normalization unit:

$$c(e) = 0, \qquad H_e = 1, \qquad m_e \equiv 1.$$

Therefore, formula (A26) applies primarily to the relative masses of higher generations, whereas the intrinsic self-normalization of the electron path is fixed by the choice of the scale m_e.

Remark A7 (Logical status of the lepton hierarchy)**.** *Formulas (A25)–(A26) do not constitute a complete theorem on the lepton spectrum. This is a partially predictive topological hypothesis: the muon case provides a strong leading numerical anchor without individual fitting of ρ_μ, whereas the tau sector reduces to specific problems of deriving κ_{emb}, f_{4_1}, and small polarization corrections from the spectrum of U_m on the complement of the figure-eight knot and its peripheral torus.*

Muon: Toric Trefoil

The muon is associated with the trefoil 3_1:

$$c(3_1) = 3, \qquad H_{3_1} = 1.$$

© 2026 by the author(s). Distributed under a Creative Commons CC BY license.

Preprints.org (www.preprints.org) | NOT PEER-REVIEWED | Posted: 9 June 2026 doi:10.20944/preprints202606.0589.v1

Since the trefoil is a toric knot without a hyperbolic volume core, its phase route is completely open to the external $U(1)$ channel:

$$f_{3_1} = 1.$$

Consequently,

$$\frac{m_\mu}{m_e} = 6^3\left(1 - 6\alpha_{\text{top}} + \delta_\mu^{\text{pol}}\right).$$

The leading term without δ_μ^{pol} is

$$\left(\frac{m_\mu}{m_e}\right)_{\text{top}} = 6^3(1 - 6\alpha_{\text{top}}) \approx 206.543,$$

where

$$\alpha_{\text{top}}^{-1} = 4\pi^3 + \pi^2 + \pi \approx 137.0363038.$$

The remaining relative discrepancy with the observed mass ratio is of the order of 10^{-3}. In IKT, it is not considered a free tuning of ρ_μ, but is attributed to small graph polarization effects $\Pi_{\text{IKT}}(\mathcal{Q}^2)$ and to the difference between the pure topological anchor α_{top} and the physical infrared coupling $\alpha(0)$.

Tau lepton: hyperbolic octet

The tau lepton corresponds to the 4_1 knot:

$$c(4_1) = 4.$$

Unlike the toric trefoil, the complement of the 4_1 knot has a non-trivial hyperbolic volume

$$V_H(4_1) \approx 2.02988.$$

In continuous topology, this volume is measured in ideal abstract units. In discrete IKT, it must be projected onto a stochastic graph network.

Hypothesis A5 (Spectral density of the hyperbolic core)**.** *The conversion of a continuous hyperbolic volume into the algorithmic phase capacity H_{4_1} on a random graph requires the embedding spectral density coefficient κ_{emb}:*

$$H_{4_1} = \kappa_{\text{emb}} V_H(4_1).$$

In a rigorous stochastic formalism, κ_{emb} is not postulated a priori. Its exact value must be obtained as a spectral invariant of the operator U_m acting on an ensemble of random graphs restricted to the complement topology of 4_1. Until this analytical calculation is completed, $\kappa_{\text{emb}} \sim O(1)$ retains the status of a phenomenological tuning parameter linking the continuous geometry of a node to the discrete capacity of the network.

Remark A8 (Status of lepton mass anchors)**.** *Charged lepton anchors have varying levels of evidence. The electron mass is a laboratory projection anchor and simultaneously the target of a monodromic inference via $K_e \Rightarrow \Theta_e$. The muon anchor relies on a toric trefoil and is a more robust topological leading-order statement. The tau anchor depends on the as-yet-uncalculated spectral invariant of embedding κ_{emb}.*

Quantity	*Topological source*	*Status*
m_e	$K_e \Rightarrow \Theta_e \Rightarrow M_{K_e}$	*projection anchor / target derivation*
m_μ/m_e	*toric trefoil*, $H_{3_1} = 1$, $f_{3_1} = 1$	*leading topological anchor*
m_τ/m_e	*hyperbolic knot* 4_1, $H_{4_1} = \kappa_{\text{emb}} V_H(4_1)$	*conditional on* κ_{emb}

© 2026 by the author(s). Distributed under a Creative Commons CC BY license.

Preprints.org (www.preprints.org) | NOT PEER-REVIEWED | Posted: 9 June 2026 doi:10.20944/preprints202606.0589.v1

The basic phase capacitance of the tau lepton in this representation is given by

$$m_\tau^{(0)} = m_e 6^4 \kappa_{\text{emb}} V_H(4_1).$$

With a simplicial proxy $\kappa_{\text{emb}} \approx 4/3$, this gives a numerical estimate of the order of 1790 MeV.

The hyperbolic octet has a bulk core that is partially shielded from external $U(1)$ traffic. Therefore, the electromagnetic subtraction acts only on the boundary component:

$$\frac{m_\tau}{m_e} = 6^4 \kappa_{\text{emb}} V_H(4_1)\left(1 - 6\alpha_{\text{top}} f_{4_1} + \delta_\tau^{\text{pol}}\right).$$

In the equivalent volume-boundary form

$$M_\tau = M_{\text{core}} + M_{\text{boundary}}(1 - 6\alpha_{\text{top}}), \qquad f_{4_1} = \frac{M_{\text{boundary}}}{M_{\text{core}} + M_{\text{boundary}}}.$$

The benchmark derived from the physical mass of the tau corresponds to

$$f_{4_1}^{\text{obs}} \approx 0.20.$$

The next task of IKT is to derive κ_{emb}, f_{4_1}, and a small correction δ_τ^{pol} from the spectrum of U_m on a stochastic graph ensemble of the complement of the figure-eight knot and its peripheral torus.

Hypothesis A6 (Absence of a stable fourth generation)**.** *For knot classes with $C_K \geq 5$, IKT expects local routing to saturate: the phase traffic density on the peripheral region of the knot approaches the limit $p_{\text{stay}}^{\text{loc}} \to 1$. In this regime, a closed lepton cycle is not a stable long-lived excitation, but decays or transitions into baryon-confinement and resonant topological sectors. This statement has the status of a testable saturation hypothesis, not a strict theorem; to prove it, one must derive the function $p_{\text{stay}}^{\text{loc}}(C_K)$ from the microdynamics U_m.*

Tau lifetime

The law $\Gamma \propto M^5$ remains a natural leading-order consequence of the volume-surface nature of the topological discontinuity:

$$\Gamma \propto M^3 M^2 = M^5, \qquad \frac{\tau_\tau}{\tau_\mu} \approx \left(\frac{m_\mu}{m_\tau}\right)^5.$$

The numerical agreement with the lepton decay branch should be regarded as a strong, but still phenomenological, test of the decay measure hypothesis.

Appendix C.2.3. Neutrinos as One-Dimensional Error Correction Packets

In the minimal microscopic description of IKT, the neutrino is not a stable charged 4π-cycle and does not possess an intrinsic local topological rest mass:

$$m_{\text{top}}^{\text{local}}(\nu) = 0.$$

It is modeled as a one-dimensional graph phase correction packet arising from weak route re-linking. Therefore, its effective propagation mass is not the monodromic mass of a closed cycle. It may appear as an imprint of the background graph generation at the moment of the packet's birth.

The three neutrino flavors correspond to three types of weak decoupling and mix as eigenmodes of the correction packet's propagation. In the effective form:

$$|\nu_\alpha\rangle = \sum_i U_{\alpha i}^{\text{PMNS}} |\nu_i\rangle.$$

© 2026 by the author(s). Distributed under a Creative Commons CC BY license.

Preprints.org (www.preprints.org) | NOT PEER-REVIEWED | Posted: 9 June 2026 doi:10.20944/preprints202606.0589.v1

In this minimal description, the matrix U_{PMNS} has the status of a weak/flavor interface and must be derived from the topological weak gluing operator in subsequent work.

Small Cross Section and Topological Sliding

The neutrino has no open $U(1)$ flow and no color end. It is not a charged 4π-cycle and therefore is not retained as a local massive knot. Its interaction with ordinary matter requires a one-dimensional correction packet to hit the moment and location of the weak graph gluing:

$$\nu + \text{weak bottleneck} \longrightarrow \text{route surgery}.$$

This provides a topological interpretation of the small cross-section of neutrino processes: the neutrino slides through most graph routes without forming a stable local node.

Dark-Energy Scale of Neutrino Mass Birth

After transitioning to two-component dark energy, the total density of graph generation takes the form

$$\rho_{\mathrm{gen}}(t) = \rho_{\mathrm{par}}(t) + \rho_{\mathrm{noise}}^{\mathrm{valve}}(t).$$

Here, ρ_{par} corresponds to the parent throughput background, and $\rho_{\mathrm{noise}}^{\mathrm{valve}}$ corresponds to the valve-limited noise tail of the residual insertion. This density is the energy form of the same physically realizable graph generation, which in the cosmological block is described in terms of $\Lambda_{\mathrm{par},time}$, $\Lambda_{\mathrm{noise},time}^{\mathrm{valve}}$, and the finite throughput of the parent valve.

A one-dimensional neutrino packet does not contain its own internal $3D$ volume and does not distinguish the source of graph generation. Therefore, the minimum energy scale that it can obtain from the homogeneous background density ρ_{gen} is determined by a self-consistent quantum cell. If the energy of the packet is E_ν, its quantum length is of the order of

$$\ell_\nu \sim \frac{\hbar c_0}{E_\nu}.$$

Then the energy of background generation in such a cell satisfies the estimate

$$E_\nu \sim \rho_{\mathrm{gen}} \left(\frac{\hbar c_0}{E_\nu} \right)^3.$$

This gives rise to a quarter-root scale

$$E_\nu \sim \left[\rho_{\mathrm{gen}} (\hbar c_0)^3 \right]^{1/4}.$$

Unlike the linear hypothesis, this dependence does not require a new dimensional constant of the form MT^2 and significantly mitigates the early cosmological drift.

Let us introduce dimensionless flavor/topology factors β_i associated with the type of weak gluing and the corresponding neutrino regime. The hypothesis of the birth of the effective neutrino mass takes the form

$$\boxed{m_{\nu,i}^{\mathrm{birth}}(t_b) c_0^2 = \beta_i \left[\rho_{\mathrm{gen}}(t_b) (\hbar c_0)^3 \right]^{1/4}}. \tag{A27}$$

The factors β_i are topological amplification factors of the weak/flavor sector. Their role is to encode the distinction between the three types of weak couplings; they need not be massive hierarchical coefficients.

The current dark energy scale

$$E_{\Lambda,0} = \left[\rho_{\Lambda,0} (\hbar c_0)^3 \right]^{1/4} \simeq 2.3\,\mathrm{meV}$$

© 2026 by the author(s). Distributed under a Creative Commons CC BY license.

Preprints.org (www.preprints.org) | NOT PEER-REVIEWED | Posted: 9 June 2026 doi:10.20944/preprints202606.0589.v1

naturally falls within the neutrino sector. Oscillation scales require moderate topological factors β_i, rather than large Yukawa hierarchies or a superheavy seesaw scale.

Valve-limited early density.

In equation (A27), we use not the bare mathematical asymptotic $1/t^2$, but a physically realizable generation density. The noise component is limited by the finite throughput of the parent throat channel, which opens the daughter branch at the critical scale

$$M_{\rm ign} \sim 0.6\, M_{\rm Moon}.$$

In dimensionless form, this limit is equivalent to a valve-limited tail

$$\lambda^{\rm valve}_{\rm noise}(m) = \frac{\lambda_{\rm raw}(m)\lambda_{\rm valve}(m)}{\lambda_{\rm raw}(m) + \lambda_{\rm valve}(m)}, \qquad \lambda_{\rm raw}(m) = \frac{\lambda_{\rm max}}{m^2}.$$

If the early valve bandwidth is nearly constant, then the compact form

$$\Lambda^{\rm valve}_{{\rm noise},time}(t) = \frac{1}{\tau_0^2}\frac{\lambda_{\rm max}}{d_0^2 + (t/\tau_0)^2}$$

follows from the relation

$$d_0^2 = \frac{\lambda_{\rm max}}{\lambda_{\rm valve}} = \frac{\lambda_{\rm max}}{\tau_0^2 \Lambda_{\rm valve}}.$$

Thus, the early neutrino mass is limited not by an artificial saturated response function, but by the finite energy and channel budget of the parent valve.

Mass freezing after birth.

After birth, the neutrino hardly participates in strong graph-surgery events. Therefore, its propagation mass retains the imprint of the birth epoch:

$$\boxed{m^{\rm eff}_{\nu,i}(t_{\rm obs}; t_b) \simeq m^{\rm birth}_{\nu,i}(t_b)} \tag{A28}$$

provided that

$$\Gamma_{\nu{\rm reset}}(t_{\rm obs} - t_b) \ll 1.$$

Here, $\Gamma_{\nu{\rm reset}}$ is the rate of rare events capable of resetting the neutrino correction package. Rapid relaxation of the mass to the current background is not introduced, since it would require strong interaction of the neutrino with the graph and would contradict its interpretation as a weakly interacting $1D$ packet.

The cosmological memory of the neutrino mass in IKT refers to the difference between populations born in different epochs, rather than a continuous change in the mass of the same neutrino. For two birth epochs, we have

$$\frac{m^{\rm birth}_{\nu,i}(t_1)}{m^{\rm birth}_{\nu,i}(t_2)} = \left[\frac{\rho_{\rm gen}(t_1)}{\rho_{\rm gen}(t_2)}\right]^{1/4}.$$

Therefore, $C\nu B$-relic neutrinos may have an effective propagation mass different from that of modern solar or laboratory neutrinos, but the fourth root makes this drift significantly milder than a linear dependence on the generation density.

For a standard $C\nu B$ population, the ratio

$$R_\nu^{C\nu B} = \left[\frac{\rho_{\rm gen}(t_{\rm dec})}{\rho_{\rm gen}(t_0)}\right]^{1/4}$$

must be consistent with cosmological constraints on $\sum m_\nu$ in the chosen dark sector model.

© 2026 by the author(s). Distributed under a Creative Commons CC BY license.

Preprints.org (www.preprints.org) | NOT PEER-REVIEWED | Posted: 9 June 2026 doi:10.20944/preprints202606.0589.v1

Very early inflationary or pre-geometric correction packets may be heavier, but their number is limited by the finite energy budget of the valve:

$$N_\nu^{\text{early}} m_\nu^{\text{early}} c_0^2 \lesssim \epsilon_\nu M_{\text{ign}} c_0^2.$$

Therefore, heavy early neutrino-like packets are not required to form a numerous ordinary active $C\nu B$ population; they may dissociate, escape into the dark sector, or have a strongly suppressed density.

Remark A9 (Hypothesis Status)**.** *Equation* (A27) *is the minimal IKT hypothesis for the birth of the effective neutrino mass from the graph generation density. It relates the neutrino scale to the dark-energy scale* $\rho_{\text{gen}}^{1/4}$*, preserves the mass freeze-out at birth, and remains falsifiable via* $C\nu B$*, constraints on* $\sum m_\nu$*, laboratory masses, and the weak/flavor sector.*

Appendix C.3. Baryon Spectrum and Nucleon Topology

Appendix C.3.1. Minimal Confinement Cell and Baryon Route

In the Standard Model, the proton mass has a predominantly non-perturbative origin: it is determined not by the sum of the bare masses of quarks, but by the confinement energy, the gluon field, and the kinetic energy of the quark degrees of freedom. In IKT, this energy is interpreted as the integral algorithmic phase delay of the baryon knot. Therefore, the natural object is not the perturbative sum of quark masses, but the phase capacity of the minimal confinement cell.

Definition A16 (Baryon binding node)**.** *The proton is modeled as a confinement binding of three fermionic arcs connected in a color singlet. Color neutrality is given by the normalized invariant combination*

$$|B\rangle_{\text{col}} = \frac{1}{\sqrt{6}} \epsilon_{abc} |q_1^a q_2^b q_3^c\rangle.$$

For the proton, we can write

$$|p\rangle_{\text{col}} = \frac{1}{\sqrt{6}} \epsilon_{abc} |u^a u^b d^c\rangle,$$

where the complete fermion wave function also includes the spin-flavor-space sector. The indices a, b, c *denote color indices, and the baryon node itself is a local region of the graph in which the operator* U_m *routes three fermionic channels through a common singlet confinement gate.*

Appendix C.3.2. The Proton Mass as the Spectral-Channel Capacity of the Minimal Confinement Cell

Lemma A8 (Spectral-channel measure of the confinement cell)**.** *The minimal baryon confinement cell in IKT is described as the product of a longitudinal arc sector and a neutral color sector:*

$$\mathcal{C}_p = \mathcal{C}_{\text{arc}} \times \mathcal{C}_{\text{col}}.$$

The longitudinal sector consists of three open fermionic arcs bounded by a baryon gate. The leading Dirichlet mode of the phase delay on each such arc determines the canonical phase coordinate

$$\varphi_a \in [0, \pi], \qquad a = 1, 2, 3.$$

Therefore, the channel measure of the three longitudinal arcs is

$$\mu_{\text{arc}} = \prod_{a=1}^{3} \int_0^\pi d\varphi_a = \pi^3.$$

The color sector of the minimal singlet coupling is given by two neutral Cartan holonomies corresponding to the rank of the color group:

$$\operatorname{rank} SU(3) = 2.$$

© 2026 by the author(s). Distributed under a Creative Commons CC BY license.

Preprints.org (www.preprints.org) | NOT PEER-REVIEWED | Posted: 9 June 2026 doi:10.20944/preprints202606.0589.v1

The leading IKT normalization uses neither the full Haar measure on $SU(3)$ nor the full Weyl chamber of the group, but rather the flat channel measure of the minimal neutral Cartan gate of the singlet coupling:

$$\eta_1, \eta_2 \in [0, \pi], \qquad \mu_{\mathrm{col}}^{\mathrm{ch}} = \int_0^{\pi} d\eta_1 \int_0^{\pi} d\eta_2 = \pi^2.$$

Therefore,

$$\mu_p(\mathcal{C}_p) = \mu_{\mathrm{arc}} \mu_{\mathrm{col}}^{\mathrm{ch}} = \pi^5.$$

Proof. The longitudinal part follows from the three independent first Dirichlet modes of open fermionic arcs. The color part uses only the minimal neutral Cartan channel of the singlet gluon, rather than the full group measure $SU(3)$. Therefore, the result has the status of a spectral-channel derivation under the adopted normalization of the phase coordinates U_m. □

Hypothesis A7 (External 3D routing of the baryon nucleus)**.** *The leading macroscopic inertial delay of a baryon node within the marginal rigidity hypothesis is obtained as a relation between the internal confinement capacity and the isotropic external routing channels of the vacuum graph. In a three-dimensional network, the number of such channels is equal to the degree of a local isotropic node:*

$$k_{\mathrm{ext}} = 2D = 6.$$

This number is not the trace of a unitary shift operator. It represents the external channel multiplicity of the connection between the internal baryon nucleus and the vacuum. This hypothesis is a baryonic application of the general marginal rigidity hypothesis from Hypothesis A1; it is not a return to a cubic lattice.

Conditional Corollary 4 (Leading topological formula for the proton mass)**.** *The dimensionless topological delay of proton confinement is equal to*

$$\Theta_p^{(0)} = k_{\mathrm{ext}} \mu_p(\mathcal{C}_p) = 6\pi^5.$$

If the electron mass m_e is used as the unit of the minimum stable fermionic delay, then the leading topological formula for the mass ratio takes the form

$$\boxed{\left(\frac{m_p}{m_e}\right)_{\mathrm{top}} = 6\pi^5}.$$

Proof. Under the adopted spectral-channel measure, the internal confinement space of the minimal proton node has a phase capacity of π^5. Isotropic external routing in a three-dimensional network yields six channels of communication between the internal baryonic nucleus and the vacuum. By the product rule for channel measures

$$\Theta_p^{(0)} = k_{\mathrm{ext}} \mu_p(\mathcal{C}_p) = 6\pi^5.$$

The electron is the minimal stable fermionic route in this IKT formalism; its mass defines the unit of fermionic phase delay:

$$\Theta_e = 1, \qquad m_e \leftrightarrow \Theta_e.$$

Therefore,

$$\left(\frac{m_p}{m_e}\right)_{\mathrm{top}} = \frac{\Theta_p^{(0)}}{\Theta_e} = 6\pi^5.$$

□

© 2026 by the author(s). Distributed under a Creative Commons CC BY license.

Preprints.org (www.preprints.org) | NOT PEER-REVIEWED | Posted: 9 June 2026 doi:10.20944/preprints202606.0589.v1

Numerically

$$6\pi^5 = 1836.1181087\ldots.$$

For $m_e = 0.51099895069\,\mathrm{MeV}$, this gives

$$m_p^{\mathrm{top}} \approx 938.2544\,\mathrm{MeV}.$$

The physical value

$$m_p^{\mathrm{exp}} \approx 938.2721\,\mathrm{MeV}$$

differs by a relative amount of the order of

$$1.9 \times 10^{-5}.$$

Therefore, a more accurate expression is

$$\frac{m_p^{\mathrm{phys}}}{m_e} = 6\pi^5 \rho_p, \qquad \rho_p \simeq 1.0000188.$$

The small correction ρ_p must account for isospin splitting, electromagnetic self-energy, finite current masses of quarks, and residual deformation of the confinement phase cell. The main result of IKT is that the overwhelming majority of baryon mass arises as the spectral-channel phase capacity of the confinement node, rather than as the sum of the Higgs masses of the constituent quarks.

Appendix C.3.3. Topological Anchor of the Strong Interaction and Graph Polarization

In the Standard Model, the strong coupling α_s is defined as a running constant at a chosen energy scale and in a chosen renormalization scheme. Typically, the value at the M_Z scale is used as a reference, after which the coupling is transferred to other energies via renormalization group equations. In IKT, the natural object is not a universal constant α_s at all energies, but a topological anchor of the strong coupling at the scale of the minimum baryon binding.

From the spectral-channel cell of proton confinement, the following decomposition follows

$$\mathcal{C}_p = \mathcal{C}_{\mathrm{arc}} \times \mathcal{C}_{\mathrm{col}} = [0,\pi]^3_{\mathrm{arc}} \times [0,\pi]^2_{\mathrm{col}}.$$

Here, $\mathcal{C}_{\mathrm{arc}}$ describes the longitudinal phase delays of the three fermionic arcs, and $\mathcal{C}_{\mathrm{col}}$ describes the two independent neutral Cartan holonomies of the singlet coupling. The corresponding channel measures are

$$\mu_{\mathrm{arc}} = \pi^3, \qquad \mu_{\mathrm{col}}^{\mathrm{ch}} = \pi^2.$$

The eight gluon directions $\dim SU(3) = 8$ do not disappear in this context: they relate to the dynamics of color gluing and to the spectrum of adjoint excitations, whereas π^2 describes the minimal neutral holonomy of the baryon singlet.

Hypothesis A8 (Geometric cross-section of the strong interaction)**.** *The strong interaction in the baryon singlet is an internal act of topological gluing of fermionic arcs through a color confinement gate. Therefore, the leading dimensionless weight of the color gluing is defined not as the fraction of the color sector in the total measure $\mathcal{C}_p$, but as the ratio of the phase capacity of the binding channel to the phase capacity of the bound longitudinal arcs:*

$$\alpha_{s,\mathrm{top}}(\mathcal{Q}_{\mathrm{conf}}) = \frac{\mu_{\mathrm{col}}^{\mathrm{ch}}}{\mu_{\mathrm{arc}}}.$$

Here, $\mathcal{Q}_{\mathrm{conf}}$ is the scale of the minimum baryon binding.

© 2026 by the author(s). Distributed under a Creative Commons CC BY license.

Preprints.org (www.preprints.org) | NOT PEER-REVIEWED | Posted: 9 June 2026 doi:10.20944/preprints202606.0589.v1

Substituting the channel measures, we obtain

$$\boxed{\alpha_{s,\mathrm{top}}(\mathcal{Q}_{\mathrm{conf}}) = \frac{\pi^2}{\pi^3} = \frac{1}{\pi} \approx 0.31831}.$$

In the standard normalization

$$\alpha_s = \frac{g_s^2}{4\pi}$$

this corresponds to the simple topological amplitude

$$g_{s,\mathrm{top}} = 2.$$

It is important to note that $\alpha_{s,\mathrm{top}} = 1/\pi$ is not a statement about the limit of $\alpha_s(Q \to 0)$ in perturbative QCD. This is the IKT matching condition at the scale of the confinement seam. The physical running relation must arise via the graph polarization of the color channels.

Graph Polarization and Roadmap for Deriving the Running $\alpha_s(\mathcal{Q}^2)$

The topological anchor

$$\alpha_{s,\mathrm{top}}(\mathcal{Q}_{\mathrm{conf}}) = \frac{1}{\pi}$$

specifies the strong-coupling channel normalization at the scale of the minimal confinement gauge. This quantity is not the universal limit $\alpha_s(Q \to 0)$ in perturbative QCD. It plays the role of the IKT matching condition at the hadronic scale.

For the running sector, it is necessary to calculate the graph polarization of the color channels. The leading hypothesis of IKT is that the short-wavelength bypass routes of the operator U_m give a low-energy analogue of the single-loop color β-function:

$$\mathcal{Q}^2 \frac{\partial \alpha_s^{\mathrm{eff}}}{\partial \mathcal{Q}^2} = -\frac{b_0^{\mathrm{IKT}}}{4\pi}(\alpha_s^{\mathrm{eff}})^2 + \mathcal{O}\big((\alpha_s^{\mathrm{eff}})^3\big),$$

$$b_0^{\mathrm{IKT}} = 11 - \frac{2}{3}n_f.$$

In this expression, the term $-2n_f/3$ corresponds to fermionic screening of accessible quark routes, while the positive term $+11$ corresponds to color antiscreening of neutral gluon detour channels. A complete microderivation of this number requires obtaining graph analogues of the group invariants

$$C_A = 3, \qquad T_R = \frac{1}{2},$$

and therefore remains a separate computational task.

In the leading-log approximation between flavor thresholds:

$$\alpha_s^{\mathrm{eff}}(\mathcal{Q}^2) = \frac{\alpha_{s,\mathrm{top}}}{1 + \dfrac{b_0^{\mathrm{IKT}}}{4\pi}\alpha_{s,\mathrm{top}} \ln(\mathcal{Q}^2/\mathcal{Q}^2_{\mathrm{conf}})}.$$

As the thresholds c, b, t are crossed, the value of n_f and the matching scheme change. Using $\alpha_{s,\mathrm{top}} = 1/\pi$ as an initial condition at the hadronic scale of the order of 1–2 GeV and standard stepwise evolution across flavor thresholds leads to the estimate

$$\alpha_s^{\mathrm{eff}}(M_Z) \sim 0.12,$$

which lies within the correct range of the observed value $\alpha_s(M_Z) \simeq 0.118$ [17]. An exact verification requires two- and three-loop graph β-functions, matching thresholds, and an explicit specification of the renormalization scheme.

© 2026 by the author(s). Distributed under a Creative Commons CC BY license.

Preprints.org (www.preprints.org) | NOT PEER-REVIEWED | Posted: 9 June 2026 doi:10.20944/preprints202606.0589.v1

Thus, IKT does not replace the running of the strong coupling with a single constant. It proposes the initial topological condition

$$\alpha_{s,\mathrm{top}}(\mathcal{Q}_{\mathrm{conf}}) = \frac{1}{\pi},$$

after which the scale dependence, flavor thresholds, the negative sign of the β-function, and matching to M_Z remain a mandatory computational layer.

Appendix C.3.4. Neutron: Algorithmic Work on the Compactification of the $U(1)$ Flow and Isospin Splitting

The proton and neutron share a common leading baryonic framework: three fermionic arcs connected by neutral color holonomies of the minimal confinement cell $\mathcal{C}_p$. Therefore, in the leading topological approximation, their basic confinement mass is the same.

The difference between the proton and the neutron arises not from a change in the three-arc cell itself, but from different routing of the transverse $U(1)$ flux. In IKT, the mass difference $m_n - m_p$ is interpreted as the energy cost of the internal closure of the charge flux in a neutral baryon. In standard theory, this splitting includes strong isospin violation, electromagnetic self-energy, and non-perturbative QCD+QED dynamics [15]; in IKT, these contributions appear as infrared deformations around the leading topological closure anchor.

Hypothesis A9 (Logarithmic work of the internal $U(1)$-compactification)**.** *The open $U(1)$-flow of the proton baryon framework has an outer angular routing measure*

$$\mu_{\mathrm{open}} = \mathrm{Vol}_\Omega(S^2) = 4\pi$$

in the canonical normalization of the unit angular sphere. This measure is not the internal volume of the $U(1)$ group; it specifies the number of external angular channels through which the charge current can flow into the surrounding three-dimensional vacuum graph.

A neutron has the same internal charged arcs but zero external divergence $Q = 0$. Therefore, the open phase flux must be compactified into the internal unit channel of the confinement cell:

$$\mu_{\mathrm{closed}} = 1.$$

In a stochastic quantum walk network, the algorithmic resistance to phase flow compression is assumed to be inversely proportional to the available channel measure:

$$F_\mu \propto \frac{1}{\mu}.$$

Then the dimensionless work of phase compactification is equal to

$$\Delta\theta_{\mathrm{closure}} = \int_1^{4\pi} \frac{d\mu}{\mu} = \ln(4\pi).$$

Hypothesis A10 (Isomorphism of the minimal compensating loop)**.** *The minimal internal route capable of compensating for one quantum of $U(1)$ divergence and preserving 4π-spinor holonomy has the same topological class as the minimal free electronic cycle K_e. Therefore, the dimensional scale of the phase compactification is given by the monodromic mass of the electronic route:*

$$M_{K_e} c_0^2 = \frac{\hbar}{T_{K_e}} |\Theta_{K_e}|.$$

© 2026 by the author(s). Distributed under a Creative Commons CC BY license.

Preprints.org (www.preprints.org) | NOT PEER-REVIEWED | Posted: 9 June 2026 doi:10.20944/preprints202606.0589.v1

From hypotheses A9 and A10, the topological anchor of the internal charge closure follows:

$$\boxed{\Delta m^{\text{top}}_{\text{closure}} = M_{K_e} \ln(4\pi)}. \tag{A29}$$

Equation (A29), in the laboratory SI projection $M_{K_e} \to m_e$, yields the following expression for the physical mass of the neutron:

$$m_n = m_p + m_e \ln(4\pi) + \delta^{\text{IR}}_{np}, \tag{A30}$$

In equation (A30), the quantity δ^{IR}_{np} denotes the residual infrared deformation correction: graph polarization, electromagnetic self-energy, and color refractions after selecting the base topological closure anchor.

Numerically,

$$\ln(4\pi) = 2.53102425,$$

whereas the observed ratio

$$\frac{m_n - m_p}{m_e} = 2.53098858$$

follows from the CODATA values $m_n - m_p = 1.29333251\,\text{MeV}$ and $m_e = 0.51099895069\,\text{MeV}$ [14]. Thus, the logarithmic phase compactification provides a strong topological anchor for isospin splitting:

$$\delta^{\text{IR}}_{np} \approx -18\,\text{eV}.$$

A complete derivation of the neutron lifetime requires a separate weak-gateway calculation, including axial overlap, phase volume, V_{ud}, g_A, and radiation corrections.

Deformation correction: internal topological atom

The negative sign δ^{IR}_{np} indicates that maintaining a compensating $U(1)$ loop inside a baryonic cell is slightly cheaper than maintaining a free electron cycle in empty vacuum. In IKT, this is interpreted as a bound state of the internal charge loop with the baryonic framework.

The natural scale of such a correction is given by the Rydberg parameter of electromagnetic coupling:

$$E^{\text{top}}_R = \frac{1}{2}\alpha^2_{\text{top}} m_e \approx 13.6\,\text{eV}.$$

Therefore, the residual can be written as

$$\delta^{\text{IR}}_{np} = -C_{\text{bind}}\alpha^2_{\text{eff}} m_e + \delta_{\text{rad}} + \delta_{\text{col}},$$

where $C_{\text{bind}} \sim 1/2$, α_{eff} is the effective $U(1)$ coupling inside the dense confinement cell, δ_{rad} is the radiative electroweak correction, and δ_{col} is the deformation caused by color graph refraction. The proximity of the scale $|\delta^{\text{IR}}_{np}| \sim 18\,\text{eV}$ to E^{top}_R is not independent evidence, but indicates that the residual correction has a natural electromagnetic scale rather than a new free MeV parameter.

Beta Decay as a Weak Relaxation of Internal Closure

A free neutron is metastable because the internal $U(1)$ closure loop has a larger phase delay than the open proton path. Beta decay

$$n \to p + e^- + \bar{\nu}_e$$

is interpreted in IKT as a weak relaxation of this internal closure.

The topological formula immediately gives the energy balance of the decay:

$$Q^{\text{top}}_\beta = \Delta m^{\text{top}}_{\text{closure}} - m_e = m_e[\ln(4\pi) - 1].$$

Numerically

$$Q^{\text{top}}_\beta \approx 0.78235\,\text{MeV},$$

© 2026 by the author(s). Distributed under a Creative Commons CC BY license.

Preprints.org (www.preprints.org) | NOT PEER-REVIEWED | Posted: 9 June 2026 doi:10.20944/preprints202606.0589.v1

which agrees with the physical $Q_\beta = m_n - m_p - m_e \approx 0.78233\,\mathrm{MeV}$ up to the same small correction $\delta_{np}^{\mathrm{IR}}$.

Upon decay, the internal charge-closing loop breaks:

1. the baryonic framework relaxes into a proton state with open external divergence $Q = +1$;
2. the electron-like compensating loop $C_K = 0$ exits into the external three-dimensional lattice as an electron;
3. a one-dimensional neutrino packet carries away the residual momentum, phase, and lepton number.

Roadmap of the weak gate and the neutron lifetime

The topological formula fixes Q_β, but does not in itself determine the lifetime of a free neutron. The latter depends on the weak charged-current gate $\mathcal{G}_W$, the phase volume of the three-body decay, the axial structure of the nucleon transition, and radiation corrections. In an effective form

$$\Gamma_n^{\mathrm{IKT}} = \frac{1}{\tau_n} = \Gamma_{\mathcal{G}_W}\, \mathcal{F}_\beta(q_\beta)\, \mathcal{M}_{\mathrm{closure}},$$

where

$$q_\beta = \frac{Q_\beta}{m_e} = \ln(4\pi) - 1 + \frac{\delta_{np}^{\mathrm{IR}}}{m_e}.$$

In the low-energy limit, this structure should reduce to the standard form of weak decay:

$$\Gamma_n = \frac{G_{F,\mathrm{IKT}}^2 |V_{ud}^{\mathrm{IKT}}|^2}{2\pi^3}(1 + 3g_{A,\mathrm{IKT}}^2) m_e^5 f(q_\beta)(1 + \delta_R^{\mathrm{IKT}}).$$

The chiral stiffness of the orthogonal baryon tripod can serve as the leading geometric anchor for the axial factor:

$$g_A^{(0)} = \frac{4}{\pi} \approx 1.273.$$

This value is close to the physical axial factor, but is not a complete calculation of g_A. It is necessary to derive a correction

$$g_A^{\mathrm{IKT}} = \frac{4}{\pi} + \delta_A^{\mathrm{graph}}$$

from the graph polarization of the weak gate and the color environment. Consequently, IKT already fixes the topological source Q_β and provides a geometric anchor $g_A^{(0)}$, but the complete derivation of the observed lifetime $\tau_n \simeq 878$–$880\,\mathrm{s}$ [16] requires the calculation of G_F, V_{ud}, g_A, δ_R, and the phase volume of the weak recoupling.

Inside stable nuclei, the decay of a bound neutron may be energetically closed or suppressed by the collective delocalization of the multinucleon graph. In beta-active nuclei, on the other hand, the mass balance of the entire nuclear graph yields a positive Q_β^{nuc}, and the same mechanism becomes allowed.

Appendix C.4. Scalar Sector: Graph-Elastic Response and the Observed 125 GeV *Channel*

Appendix C.4.1. The observed 125 GeV scalar channel as a graph-elastic reaction

This subsection is not part of the minimal mass derivation in IKT. The masses of stable particles in the main logic arise from the monodromy of closed routes $W_K^{\mathrm{eff}} \to \Theta_K \to M_K$. The observed 0^{++} resonance near 125 GeV is considered below only as an observational scalar-channel matching layer, that is, as a way to match the longitudinal graph susceptibility with experimental amplitudes.

In this subsection, the language of the Higgs sector is used not as a microscopic ontology, but as a phenomenological interface with the experiment. The methodological principle of IKT is as follows: the theory bears no obligations to the Standard Model Lagrangian, the geometric formalism of GR-STO, or any other existing theoretical framework as a fundamental reality. The only obligation

© 2026 by the author(s). Distributed under a Creative Commons CC BY license.

Preprints.org (www.preprints.org) | NOT PEER-REVIEWED | Posted: 9 June 2026 doi:10.20944/preprints202606.0589.v1

is to reproduce the observed invariants: masses, charges, cross sections, lifetimes, branching ratios, spectral poles, weak mixing, and gravitational effects in the regions where they are measured.

Therefore, IKT does not postulate a fundamental scalar field, a distinct mass-carrying particle, or independent Yukawa constants. The observed resonance near 125 GeV is interpreted as a collective longitudinal mode of the graph phase capacitance, that is, as an elastic response of the vacuum graph to a local topological delay. The variables $h(x)$, F_h, g_{hff}, g_{hVV}, and λ_K below are coordinates of a low-energy detector projection, not proof of the existence of a fundamental bare Higgs field in the microdynamics of the graph.

In the Standard Model, the observed masses and scalar amplitudes are conveniently parameterized in terms of the Higgs field and Yukawa coefficients,

$$m_f = \frac{y_f v_{\mathrm{EW}}}{\sqrt{2}}, \qquad g_{hff}^{\mathrm{SM}} = \frac{m_f}{v_{\mathrm{EW}}}.$$

In IKT, this expression is regarded as a successful phenomenological map, but not as an ontological explanation of mass. The microscopic source of inertia is the integral phase delay θ_M of a stable topological cycle. The task of IKT is not to literally reconstruct the Higgs mechanism, but to derive the observable effects it encodes: the scalar 0^{++} resonance channel, mass-dependent creation and decay amplitudes, branching ratios, and the unitarization of longitudinal WW scattering.

Appendix C.4.2. Graph Elasticity and Universal Susceptibility of the Scalar Response

Let $\Phi(x)$ denote the local phase capacitance of the vacuum graph. It is convenient to write a small longitudinal deformation as

$$\Phi(x) = \Phi_0 e^{\varphi(x)},$$

where Φ_0 is the equilibrium capacitance, and $\varphi(x)$ is the dimensionless deformation. We define the detector coordinate of the observed scalar channel as

$$h_{\mathrm{obs}}(x) = F_h \varphi(x).$$

Here F_h is not a fundamental field constant, but an elastic scale through which the laboratory projection maps the dimensionless deformation of the graph to the amplitude of the observed 0^{++} channel.

The mass of the topological cycle K depends on the local phase capacitance:

$$M_K(\Phi) = M_K^{(0)} \exp(\lambda_K \varphi),$$

where

$$\lambda_K = \left. \frac{\partial \ln M_K}{\partial \ln \Phi} \right|_{\Phi_0}$$

— the elastic susceptibility of this topological class.

Hypothesis A11 (Universal elastic susceptibility)**.** *In linear mode, the longitudinal deformation of the graph capacitance scales the integral phase delay of any stable massive cycle identically:*

$$\lambda_K = 1 + \delta_K, \qquad |\delta_K| \ll 1.$$

The leading term $\lambda_K \simeq 1$ implies that the measured relaxation amplitude of the scalar channel is proportional to the mass of the topological cycle. The deviations δ_K must have a graph-topological structure and correlate with the particle's knot class.

If we write the low-energy response in the familiar form of the effective mass term,

$$\mathcal{L}_K^{\mathrm{eff}} = -M_K(\Phi)\bar{\psi}_K \psi_K,$$

© 2026 by the author(s). Distributed under a Creative Commons CC BY license.

Preprints.org (www.preprints.org) | NOT PEER-REVIEWED | Posted: 9 June 2026 doi:10.20944/preprints202606.0589.v1

then the expansion in terms of $h_{\rm obs}/F_h$ yields the observed scalar response coefficient

$$\boxed{g^{\rm obs}_{hKK} = \frac{\lambda_K M_K}{F_h}}.$$

In the universal limit $\lambda_K \simeq 1$, this coefficient has mass proportionality

$$g^{\rm obs}_{hKK} \simeq \frac{M_K}{F_h}.$$

This formula does not introduce individual Yukawa parameters as initial constants. It merely states that the observed scalar response is the logarithmic derivative of the topological mass with respect to the total graph capacity.

Neutrino effective masses do not enter this local elastic response on the same footing as the masses of charged leptons, since the neutrino is not a stable local node. Their small propagation masses must arise from the bridge phase, weak mixing, and cosmological memory of the birth mass.

Appendix C.4.3. Connection to Massive Weak Channels

The same graph-elastic principle should yield the observed scalar channel response to massive weak modes. Here, W and Z are understood not as fundamental carriers, but as the names of low-energy resonant channels of the weak gate. If the mass of a vector mode is determined by the elastic energy of the phase-calibration channel, then the natural scale form is

$$m_V^2(\Phi) = m_V^2(\Phi_0)e^{2\varphi}.$$

Then

$$m_V^2(\Phi) = m_V^2\left(1 + 2\frac{h_{\rm obs}}{F_h} + \mathcal{O}(h_{\rm obs}^2)\right),$$

and the observed response coefficient takes the form

$$\boxed{g^{\rm obs}_{hVV} = \frac{2m_V^2}{F_h}}.$$

When $F_h \simeq v_{\rm EW}$, this yields the same mass-squared dependence of the WW and ZZ amplitudes that is experimentally described by the Higgs sector of the Standard Model. In IKT, such a coincidence is a requirement of observational equivalence, not an acceptance of the Higgs mechanism as the microscopic cause of mass.

Appendix C.4.4. The Meaning of the 125 GeV Mass

In IKT ontology, the mass of the observed 125 GeV resonance is not the bare mass of a fundamental point scalar field. It defines the spectral gap of the collective longitudinal mode of the graph capacitance:

$$m_{0^{++}}^2 = \frac{1}{F_h^2}\frac{\partial^2 U_{\rm graph}}{\partial \varphi^2}\bigg|_{\varphi=0},$$

where $U_{\rm graph}(\varphi)$ is the effective elastic deformation energy of the vacuum graph. In this sense, $m_{0^{++}} \simeq 125$ GeV is the eigenfrequency of the "ringing" of local connectivity near the saturation limit $p_{\rm stay} \to 1$, projected into laboratory units.

The decay channels of the observed scalar resonance are interpreted as relaxation channels of this graph mode into accessible topological sectors. The leading branching relations must follow from the same response coefficients $g^{\rm obs}_{hKK}$ and $g^{\rm obs}_{hVV}$, and the loop channels $h \to \gamma\gamma$ and $h \to gg$ must arise via charged and color topological channels.

© 2026 by the author(s). Distributed under a Creative Commons CC BY license.

Preprints.org (www.preprints.org) | NOT PEER-REVIEWED | Posted: 9 June 2026 doi:10.20944/preprints202606.0589.v1

Appendix C.4.5. Status of the Hierarchy Problem

Since IKT does not postulate a fundamental scalar field with an arbitrary bare mass, the hierarchy problem is reduced to the task of calculating the finite spectral gap of a longitudinal elastic mode of a discrete graph. A complete solution requires deriving from the microdynamics U_m the quantities that, in the laboratory projection, are measured as

$$F_h, \qquad m_{0^{++}}, \qquad \lambda_K, \qquad \lambda_h.$$

The leading testable hypothesis of IKT is that

$$F_h \simeq v_{\mathrm{EW}}, \qquad \lambda_K \simeq 1,$$

and the observed 125 GeV resonance is a collective scalar mode of graph strength, rather than a fundamental field independent of the topological structure of the masses.

Appendix C.4.6. Status of the Scalar Sector: Observational Matching, Not Mass Origin

The scalar sector in IKT is not the source of the inertial masses of stable routes. Particle masses in the minimal ontology are determined by the monodromic phase gaps of closed topological cycles. The observed 125 GeV channel plays the role of an experimental coordinate of the longitudinal graph-elastic response, which the theory must reproduce via the U_m spectrum and the susceptibility of saturated local subgraphs. Therefore, all parameters F_h, $m_{0^{++}}$, λ_K, and λ_h in this section have the status of observational/scalar-interface matching, rather than fundamental constants of microdynamics.

Appendix C.5. Summary of the Microscopic Limit and Status of Spectral Anchors

Appendix C.5.1. Summary Table of Particles and Topological Classes

Object	IKT Interpretation	Status
e	minimal charged 4π-path K_e	spectral target / normalization anchor
$n_e^{(0)} = 10$	factored parameter-rank of the electronic path	conditional parameter-rank result
μ	toric trefoil 3_1	leading topological anchor
τ	hyperbolic knot 4_1	conditional on κ_{emb}
ν	one-dimensional graph error correction package	weak/flavor hypothesis
p	minimal confinement cell of the baryon singlet	spectral-channel anchor
$n - p$	internal $U(1)$ compactification and isospin splitting	topological anchor + IR residual
0^{++} near 125 GeV	longitudinal graph-elastic response	observational matching

Appendix C.5.2. Status of Numerical Anchors

Numerical relations in the microscopic sector have varying logical statuses. The formulas for m_μ/m_e, m_p/m_e, and $m_n - m_p$ are strong topological anchors, but contain different levels of residual corrections and matching conditions. The tau lepton requires the calculation of the embedding spectral coefficient κ_{emb}, and the scalar 125 GeV channel is an observational coordinate of the longitudinal response, not the underlying mass mechanism.

$$\boxed{\text{mass anchors} \neq \text{all-order spectrum theorem}}$$

Appendix C.5.3. Open Spectral Problems in the Microscopic Sector

To complete the microscopic predictive layer of IKT, the following independent computations must be performed:

1. derive the monodromic mass of the electronic path M_{K_e} from $W_{K_e}^{\mathrm{eff}}$;
2. calculate Γ_e and the correlation factor Ξ_e in $|\Omega_e|_{\mathrm{eff}}$;

© 2026 by the author(s). Distributed under a Creative Commons CC BY license.

Preprints.org (www.preprints.org) | NOT PEER-REVIEWED | Posted: 9 June 2026 doi:10.20944/preprints202606.0589.v1

3. obtain κ_{emb} and f_{4_1} for the hyperbolic nucleus 4_1;
4. derive the graph corrections δ_K^{pol} to the lepton mass anchors;
5. construct the spectral derivation $\alpha_s(\mathcal{Q}^2)$ and the flavor-matching thresholds;
6. obtain the PMNS/CKM matrices as matrix elements of the topological gluing;
7. compute the longitudinal scalar spectrum of the graph-elastic response.

These tasks do not negate the microscopic reduction, but they define the boundary between the already specified topological framework and the future computational program.

Appendix C.5.4. Hard Closure Problems for Future Versions

The following problems are not phenomenological extensions, but closure problems of the core IKT program. Their solution would convert several conditional anchors into genuine microscopic predictions.

1. Spectral equipartition theorem for α_{top}.

The topological fine-structure anchor

$$\alpha_{\mathrm{top}}^{-1} = 4\pi^3 + \pi^2 + \pi$$

requires not only the admissibility of the three recombination strata

$$\mathcal{C}_4, \qquad \mathcal{C}_2, \qquad \mathcal{C}_1,$$

but also the equality of their normalized spectral densities,

$$\rho_4 = \rho_2 = \rho_1 = 1.$$

The required future theorem is not the equality of raw probabilities of the strata, but the equality of spectral density per canonical information capacity:

$$\rho_s = \frac{\text{spectral weight of the stratum } \mathcal{C}_s}{\text{canonical channel capacity } \mu_s} = 1.$$

A possible route is to analyze the prethermal electromagnetic routing block of the microoperator U_m as a unitary quantum walk with a maximally symmetric coin on the admissible $U(1) \times SU(2)$ route space. Since a closed unitary system does not converge to a stationary distribution in the classical sense, the relevant object should be the Cesaro-averaged or prethermally dephased spectral measure of the corresponding Floquet operator. Peter–Weyl decomposition of the edge Hilbert space into irreducible representations can then be used to show that, in the absence of a stratum-selective term in the coin/update operator, the normalized channel densities are equal up to finite-size and anisotropy corrections:

$$\rho_s = 1 + O(\epsilon_{\mathrm{aniso}}) + O(N_{\mathrm{graph}}^{-1/2}).$$

Proving this result would upgrade α_{top} from a conditional no-fit channel anchor to a microscopic spectral prediction.

2. Inverse phase-impedance theorem and the origin of $\gamma = 1$.

The weak-field gravitational interface of IKT uses

$$\Pi_G = e^{-\chi_G}, \qquad d\tau = \Pi_G dt, \qquad d\ell_{\mathrm{ph}} = \Pi_G^{-1} d\ell.$$

© 2026 by the author(s). Distributed under a Creative Commons CC BY license.

Preprints.org (www.preprints.org) | NOT PEER-REVIEWED | Posted: 9 June 2026 doi:10.20944/preprints202606.0589.v1

The first relation fixes the time component of the metric. The second, inverse phase-impedance relation fixes the spatial component and yields the PPN parameter

$$\gamma = 1.$$

In a more general parametrization,

$$d\ell_{\mathrm{ph}} = \Pi_G^{-a} d\ell,$$

one would obtain $\gamma = a$. Therefore the central future task is to derive $a = 1$ directly from U_m.

A possible proof route is graph homogenization. One should start from a locally statistically isotropic stochastic graph with a localized mass-delay defect and derive the macroscopic eikonal equation of coherent phase transport from the discrete operator U_m or its effective graph Laplacian. The required result is that conservation of phase current in the isotropic prethermal graph medium is equivalent, after homogenization, to a conformal spatial phase metric

$$d\ell_{\mathrm{ph}}^2 = e^{2\chi_G} d\mathbf{r}^2$$

whenever the local clock rate is

$$d\tau = e^{-\chi_G} dt.$$

Equivalently, the Green function of a localized graph-delay defect must produce

$$\chi_G(r) \sim \frac{GM}{c_0^2 r}$$

and the reciprocal spatial impedance

$$d\ell_{\mathrm{ph}} = e^{\chi_G} d\ell.$$

This would turn the current PPN interface into a theorem of microscopic phase-current conservation and graph homogenization.

3. Hyperbolic embedding spectral density for the tau lepton.

The tau-lepton anchor depends on the hyperbolic figure-eight knot

$$4_1$$

through the factor

$$H_{4_1} = \kappa_{\mathrm{emb}} V_H(4_1).$$

Here $V_H(4_1)$ is the hyperbolic volume of the knot complement, while κ_{emb} is the conversion coefficient from continuous hyperbolic volume to discrete graph phase capacity. In the current version κ_{emb} is a conditional spectral coefficient, not yet a derived invariant.

A possible route is to combine hyperbolic knot theory, Mostow–Prasad rigidity, and spectral geometry of graph Laplacians. The figure-eight complement has a rigid finite-volume hyperbolic structure, but its cusp and peripheral torus must be treated explicitly. The future calculation should construct a canonical weighted graph or simplicial approximation of the 4_1 complement, define the corresponding restriction of the microoperator U_m, and compute the cusp-renormalized spectral density of the graph Laplacian or transfer operator. The goal is to obtain

$$\kappa_{\mathrm{emb}}$$

as a genuine spectral invariant of the stochastic complement ensemble, rather than as a phenomenological embedding factor.

© 2026 by the author(s). Distributed under a Creative Commons CC BY license.

Preprints.org (www.preprints.org) | NOT PEER-REVIEWED | Posted: 9 June 2026 doi:10.20944/preprints202606.0589.v1

A complete solution should also determine the boundary susceptibility factor f_{4_1} and the small polarization correction $\delta_\tau^{\mathrm{pol}}$. This would promote the tau mass relation from a conditional hyperbolic-topological estimate to a hard prediction of the lepton hierarchy.

Appendix D. Calculation of Topological Transitions: TTC

Appendix D.1. Mathematical apparatus for calculating topological transitions

Until now, IKT has defined the kinematics of stable topological carriers: masses, charges, phase capacitances, graph delays, and macroscopic fields as coarse-grained projections of the operator U_m. To connect with experimental physics, the following layer is needed: a rule for calculating transition amplitudes, scattering cross sections, and decay widths.

In QFT, such quantities are calculated via the Lagrangian, path integrals, and Feynman diagrams. In TTC, these diagrams are not accepted as a microscopic ontology. They must arise as a low-energy linearization of a more general process: local surgery on the adjacency matrix, in which phase routes are re-connected, broken, stitched together, or transferred to bypass channels of the graph.

Let us call the corresponding computational layer the Topological Transition Calculus:

$$\mathrm{TTC} = \text{Topological Transition Calculus.}$$

Its task is not to repostulate virtual carrier particles, but to provide a procedure

$$\text{graph surgery} \longrightarrow \mathcal{M}_{\beta\alpha} \longrightarrow d\sigma, \Gamma,$$

where $\mathcal{M}_{\beta\alpha}$ is the observed transition amplitude between asymptotic topological states.

Remark A10 (TTC Status)**.** *In this work, TTC is introduced as a minimal computational interface. The complete microderivation of all vertices from the operator U_m remains an open problem. Therefore, four levels are distinguished below: elementary graph cobordism, the definition of asymptotic states, the graph-surgery ansatz for the amplitude, and low-energy matching to the observed cross-sections and decay widths.*

Appendix D.1.1. Elementary Topological Transition: Cobordism, Kernel, and Measure

An elementary TTC transition is defined by a local cobordism of graph routes

$$\mathfrak{C} : (G_{\mathrm{in}}, K_{\mathrm{in}}) \longrightarrow (G_{\mathrm{out}}, K_{\mathrm{out}}),$$

where K_{in} and K_{out} denote the input and output stable topological carriers. A cobordism is admissible if it satisfies the locality of the graph gluing, the preservation of admissible topological indices, and the boundary conditions of the chosen interface sector.

Let us denote the set of admissible transitions between asymptotic states α and β by

$$\mathrm{Adm}(\alpha \to \beta).$$

The total TTC amplitude takes the form of a discrete sum over admissible graph surgeries:

$$\boxed{\mathcal{M}_{\beta\alpha}^{\mathrm{TTC}} = \sum_{\mathfrak{C} \in \mathrm{Adm}(\alpha\to\beta)} \mathcal{A}[\mathfrak{C}]}. \tag{A31}$$

The weight of a single cobordism is written as

$$\mathcal{A}[\mathfrak{C}] = \mathcal{N}[\mathfrak{C}] \exp\left(\frac{i}{\hbar_{\mathrm{graph}}} S_{\mathrm{top}}[\mathfrak{C}]\right) \mathcal{K}_{\mathrm{loc}}[\mathfrak{C}] \prod_{e\in\mathfrak{C}} \mathcal{G}_e \prod_K F_K(q_K^2).$$

© 2026 by the author(s). Distributed under a Creative Commons CC BY license.

Preprints.org (www.preprints.org) | NOT PEER-REVIEWED | Posted: 9 June 2026 doi:10.20944/preprints202606.0589.v1

Here, $\mathcal{N}[\mathfrak{C}]$ is the automorphism norm, S_{top} isthe topological transition action, $\mathcal{K}_{\text{loc}}$ is the local gluing kernel, $\mathcal{G}_e$ are the effective Green's functions, and F_K are the form factors of stable cycles.

Unlike the continuous path integral, the TTC sum is a sum over discrete classes of graph surgery. UV finiteness is ensured by finite graph resolution, a finite number of available local reconnections at a fixed scale, and the suppression of short-wavelength transitions in the form factors. Infrared problems of long-range channels, especially $U(1)$, do not disappear automatically and must be considered via inclusive sums over soft link excitations.

Appendix D.1.2. Asymptotic States and Transition Matrix

An asymptotic state in TTC is defined not by a point particle in the continuum, but by a stable topological carrier together with its macroscopic envelope:

$$|\alpha\rangle = |K_1, p_1, s_1, c_1; \ldots; K_n, p_n, s_n, c_n\rangle.$$

Here, K_i denotes the class of a topological cycle, p_i denotes the emergent four-momentum of its envelope, s_i denotes the frame spin/chirality, and c_i denotes the internal color or channel index, if applicable.

The photon state in this notation is a transverse $U(1)$-link excitation,

$$|\gamma\rangle = |U(1)^{\perp}_{\text{link}}, \mathbf{k}, \lambda\rangle,$$

and the fermionic state is a stable closed path with a Dirac/Floquet envelope,

$$|e^-\rangle = |K_e, \Theta_e, Q_{\text{top}}, s\rangle.$$

The transition matrix is written as

$$S_{\beta\alpha} = \delta_{\beta\alpha} + i(2\pi)^4 \delta^{(4)}(P_\beta - P_\alpha)\mathcal{M}^{\text{TTC}}_{\beta\alpha}.$$

This expression is the laboratory/IR projection. On the microscopic graph, the fundamental object is the sum over cobordisms (A31); the energy-momentum delta function arises only after coarse-graining to the effective translational envelope.

In the low-energy limit, when external wavelengths are much larger than the graph step size, admissible histories are grouped into a small number of effective channels. Then (A31) reduces to the familiar diagrammatic structure: vertices, propagators, external lines, and phase space. In IKT, this structure is not a microscopic ontology, but a convenient macroscopic representation of linearized graph theory.

Appendix D.1.3. Green's Functions, Spectral Densities, and Observable Phase Space

For each channel X, the effective phase shift transfer is given by the inverse operator of the corresponding coarse-grained Laplacian:

$$\mathcal{G}_X(q) = \frac{P_X(q)}{L_X(q) + \mu_X^2 + \Pi_X(q)}.$$

Here P_X is the channel projector, $L_X(q)$ is the eigenvalue of the graph Laplacian in a given sector, μ_X is the possible infrared mass or channel locking, and $\Pi_X(q)$ is the polarization of the vacuum graph.

For the electromagnetic channel

$$\mu_{\text{em}} = 0, \qquad P_X = P_\perp,$$

© 2026 by the author(s). Distributed under a Creative Commons CC BY license.

Preprints.org (www.preprints.org) | NOT PEER-REVIEWED | Posted: 9 June 2026 doi:10.20944/preprints202606.0589.v1

and in the long-wavelength limit, we require

$$L_\perp(q) = Z_\perp q^2 + O(q^4).$$

The calibration normalization is chosen such that $Z_\perp = 1$ in the laboratory projection. This is an observable matching condition, not a postulate of the continuous field.

To transition from the discrete graph spectrum to the observed phase volume, the effective spectral density of accessible harmonics is introduced

$$\rho_X(E) = \sum_{n \in X} \delta_{\mathrm{cg}}(E - E_n),$$

where δ_{cg} denotes the observer's coarse-grained energy resolution. In the infrared limit, the sum over graph harmonics becomes the standard phase volume

$$\sum_{\text{graph harmonics}} \longrightarrow \int d\Pi_n \qquad (qa_0 \ll 1).$$

For n finite particles, the observed phase volume takes the form

$$d\Pi_n = (2\pi)^4 \delta^{(4)}\left(P_{\mathrm{in}} - \sum_f p_f\right) \prod_{f=1}^{n} \frac{d^3 p_f}{(2\pi)^3 2E_f}.$$

In TTC, this object is the IR limit of the spectral sum, not a fundamental measure of the continuum space.

Appendix D.1.4. Observed Cross Sections and Decay Widths

At the fundamental level, the transition rate is determined by the number of admissible graph cobordisms per operational clock-time and the spectral condition of phase-frequency coincidence:

$$\Gamma^{\mathrm{graph}}_{\alpha\to\beta} = \frac{1}{T_{\mathrm{clock}}} \sum_{\mathfrak{C}:\alpha\to\beta} |\mathcal{A}[\mathfrak{C}]|^2 \delta_{\mathrm{cg}}(E_\alpha - E_\beta).$$

In the infrared laboratory frame, this formula takes the standard form.

In natural units $\hbar = c_0 = 1$, the differential cross section of the $2 \to n$ transition is given by the observable form

$$d\sigma_{\alpha\to\beta} = \frac{|\mathcal{M}^{\mathrm{TTC}}_{\beta\alpha}|^2}{4\sqrt{(p_1 p_2)^2 - m_1^2 m_2^2}} d\Pi_n.$$

The width of the decay of state A:

$$d\Gamma_{A\to\beta} = \frac{|\mathcal{M}^{\mathrm{TTC}}_{\beta A}|^2}{2M_A} d\Pi_n.$$

The dimensional SI projection is performed only after calculating the dimensionless amplitude: masses are converted to energies via c_0^2, and times and lengths via $\hbar$ and c_0. Therefore, TTC does not introduce new dimensional constants beyond the already calibrated metric projections of IKT.

Appendix D.2. Phenomenological Scattering and Decay Interfaces

Appendix D.2.1. Selection of Benchmark Processes and Status of Approximations

Below, we consider three minimal TTC benchmark processes: electromagnetic electron scattering, lepton weak decay of the muon, and baryon weak decay of the neutron. These examples do not fully replace all QCT calculations. Their purpose is to show how graph surgery reduces to known IR forms of amplitudes and where specific IKT corrections should appear.

© 2026 by the author(s). Distributed under a Creative Commons CC BY license.

Preprints.org (www.preprints.org) | NOT PEER-REVIEWED | Posted: 9 June 2026 doi:10.20944/preprints202606.0589.v1

The strong sector is not used as a full scattering benchmark in this work: this requires a separate RG bridge $\alpha_s(\mu)$, a hadronization mechanism, and hadron spectral form factors. The minimal role of the strong sector is already captured in the singlet-routing constraint; a full-fledged strong TTC benchmark is left as an open problem at the end of the section.

Appendix D.2.2. Electromagnetic Sector: Coulomb Limit and Møller Scattering

Consider the elastic scattering of two electron loops

$$e^-e^- \to e^-e^-.$$

In TTC, the electron is a stable 4π-frame cycle of class 0_1, and the electromagnetic interaction corresponds to a local reset of the transverse $U(1)$ phase in the bypass channel of the graph.

At the tree level, the amplitude has direct and exchange terms:

$$\mathcal{M}_{ee}^{\mathrm{TTC}} = -g_{\mathrm{em}}^2 \left[\frac{J_{31}^{\mu} P_{\mu\nu}^{\perp}(q_t) J_{42}^{\nu}}{L_{\perp}(q_t)} - \frac{J_{41}^{\mu} P_{\mu\nu}^{\perp}(q_u) J_{32}^{\nu}}{L_{\perp}(q_u)} \right] F_e(q_t^2) F_e(q_u^2) + O(g_{\mathrm{em}}^4).$$

Here

$$g_{\mathrm{em}}^2 = 4\pi\alpha_{\mathrm{top}},$$

J^{μ} — emergent frame currents of electron envelopes, $P_{\mu\nu}^{\perp}$ — transverse projector, and F_e — electron topological form factor. The minus between the t- and u-channels is not an external anticommutation postulate, but the FR-phase of exchange of two 4π-cycles:

$$\rho([E_{12}]) = -1.$$

In the non-relativistic long-wavelength limit, the currents reduce to charge densities, $F_e \to 1$, and

$$L_{\perp}(\mathbf{q}) = |\mathbf{q}|^2 + O(|\mathbf{q}|^4).$$

Then the effective potential is:

$$V(r) = g_{\mathrm{em}}^2 \int \frac{d^3\mathbf{q}}{(2\pi)^3} \frac{e^{i\mathbf{q}\cdot\mathbf{r}}}{|\mathbf{q}|^2} = 4\pi\alpha_{\mathrm{top}} \frac{1}{4\pi r} = \frac{\alpha_{\mathrm{top}}}{r}.$$

This is the first normalization test of TTC: the topological anchor $g_{\mathrm{em}}^2 = 4\pi\alpha_{\mathrm{top}}$ and the three-dimensional Green's function jointly reproduce the Coulomb limit without introducing a fundamental carrier.

Remark A11 (Soft $U(1)$-link modes)**.** *The UV finiteness of the TTC does not automatically eliminate the infrared problem of soft transverse $U(1)$-link excitations. The physical observables in the electromagnetic sector are the inclusive cross sections, summed over the unresolved soft link modes:*

$$\sigma_{\mathrm{obs}} = \sum_{\gamma_{\mathrm{soft}}} \sigma(e^-e^- \to e^-e^- + \gamma_{\mathrm{soft}}).$$

Thus, TTC distinguishes between discrete UV finiteness and the usual IR inclusivity of the long-range $U(1)$ channel.

Appendix D.2.3. Weak Topological Gateway: Muon Decay and G_F-Matching

The

$$\mu^- \to e^- + \bar{\nu}_e + \nu_{\mu}$$

© 2026 by the author(s). Distributed under a Creative Commons CC BY license.

Preprints.org (www.preprints.org) | NOT PEER-REVIEWED | Posted: 9 June 2026 doi:10.20944/preprints202606.0589.v1

in TTC is a low-energy manifestation of the unravelling of the over-stressed cycle 3_1 into the electronic cycle 0_1 with the emission of two 1D error correction packets. Local surgery is performed by the weak gateway $\mathcal{G}_W$.

In the infrared limit, the amplitude must take the form

$$\mathcal{M}_{\mu}^{\mathrm{TTC}} = \frac{G_{F,\mathrm{IKT}}}{\sqrt{2}} \mathcal{F}_{\mu e}^{\mathrm{topo}} \left[J_L^{(\mu \nu_\mu)} J_L^{(e \nu_e)} \right] + O(q^2/M_W^2),$$

where $\mathcal{F}_{\mu e}^{\mathrm{topo}}$ is the topological overlap of the $3_1 \to 0_1$ decoupling operator.

In natural units, the decay width is:

$$\Gamma_{\mu}^{\mathrm{TTC}} = \frac{G_{F,\mathrm{IKT}}^2 m_\mu^5}{192\pi^3} |\mathcal{F}_{\mu e}^{\mathrm{topo}}|^2 F(x_e) \Big(1 + \delta_{\mathrm{rad}} + \delta_{\mathrm{graph}}\Big),$$

where

$$x_e = \frac{m_e^2}{m_\mu^2},$$

and

$$F(x) = 1 - 8x + 8x^3 - x^4 - 12x^2 \ln x$$

is the triplet phase-volume factor of the electron's finite mass. In SI notation, if masses are given in kilograms, the corresponding decay rate is:

$$\tau_{\mu}^{-1} = \frac{G_{F,\mathrm{IKT}}^2 m_\mu^5 c_0^4}{192\pi^3 \hbar^7} |\mathcal{F}_{\mu e}^{\mathrm{topo}}|^2 F(x_e) \Big(1 + \delta_{\mathrm{rad}} + \delta_{\mathrm{graph}}\Big).$$

Lepton universality in TTC does not necessarily imply that $\mathcal{F}_{\mu e}^{\mathrm{topo}} = 1$ literally, but rather that the weak topological overlaps for different lepton transitions are equal up to small polarization corrections:

$$\mathcal{F}_{\mu e}^{\mathrm{topo}} \simeq \mathcal{F}_{\tau e}^{\mathrm{topo}} \simeq \mathcal{F}_{\tau \mu}^{\mathrm{topo}}.$$

A rigorous derivation of these equalities must be obtained from the weak gate algebra $\mathcal{G}_W$ and the FR-structure of lepton cycles.

Appendix D.2.4. Baryon Surgery: Neutron Beta Decay

A free neutron in IKT is described as a metastable baryonic framework in which a compactified compensating $U(1)$ loop is confined within a proton node. Beta decay

$$n \to p + e^- + \bar{\nu}_e$$

corresponds to the breaking of this compactification by the weak gauge group $\mathcal{G}_W$.

The topological part of the energy balance is given by the transition of the routing angle measure

$$\mu_{\mathrm{closed}} = 1 \longrightarrow \mu_{\mathrm{open}} = 4\pi,$$

which yields the contribution

$$\Delta m_{\mathrm{closure}}^{\mathrm{top}} = m_e \ln(4\pi).$$

After electromagnetic, graph-polarization, and IR corrections, the observed decay energy is determined as

$$Q_\beta = m_n - m_p - m_e.$$

© 2026 by the author(s). Distributed under a Creative Commons CC BY license.

Preprints.org (www.preprints.org) | NOT PEER-REVIEWED | Posted: 9 June 2026 doi:10.20944/preprints202606.0589.v1

In the allowed limit, the TTC width of the neutron decay must take the form

$$\tau_n^{-1} = \frac{G_{F,\mathrm{IKT}}^2 |V_{ud}^{\mathrm{IKT}}|^2 m_e^5}{2\pi^3} \left(1 + 3g_{A,\mathrm{IKT}}^2\right) f_R(Q_\beta) |\mathcal{F}_{np}^{\mathrm{topo}}|^2 \left(1 + \delta_{\mathrm{graph}}^{(n)}\right)$$

in natural units. Here $f_R(Q_\beta)$ denotes the phase volume with radiation and Coulomb corrections, and $\mathcal{F}_{np}^{\mathrm{topo}}$ denotes the overlap of the $n \to p$ baryon surgery.

The IKT axial anchor gives the bare value

$$g_A^{(0)} = \frac{4}{\pi}.$$

The physical value must include baryon polarization, pion-like graph tails, and the finite size of the baryon lattice:

$$g_{A,\mathrm{IKT}} = g_A^{(0)} \left(1 + \delta_A^{\mathrm{pol}}\right).$$

Thus, TTC translates the qualitative picture of neutron decoupling into a testable problem: one must derive V_{ud}^{IKT}, $\mathcal{F}_{np}^{\mathrm{topo}}$, δ_A^{pol}, and $\delta_{\mathrm{graph}}^{(n)}$ from graph microdynamics.

Appendix D.2.5. Roadmap for a Strong TTC Benchmark

The strong sector in the current version of TTC defines the color-routing interface, the color current, and the singlet-routing constraint, but does not contain a complete scattering benchmark. For such a benchmark, it is necessary to construct:

1. an RG bridge from α_s^{top} to the running constant $\alpha_s(\mu)$;
2. graph form factors for mesons and baryons;
3. a hadronization mechanism as a final topological rearrangement of color routes;
4. a minimal process, such as a singlet color form factor or low-energy π-like scattering.

Until these objects are constructed, the strong TTC benchmark retains the status of a roadmap rather than a completed computational test.

Appendix D.3. Test Conditions and Analytical Properties of TTC

Appendix D.3.1. Unitarity of the S-matrix and the Optical Theorem on the Graph

On the full space of graph transitions, TTC must define a unitary S-matrix:

$$S_{\mathrm{full}}^\dagger S_{\mathrm{full}} = 1.$$

In the infrared observable sector, this leads to the optical theorem only after the inclusive sum over unresolved graph channels:

$$2\,\mathrm{Im}\,\mathcal{M}_{\alpha\alpha} = \sum_\beta \int d\Pi_\beta |\mathcal{M}_{\beta\alpha}|^2.$$

If a portion of the graph-surgery channels is traced as a hidden sector, the reduced amplitude may appear non-unitary. The physically observable version is the inclusive version, in which the sum over hidden or soft channels restores the probability balance.

Appendix D.3.2. Transversality of the Electromagnetic Channel and Ward's Graph Identities

For the $U(1)$ sector, the graph continuity equation must hold:

$$\Delta_m \rho_i + \sum_{j\sim i} J_{ij} = 0.$$

After coarse-graining, it yields

$$\partial_\mu j^\mu = 0.$$

© 2026 by the author(s). Distributed under a Creative Commons CC BY license.

Preprints.org (www.preprints.org) | NOT PEER-REVIEWED | Posted: 9 June 2026 doi:10.20944/preprints202606.0589.v1

Consequently, under the gauge shift $A_\mu \to A_\mu + \partial_\mu \Lambda$, the variation of the TTC amplitude is given by

$$\delta_\Lambda \mathcal{M}_{\text{em}} = g_{\text{em}} \int d^4x\, \partial_\mu \Lambda\, j^\mu = -g_{\text{em}} \int d^4x\, \Lambda\, \partial_\mu j^\mu = 0.$$

The equivalent momentum-space form — Ward-like identity

$$q_\mu \mathcal{M}^\mu = 0.$$

The transversality of the photon channel is not an additional gauge fixing, but follows from the closed nature of the $U(1)$ phase flux on the graph.

Appendix D.3.3. FR Statistics, Locality, and Discrete UV Finiteness

FR statistics.

The exchange of identical 4π-cycles defines the element $[E_{12}]$ of the fundamental group of the configuration space of routes. For the fermion sector

$$\rho([E_{12}]) = -1.$$

This ensures the antisymmetry of fermionic amplitudes without separately postulating anticommuting fields.

Locality and causal support.

Nonlocal graph detour routes should not give rise to observable superluminal signal transmission. In the infrared limit, their contribution must reduce to the causal retarded/advanced Green's functions of the effective channels. This locality is a property of the observable prethermal/coarse-grained sector, not a statement about the existence of a predefined continuous background.

Discrete UV finiteness.

For $qa_0 \sim 1$, the amplitudes are suppressed by topological form factors:

$$F_K(q^2) \to 0 \qquad (qa_0 \to 1),$$

which replaces the continuous UV divergences with a finite discrete sum over graph harmonics. However, the long-range $U(1)$ sector may preserve infrared soft-link features. Therefore, the correct formulation of the TTC status is:

TTC is graph-UV finite, while IR-safe observables are inclusive.

Appendix D.3.4. TTC Applicability Limits and Open Computational Benchmarks

In this work, TTC is a minimal computational framework, not a complete replacement for the entire perturbative QCD. The following properties must be proven or established in future versions:

1. crossing symmetry as a consequence of automorphisms of graph cobordisms;
2. full reconstruction of renormalized QCD and running $\alpha_s(\mu)$;
3. derivation of CKM/PMNS matrices as matrix elements of weak-gateway surgery;
4. multi-loop electroweak corrections as repeated local gluing;
5. hadronization as the finite topological closure of color routes;
6. cluster decomposition for spatially separated graph defects.

These open issues do not invalidate TTC as a computational layer, but they define the boundary between the already established topology-to-amplitude interface and the future program of exact calculations.

© 2026 by the author(s). Distributed under a Creative Commons CC BY license.

Preprints.org (www.preprints.org) | NOT PEER-REVIEWED | Posted: 9 June 2026 doi:10.20944/preprints202606.0589.v1

Appendix E. Cosmological Limit: Birth, Expansion, Structure, and Limit Regimes

Appendix E.1. Algorithmic Inflation and the Initiation of the Universe

Within the framework of classical General Relativity (GR), cosmology is based on the metric tensor of continuous spacetime. This approach triumphantly describes the evolution of the Universe on macroscopic scales, but inevitably leads to a mathematical catastrophe at the moment $t = 0$ (the Big Bang) and inside black holes, where the equations predict non-physical singularities with infinite density. In Information-Kinetic Theory (IKT), the continuum is merely a macroscopic illusion of the thermodynamic limit ($N \to \infty$). Cosmological evolution is viewed as a process of sequential changes in the number of vertices, connectivity, and topology of the base graph G_m.

In all subsequent cosmological formulas, the causal layer m is the graph update index, not external Newtonian time. The dimensional notation

$$t = m\tau_0$$

is an operational SI-projection following the choice of metric calibration and coarse-graining. Therefore, the quantities $H(t)$, $\mathcal{E}_{\exp}(t)$, $\Lambda^{\mathrm{IKT}}_{\mathrm{DE,time}}(t)$, and the lifetimes of cosmological regimes do not introduce a fundamental external time; they are observable coordinates of the reduced graph dynamics.

Appendix E.1.1. Pre-geometric Singularity, Distributed Injection, and the Topological Archipelago

The fundamental problem of the classical description of the Big Bang lies in the emergence of a singularity: the mathematical extrapolation of the finite mass of the Universe into a zero geometric volume. In the IKT paradigm, empty geometric volume does not exist. The set of vertices V_m itself expands, as does the dimension of the associated state space $\mathcal{H}_m$.

In the simplest local description, the initial pre-geometric state of a daughter universe can be idealized as a single oversaturated clique K_{N_0}. However, this picture is a local limit of a more general mechanism. If the daughter universe is born from a macroscopic parent network, then the topological breakdown may occur not at a single absolutely symmetric point, but in a set of overstressed parent clusters.

Hypothesis A12 (Topological Archipelago)**.** *The initial state of the daughter graph need not be a single isolated clique. In the general case, it is a system of saturated subgraphs*

$$\mathcal{A}_0 = \left\{ G^{(a)}_{\mathrm{sat}} \right\}_{a=1}^{N_{\mathrm{gate}}}, \qquad p^{(a)}_{\mathrm{stay}} \to 1,$$

where N_{gate} is the number of parent phase gates involved in the initialization of the daughter universe. Each subgraph $G^{(a)}_{\mathrm{sat}}$ is a local analogue of a primary clique, but the entire initial configuration forms not a single point, but a distributed pre-geometric archipelago.

Physically, such a distributed injection arises because the supermassive black holes of the parent universe are not formed uniformly, but at the nodes of its own large-scale structure. Therefore, the topological break inherits not the metric geometry of the parent world, but the discrete pattern of its phase gates. At time $t = 0$, this pattern is not yet a space in the usual sense, but it specifies the initial inhomogeneities of graph connectivity, from which primary perturbations of the effective density arise after the inflationary break.

The case of a single primary clique is recovered as a limit

$$N_{\mathrm{gate}} = 1, \qquad \mathcal{A}_0 = K_{N_0}.$$

Therefore, the local primary clique is preserved as a limiting case of a more general multipoint mechanism.

© 2026 by the author(s). Distributed under a Creative Commons CC BY license.

Preprints.org (www.preprints.org) | NOT PEER-REVIEWED | Posted: 9 June 2026 doi:10.20944/preprints202606.0589.v1

The Local Primary Clique as the Limit $N_{\text{gate}} = 1$

During the macroscopic evolution of the Parent Universe (for example, during the collapse of a supermassive star), a local region of the graph begins to become catastrophically entangled. The local connectivity of the subgraph grows rapidly, and the probability of staying approaches unity ($p_{\text{stay}} \to 1$). The external phase interface can no longer reconstruct this cluster as an ordinary interior; a finite graph-accessibility neck forms. The connections linking the overloaded cluster to the external network become a small Cheeger bottleneck rather than a continuum event horizon. **Topological unknotting** occurs. At the moment of unknotting, this local cluster completely drops out of the space and time of the Parent Universe. The graph becomes completely self-connected, forming an ideal clique (complete graph) from the minimal initial number N_0 of algorithmic vertices. Each vertex is directly connected to all others ($\langle k \rangle = N_0 - 1$). The topological diameter of the network is equal to 1. This unbound state is our **Tick 0 (Pre-geometric singularity)**. In it, phase translation is blocked ($p_{\text{stay}} \simeq 1$). Macroscopic time stands still. A singularity with infinite density is forbidden: the density cannot go to infinity, since the probability of a delay is bounded by unity.

Trigger Mechanism: Algorithmic Interruption

From the perspective of phase translation, the state of a complete graph is a state of maximum frustration. The insertion algorithm (Postulate 4) is a mechanism for protecting the network from logical collapse (overflow interruption). As soon as the delay reaches the limit ($p_{\text{stay}} \to 1$), the algorithm must forcibly break the congestion. At the moment of transition to Tick 1, each of the N_0 overloaded vertices generates a new "empty" satellite vertex to reset the phase. The ideal symmetry of the clique is permanently destroyed. The average connectivity $\langle k \rangle$ drops instantly, the probability of delay p_{stay} becomes $1 - \epsilon$, and the phase gains a microscopic chance to move. The topological singularity rupture irreversibly triggers an avalanche of algorithmic inflation.

Appendix E.1.2. Discrete Exponent and Percolation Chiral Selection

In IKT, the evolution of the system is described by discrete cycles. The system relieves critical algorithmic tension by inserting new nodes. The most general recurrent form of node growth is written as

$$N_{m+1} = N_m + \Delta N_m = B_{\text{eff}} N_m,$$

where B_{eff} is the effective volumetric branching coefficient of the given regime. Then

$$N_m = N_0 B_{\text{eff}}^m.$$

The initial topological trigger, in which each overloaded vertex gives rise to a single satellite, corresponds to a local binary reset $B_{\text{top}} = 2$. However, this early event is not yet the growth law of the already formed three-dimensional geometry: it describes the exit of the primary clique from a state of frustration.

After the emergence of the effective dimensional regime, one must distinguish between the growth of the abstract number of vertices and the growth of the geometrized scale $a_{\cos}$. To this end, a separate principle of the maximum geometric avalanche is introduced.

Postulate A9 (Maximum Isotropic Binary Geometrization)**.** *In a saturated inflationary regime, each fundamental cycle adds one binary address bit to each independent direction of the effective geometry. If the effective dimension is D_{eff}, then the volume number of cells grows as*

$$N_{m+1} = 2^{D_{\text{eff}}} N_m,$$

and the linear scale as

$$a_{\cos,m+1} = 2 a_{\cos,m}.$$

© 2026 by the author(s). Distributed under a Creative Commons CC BY license.

Preprints.org (www.preprints.org) | NOT PEER-REVIEWED | Posted: 9 June 2026 doi:10.20944/preprints202606.0589.v1

For the observed three-dimensional geometrized regime, $D_{\text{eff}} = 3$, *so*

$$B_{\text{eff}} = 2^3 = 8, \qquad N_{m+1} = 8N_m.$$

Thus, exponential inflation in IKT is not the Guth–Linde scalar field, but a discrete binary avalanche of address space. The doubling of the linear scale is not postulated for the sake of preserving a numerical coefficient; it follows from the isotropic application of the minimal binary operation to each independent direction of an already geometrized graph.

Percolation chiral selection and possible baryogenesis

As N grows exponentially, the network becomes less dense. When $p_{\text{stay}} < 1$, the first stable chiral cycle (the first particle) closes randomly. As soon as it is fixed, it creates a topological template. It is "cheaper" for the algorithm to form new stable cycles with the same chirality. A percolation cascade arises: the chirality of the first random particle is exponentially copied across the entire expanding volume of the graph. The possible baryonic asymmetry in this picture is linked to the nonlinear amplification of the microscopic chiral fluctuation by the inflationary avalanche B_{eff}^m; in the saturated 3D regime, this factor is equal to 8^m. To translate this picture into a quantitative baryogenesis model, it is necessary to derive separately the CP-asymmetric weak couplings, the violation of the effective baryon number, and the non-equilibrium freeze-out dynamics.

Appendix E.1.3. Calibration of Avalanche Expansion and CMB Perturbations

In standard phenomenological language, early accelerated expansion is often characterized by the number of e-folds

$$N_{\text{exp}} = \ln \frac{a_{\text{end}}}{a_{\text{start}}}.$$

In IKT, this parameter is not introduced as a constraint imposed by the scalar-field inflationary ontology. It is used only as a convenient observational measure of the sufficient early growth of the scale factor required to reconcile the theory with the horizon problem, the flatness problem, and CMB data. Thus, the theory is calibrated not by the inflaton model, but by the measurable requirement of large early expansion.

The postulate of maximum isotropic binary geometrization gives

$$B_{\text{eff}} = 2^{D_{\text{eff}}} = 2^3 = 8, \qquad N_{m+1} = 8N_m.$$

Since the geometrized volume scales as

$$N \propto a_{\text{cos}}^3,$$

the linear scale doubles in one fundamental cycle:

$$a_{\text{cos},m+1} = 2a_{\text{cos},m}, \qquad a_{\text{cos}}(m) = a_{\text{cos},0}2^m.$$

Consequently, the graph number of e-folds after m cycles is equal to

$$N_{\text{exp}}^{\text{IKT}}(m) = \ln \frac{a_{\text{cos}}(m)}{a_{\text{cos},0}} = m \ln 2.$$

Hence, the number of cycles corresponding to a given observational benchmark N_{obs} is equal to

$$\boxed{m_{\text{inf}} = \frac{N_{\text{obs}}}{\ln 2}}.$$

For example, for $N_{\text{obs}} = 60$ we obtain

$$m_{\text{inf}} \approx 86.6 \approx 87.$$

© 2026 by the author(s). Distributed under a Creative Commons CC BY license.

Preprints.org (www.preprints.org) | NOT PEER-REVIEWED | Posted: 9 June 2026 doi:10.20944/preprints202606.0589.v1

In this case, the linear scale increases as

$$2^{m_{\rm inf}} = e^{N_{\rm obs}} \approx e^{60} \sim 10^{26},$$

and the geometric volume as

$$8^{m_{\rm inf}} = e^{3N_{\rm obs}} \approx e^{180} \sim 10^{78}.$$

If we round to the nearest integer, $m = 87$, then the actual graph number of e-folds is $87 \ln 2 \simeq 60.3$. Therefore, an order of 60 e-folds in the observational language corresponds to an order of 90 fundamental cycles of the graph avalanche.

The physical SI projection of the duration of such a phase is written as

$$\Delta t_{\rm inf}^{\rm SI} = m_{\rm inf}\tau_0, \qquad \tau_0 = \frac{\tau_e}{|\Omega_e|_{\rm eff}}, \qquad \tau_e = \frac{\hbar}{m_e c_0^2}.$$

If $|\Omega_e|_{\rm eff}$ is calibrated via the observed gravitational normalization

$$\alpha_G^{(e)} = \frac{G m_e^2}{\hbar c_0} = \frac{1}{|\Omega_e|_{\rm eff}^2},$$

then

$$\tau_0 = \tau_e \sqrt{\alpha_G^{(e)}} = \sqrt{\frac{\hbar G}{c_0^5}} = t_{\rm Pl}.$$

Numerically, this gives

$$\tau_0 \simeq 5.39 \times 10^{-44}\,{\rm s}, \qquad \Delta t_{\rm inf}^{\rm SI} \simeq 87\tau_0 \simeq 4.7 \times 10^{-42}\,{\rm s}.$$

This coincidence with the Planck time is an algebraic consequence of gravitational calibration. It will become an independent verification of IKT only after $|\Omega_e|_{\rm eff}$ is derived from the microdynamics of the electronic topological route without using the observed G.

The maximum rate of graph geometrization is equal to

$$H_{\rm alg,max} = \frac{1}{3\tau_0} \ln B_{\rm eff} = \frac{\ln 2}{\tau_0}.$$

Here, $H_{\rm alg,max}$ denotes not necessarily the slow-roll Hubble parameter of scalar-field inflation, but the limiting rate of algorithmic growth of the geometrized address space. The relationship between this quantity and the observed scalar and tensor CMB spectra requires a separate coarse-graining calculation. Until such a calculation is performed, $H_{\rm alg,max}$ should not be directly identified with the parameter constrained via tensor modes.

Primordial CMB Perturbations: Avalanche Cooling and Archipelago Residual

The observed CMB requires not only a large early growth of the scale factor, but also the correct statistics of primordial perturbations. In the phenomenological formalism, the scalar spectrum is usually parameterized as

$$\mathcal{P}_\zeta(q) = A_s \left(\frac{q}{q_*}\right)^{n_s - 1}, \qquad n_s \simeq 0.965,$$

where q denotes the cosmological Coma wave number. We use q rather than k to avoid confusion with the graph's degree of connectivity k. This notation does not imply a commitment to slow-roll inflation or a fundamental scalar field. It is used solely as an observational coordinate of the primordial CMB spectrum, which the graph microdynamics must reproduce.

© 2026 by the author(s). Distributed under a Creative Commons CC BY license.

Preprints.org (www.preprints.org) | NOT PEER-REVIEWED | Posted: 9 June 2026 doi:10.20944/preprints202606.0589.v1

The average growth of the geometrized volume in the saturated three-dimensional regime remains

$$N_{m+1} = 8N_m, \qquad \frac{d\ln N}{dm} = \ln 8.$$

Therefore, the probability of oversaturated connectivity $p_{\mathrm{stay}}^{\mathrm{conn}}$ should not be equated with the average volume growth rate itself. It governs the amplitude of the residual algorithmic tension and, consequently, the power of the stochastic avalanche noise:

$$\mathcal{D}_{\mathrm{ins}}(m) = \mathcal{D}_* \exp[-\gamma_{\mathrm{cool}}(m - m_*)], \qquad \gamma_{\mathrm{cool}} > 0.$$

Microscopically, this slow relaxation must be derived from the function

$$\mathcal{D}_{\mathrm{ins}}(m) \propto \left[p_{\mathrm{stay}}^{\mathrm{conn}}(\langle k\rangle_m)\right]^{\beta} \mathcal{C}_{\mathrm{mix}}(m), \qquad p_{\mathrm{stay}}^{\mathrm{conn}}(\langle k\rangle) = \max\left(0, 1 - \frac{6}{\langle k\rangle}\right),$$

where β determines the sensitivity of the noise to excess connectivity, and $\mathcal{C}_{\mathrm{mix}}$ describes the coarse-grained mixing of insertion domains.

In a first approximation, the cosmological mode q leaves the graph horizon when

$$\frac{d\ln q}{dm} = \ln 2 + \frac{d\ln H_{\mathrm{alg}}}{dm} \simeq \ln 2,$$

if H_{alg} varies slowly within the observable window. Then

$$n_s - 1 = \frac{d\ln \mathcal{P}_\zeta}{d\ln q} \simeq -\frac{\gamma_{\mathrm{cool}}}{\ln 2}.$$

For the observational benchmark $n_s \simeq 0.965$, this gives

$$\gamma_{\mathrm{cool}} \simeq (1 - n_s)\ln 2 \simeq 2.4 \times 10^{-2}.$$

In other words, the red slope corresponds not to a sharp cutoff of the avalanche, but to a gentle decay of the power of the primary insertion noise at a rate of a few percent per fundamental cycle in the range m that is projected onto the observed CMB scales.

To be consistent with quasi-Gaussian statistics, the primary perturbations must be decomposed into two components:

$$\zeta(\mathbf{x}) = \zeta_{\mathrm{lav}}(\mathbf{x}) + \zeta_{\mathrm{arch}}(\mathbf{x}).$$

The component ζ_{lav} is the sum of a large number of local insertion noises. With a large number of independent coarse-grained domains $N_{\mathrm{corr}}(q) \gg 1$, central limit theorem averaging makes it nearly Gaussian:

$$f_{\mathrm{NL}}^{\mathrm{IKT}} \sim N_{\mathrm{corr}}^{-1/2} \ll 1.$$

The component ζ_{arch} is the residual of the distributed boundary condition of the Topological Archipelago. It should not dominate in the acoustic CMB range:

$$\mathcal{P}_\zeta(\mathbf{q}) = \mathcal{P}_{\mathrm{lav}}(q)[1 + \Delta_{\mathrm{arch}}(\mathbf{q})], \qquad |\Delta_{\mathrm{arch}}(\mathbf{q})| \ll 1 \quad \text{for } q \gg q_{\mathrm{arch}}.$$

In this regime, the statistical isotropy of the CMB is not a property of a single parent gate, but rather the result of coarse-graining a large number of insertion domains and the suppression of the directional archipelago residual on subhorizon scales.

© 2026 by the author(s). Distributed under a Creative Commons CC BY license.

Preprints.org (www.preprints.org) | NOT PEER-REVIEWED | Posted: 9 June 2026 doi:10.20944/preprints202606.0589.v1

Finally, compatibility with acoustic peaks requires that avalanche perturbations after reheating enter the baryon-photon and primary vortex sectors as a common refractive/curvature mode:

$$S_{i,\gamma} = \delta_i - \frac{3}{4}\delta_\gamma \approx 0,$$

with a small permissible isocurvature admixture. This condition is an observational constraint on IKT coarse-graining, not a consequence of the slow-roll ontology.

Remark A12 (Status of large-scale CMB residuals)**.** *The Topological Archipelago should not provide a dominant anisotropic source on CMB acoustic scales. Its admissible observational trace in IKT is a subdominant low-multipole component $\zeta_{\rm arch}$, capable of manifesting only on the very largest angular scales. Therefore, the so-called lower-multipole CMB anomalies, including quadrupole-octopole alignments and hemispheric asymmetry, can be regarded in IKT only as a possible projection of the Archipelago boundary condition, but not as evidence for this picture. The main CMB spectrum must remain nearly Gaussian, nearly statistically isotropic, and nearly adiabatic.*

Exit from Inflation: Emergent Dimension

For the formation of macroscopic 3D geometry, the average coordination number is modeled as being stabilized: $k_{\rm crit} = 2D = 6$. The probability of algorithmic delay associated with excess connectivity is determined by the ratio of the number of excess paths to the total number of paths:

$$p_{\rm stay}^{\rm conn}(k) = \max\left(0, 1 - \frac{k_{\rm crit}}{k}\right).$$

The index "conn" emphasizes that this is neither the mass delay $p_{\rm stay} = 1 - e^{-\theta_M}$ nor the gravitational delay $p_G = 1 - e^{-\chi_G}$, but rather the threshold delay of oversaturated connectivity. When insertion dilutes the graph and excess bonds are destroyed ($k \to 6$), the delay of an empty node becomes zero:

$$p_{\rm stay}^{\rm conn}(6) = 0.$$

The speed of light in a vacuum reaches its absolute maximum c_0. Inflation stops. The accumulated algorithmic tension of the overstressed links is released into the primary translational kinetics of the phase. This defines a graph-theoretic analogue of reheating; a possible connection between this phase and baryogenesis requires a separate mechanism of asymmetry and is not considered a complete conclusion.

Appendix E.1.4. Relativistic Time Synchronization and the Holographic Limit of Inflation

To integrate the inflation process into the global Multiverse, it is necessary to relate the internal time scale m to the coordinate time of the parent network t_p. In the saturated geometrized regime

$$N_m = N_0 B_{\rm eff}^m,$$

and the external node-supply flux through the parent graph-gate is limited by its finite B3 area:

$$\Phi_{\mathcal{N},\rm in}^{\rm cap} = \kappa_{\mathcal{N},\rm in} M^2.$$

Here the symbol denotes a node or graph-channel supply rate after the energy-to-channel conversion of Section E.4.1.2, not an energy power. The discrete increment per tick is equal to

$$\Delta N_m = (B_{\rm eff} - 1) N_m.$$

© 2026 by the author(s). Distributed under a Creative Commons CC BY license.

Preprints.org (www.preprints.org) | NOT PEER-REVIEWED | Posted: 9 June 2026 doi:10.20944/preprints202606.0589.v1

Therefore, the finite parent time interval required for a single internal tick is estimated as

$$\Delta t_p = \frac{\Delta N_m}{\Phi^{\mathrm{cap}}_{\mathcal{N},\mathrm{in}}} = \frac{(B_{\mathrm{eff}} - 1) N_0 B^m_{\mathrm{eff}}}{\kappa_{\mathcal{N},\mathrm{in}} M^2}.$$

In a smooth shell, where $dN/dm = N \ln B_{\mathrm{eff}}$, we obtain the differential form of the time relation:

$$\frac{dm}{dt_p} = \frac{\kappa_{\mathcal{N},\mathrm{in}} M^2}{N_0 B^m_{\mathrm{eff}} \ln B_{\mathrm{eff}}}.$$

This equation demonstrates:

- **Gravitational time dilation:** from the perspective of an external observer, the rate of time flow inside the black hole (dm/dt_p) slows down exponentially as the daughter space (B^m_{eff} in the denominator) grows. For an internal observer, inflation proceeds as an instantaneous local explosion.
- **Graph-gate limit:** the maximum rate of inflation of the geometrized volume of the daughter universe ($N \propto B^m_{\mathrm{eff}}$) is limited by the 2D area of the parent B3 graph-gate ($A_{\mathrm{gate}} \propto M^2$). This establishes the IKT area-throughput scaling at the level of the phase gate. Matching the Bekenstein–Hawking coefficient, if desired, is a separate TTC neck-spectrum problem rather than an assumption.

Appendix E.1.5. Status of the IKT Inflationary Scenario

Algorithmic inflation in IKT has the status of a conditional graph-growth scenario. Its hard core is specified by a discrete insertion avalanche and the condition of maximum isotropic binary geometrization. Observable quantities, such as the number of e-folds, the spectral slope, and the amplitude of CMB perturbations, are interface calibrations of this graph scenario. A complete derivation of the initial spectrum requires a separate calculation of the statistics of the Topological Archipelago and the prethermal noise of the early graph.

Appendix E.2. Dark Energy as Parent Throughput and Residual Algorithmic Noise

Remark A13 (Status of the multiverse extension)**.** *The following section is a high-level cosmological extension of the graph growth mechanism. It is not used in the local derivation of $U_m \Rightarrow$ Weyl/wave envelope, interaction interfaces, α_{top}, or G. Its role is to describe a possible global source of late acceleration and a small dynamic correction from residual insertion. Therefore, claims regarding parent throughput, homeostasis, and the multiverse have the status of a cosmological-interface hypothesis, rather than a proven part of the IKT minimal core.*

Dark energy in IKT is described as the sum of two contributions:

$$\boxed{\Lambda^{\mathrm{IKT}}_{\mathrm{DE,time}}(t) = \Lambda_{\mathrm{par},time}(t) + \Lambda^{\mathrm{valve}}_{\mathrm{noise},time}(t)}. \tag{A32}$$

The first term is the dynamic parent or homeostatic throughput background associated with the external phase flow through topological valves between parent and child graph branches. The second term is the valve-limited residual insertion noise, preserving the old idea of a regularized algorithmic tail while replacing the singular early asymptote by a finite parent-valve bandwidth.

The notation in Equation (A32) is deliberately strict: $\Lambda^{\mathrm{IKT}}_{\mathrm{DE,time}}$ denotes only the effective dark-energy source of the IKT cosmological interface. It must not be identified with the total expansion scalar $3H^2$, which also contains matter, radiation, neutrinos, the vortex/dark-matter component, curvature, and possible coarse-graining corrections.

© 2026 by the author(s). Distributed under a Creative Commons CC BY license.

Preprints.org (www.preprints.org) | NOT PEER-REVIEWED | Posted: 9 June 2026 doi:10.20944/preprints202606.0589.v1

Appendix E.2.1. Expansion Scalar versus Dark-Energy Component

The time variable in this section is always a coarse-grained projection of the causal layer m, not fundamental external time. The normalized node-growth rate and the Hubble parameter are

$$\lambda_N(t) = \frac{1}{N}\frac{dN}{dt}, \qquad H(t) = \frac{1}{a_{\cos}}\frac{da_{\cos}}{dt} = \frac{1}{3}\lambda_N(t),$$

where $N \propto a_{\cos}^3$ is the number of nodes in the effective volume. The quantities λ_N and H have dimension T^{-1}.

The total kinematic expansion scalar is

$$\boxed{\mathcal{E}_{\exp}(t) \equiv 3H^2(t)}, \qquad \mathcal{E}_{\exp,\mathrm{geom}}(t) = \frac{\mathcal{E}_{\exp}(t)}{c_0^2}. \tag{A33}$$

This scalar has dimension T^{-2} and measures the total coarse-grained expansion of the daughter branch. It is not, by itself, the dark-energy component. The geometric IKT dark-energy term is instead

$$\Lambda^{\mathrm{IKT}}_{\mathrm{DE,geom}}(t) = \frac{\Lambda^{\mathrm{IKT}}_{\mathrm{DE,time}}(t)}{c_0^2}. \tag{A34}$$

The total expansion scalar obeys a Friedmann-like bookkeeping relation,

$$\boxed{\mathcal{E}_{\exp} = \mathcal{C}_b + \mathcal{C}_r + \mathcal{C}_\nu + \mathcal{C}_{\mathrm{vort}} + \Lambda^{\mathrm{IKT}}_{\mathrm{DE,time}} + \mathcal{C}_k + \mathcal{C}_{\mathrm{corr}}}. \tag{A35}$$

Here

$$\mathcal{C}_X(t) = \frac{8\pi G}{c_0^2}\rho_X(t) \tag{A36}$$

for an energy density ρ_X, while

$$\mathcal{C}_k(t) = -\frac{3kc_0^2}{a_{\cos}^2(t)} \tag{A37}$$

is the curvature contribution. The term $\mathcal{C}_{\mathrm{vort}}$ denotes the IKT vortex component which plays the role normally assigned to cold dark matter. The term $\mathcal{C}_{\mathrm{corr}}$ collects possible small interaction, leakage, or coarse-graining corrections.

Therefore the observationally reconstructed dark-energy term is not $3H^2$ itself, but the residual

$$\boxed{\Lambda^{\mathrm{obs}}_{\mathrm{DE,time}} = 3H^2 - \mathcal{C}_b - \mathcal{C}_r - \mathcal{C}_\nu - \mathcal{C}_{\mathrm{vort}} - \mathcal{C}_k - \mathcal{C}_{\mathrm{corr}}}. \tag{A38}$$

The IKT dark-energy model is tested by the comparison

$$\Lambda^{\mathrm{IKT}}_{\mathrm{DE,time}}(z) \simeq \Lambda^{\mathrm{obs}}_{\mathrm{DE,time}}(z), \tag{A39}$$

not by the identification $\Lambda^{\mathrm{IKT}}_{\mathrm{DE,time}} = 3H^2$.

Appendix E.2.2. Two Sources of Dark Energy

The parent contribution describes the phase throughput coming from the parent graph branch. Unlike local insertion noise, this contribution is not required to follow a t^{-2} law. Its natural form is a slowly varying throughput window:

$$\boxed{\Lambda_{\mathrm{par},time}(t) = \Lambda_* \mathcal{F}_{\mathrm{par}}(T_{\mathrm{par}}(t))}. \tag{A40}$$

© 2026 by the author(s). Distributed under a Creative Commons CC BY license.

Preprints.org (www.preprints.org) | NOT PEER-REVIEWED | Posted: 9 June 2026 doi:10.20944/preprints202606.0589.v1

Here, $T_{\rm par}(t)$ is the effective time of the parent branch, projected onto the cosmological time of the daughter universe, and $\mathcal{F}_{\rm par}$ defines the rise, plateau, and subsequent decay of the parent throughput channel.

Qualitatively, this channel goes through three phases:

valve opening $\longrightarrow$ plateau / maximum flux $\longrightarrow$ topological extinction of the parent branch.

The valves open when the black holes of the parent branch reach a critical threshold

$$M_{\rm BH} \gtrsim M_{\rm valve}, \qquad M_{\rm valve} \sim 0.6\, M_{\rm Moon}.$$

One minimal parameterization of the window function is given by

$$\mathcal{F}_{\rm par}(T) = \frac{1}{1+\exp[-(T-T_{\rm on})/\Delta_{\rm on}]}\,\frac{1}{1+\exp[(T-T_{\rm off})/\Delta_{\rm off}]}. \tag{A41}$$

In the present era, the observed $w \simeq -1$ requires that the parent channel be on a broad plateau or in a state of very slow change.

Appendix E.2.3. Valve-limited Regularization of Residual Algorithmic Noise

The noise component remains a local tail of the residual insertion, but its early limit is not an infinite asymptote. The daughter graph branch starts through a finite parent throat channel; therefore, the physically realizable noise generation density is limited by the valve bandwidth $\Lambda_{\rm valve}(t)$.

Let us introduce the dimensionless quantities

$$m = \frac{t}{\tau_0}, \qquad \lambda_{\rm valve}(m) = \tau_0^2 \Lambda_{\rm valve}(t).$$

The bare scale-invariant asymptotic form of the residual noise is

$$\lambda_{\rm raw}(m) = \frac{\lambda_{\max}}{m^2},$$

but it is not physically realizable as $m \to 0$. The realizable noise density is given by the valve-limited expression

$$\boxed{\lambda^{\rm valve}_{\rm noise}(m) = \frac{\lambda_{\rm raw}(m)\lambda_{\rm valve}(m)}{\lambda_{\rm raw}(m)+\lambda_{\rm valve}(m)}}. \tag{A42}$$

In the regime of nearly constant initial bandwidth $\lambda_{\rm valve} \simeq$ const, this expression takes the familiar regularized form

$$\boxed{\lambda^{\rm valve}_{\rm noise}(m) = \frac{\lambda_{\max}}{d_0^2+m^2}}, \qquad \boxed{d_0^2 = \frac{\lambda_{\max}}{\lambda_{\rm valve}} = \frac{\lambda_{\max}}{\tau_0^2\Lambda_{\rm valve}}}. \tag{A43}$$

After dimensional projection $t = m\tau_0$, we obtain

$$\boxed{\Lambda^{\rm valve}_{{\rm noise},time}(t) = \frac{1}{\tau_0^2}\,\frac{\lambda_{\max}}{d_0^2+(t/\tau_0)^2}}. \tag{A44}$$

Thus, d_0 is not an independent empirical regularization of the singularity $1/t^2$. It is a dimensionless valve-depth variable, that is, a compact representation of the finite initial bandwidth of the parent throat channel.

For $t \gg d_0\tau_0$, the noise component has the asymptotic behavior

$$\Lambda^{\rm valve}_{{\rm noise},time}(t) \approx \frac{\lambda_{\max}}{t^2},$$

© 2026 by the author(s). Distributed under a Creative Commons CC BY license.

Preprints.org (www.preprints.org) | NOT PEER-REVIEWED | Posted: 9 June 2026 doi:10.20944/preprints202606.0589.v1

and at $t = 0$ there is a finite early plateau

$$\Lambda^{\text{valve}}_{\text{noise},time}(0) = \Lambda_{\text{valve}} = \frac{\lambda_{\max}}{d_0^2 \tau_0^2}. \tag{A45}$$

In other words, the finite throughput of the parent valve physically justifies the regularized plateau of the noise tail. Therefore, the t^{-2} law is not the entire late dark energy, but rather a small dynamic correction to the parent throughput background and, simultaneously, a valve-limited early noise plateau.

Amplitude $\lambda_{\max}$ from maximum binary geometrization

The parameter $\lambda_{\max}$ determines the dimensionless amplitude of the noise component. For the volumetric branching coefficient

$$N_{m+1} = B_{\text{eff}} N_m$$

and $N \propto a^3_{\cos}$, the maximum rate of graph geometrization is equal to

$$H_{\text{alg},\max} = \frac{1}{3\tau_0} \ln B_{\text{eff}}.$$

The postulate of maximum isotropic binary geometrization yields for the three-dimensional case

$$B_{\text{eff}} = 2^{D_{\text{eff}}} = 8.$$

Therefore,

$$\boxed{\lambda_{\max} = 3(\ln 2)^2 \simeq 1.441}. \tag{A46}$$

This coefficient refers to the valve-limited noise tail $\Lambda^{\text{valve}}_{\text{noise}}$, not to the total late dark energy.

Appendix E.2.4. Time Hierarchy and the Naturalness of the Parent Plateau

A rough estimate of the lifetime of a multiverse generation gives

$$T_{\text{life}} \sim 10^{33}\,\text{yr}.$$

If the characteristic time of change of the parent throughput background is of the same order,

$$T_{\text{drift}} \sim T_{\text{life}},$$

then at the present Hubble time $H_0^{-1} \sim 10^{10}\,\text{yr}$, the logarithmic slope of the parent component is suppressed:

$$\epsilon_{\text{par}} \equiv \left| \frac{d \ln \Lambda_{\text{par},time}}{d \ln a} \right| \sim \frac{1}{H_0 T_{\text{drift}}} \sim 10^{-23}. \tag{A47}$$

Therefore, for an observer inside the daughter branch, the parent throughput background appears practically constant:

$$\Lambda_{\text{par},time}(t) \simeq \Lambda_*$$

at times of the order of the age of the observable universe. In this sense, the current $w_{\text{DE}} \simeq -1$ is a natural consequence of the enormous hierarchy between the Hubble time and the evolution time of the parent channel, rather than a separate fine-tuning.

© 2026 by the author(s). Distributed under a Creative Commons CC BY license.

Preprints.org (www.preprints.org) | NOT PEER-REVIEWED | Posted: 9 June 2026 doi:10.20944/preprints202606.0589.v1

Appendix E.2.5. Effective Equation of State and Constraint on the Noise Tail

Let us define the fractions of the two dark-energy components with respect to the IKT dark-energy source, not with respect to the total expansion scalar:

$$f_{\rm par}(t) = \frac{\Lambda_{{\rm par},time}(t)}{\Lambda^{\rm IKT}_{\rm DE,time}(t)}, \qquad f_{\rm noise}(t) = \frac{\Lambda^{\rm valve}_{{\rm noise},time}(t)}{\Lambda^{\rm IKT}_{\rm DE,time}(t)}.$$

If the IKT dark-energy source is treated as an effective separately projected component, its equation of state is defined by

$$w^{\rm IKT}_{\rm DE} + 1 = -\frac{1}{3}\frac{d\ln \Lambda^{\rm IKT}_{\rm DE,time}}{d\ln a_{\rm cos}}.$$

For the two-component structure of Equation (A32), we obtain the estimate

$$\boxed{w^{\rm IKT}_{\rm DE} + 1 \simeq -\frac{1}{3} f_{\rm par}\frac{d\ln \Lambda_{{\rm par},time}}{d\ln a_{\rm cos}} + f_{\rm noise}\frac{2}{3Ht}}. \tag{A48}$$

If the present epoch is on the parent plateau, the first term is suppressed, and the proximity of the reconstructed dark-energy equation of state to -1 requires a small present-day fraction of the noise tail:

$$\boxed{f_{\rm noise,0} \lesssim 0.05\text{–}0.1.} \tag{A49}$$

Possible small deviations of $w_{\rm DE}(z)$ from -1 in the IKT serve as a test of the slope of the parent window $\mathcal{F}_{\rm par}$ and the fraction of residual insertion $f_{\rm noise}$. This $w_{\rm DE}$ must be reconstructed from the dark-energy residual of Equation (A38), not from the logarithmic derivative of $3H^2$ itself.

Appendix E.2.6. The Coincidence Problem and the Vacuum Catastrophe

In this interpretation, the observed dark-energy residual is not the sum of the zero energies of all continuous quantum fields. It is the operational interface of two graph processes: the parent throughput background and the residual insertion noise. Therefore, the 10^{120}-order error in the standard estimate of the vacuum energy does not arise in its original form: it is not the energy density of the continuous vacuum and the reconstructed dark-energy residual that are compared, but rather the finite graph flows and their coarse-grained metric projection.

The coincidence problem also changes status. The later acceleration is determined by the slow parent background, and the t^{-2} tail of the insertion is a small correction to the dark-energy residual, not to the total $3H^2$ budget. The current value $w_{\rm DE} \simeq -1$ requires either a broad parent plateau or compensation for the slopes of the two components in formula (A48). A complete verification requires a joint fit module for $H(z)$, the reconstructed residual $\Lambda^{\rm obs}_{\rm DE,time}(z)$, $w_{\rm DE}(z)$, BAO, SN, and CMB.

Appendix E.2.7. Observational Interface: $H(z)$, $w_{\rm DE}(z)$, BAO/SN/CMB

The two-component IKT dark energy is tested not by a single local formula, but by expansion and distance functions:

$$H(z), \qquad w_{\rm DE}(z), \qquad D_L(z), \qquad D_A(z).$$

The observational comparison proceeds in two steps. First, the total expansion scalar $3H^2(z)$ is reconstructed from distance, expansion, and structure data. Second, baryonic matter, radiation, neutrinos, curvature, the IKT vortex/dark-matter component, and possible coarse-graining corrections are subtracted according to Equation (A38). The residual $\Lambda^{\rm obs}_{\rm DE,time}(z)$ is then compared with the IKT source $\Lambda^{\rm IKT}_{\rm DE,time}(z)$.

Comparison with BAOs, SN Ia, and the CMB acoustic scale should therefore constrain three classes of quantities: the level of the parent throughput background Λ_*, the window shape $\mathcal{F}_{\rm par}$, and the present-day noise tail fraction $f_{\rm noise,0}$. Unlike the pure t^{-2} model, the two-component interface

© 2026 by the author(s). Distributed under a Creative Commons CC BY license.

Preprints.org (www.preprints.org) | NOT PEER-REVIEWED | Posted: 9 June 2026 doi:10.20944/preprints202606.0589.v1

naturally allows for $w_{\mathrm{DE}} \simeq -1$ today and a small dynamic evolution of $w_{\mathrm{DE}}(z)$. Thus $w_{\mathrm{DE}}(z)$ is not extracted from the logarithmic derivative of $3H^2$ itself, but from the reconstructed dark-energy residual.

Appendix E.2.8. The Status of Dark Energy in IKT

Dark energy in IKT has the status of a two-component cosmological interface. The parent throughput background is the boundary-condition / homeostatic fixed-point hypothesis, and the noise component is the regularized tail of the residual graph insertion. The numerical success of this mechanism should be evaluated by the joint reproduction of $H(z)$, the residual $\Lambda^{\mathrm{obs}}_{\mathrm{DE,time}}(z)$, BAO/SN/CMB-distance data, structure growth, and admissible deviations of $w_{\mathrm{DE}}(z)$ from -1. The total expansion scalar $3H^2$ is not the IKT dark-energy component; it is the bookkeeping sum of all cosmological components.

Appendix E.3. Dark Matter as a Macroscopic Topological Vortex

The problem of hidden mass is traditionally solved by introducing an invisible particle halo. In IKT, an alternative mechanism links the excess gravity to a macroscopic vortex response of the graph. It is important to note that this section uses not the probability p_j, but a separate potential χ_{vort}.

In the cosmological section, the primary component $\chi^{\mathrm{prim}}_{\mathrm{vort}}$ was introduced, which is necessary for the CMB and LSS. Below, we consider the late galactic limit of the same physics. Therefore, dark matter in IKT is understood not as a single mechanism, but as two modes of a unified vortex field:

$$\chi_{\mathrm{vort}} = \chi^{\mathrm{prim}}_{\mathrm{vort}} + \chi^{\mathrm{gal}}_{\mathrm{vort}}.$$

The primordial component defines pre-galactic potential wells, while the galactic component arises from the interaction of this field with a rotating baryonic disk.

Appendix E.3.1. Primordial Vortex Component: Pre-galactic Halo and CMB/LSS

The galactic vortex mechanism, discussed below in the section on dark matter, describes the late regime: a rotating baryonic disk forms a quasi-two-dimensional topological waveguide and thereby generates flat rotation curves. However, this late mechanism alone cannot explain the acoustic peaks in the cosmic microwave background and the growth of large-scale structure, since stable galactic disks did not yet exist during the recombination era.

Therefore, the IKT vorticity potential must be decomposed into two components:

$$\chi_{\mathrm{vort}} = \chi^{\mathrm{prim}}_{\mathrm{vort}} + \chi^{\mathrm{gal}}_{\mathrm{vort}}.$$

Here, $\chi^{\mathrm{prim}}_{\mathrm{vort}}$ is the primary pre-galactic component, determined by the initial conditions of the Topological Archipelago, and $\chi^{\mathrm{gal}}_{\mathrm{vort}}$ is the late component, induced by rotating baryonic disks.

Similarly, the macroscopic vorticity field is expressed as

$$\boldsymbol{\Omega} = \boldsymbol{\Omega}_{\mathrm{prim}} + \boldsymbol{\Omega}_{\mathrm{bar}}.$$

The component $\boldsymbol{\Omega}_{\mathrm{bar}}$ arises from the late baryon current $\mathbf{J}_{\mathrm{bar}}$, whereas $\boldsymbol{\Omega}_{\mathrm{prim}}$ is the relic field of the initial graph injection.

Hypothesis A13 (Primary cold vortex component)**.** *Distributed injection through the Topological Archipelago sets the initial inhomogeneities of graph connectivity and the primary macroscopic vorticity* $\boldsymbol{\Omega}_{\mathrm{prim}}$*. After inflationary coarse-graining, the observable gravitational source is not the vector vortex itself, but the scalar refractive density associated with its invariant amplitude:*

$$n^{\mathrm{prim}}_{\mathrm{vort}} \simeq 1 + \chi_{\mathrm{algo}} |\boldsymbol{\Omega}_{\mathrm{prim}}|^2,$$

© 2026 by the author(s). Distributed under a Creative Commons CC BY license.

Preprints.org (www.preprints.org) | NOT PEER-REVIEWED | Posted: 9 June 2026 doi:10.20944/preprints202606.0589.v1

$$\delta_{\rm vort}^{\rm prim} \propto |\mathbf{\Omega}_{\rm prim}|^2 - \left\langle |\mathbf{\Omega}_{\rm prim}|^2 \right\rangle.$$

This scalar component acts as effective cold dark matter prior to recombination.

Effective scalar dynamics of the primary vortical component

The previous hypothesis asserts that the primary source $\mathbf{\Omega}_{\rm prim}$ has a vortical topological nature. However, the CMB and LSS are sensitive not to the direction of the microscopic vorticity, but to its coarse-grained gravitational projection. Therefore, it is necessary to explicitly separate the vector initial-boundary variable $\mathbf{\Omega}_{\rm prim}$ from the scalar observable component $\chi_{\rm vort}^{\rm prim}$.

Let

$$\mathcal{I}_\Omega(\eta, \mathbf{x}; L) = \left\langle |\mathbf{\Omega}_{\rm prim}|^2 \right\rangle_L$$

denotes the invariant amplitude of the primary vorticity after averaging over a scale L exceeding the size of individual Archipelago insertion domains. Then the effective density of the primary vorticity component is given not by the direction $\mathbf{\Omega}_{\rm prim}$, but by the scalar

$$n_{\rm vort}^{\rm prim} = \overline{n}_{\rm vort}(1 + \delta_{\rm vort}), \qquad \delta_{\rm vort} = \beta_\Omega \frac{\mathcal{I}_\Omega - \bar{\mathcal{I}}_\Omega}{\bar{\mathcal{I}}_\Omega} + O(\Sigma_\Omega^2).$$

Here, β_Ω is a dimensionless coarse-graining coefficient, and Σ_Ω denotes the residual orientational anisotropy, defined below.

The low-field refractive projection $\chi_{\rm vort}^{\rm prim}$ is related to this density by Poisson's equation under the convention $\chi = -\Phi/c_0^2$:

$$\nabla^2 \chi_{\rm vort}^{\rm prim} = -\frac{4\pi G_{\rm eff}}{c_0^2} a^2 \bar{\rho}_{\rm vort} \delta_{\rm vort}, \qquad q^2 \chi_{\rm vort}^{\rm prim}(q) = \frac{4\pi G_{\rm eff}}{c_0^2} a^2 \bar{\rho}_{\rm vort} \delta_{\rm vort}(q).$$

Thus, $\chi_{\rm vort}^{\rm prim}$ is not a fundamental field-particle, but rather a scalar refractive projection of the primary vorticity density.

The minimal effective action for this component can be written as the action of a cold barotropic medium:

$$S_{\rm vort}^{(0)} = \int d^4x \sqrt{-g} \left[-\rho_{\rm vort}(n) - n u^\mu \partial_\mu \vartheta + \lambda (u_\mu u^\mu + 1) \right]. \tag{A50}$$

Here, u^μ is the effective velocity of the coarse-grained refractive medium, ϑ is the scalar displacement potential, and λ fixes the normalization $u_\mu u^\mu = -1$. This action serves as an observational interface for CMB/LSS calculations, rather than a postulate regarding the existence of a new fundamental dark matter particle.

The parameters $\mu_{\rm vort}$ and $K_{\rm vort}$ are not fundamental IKT constants. They represent fluid-interface coefficients arising after coarse-graining the vortex deformations of local graph coordinates. For the observable CMB/LSS interface, it is convenient to temporarily write the equation of state as a small elastic correction to the frozen topological lag:

$$\rho_{\rm vort}(n) = \mu_{\rm vort} n + \frac{K_{\rm vort}}{2} n^2 + O(n^3),$$

from which

$$p_{\rm vort} = n \frac{d\rho_{\rm vort}}{dn} - \rho_{\rm vort} = \frac{K_{\rm vort}}{2} n^2 + O(n^3),$$

and

$$w_{\rm vort}^{\rm prim} \simeq \frac{K_{\rm vort} \overline{n}_{\rm vort}}{2\mu_{\rm vort}}, \qquad c_{s,\rm vort}^2 \simeq \frac{K_{\rm vort} \overline{n}_{\rm vort}}{\mu_{\rm vort}}.$$

However, the ratio $K_{\rm vort}\overline{n}_{\rm vort}/\mu_{\rm vort}$ should not be regarded as a free phenomenological parameter. The primary vorticity field $\mathbf{\Omega}_{\rm prim}$ is a macroscopic measure of the coherent distortion of local reference

© 2026 by the author(s). Distributed under a Creative Commons CC BY license.

Preprints.org (www.preprints.org) | NOT PEER-REVIEWED | Posted: 9 June 2026 doi:10.20944/preprints202606.0589.v1

frames $\hat{n}_{ij}$. Therefore, its elastic compressibility must be determined by the same spectral resistance of the stochastic vacuum to short-wavelength deformations that appears in the isotropic DSR dispersion:

$$\omega^2 = c_0^2 k^2 - c_0^2 a_0^2 A_4 k^4 + O(k^6 a_0^4),$$

where

$$A_4 = \eta_4 - \frac{\lambda_{\text{wave}}}{12}.$$

For a stable vortical fluid component, the square of the speed of sound must be positive. In this normalization, this yields the stability condition

$$\boxed{\mathcal{C}_{\text{vort}} A_4 \geq 0}. \tag{A51}$$

If the sign of A_4 for the chosen stochastic vacuum ensemble is opposite to the sign required for positive vortical compressibility, then matching the vortical fluid interface requires either changing the sign of $\mathcal{C}_{\text{vort}}$ or revising the fluid-interface ansatz itself.

In the long-wavelength fluid limit, the effective sound speed of the primary vortical component has the scaling form

$$\boxed{\frac{c_{s,\text{vort}}^2(k_{\text{phys}})}{c_0^2} = \mathcal{C}_{\text{vort}} A_4 (k_{\text{phys}} a_0)^2 + O((k_{\text{phys}} a_0)^4)}.$$

Here, $\mathcal{C}_{\text{vort}} = O(1)$ — the dimensionless spectral matching invariant of the transition from the graph Laplacian to the vortical fluid action. It is not a new fundamental constant, but must be calculated for the chosen stochastic vacuum ensemble. The stability condition (A51) fixes the sign of the effective vorticity compressibility.

For perturbations averaged over the scale L, one can set $k_{\text{phys}} \sim L^{-1}$ and introduce

$$\epsilon_{\text{comp}}(L) \equiv \frac{c_{s,\text{vort}}^2}{c_0^2} \simeq \mathcal{C}_{\text{vort}} A_4 \left(\frac{a_0}{L}\right)^2.$$

On cosmological scales, $L \gg a_0$, so

$$w_{\text{vort}}^{\text{prim}} \simeq \frac{1}{2}\epsilon_{\text{comp}}(L) \ll 1, \qquad \frac{c_{s,\text{vort}}^2}{c_0^2} \simeq \epsilon_{\text{comp}}(L) \ll 1.$$

Thus, the coldness of the primary vortical component is not a fitting parameter, but a conditional fluid consequence of the high isotropy of the stochastic vacuum and the smallness of the graph UV scale relative to the wavelength of cosmological perturbations. In the Newtonian scalar-sector projection

$$ds^2 = a^2(\eta)\left[-(1+2\Psi)d\eta^2 + (1-2\Phi)d\mathbf{x}^2\right],$$

linear perturbations of this component satisfy

$$\begin{aligned}
\bar{\rho}'_{\text{vort}} + 3\mathcal{H}(1+w_{\text{vort}})\bar{\rho}_{\text{vort}} &= 0,\\
\delta'_{\text{vort}} &= -(1+w_{\text{vort}})(\theta_{\text{vort}} - 3\Phi') - 3\mathcal{H}\left(c_{s,\text{vort}}^2 - w_{\text{vort}}\right)\delta_{\text{vort}},\\
\theta'_{\text{vort}} &= -\mathcal{H}\left(1 - 3c_{s,\text{vort}}^2\right)\theta_{\text{vort}} + \frac{c_{s,\text{vort}}^2}{1+w_{\text{vort}}} q^2 \delta_{\text{vort}} + q^2\Psi - q^2\sigma_{\text{vort}}.
\end{aligned}$$

In the cold limit

$$w_{\text{vort}}^{\text{prim}} \to 0, \qquad c_{s,\text{vort}}^2 \to 0, \qquad \sigma_{\text{vort}} \to 0$$

© 2026 by the author(s). Distributed under a Creative Commons CC BY license.

Preprints.org (www.preprints.org) | NOT PEER-REVIEWED | Posted: 9 June 2026 doi:10.20944/preprints202606.0589.v1

we obtain

$$\delta'_{\rm vort} = -\theta_{\rm vort} + 3\Phi', \qquad \theta'_{\rm vort} = -\mathcal{H}\theta_{\rm vort} + q^2\Psi.$$

This is the CDM-like limit of the primary vortex refractive medium.

The residual anisotropic stress is determined not by the mere existence of the vector $\mathbf{\Omega}_{\rm prim}$, but by the incomplete averaging of its directions. Let us introduce the correlation tensor

$$\langle \Omega_i \Omega_j \rangle_L = \frac{1}{3}\delta_{ij}\mathcal{I}_\Omega + \Sigma_{ij}, \qquad \Sigma^i{}_i = 0.$$

The parameter of residual orientation anisotropy:

$$\epsilon_\Sigma = \frac{(\Sigma_{ij}\Sigma^{ij})^{1/2}}{\mathcal{I}_\Omega}.$$

Then

$$(\Pi_{\rm vort})^i{}_j = \xi_\Pi \bar{\rho}_{\rm vort}\frac{\Sigma^i{}_j}{\mathcal{I}_\Omega} + O(\Sigma^2), \qquad |\Pi_{\rm vort}| \lesssim \epsilon_\Sigma |\delta_{\rm vort}|.$$

Therefore, the condition

$$|\Pi_{\rm vort}| \ll |\delta_{\rm vort}|$$

reduces to the observationally verifiable requirement

$$\epsilon_\Sigma \ll 1.$$

Similarly, the velocity can be decomposed into scalar and vector parts:

$$v_i = \partial_i v + v_i^{(V)}, \qquad \partial_i v_i^{(V)} = 0.$$

The action (A50) describes the leading scalar component. The residual vector mode is a measure of the Archipelago's incomplete mixing:

$$\epsilon_V = \frac{|v^{(V)}|}{|\nabla v|/q} \ll 1.$$

The corresponding vector metric has the schematic constraint

$$q^2 B_i^{(V)} = 16\pi G_{\rm eff} a^2 (\bar{\rho}_{\rm vort} + \bar{p}_{\rm vort}) v_i^{(V)} + 8\pi G_{\rm eff} a^2 i q_j (\Pi_{\rm vort}^{(V)})^j{}_i.$$

Consequently, the vector modes are suppressed as

$$B_i^{(V)} = O(\epsilon_V, \epsilon_\Sigma).$$

Finally, parity-odd CMB signals require a nonzero spin of the primary vorticity:

$$\mathcal{H}_\Omega = \langle \mathbf{\Omega}_{\rm prim} \cdot (\nabla \times \mathbf{\Omega}_{\rm prim}) \rangle_L.$$

Let us define

$$\epsilon_H(q) = \frac{|\mathcal{H}_\Omega|}{q\mathcal{I}_\Omega}.$$

Then the possible TB- and EB-signals have the status of small relic traces:

$$C_\ell^{TB},\ C_\ell^{EB} = O(\epsilon_H, \epsilon_V, \epsilon_\Sigma).$$

© 2026 by the author(s). Distributed under a Creative Commons CC BY license.

Preprints.org (www.preprints.org) | NOT PEER-REVIEWED | Posted: 9 June 2026 doi:10.20944/preprints202606.0589.v1

An almost adiabatic entry into the baryon-photon plasma implies that the initial vorticity density inherits the same curvature modulus ζ_{lav} as the radiation:

$$S_{\text{vort},\gamma} = \delta_{\text{vort}} - \frac{3}{4}\delta_\gamma \approx 0,$$

with a small permissible isocurvature admixture. In this form, the primary vorticity component reproduces the observed CDM limit without introducing WIMP particles and without transforming $\mathbf{\Omega}_{\text{prim}}$ into a fundamental vector field of matter.

The vector variable $\mathbf{\Omega}_{\text{prim}}$ does not disappear in this process: it defines the initial-boundary condition from which, after coarse-graining, the scalar density δ_{vort} and the potential $\chi_{\text{vort}}^{\text{prim}}$ are obtained. It is convenient to write its effective equation not as a late baryonic source, but as a trace of the Topological Archipelago:

$$\mathcal{L}_{\cos}\mathbf{\Omega}_{\text{prim}} = S_{\text{arch}},$$

where $\mathcal{L}_{\cos}$ is the cosmological propagation operator for a vortex perturbation in an expanding graph, and S_{arch} is the effective pre-galactic source, given by the distribution of parent phase gates. In formal notation, it can be related to the parent phase current:

$$S_{\text{arch}} \sim -\mu_{\text{algo}}\nabla \times \mathbf{J}_{\text{parent}}^{\text{eff}},$$

but $\mathbf{J}_{\text{parent}}^{\text{eff}}$ is not the matter current in our already geometrized Universe. It is the boundary trace of the parent graph that has been transferred to the initial conditions of the daughter graph.

Observationally, this hypothesis should reproduce three modes.

1. **CMB acoustic peaks.** Before recombination, the baryon-photon plasma oscillates in gravitational wells defined by the primary cold vortex component $\chi_{\text{vort}}^{\text{prim}}$. Therefore, the IKT component must reproduce the effective density of cold dark matter

$$\Omega_{\text{vort}}h^2 \simeq \Omega_c h^2,$$

as well as the relative heights of the first acoustic peaks measured in CMB spectra [7].
2. **Large-scale structure.** After recombination, baryons do not fall into an empty vacuum, but into an already existing primary vortical refraction framework $\chi_{\text{vort}}^{\text{prim}}$. Therefore, galactic filaments and voids are the result of baryon growth on a pre-galactic vortical template.
3. **Late-stage galaxies.** After the formation of rotating disks, the primary component $\chi_{\text{vort}}^{\text{prim}}$ is locally amplified and reoriented by the baryon current $\mathbf{J}_{\text{bar}}$. This late-stage regime is described by the waveguide reduction:

$$\chi_{\text{vort}}^{\text{gal}} = \chi_{\text{2D}}(r)Z_0(z;r) + \chi_{\text{leak}}(r,z),$$

which leads to flat rotation curves and a flattened hidden halo.

Early JWST Galaxies.

The primary vortex component may also facilitate the early assembly of massive galaxies. In this picture, baryons do not form gravitational wells from scratch after recombination, but settle into an already existing refractive framework $\chi_{\text{vort}}^{\text{prim}}$. Therefore, IKT allows for the earlier formation of massive baryonic structures without introducing additional dark matter particles. This point has the status of observational motivation rather than proof: the interpretation of JWST data on galaxies at $z \gtrsim 10$ remains a subject of active debate.

Thus, the galactic disk in IKT does not create dark matter from scratch. It acts as a late nonlinear amplifier and waveguide organizer of the primary vortex component that already existed during the recombination era.

© 2026 by the author(s). Distributed under a Creative Commons CC BY license.

Preprints.org (www.preprints.org) | NOT PEER-REVIEWED | Posted: 9 June 2026 doi:10.20944/preprints202606.0589.v1

Appendix E.3.2. Algorithmic Drag Effect and 2D Waveguide Reduction

Algorithmic drag effect

The total weak-field acceleration is given by

$$\mathbf{g} = c_0^2 \nabla(\chi_G + \chi_{\text{vort}}).$$

For an isolated spherical mass, $\chi_G \propto 1/r$. A rotating galactic disk creates an additional vortical contribution associated with the non-commutative part of the routing:

$$\mathcal{U}_{ij}^{\text{eff}} = \mathcal{U}_{ij}^{(0)} \exp\left[i\, \eta_{\text{vort}} \frac{\mathbf{\Omega} \cdot (\mathbf{r}_i \times \mathbf{r}_j)}{c_0 |\mathbf{r}_i - \mathbf{r}_j|} \right].$$

If the z-axis is chosen perpendicular to the galactic disk,

$$\mathbf{\Omega} = (0, 0, \Omega_z),$$

then the additional phase predominantly renormalizes the azimutal circulation channels in the disk plane. For purely vertical steps, the contribution of the vortex factor vanishes. Therefore, the vortex does not prevent three-dimensional phase translation but creates macroscopic anisotropy in the graph conductance: circulation transport near the disk becomes dominant, while vertical leakage is suppressed but not zero.

Asymptotic 2D Reduction of the Vortex and the Topological Waveguide

In the strict formalism of quantum walk, phase translation remains three-dimensional. Therefore, the 2D reduction of the vortex field cannot be understood as the absolute confinement of phase traffic within an infinite cylinder. The correct interpretation is that the rotating baryonic disk forms a quasi-two-dimensional topological waveguide.

The weak-field formula for the reduction of the coherent phase translation velocity is not taken as a fundamental saturation law. It is the small-holonomy expansion of a compact edge phase. Let the local vortical phase be

$$\theta_{ij}^{\text{vort}} = \eta_{\text{vort}} \frac{\mathbf{\Omega} \cdot (\mathbf{r}_i \times \mathbf{r}_j)}{c_0 |\mathbf{r}_i - \mathbf{r}_j|}.$$

The physical transporter depends on $e^{i\theta_{ij}^{\text{vort}}}$, not on an unbounded real variable $\theta_{ij}^{\text{vort}}$. Therefore the coherent propagation factor is defined by the compact phase average

$$F_\Omega = \left| \left\langle e^{i\theta_{\text{vort}}} \right\rangle \right|, \qquad 0 \le F_\Omega \le 1.$$

The effective coherent velocity is

$$c_{\text{eff}} = c_0 F_\Omega.$$

For a narrow phase distribution,

$$F_\Omega = 1 - \frac{1}{2} \operatorname{Var}(\theta_{\text{vort}}) + \cdots .$$

If

$$\frac{1}{2} \operatorname{Var}(\theta_{\text{vort}}) = \chi_{\text{algo}} |\mathbf{\Omega}|^2, \qquad \chi_{\text{algo}} |\mathbf{\Omega}|^2 \ll 1,$$

then the previous phenomenological expression is recovered as the weak-holonomy limit:

$$c_{\text{eff}} \simeq c_0 \left(1 - \chi_{\text{algo}} |\mathbf{\Omega}|^2 \right).$$

© 2026 by the author(s). Distributed under a Creative Commons CC BY license.

Preprints.org (www.preprints.org) | NOT PEER-REVIEWED | Posted: 9 June 2026 doi:10.20944/preprints202606.0589.v1

The corresponding graph refractive index is

$$n_{\text{vort}} = \frac{1}{F_\Omega} \simeq 1 + \chi_{\text{algo}} |\mathbf{\Omega}|^2.$$

Thus the saturation of vortical graph dragging is not an empirical patch: it follows from the compactness of edge holonomy. Since $|\mathbf{\Omega}|$ is maximized near the baryonic disk and decreases with distance from it, the disk becomes a region of elevated phase refractive index. In accordance with the graph-theoretic analogue of Fermat's principle, phase trajectories extending along the z-axis undergo refractive return to the equatorial plane. It is precisely this, rather than an absolute prohibition on vertical edges, that determines the asymptotic two-dimensionality of the vortex regime.

The macroscopic equation for the vorticity potential in this regime has an anisotropic form

$$\nabla \cdot (\mathbf{D}_{\text{vort}} \nabla \chi_{\text{vort}}) = S_{\text{vort}},$$

where

$$\mathbf{D}_{\text{vort}} = \text{diag}(D_r, D_\phi, D_z), \qquad \epsilon_z = \frac{D_z}{D_\phi} \ll 1.$$

The parameter ϵ_z measures the relative vertical phase leakage. In the limit $\epsilon_z \to 0$, the ideal 2D reduction is restored, but for finite ϵ_z, the vortex halo has a finite vertical thickness.

Postulate A10 (Asymptotic waveguide reduction of a vortex)**.** *A vortex disk does not remove the vertical edges of the graph, but creates anisotropic phase transport conductivity. The ideal two-dimensional reduction is only a limit as $\epsilon_z \to 0$. A physically realizable galactic mode has a small but nonzero vertical leakage, so its hidden gravitational component is a flattened halo of finite thickness.*

The transverse structure of the waveguide is determined by the lowest bound eigenmode:

$$\left[-\frac{\partial}{\partial z} D_z(r,z) \frac{\partial}{\partial z} + V_{\text{guide}}(r,z) \right] Z_0(z;r) = \kappa_z^2(r) Z_0(z;r),$$

where V_{guide} is the effective confining potential generated by the gradient of n_{vort}. Outside the disk core, the bound mode has an evanescent asymptote

$$Z_0(z;r) \sim \exp\left(-\frac{|z|}{h_{\text{vort}}(r)} \right), \qquad h_{\text{vort}}(r) = \kappa_z^{-1}(r).$$

Consequently, the late galactic component of the vortex potential takes a quasi-separable form

$$\chi_{\text{vort}}^{\text{gal}}(r,z) = \chi_{\text{2D}}(r) Z_0(z;r) + \chi_{\text{leak}}(r,z),$$

where

$$\frac{\|\chi_{\text{leak}}\|}{\|\chi_{\text{2D}} Z_0\|} = O(\epsilon_z).$$

Inside the waveguide region, for $|z| \ll h_{\text{vort}}(r)$, we have $Z_0 \simeq 1$, and the effective equation for the radial profile reduces to the two-dimensional Laplace equation:

$$\frac{1}{r} \frac{\partial}{\partial r} \left(r \frac{\partial \chi_{\text{2D}}}{\partial r} \right) \simeq 0.$$

Therefore

$$\chi_{\text{2D}}(r) = A \ln \frac{r}{r_0} + B.$$

© 2026 by the author(s). Distributed under a Creative Commons CC BY license.

Preprints.org (www.preprints.org) | NOT PEER-REVIEWED | Posted: 9 June 2026 doi:10.20944/preprints202606.0589.v1

Appendix E.3.3. Flat Curves of Rotation, BTFR, and Flattened Halo

Flat rotation curves and BTFR

The dimension-consistent logarithmic profile of the late galactic component in the disk plane is given by

$$\chi^{\rm gal}_{\rm vort}(r,0) = -\frac{\sqrt{GM_{\rm bar}a_{\rm vort}}}{c_0^2}\ln\left(\frac{r}{r_0}\right),$$

where $M_{\rm bar}$ is the baryonic mass of the galaxy, and $a_{\rm vort}$ is the saturation acceleration scale of the vortex waveguide. Then, inside the waveguide zone

$$g_{\rm vort} = c_0^2\frac{\partial\chi^{\rm gal}_{\rm vort}}{\partial r} = -\frac{\sqrt{GM_{\rm bar}a_{\rm vort}}}{r}. \tag{A52}$$

Setting $v_f^2/r = |g_{\rm vort}|$, we obtain

$$v_f^2 = \sqrt{GM_{\rm bar}a_{\rm vort}}, \qquad v_f^4 = GM_{\rm bar}a_{\rm vort}.$$

Thus, the Tally–Fisher baryon relation arises not from the absolute two-dimensionality of all gravity, but from the asymptotically two-dimensional waveguide sector of the vortex potential.

Self-focusing and saturation of the waveguide cross-section

The quasi-two-dimensional vortex waveguide of a galaxy is not a rigid cylinder. It is a phase soliton whose cross-section self-focuses to saturation. Let $h_{\rm coh}$ denote the effective height of the coherent waveguide channel. Then the flux of vortical acceleration through the lateral surface of a cylinder of radius r and height $h_{\rm coh}$ satisfies the weak-field Gaussian norm

$$|g_{\rm vort}|\,2\pi r h_{\rm coh} = 4\pi GM_{\rm bar}.$$

Hence

$$|g_{\rm vort}| = \frac{2GM_{\rm bar}}{rh_{\rm coh}}. \tag{A53}$$

Equivalently, for a dimensionless refractive potential

$$\left|\partial_r\chi^{\rm gal}_{\rm vort}\right| = \frac{2GM_{\rm bar}}{c_0^2 rh_{\rm coh}}.$$

To obtain the asymptotic relation $|g_{\rm vort}| \propto \sqrt{M_{\rm bar}}/r$, the transverse scale of the coherent waveguide must grow as $\sqrt{M_{\rm bar}}$. Let us introduce the transverse coherence radius

$$R_\perp^2 = \frac{GM_{\rm bar}}{a_{\rm vort}}, \qquad h_{\rm coh} = 2R_\perp. \tag{A54}$$

Then

$$h_{\rm coh} = 2\sqrt{\frac{GM_{\rm bar}}{a_{\rm vort}}}, \qquad A_\perp = \pi R_\perp^2 = \frac{\pi GM_{\rm bar}}{a_{\rm vort}}.$$

Substituting (A54) into (A53) gives

$$|g_{\rm vort}| = \frac{\sqrt{GM_{\rm bar}a_{\rm vort}}}{r},$$

that is, exactly the profile (A52). Therefore, $a_{\rm vort}$ acquires the geometric meaning of the limiting transverse phase density, or tension, held by the graph waveguide.

© 2026 by the author(s). Distributed under a Creative Commons CC BY license.

Preprints.org (www.preprints.org) | NOT PEER-REVIEWED | Posted: 9 June 2026 doi:10.20944/preprints202606.0589.v1

Cosmological calibration of a_{vort}

It remains to determine the absolute value of the limiting tension a_{vort}. In IKT, the waveguide does not exist in empty continuous space, but in the background of residual cosmological insertion noise. This background creates a late-time dephasing of the graph with a characteristic acceleration scale

$$a_{\mathrm{bg}} = c_0 H_{\mathrm{bg}},$$

where H_{bg} is the effective rate of background cosmological dephasing. In the current SI projection, $H_{\mathrm{bg}} \simeq H_0$.

For the circular fundamental mode of a cylindrical waveguide, the dephasing is averaged over one complete azimuthal circuit. The minimum geometric factor of this mode is

$$\eta_{\mathrm{circ}} = \frac{1}{2\pi}.$$

Thus, the minimum cosmological calibration of the vortex tension takes the form

$$\boxed{a_{\mathrm{vort}} = \eta_{\mathrm{circ}} c_0 H_{\mathrm{bg}} = \frac{c_0 H_{\mathrm{bg}}}{2\pi}}. \tag{A55}$$

With CMB normalization $H_{\mathrm{bg}} = 67.4\,\mathrm{km\,s^{-1}\,Mpc^{-1}}$ [7], the current projection yields

$$a_{\mathrm{vort}} \simeq 1.04 \times 10^{-10} \left(\frac{H_{\mathrm{bg}}}{67.4\,\mathrm{km\,s^{-1}\,Mpc^{-1}}} \right) \mathrm{m\,s^{-2}}.$$

If we use the local ladder calibration $H_0 \simeq 73\,\mathrm{km\,s^{-1}\,Mpc^{-1}}$, the value shifts to $1.1 \times 10^{-10}\,\mathrm{m\,s^{-2}}$. Therefore, IKT relates the galactic acceleration scale not to a new free parameter, but to a late-time cosmological dephasing of the vacuum graph.

Remark A14 (Status of the 2π factor)**.** *Equation* (A55) *is a minimal waveguide calibration, not a MOND postulate. The 2π factor is interpreted as the geometric factor of the fundamental circular mode of a cylindrical waveguide. A complete microscopic derivation must be obtained from the spectrum of transverse modes of the vortex phase conductivity tensor $\mathbf{D}_{\mathrm{vort}}$ and from the mechanism of vertical leakage χ_{leak}. Until such a conclusion is reached,* (A55) *should be regarded as a testable conjecture of IKT.*

A Flattened Vortex Halo as a Testable Prediction

The waveguide reduction predicts that the algorithmic halo is neither an isotropic sphere nor a non-physical infinite cylinder. An evanescent vertical leakage forms a flattened distribution of hidden gravity with finite height $h_{\mathrm{vort}}(r)$:

$$\chi^{\mathrm{gal}}_{\mathrm{vort}}(r,z) \approx -\frac{\sqrt{G M_{\mathrm{bar}} a_{\mathrm{vort}}}}{c_0^2} \ln\left(\frac{r}{r_0}\right) \exp\left(-\frac{|z|}{h_{\mathrm{vort}}(r)}\right) + \chi_{\mathrm{leak}}(r,z).$$

Consequently, the shape of the effective dark halo must be correlated not only with the baryonic mass but also with the angular momentum of the disk: a large macroscopic torsion $|\mathbf{\Omega}|$ should correspond to a more pronounced flattening and a smaller relative vertical leakage ϵ_z. In the asymptotic saturated regime, the characteristic coherent height is related to the BTFR calibration as $h_{\mathrm{coh}} = 2\sqrt{G M_{\mathrm{bar}}/a_{\mathrm{vort}}}$, whereas the actual function $h_{\mathrm{vort}}(r)$ contains local corrections from the disk, the modal structure, and vertical leakage.

The observational test of this part of the IKT consists of reconstructing the three-dimensional shape of the gravitational potential from stellar streams, polar rings, gas disks, and weak lensing. The model predicts that for stable rotating disk galaxies, the principal plane of the hidden gravitational component must be aligned with the plane of the baryonic disk, and the orientation of the halo axes

© 2026 by the author(s). Distributed under a Creative Commons CC BY license.

Preprints.org (www.preprints.org) | NOT PEER-REVIEWED | Posted: 9 June 2026 doi:10.20944/preprints202606.0589.v1

must correlate with the macroscopic vorticity field $\mathbf{\Omega}$. The detection of universally spherical halos, unrelated to the direction of the baryonic angular momentum, would be a direct falsification of this vortex mechanism.

Appendix E.3.4. Spiral Modes as Non-Axisymmetric Excitation of a Waveguide

The finite vertical leakage of the vortex waveguide has another important consequence. It not only forms a flattened halo, but also opens a channel for three-dimensional non-axisymmetric perturbations. In the ideal limit

$$\epsilon_z = \frac{D_z}{D_\phi} = 0$$

the vortex field reduces to an axisymmetric two-dimensional profile

$$\chi_{2D}(r) \propto \ln r,$$

which explains the flat curves of rotation but does not in itself generate spiral morphology. With a small but finite vertical leakage

$$0 < \epsilon_z \ll 1$$

the waveguide sustains transverse eigenmodes

$$Z_n(z;r), \qquad n = 0, 1, 2, \ldots,$$

and azimuthal non-axisymmetric perturbations of the form

$$\delta\chi_{\text{vort}} = A_m(r) Z_n(z;r) e^{i(m\phi - \omega t)}.$$

Here, $m = 0$ corresponds to the axisymmetric mode, $m = 1$ to the single-arm or displaced mode, $m = 2$ to the two-arm grand-design structure, and $m > 2$ to multi-arm and flocculent regimes.

Taking into account the radial wave number, the perturbation takes the form

$$\delta\chi_{\text{vort}} = A(r) Z_n(z;r) \exp\left[i \left(m\phi + \int k_r(r)\, dr - \omega t \right) \right].$$

Constant-phase lines satisfy the condition

$$m\phi + \int k_r(r)\, dr - \omega t = \text{const}.$$

This equation defines a spiral curve in the plane of the disk. The local pitch angle of the spiral arm is given by the expression

$$\tan i_{\text{pitch}} = \frac{m}{|k_r| r}.$$

Thus, in IKT, spiral arms are interpreted not as an independent fundamental entity, but as a baryonic response to non-axisymmetric eigenmodes of the vortex waveguide. Vertical leakage is not the sole cause of the spiral structure: it serves as a channel for the excitation and selection of m-modes, which are then amplified by the differential rotation of the disk and baryonic self-gravity.

Physically, there are three regimes:

$$\epsilon_z = 0: \quad \text{ideal axisymmetric 2D limit},$$

$$0 < \epsilon_z \ll 1: \quad \text{quasi-two-dimensional waveguide with spiral modes},$$

$$\epsilon_z \sim 1: \quad \text{breakdown of the waveguide reduction and return to 3D diffusion}.$$

© 2026 by the author(s). Distributed under a Creative Commons CC BY license.

Preprints.org (www.preprints.org) | NOT PEER-REVIEWED | Posted: 9 June 2026 doi:10.20944/preprints202606.0589.v1

Consequently, the pronounced spiral morphology should arise not when the vortex is completely confined in the plane, but in an intermediate regime of small but finite vertical leakage.

Appendix E.3.5. Vortex soliton detachment: kinematics of the Pule cluster

In the presence of a massive rotating source, the evolution equation for the macroscopic vorticity field $\mathbf{\Omega}(\mathbf{r}, t)$ takes the form of a non-homogeneous wave equation:

$$\Box\mathbf{\Omega} \equiv \left(\nabla^2 - \frac{1}{c_0^2}\frac{\partial^2}{\partial t^2}\right)\mathbf{\Omega} = -\mu_{\text{algo}}\nabla \times \mathbf{J}_{\text{bar}},$$

where $\mathbf{J}_{\text{bar}} = \rho_B \mathbf{v}_B$ is the baryon mass current, and μ_{algo} is the coupling coefficient of the vacuum network. In IKT, the vacuum is nonlinear: phase traffic contributes to the vortex potential χ_{vort} and reduces the effective translation velocity,

$$c_{\text{eff}} = c_0\left(1 - \chi_{\text{algo}}|\mathbf{\Omega}|^2\right).$$

Substituting this modified velocity and expanding the denominator into a Taylor series, we obtain the effective nonlinear vortex evolution equation with cubic self-focusing:

$$\Box\mathbf{\Omega} - \frac{2\chi_{\text{algo}}}{c_0^2}|\mathbf{\Omega}|^2\frac{\partial^2\mathbf{\Omega}}{\partial t^2} = -\mu_{\text{algo}}\nabla \times \mathbf{J}_{\text{bar}}.$$

During the collision of two clusters (Bullet Cluster 1E 0657-56, [6]), the hot baryonic gas experiences electromagnetic drag and shock braking. The macroscopic velocity of the gas drops sharply, the baryon current $\mathbf{J}_{\text{bar}}$ decreases, and the right-hand side of the equation for the detached vortex component enters a near-vacuum regime.

Since the vortex $\mathbf{\Omega}$ has no electric charge, it does not participate in electromagnetic drag. The full 3D problem depends on the conductivity tensor $\mathbf{D}_{\text{vort}}$, the vertical leakage ϵ_z, and the collision boundary conditions. Therefore, rather than a universal exact solution, we use a leading soliton-like ansatz for a bound phase packet propagating along the collision axis x with the initial orbital velocity of the cluster v_c:

$$\mathbf{\Omega}(\mathbf{r}, t) \simeq \mathbf{\Omega}_0 \operatorname{sech}\left(\frac{x - v_c t}{L_{\text{sol}}}\right).$$

where L_{sol} is the characteristic effective width of the bound vortex packet, depending on the vacuum dispersion and the waveguide thickness h_{vort}. Thus, the gravitational lens observed behind the decelerated baryonic gas is a macroscopic map of the distribution $\chi_{\text{vort}} \propto |\mathbf{\Omega}|^2$. The detached topological vortex of the effective edge core continues its motion by inertia as a weakly dissipative phantom soliton, mimicking the kinematics of hypothetical collisionless dark matter particles without introducing a new particle.

Unified refractive potential for lensing

Gravitational refraction and the vortex dark sector must use the same eikonal lensing interface. Therefore, in systems where an additional vortex delay is present, the lensing metric includes not only the baryonic delay χ_G, but the total refractive delay

$$\boxed{\chi_{\text{lens}} = \chi_G + \chi_{\text{vort}}^{\text{prim}} + \chi_{\text{vort}}^{\text{gal}}}.$$

In baryon-dominated systems, the dominant term is χ_G. In galaxies and cluster collisions, the vortical contribution provides an additional effective lensing density. Thus, the vortical sector does not introduce a separate metric: it adds the refractive delay to the same eikonal functional used in the gravitational interface.

© 2026 by the author(s). Distributed under a Creative Commons CC BY license.

Preprints.org (www.preprints.org) | NOT PEER-REVIEWED | Posted: 9 June 2026 doi:10.20944/preprints202606.0589.v1

Minimal lensing-forward ansatz for cluster collisions

A qualitative statement about the kinematic separation of the vortex component from the decelerating X-ray gas must be translated into observational quantities of weak and strong lensing. Therefore, we introduce a minimal forward-model interface between the vorticity field $\boldsymbol{\Omega}$ and the lensing maps. This block is not a complete hydrodynamic fit of the 1E 0657–56 system; it defines a computable procedure that can be compared with X-ray/SZ, optical, and strong/weak-lensing data.

In the thin-lens approximation, the observed two-dimensional lensing potential function is given by

$$\psi_{\rm IKT}(\boldsymbol{\theta}) = \frac{2}{c_0^2}\frac{D_{ls}}{D_l D_s}\int dz\, \Phi_{\rm lens}^{\rm IKT}(D_l\boldsymbol{\theta}, z),$$

where D_l, D_s, D_{ls} are the angular distances to the lens, to the source, and between the lens and the source, respectively. In IKT, the lensing potential is decomposed into baryonic and vortex components:

$$\Phi_{\rm lens}^{\rm IKT} = \Phi_{\rm bar} + \Phi_{\Omega}.$$

Here, Φ_{Ω} is not the potential of a new material particle; it is the refractive projection of macroscopic graphic curl.

Convergence and shear are given by the derivatives of the two-dimensional potential:

$$\kappa(\boldsymbol{\theta}) = \frac{1}{2}\nabla_{\boldsymbol{\theta}}^2\psi_{\rm IKT}, \qquad \gamma_1 = \frac{1}{2}\left(\partial_{\theta_1}^2 - \partial_{\theta_2}^2\right)\psi_{\rm IKT}, \qquad \gamma_2 = \partial_{\theta_1}\partial_{\theta_2}\psi_{\rm IKT}.$$

Equivalently, one can introduce an effective lensing surface density

$$\kappa(\mathbf{R}) = \frac{\Sigma_{\rm eff}(\mathbf{R})}{\Sigma_{\rm crit}}, \qquad \Sigma_{\rm crit} = \frac{c_0^2}{4\pi G}\frac{D_s}{D_l D_{ls}},$$

where $\mathbf{R} = D_l\boldsymbol{\theta}$ is a coordinate in the lens plane. In the minimal decomposition

$$\Sigma_{\rm eff} = \Sigma_{\rm gal} + \Sigma_{\rm gas} + \Sigma_{\Omega}.$$

The first two terms are reconstructed from the optical/IR map of galaxies and the X-ray/SZ map of gas. The last term is the effective lensing projection of a vortex soliton.

For the collision of two clusters, let us introduce the x-axis along the direction of the collision, the y-axis in the sky plane transverse to the collision, and the z-axis along the line of sight. The minimal soliton ansatz for the a-th component is given by

$$\mathcal{I}_{\Omega,a}(\mathbf{r},t) = |\boldsymbol{\Omega}_a|^2 = \Omega_{0a}^2\,\mathrm{sech}^2\left(\frac{x - X_{\Omega,a}(t)}{L_{\parallel,a}}\right)\exp\left[-\frac{(y - Y_{\Omega,a})^2}{2L_{\perp,a}^2} - \frac{(z - Z_{\Omega,a})^2}{2H_{\Omega,a}^2}\right].$$

The positive effective lensing density of the vortex component is given by the closure relation

$$\rho_{\Omega}^{\rm lens} = \rho_{\Omega *}\sum_{a=1}^{2}\mathcal{I}_{\Omega,a} + \rho_{\rm bridge},$$

where $\rho_{\rm bridge}$ allows for a small bridge or tail component between subclusters. Then

$$\Sigma_{\Omega}(\mathbf{R},t) = \int dz\, \rho_{\Omega}^{\rm lens}(\mathbf{R},z,t)$$

and for the Gaussian z-projection

$$\Sigma_{\Omega}(\mathbf{R},t) = \sum_{a=1}^{2}\Sigma_{\Omega,0a}\,\mathrm{sech}^2\left(\frac{x - X_{\Omega,a}(t)}{L_{\parallel,a}}\right)\exp\left[-\frac{(y - Y_{\Omega,a})^2}{2L_{\perp,a}^2}\right] + \Sigma_{\rm bridge}(\mathbf{R},t),$$

© 2026 by the author(s). Distributed under a Creative Commons CC BY license.

Preprints.org (www.preprints.org) | NOT PEER-REVIEWED | Posted: 9 June 2026 doi:10.20944/preprints202606.0589.v1

where

$$\Sigma_{\Omega,0a} = \sqrt{2\pi}\, H_{\Omega,a}\rho_{\Omega*}\Omega_{0a}^2.$$

The two-dimensional potential from which κ and shear are constructed can be obtained directly from $\Sigma_{\rm eff}$. For $\mathbf{R} = D_l\boldsymbol{\theta}$ we have

$$\psi_{\rm IKT}(\mathbf{R}) = \frac{4G}{c_0^2}\frac{D_{ls}}{D_l D_s}\int d^2R'\,\Sigma_{\rm eff}(\mathbf{R}')\ln\!\left(\frac{|\mathbf{R}-\mathbf{R}'|}{R_*}\right) + \text{const.}$$

Here, R_* is an arbitrary length that vanishes from the observed potential derivatives. This formula defines a direct computational procedure:

$$\boldsymbol{\Omega} \longrightarrow \Sigma_\Omega \longrightarrow \Sigma_{\rm eff} \longrightarrow \psi_{\rm IKT} \longrightarrow \kappa, \gamma_1, \gamma_2.$$

The observed offset profiles are determined without reference to the ontology of dark matter particles. For each subcluster a, we define

$$\mathbf{R}_{\kappa,a} = \arg\max_{\mathcal{W}_a}\kappa(\mathbf{R}), \qquad \mathbf{R}_{\rm gas,a} = \arg\max_{\mathcal{W}_a}\Sigma_{\rm gas}(\mathbf{R}), \qquad \mathbf{R}_{\rm gal,a} = \arg\max_{\mathcal{W}_a}\Sigma_{\rm gal}(\mathbf{R}),$$

where $\mathcal{W}_a$ is the window around the corresponding subcluster. Displacements along the collision axis $\hat{\mathbf{e}}_x$:

$$\Delta_{\rm gas\to\kappa,a} = (\mathbf{R}_{\kappa,a} - \mathbf{R}_{\rm gas,a})\cdot\hat{\mathbf{e}}_x, \qquad \Delta_{\rm gal\to\kappa,a} = \left(\mathbf{R}_{\kappa,a} - \mathbf{R}_{\rm gal,a}\right)\cdot\hat{\mathbf{e}}_x.$$

The IKT limit of a detached vortex soliton corresponds to the regime

$$|\Delta_{\rm gas\to\kappa,a}| \gg |\Delta_{\rm gal\to\kappa,a}|,$$

that is, the lensing maximum follows the collisionless galactic-vortex packet, rather than the decelerating X-ray gas.

For comparison with the data, it is also convenient to introduce one-dimensional profiles along the collision axis:

$$\kappa_a^{\parallel}(s) = \kappa\big(\mathbf{R}_{\rm gas,a} + s\hat{\mathbf{e}}_x\big), \qquad \Sigma_{\rm gas,a}^{\parallel}(s) = \Sigma_{\rm gas}\big(\mathbf{R}_{\rm gas,a} + s\hat{\mathbf{e}}_x\big).$$

Then, a Bullet-like configuration in IKT implies that the maximum of $\kappa_a^{\parallel}$ is shifted relative to the maximum of $\Sigma_{\rm gas,a}^{\parallel}$, and the width and ellipticity of the κ-peak are controlled by the parameters $L_{\parallel,a}$, $L_{\perp,a}$, and $H_{\Omega,a}$.

Remark A15 (Status of the Bullet Cluster in the IKT)**.** *The equations in this subsection do not constitute a complete hydrodynamic fit of the 1E 0657–56 system. They define the minimal observational interface required to test the IKT: from a given vortex soliton, the $\Phi_{\rm lens}^{\rm IKT}$, $\Sigma_{\rm eff}$, κ, shear, and offset profiles are constructed. A complete verification requires a joint fit of the X-ray/SZ gas map, the optical galaxy map, strong/weak-lensing constraints, collision geometry, and a possible bridge component. Until such a fit is achieved, the Bullet Cluster should be considered not as proof of IKT, but as a rigorous test of its vortex sector.*

Appendix E.3.6. Unified Lensing Potential and Status of the Dark-Sector Fit

The vortex sector is included in the same eikonal lensing metric as the baryonic phase delay:

$$\chi_{\rm lens} = \chi_G + \chi_{\rm vort}^{\rm prim} + \chi_{\rm vort}^{\rm gal}.$$

The early linear limit $\chi_{\rm vort}^{\rm prim}$ is responsible for CMB/LSS-consistent cold behavior, while the late nonlinear waveguide limit $\chi_{\rm vort}^{\rm gal}$ is responsible for flat rotation curves and the BTFR. Full confirmation

© 2026 by the author(s). Distributed under a Creative Commons CC BY license.

Preprints.org (www.preprints.org) | NOT PEER-REVIEWED | Posted: 9 June 2026 doi:10.20944/preprints202606.0589.v1

of this scenario requires a unified fitting module that simultaneously tests the CMB/LSS, galactic dynamics, and cluster lensing maps.

Appendix E.4. Limit Regimes: Black Holes, Drainage, and Multiverse Homeostasis

Remark A16 (Status of the limiting extension)**.** *This section is a high-level cosmological extension of the graph insertion mechanism. It is not used in the derivation of local interactions, masses, α_{top}, G_{IKT}, or the wave-sector. Its purpose is to demonstrate a possible extension of IKT to black hole, phase-drainage, topological de-string, and cosmological aging regimes.*

Remark A17 (B3 convention for the black-hole sector)**.** *In the B3 branch, a black hole is not defined by a Schwarzschild event horizon. It is a finite graph-accessibility neck whose exterior optical interface is described by the exponential metric of Section B.4.6. The terms "capture", "gate", and "neck" therefore refer to graph-routing accessibility rather than to a pre-existing continuum surface. Standard Hawking and Bekenstein–Hawking formulae may be used only as comparison benchmarks unless the corresponding B3 neck spectrum is explicitly computed.*

Appendix E.4.1. Topological Singularity Degeneracy and the Black Hole Limit

Topological Singularity Degeneracy and the Reproduction Coefficient $R = 1$

Hypothesis A14 (Degeneracy of Saturated Knots)**.** *All regions where the saturable delay tends to the limit $p_{\text{stay}} \to 1$ belong to a single equivalence class of the absolute phase flow:*

$$i \sim j \quad \Longleftrightarrow \quad p_i \to 1,\ p_j \to 1.$$

Factorization of the graph by this class yields a single flow S_∞.

It follows from this additional hypothesis that the set of black holes in the parent universe can function as a set of parallel channels of a single daughter domain, rather than as an independent branching for each horizon. In this sense, the reproduction coefficient $R = 1$ is a consequence of the topological degeneracy postulate, rather than a result already proven by the initial kinematics.

Dimensional Separation of Energy, Entropy, Information, and Node Flux

The B3 black-hole sector uses several different flux notions. They must not be identified with one another. We reserve

$$P_E \qquad [\mathrm{J\,s^{-1}}]$$

for laboratory energy power. We use

$$\Phi_{\text{ch}} \qquad [\text{channels}\,\mathrm{s^{-1}}]$$

for graph phase-channel flux and

$$\Phi_{\mathcal{N}} \qquad [\text{nodes}\,\mathrm{s^{-1}}]$$

for effective node-production or node-drainage rate. The notation Φ_N is avoided here because it is already used for the Newtonian potential in the weak-field glossary. The dimensional projection has the ordered form

$$P_E \longrightarrow \dot{S}_{\text{gate}} \longrightarrow \dot{\mathcal{I}}_{\text{gate}} \longrightarrow \Phi_{\text{ch}} \longrightarrow \Phi_{\mathcal{N}}.$$

For the B3 graph gate,

$$A_{\text{gate}} = 4\pi e^2 \frac{G^2 M^2}{c_0^4}, \qquad N_{\text{gate}} = \frac{A_{\text{gate}}}{A_0}.$$

© 2026 by the author(s). Distributed under a Creative Commons CC BY license.

Preprints.org (www.preprints.org) | NOT PEER-REVIEWED | Posted: 9 June 2026 doi:10.20944/preprints202606.0589.v1

The gate entropy is

$$S_{\mathrm{B3}} = k_B N_{\mathrm{gate}} \ln \Omega_{\mathrm{edge}}.$$

Therefore the energy associated with one unwound gate channel is

$$\varepsilon_{\mathrm{ch}}^{B3}(M) = \frac{d(Mc_0^2)}{dN_{\mathrm{gate}}} = \frac{A_0 c_0^6}{8\pi e^2 G^2 M}. \tag{A56}$$

Equivalently,

$$\varepsilon_{\mathrm{ch}}^{B3} = k_B T_{\mathrm{B3}} \ln \Omega_{\mathrm{edge}}.$$

If an energy power is used as a benchmark source, the corresponding entropy and information rates are

$$\dot{S}_{\mathrm{gate}}^{(E)} = \frac{P_E}{T_{\mathrm{B3}}}, \qquad \dot{\mathcal{I}}_{\mathrm{gate}}^{(E)} = \frac{\dot{S}_{\mathrm{gate}}^{(E)}}{k_B}$$

in nats per second. Hence the energy-driven graph-channel flux is

$$\Phi_{\mathrm{ch}}^{(E)} = \frac{\dot{\mathcal{I}}_{\mathrm{gate}}^{(E)}}{\ln \Omega_{\mathrm{edge}}} = \frac{P_E}{\varepsilon_{\mathrm{ch}}^{B3}(M)} = \frac{8\pi e^2 G^2 M}{A_0 c_0^6} P_E. \tag{A57}$$

If a node-production or node-drainage rate is needed, a further dimensionless yield factor must be specified:

$$\Phi_{\mathcal{N}} = \nu_{\mathcal{N}} \Phi_{\mathrm{ch}}. \tag{A58}$$

The coefficient $\nu_{\mathcal{N}}$ is not an energy coefficient. It measures the mean number of effective daughter-graph nodes generated per unwound phase-channel and must ultimately be computed from the insertion/TTC operator. In a minimal bookkeeping normalization one may set $\nu_{\mathcal{N}} = 1$, but this is a convention rather than a derivation.

The maximum graph-gate capacity is a distinct quantity:

$$\Phi_{\mathrm{cap}}^{B3} = \frac{N_{\mathrm{gate}}}{\tau_0} \nu_{\mathrm{gate}} = \frac{4\pi e^2 G^2 M^2}{c_0^4 A_0 \tau_0} \nu_{\mathrm{gate}}. \tag{A59}$$

It is an upper bound or saturation capacity of the neck, not an energy power. The actual channel flux must be written as

$$\Phi_{\mathrm{ch}}^{\mathrm{actual}} = f_{\mathrm{occ}}(M,t) \min\left[\Phi_{\mathrm{cap}}^{B3}, \Phi_{\mathrm{src}}^{B3}, \Phi_{\mathrm{TTC}}^{B3}\right], \qquad 0 \le f_{\mathrm{occ}} \le 1. \tag{A60}$$

Here Φ_{src}^{B3} is the source-limited channel flux and Φ_{TTC}^{B3} is the spectrum-limited unwinding flux computed from the microscopic neck dynamics. If the source is described by laboratory energy power, then

$$\Phi_{\mathrm{src}}^{B3} = \Phi_{\mathrm{ch}}^{(E)} = \frac{P_E}{\varepsilon_{\mathrm{ch}}^{B3}(M)}.$$

Consequently, a law such as $P_E \propto M^{-2}$ does not imply $\Phi_{\mathrm{ch}} \propto M^{-2}$. For example, a Hawking-like benchmark energy power $P_E \propto M^{-2}$ corresponds, through (A57), to an energy-driven channel flux $\Phi_{\mathrm{ch}}^{(E)} \propto M^{-1}$. The scaling $\Phi_{\mathrm{cap}}^{B3} \propto M^2$ refers instead to the finite B3 gate capacity.

B3 Black-Hole Mass Limits: Gate Ignition and Fragmentation Limit

In the B3 branch the relevant macroscopic surface is not a Schwarzschild event horizon but the graph phase-gate of the exponential exterior. For a non-rotating overloaded cluster its natural area is

$$A_{\mathrm{gate}} = 4\pi e^2 M_g^2 = 4\pi e^2 \frac{G^2 M^2}{c_0^4}.$$

© 2026 by the author(s). Distributed under a Creative Commons CC BY license.

Preprints.org (www.preprints.org) | NOT PEER-REVIEWED | Posted: 9 June 2026 doi:10.20944/preprints202606.0589.v1

This area is also equal to the B3 optical capture cross-section $\pi b_{\rm ph}^2$ of the static exponential exterior. Therefore any phase-throughput or absorption law in the B3 sector must be normalized by $A_{\rm gate}$, not by the Schwarzschild horizon area, unless a separate TTC calculation proves a different effective counting area.

The fate of a daughter domain inside a graph neck is determined by source-limited channel supply, TTC unwinding, and the finite capacity of the B3 graph gate. The gate capacity is

$$\Phi_{\rm cap}^{B3} = \frac{4\pi e^2 G^2 M^2}{c_0^4 A_0 \tau_0} \nu_{\rm gate}.$$

This is a graph-channel capacity, not an energy power. If one introduces a laboratory energy benchmark, it must be denoted by P_E and converted to channel flux using (A57). A channel flux is then converted to a node flux by (A58).

For comparison only, one may define a semiclassical energy benchmark by replacing the parent bath with a thermal CMB bath and the unwinding law with the Hawking energy-power scaling:

$$P_{\rm out}^{\rm bench} = \frac{\hbar c_0^6}{15360\pi G^2 M^2}, \qquad P_{\rm in}^{B3,\rm bench} = A_{\rm gate}\sigma_{SB} T_{CMB}^4.$$

The corresponding B3 channel fluxes are

$$\Phi_{\rm out,ch}^{\rm bench} = \frac{P_{\rm out}^{\rm bench}}{\varepsilon_{\rm ch}^{B3}(M)}, \qquad \Phi_{\rm in,ch}^{B3,\rm bench} = \frac{P_{\rm in}^{B3,\rm bench}}{\varepsilon_{\rm ch}^{B3}(M)}.$$

The equality of benchmark powers and the equality of the corresponding benchmark channel fluxes give the same reference mass, because both sides are divided by the same channel energy $\varepsilon_{\rm ch}^{B3}(M)$. This gives

$$M_{\rm ign}^{B3,\rm bench} = \left(\frac{\hbar c_0^{10}}{61440\pi^2 e^2 G^4 \sigma_{SB} T_{CMB}^4} \right)^{1/4}.$$

This reference mass is not a fundamental prediction of IKT; it is only a B3-normalized comparison with the usual semiclassical energy scaling. The true ignition threshold requires the TTC neck spectrum, the source-limited channel flux, and the node-yield factor of the insertion dynamics.

The upper mass limit remains a coherence problem of the accretion vortex. In B3 it should be phrased without importing an extremal Kerr radius. Let

$$R_{\rm cap} = \zeta_{\rm cap}(a_*^{\rm IKT}) \frac{GM}{c_0^2}$$

be the B3 capture or gate-transport scale of the rotating graph neck. For the static B3 exterior, the natural choices are $\zeta_{\rm cap} = e$ for the minimal gate radius or $\zeta_{\rm cap} = 2e$ for the photon-capture impact scale. For a rotating B3 neck, $\zeta_{\rm cap}$ must be computed from the compact-holonomy dragging field $\omega_{\rm IKT}(r,\theta)$.

The fragmentation condition is then

$$R_{\rm cap} \geq R_{\rm frag},$$

where the disk fragmentation law may be kept in the phenomenological form

$$R_{\rm frag} \approx R_0 \left(\frac{M}{M_{\rm ref}} \right)^{1/27}.$$

© 2026 by the author(s). Distributed under a Creative Commons CC BY license.

Preprints.org (www.preprints.org) | NOT PEER-REVIEWED | Posted: 9 June 2026 doi:10.20944/preprints202606.0589.v1

Thus

$$M_{\mathrm{crit}}^{B3} = M_{\mathrm{ref}} \left(\frac{R_0 c_0^2}{\zeta_{\mathrm{cap}} G M_{\mathrm{ref}}} \right)^{27/26}.$$

This preserves the original IKT idea of a topological upper mass cutoff, but removes the implicit Schwarzschild/Kerr normalization. The coefficient is now a B3 observable: it must be predicted from the rotating exponential graph-neck sector.

When this threshold is exceeded, the central gateway disrupts the architecture of the incoming phase traffic. The information flow fragments into stars before reaching the graph-accessibility neck, permanently blocking further black-hole growth and forming a statistical cutoff in the observed mass function of quasars.

Appendix E.4.2. Algebraic Factorization of the State Space: From Insertion to Drainage

At the microscopic level, the algorithmic overload

$$p_{\mathrm{stay}} \to 1$$

is resolved by a local isometric insertion

$$\mathcal{I}_m : \mathcal{H}_m \to \mathcal{H}_{m+1}.$$

In the regime of macroscopic gravitational collapse, this mechanism can transition to a topological phase-separation limit.

Let the overloaded cluster $B \subset G_m$ form a narrow graph bottleneck ∂B. Its Cheeger parameter

$$h(B) = \frac{|\partial B|}{\min(|B|, |G_m \setminus B|)}$$

tends to zero:

$$h(B) \to 0.$$

Then the adjacency matrix has an almost block form:

$$A_m = \begin{pmatrix} A_{\mathrm{parent}} & B_{\mathrm{neck}} \\ B_{\mathrm{neck}}^{\dagger} & A_{\mathrm{daughter}} \end{pmatrix}, \qquad \|B_{\mathrm{neck}}\| \ll \|A_{\mathrm{parent}}\|, \|A_{\mathrm{daughter}}\|.$$

At the level of the single-particle graph space, this yields an almost direct sum:

$$\mathcal{H}_{\mathrm{total}}^{(1)} \simeq \mathcal{H}_{\mathrm{parent}}^{(1)} \oplus \mathcal{H}_{\mathrm{daughter}}^{(1)} \oplus \mathcal{H}_{\mathrm{neck}}^{(1)}.$$

At the level of the observable algebras after decoherence of the neck sector, an approximate factorization arises:

$$\mathcal{A}_{\mathrm{total}} \simeq \mathcal{A}_{\mathrm{parent}} \otimes \mathcal{A}_{\mathrm{daughter}} + O(\epsilon_{\mathrm{neck}}),$$

where

$$\epsilon_{\mathrm{neck}} \sim \frac{\|B_{\mathrm{neck}}\|}{\min(\|A_{\mathrm{parent}}\|, \|A_{\mathrm{daughter}}\|)}.$$

In this picture, what appears to be internal inflationary node generation for the daughter sector appears as reduced phase drainage through the boundary/neck layer for the parent sector:

$$\rho_{\mathrm{parent}} = \mathrm{Tr}_{\mathrm{daughter,neck}} |\Psi_{\mathrm{total}}\rangle\langle\Psi_{\mathrm{total}}|.$$

© 2026 by the author(s). Distributed under a Creative Commons CC BY license.

Preprints.org (www.preprints.org) | NOT PEER-REVIEWED | Posted: 9 June 2026 doi:10.20944/preprints202606.0589.v1

Consequently, black-hole drainage is not a new fundamental operation, but rather the large-cluster/bottleneck limit of the local insertion $\mathcal{I}_m$. This block pertains to a high-level cosmological generalization, rather than to the local minimum U_m theorem.

Appendix E.4.3. Graph Accessibility, Neck-Subalgebra, and Black Hole Information Balance

Graph accessibility instead of background "inside" and "outside".

In IKT, the graph is not embedded in a predefined space: the graph itself defines reachability relations, from which a spacetime interface then emerges. Therefore, in black hole mode, the terms "outer sector," "neck layer," and "inner cluster" denote not regions of the background space, but graph-causal domains defined by paths in G_m and the smallness of connectivity through the neck B_{neck}.

Let the formation of a black hole correspond to the emergence of a narrow neck B_{neck} for which the Cheeger connectivity is small:

$$h(B_{\text{neck}}) \ll 1.$$

Then the algebra of observables of the complete graph admits an approximate decomposition:

$$\mathcal{A}_m \simeq \mathcal{A}_{\text{out}} \otimes \mathcal{A}_{\text{neck/in}} + O(\epsilon_{\text{neck}}).$$

Here, $\mathcal{A}_{\text{out}}$ is a subalgebra of operations supported on the graph-causal domain that does not require an intersection with B_{neck} at the observed scale. This is not a spatial "outer region," but rather an operationally distinguished class of routes and observables.

The total state $|\Psi_m\rangle$ evolves unitarily in the full graph description. An observer constructed from paths of the outer domain has access only to the restriction of the state to $\mathcal{A}_{\text{out}}$:

$$\omega_{\text{out}}(O) = \langle \Psi_m | O | \Psi_m \rangle, \qquad O \in \mathcal{A}_{\text{out}}.$$

If we use an approximate factorization, this restriction can be written as a reduced state:

$$\rho_{\text{out}} = \text{Tr}_{\text{neck/in}} |\Psi_m\rangle\langle\Psi_m|.$$

Such a trace does not constitute a fundamental loss of information. It is a coarse-grained operation reflecting the restriction on available observables.

Consequently, in IKT, information is not destroyed in the "inner space." It ceases to be reconstructable from a single reduced subalgebra and is preserved in the correlations of the full graph state, including the neck layer and subsequent $1D$ unwinding paths.

Topological unwinding and Page-curve-compatible toy model.

As the neck topologically unwinds, part of the correlation structure is transferred from $\mathcal{A}_{\text{neck/in}}$ to the algebra of radiated $1D$-routes $\mathcal{A}_{\text{rad}}$. This does not mean that the information was initially "beyond the graph-accessibility neck" and then moved into the background geometry. Within IKT, this implies a change in which part of the full correlation structure becomes reconstructible from the reduced algebra of observables:

$$\mathcal{A}_{\text{neck/in}} \longrightarrow \mathcal{A}_{\text{rad}}.$$

If the initial number of neck channels is N_0, and each channel has Ω_{edge} phase-frame states, then the simplest unitary toy model of unwinding yields

$$\dim \mathcal{H}_{\text{neck}}(n) = \Omega_{\text{edge}}^{N_0 - n}, \qquad \dim \mathcal{H}_{\text{rad}}(n) = \Omega_{\text{edge}}^{n}.$$

For a typical unitary unwinding, the radiation entropy has a Page-like form:

$$S_{\text{rad}}(n) \simeq k_B \ln \Omega_{\text{edge}} \, \min(n, N_0 - n).$$

© 2026 by the author(s). Distributed under a Creative Commons CC BY license.

Preprints.org (www.preprints.org) | NOT PEER-REVIEWED | Posted: 9 June 2026 doi:10.20944/preprints202606.0589.v1

It grows until $n \simeq N_0/2$, and then decays to zero upon complete unwinding. Thus, the graph black-hole sector obtains a Page-curve-compatible information-preservation scenario: the full graph state remains unitary, and the observed thermality is a property of the reduced algebra, not a fundamental loss of information.

The quantitative limit of B3 black-hole thermodynamics.

In the B3 branch the counting surface is the finite graph phase-gate, not a Schwarzschild event horizon. For the static exterior this surface has area

$$A_{\text{gate}} = 4\pi e^2 \frac{G^2 M^2}{c_0^4}.$$

If one elementary neck channel occupies an effective graph area A_0, then

$$N_{\text{gate}} = \frac{A_{\text{gate}}}{A_0}, \qquad S_{\text{B3}} = k_B N_{\text{gate}} \ln \Omega_{\text{edge}} = k_B \frac{4\pi e^2 G^2 M^2}{c_0^4 A_0} \ln \Omega_{\text{edge}}.$$

Therefore the area law $S \propto A_{\text{gate}}$ and the mass scaling $S \propto M^2$ follow from finite edge counting. The temperature defined by the thermodynamic relation $dE = TdS$, with $E = Mc_0^2$, is

$$\boxed{T_{\text{B3}} = \frac{A_0 c_0^6}{8\pi e^2 k_B G^2 M \ln \Omega_{\text{edge}}}}$$

so the scaling $T_{\text{B3}} \propto 1/M$ is obtained without importing the Schwarzschild horizon. The numerical coefficient depends on the microscopic ratio $A_0/\ln \Omega_{\text{edge}}$ and must be computed from the B3 neck spectrum. Equating it to the Bekenstein–Hawking coefficient is allowed only as an external comparison, not as a derivation.

The detachment of 1D packets from the neck then gives an evaporation/unwinding scale of the form $\tau_{\text{unwind}} \propto M^3$, but its coefficient and greybody factors require a full TTC computation of the absorbing graph-accessibility neck.

Remark A18 (Status of the mechanism)**.** *The graph unwinding of the neck sector is not, in this work, a complete theorem of quantum black-hole gravity. Its role is to show that in IKT there exists a background-independent internal formulation of the information balance: accessibility is determined by graph paths, Cheeger necks, and subalgebras of routing operations, rather than regions of a pre-specified space. A rigorous conclusion requires constructing a complete TTC unwinding operator, computing the neck spectrum, and verifying Page-like behavior for a specific ensemble of graphs.*

Appendix E.4.4. Phase Flow Balance Through Black Holes and Hubble Tension

Multi-component flux balance and Hubble tension

Let $\Phi_{\mathcal{N},\text{in}}$, $\Phi_{\mathcal{N},\text{out}}$, and $\Phi_{\mathcal{N},\text{noise}}$ be measured at nodes per unit time. Then the node number balance takes the form

$$\frac{dN}{dt} = \Phi_{\mathcal{N},\text{in}}(t) - \Phi_{\mathcal{N},\text{out}}(t) + \Phi_{\mathcal{N},\text{noise}}(t).$$

The observed Hubble parameter is equal to the normalized node flux:

$$H_{\text{IKT}}(t) = \frac{1}{3N(t)}[\Phi_{\mathcal{N},\text{in}}(t) - \Phi_{\mathcal{N},\text{out}}(t) + \Phi_{\mathcal{N},\text{noise}}(t)].$$

© 2026 by the author(s). Distributed under a Creative Commons CC BY license.

Preprints.org (www.preprints.org) | NOT PEER-REVIEWED | Posted: 9 June 2026 doi:10.20944/preprints202606.0589.v1

This replaces dimensionally incorrect sums in which a Hubble rate, an energy power, and a node flux are combined without conversion. If a component is first estimated as a laboratory energy power P_E, it must be converted according to

$$\Phi_{\mathcal{N},\alpha}^{(E)} = \nu_{\mathcal{N}} \frac{P_{E,\alpha}}{\varepsilon_{\mathrm{ch}}^{B3}(M)}.$$

If a component is a purely topological parent-bath throughput, it is instead bounded by the B3 capacity law (A59) and by the occupation factor of the neck.

In the early Universe, endogenous noise $\Phi_{\mathcal{N},\mathrm{noise}}$ associated with graph relaxation dominates. In the late Universe, the quasi-stationary parent inflow $\Phi_{\mathcal{N},\mathrm{in}}$ and black-hole node drainage $\Phi_{\mathcal{N},\mathrm{out}}$ may play a major role. Therefore, the discrepancy between local and early-Universe estimates of H_0 is interpreted as a possible change in the dominant node-flow component, not as a direct sum of energy powers.

Balance of node and channel fluxes through B3 graph necks

The capacity of a B3 graph neck scales as the finite gate area rather than as a Schwarzschild event horizon:

$$\Phi_{\mathrm{cap}}^{B3}(M) = \kappa_{\mathrm{B3}} M^2, \qquad \kappa_{\mathrm{B3}} = \frac{4\pi e^2 G^2}{c_0^4 A_0 \tau_0} \nu_{\mathrm{gate}}.$$

Here A_0 is the effective area per graph-channel, τ_0 is the elementary update time, and ν_{gate} is the dimensionless mean number of admissible phase-transfer acts per channel per tick. In the simplest bookkeeping normalization $\nu_{\mathrm{gate}} = 1$, but in a complete TTC computation it must be derived from the neck spectrum. The actual node drainage also contains the occupation factor and the node-yield factor:

$$\Phi_{\mathcal{N},\mathrm{drain}}(M,t) = \nu_{\mathcal{N}} f_{\mathrm{occ}}(M,t) \Phi_{\mathrm{cap}}^{B3}(M).$$

For the distribution of supermassive B3 necks,

$$\Phi_{\mathcal{N},\mathrm{out}} = \nu_{\mathcal{N}} \kappa_{\mathrm{B3}} \int f_{\mathrm{occ}}(M,t) M^2 \frac{dn}{dM} dM.$$

Then the governing equation of expansion takes the form

$$\frac{dN}{dt} = \Phi_{\mathcal{N},\mathrm{in}}^{\mathrm{parent}}(t) - \nu_{\mathcal{N}} \kappa_{\mathrm{B3}} \int f_{\mathrm{occ}}(M,t) M^2 \frac{dn}{dM} dM + \Phi_{\mathcal{N},\mathrm{noise}}(t),$$

where a minimal parent-gate model may set $\Phi_{\mathcal{N},\mathrm{in}}^{\mathrm{parent}} = \nu_{\mathcal{N}} f_{\mathrm{parent}} \kappa_{\mathrm{B3}} M_{\mathrm{parent}}^2$. The observed Hubble parameter is

$$H(t) = \frac{1}{3N(t)} \frac{dN}{dt}.$$

This form preserves the original idea of Multiverse homeostasis while replacing the GR-horizon normalization by the B3 graph-gate normalization and keeping energy powers, phase-channel fluxes, and node fluxes dimensionally separated.

Appendix E.4.5. Cascade Dynamics of the Multiverse and Estimation of Lifetimes

Let $V_n(t)$ be the phase volume of the nth-generation universe. In the linear approximation, the cascade drain can be written as

$$\frac{dV_n}{dt} = \lambda_{\mathrm{drain}} V_{n-1} - \lambda_{\mathrm{drain}} V_n,$$

where λ_{drain} has the dimension T^{-1} and is equal to the node-drain flux normalized by volume:

$$\lambda_{\mathrm{drain}} = \frac{\nu_{\mathcal{N}} \kappa_{\mathrm{B3}} \sum f_{\mathrm{occ}}(M_{\mathrm{SMBH}},t) M_{\mathrm{SMBH}}^2}{V_n}.$$

© 2026 by the author(s). Distributed under a Creative Commons CC BY license.

Preprints.org (www.preprints.org) | NOT PEER-REVIEWED | Posted: 9 June 2026 doi:10.20944/preprints202606.0589.v1

The solution takes the form of the Erlang distribution:

$$V_n(t) = V_0 \frac{(\lambda_{\text{drain}} t)^n}{n!} e^{-\lambda_{\text{drain}} t}.$$

The estimate of the lifetime $\tau_{\text{life}} \sim \lambda_{\text{drain}}^{-1} \approx 10^{33}$ years remains valid as an order of magnitude, but its numerical value depends on the observed black hole mass function and on the chosen normalization of V_n.

Appendix E.4.6. Topological Dissociation and the Death of the Universe

After inflation, the basis matrix continues to add empty nodes by inertia through the IKT dark-energy component $\Lambda^{\text{IKT}}_{\text{DE,time}}$, rather than through the total expansion scalar $3H^2$. As the universe expands, the average connectivity $\langle k \rangle$ decreases. If it falls below the percolation threshold (for random networks, $k = 1$), the giant connectivity component breaks down. Algorithmic tension within the particle breaks it into trivial nodes. The universe mathematically fades away, turning into algorithmic nothingness ($A_{ij} = 0$). The cosmological cycle is complete.

Appendix F. IKT Audit

Appendix F.1. Audit of Parameters, Dependencies, and Closure Status

Appendix F.1.1. Dimensionless IKT Core

The fundamental normalization is chosen as

$$\boxed{c_{\text{graph}} = 1, \qquad \hbar_{\text{graph}} = 1, \qquad m_e^{\text{graph}} = 1}.$$

Here, $c_{\text{graph}} = 1$ denotes one local causal step per layer, $\hbar_{\text{graph}} = 1$ means that the action is a phase, and $m_e^{\text{graph}} = 1$ fixes the electron as the minimal stable fermionic scale of mass ratios. A full phase cycle has

$$h_{\text{graph}} = 2\pi.$$

It is in this form that the IKT formulas are predictive:

$$\alpha_{\text{top}}^{-1} = 4\pi^3 + \pi^2 + \pi, \qquad \alpha_{s,\text{top}} = \frac{1}{\pi},$$

$$\frac{m_p}{m_e} = 6\pi^5 \rho_p, \qquad \frac{m_n - m_p}{m_e} = \ln(4\pi) + \frac{\delta_{np}^{\text{IR}}}{m_e},$$

$$\frac{m_\mu}{m_e} = 6^3(1 - 6\alpha_{\text{top}}), \qquad \frac{Q_\beta}{m_e} = \ln(4\pi) - 1 + \frac{\delta_{np}^{\text{IR}}}{m_e}.$$

These expressions do not require meters, seconds, or kilograms.

Appendix F.1.2. Dimensional Projection into Laboratory Units

To connect with the observer's instruments, three conversion anchors must be chosen:

$$c_{\text{graph}} = 1 \mapsto c_0, \qquad \hbar_{\text{graph}} = 1 \mapsto \hbar, \qquad m_e^{\text{graph}} = 1 \mapsto m_e.$$

Here, $c_{\text{graph}} = 1$ is the dimensionless normalization of local causal reachability, and c_0 is its physically observable SI projection, which in a weak-field vacuum coincides with the speed of the coherent massless branch. Similarly, $\hbar_{\text{graph}} = 1$ means that the action in microdynamics is a phase; the dimensional $\hbar$ translates the phase angle into a laboratory action, and a full cycle has $h_{\text{graph}} = 2\pi$.

© 2026 by the author(s). Distributed under a Creative Commons CC BY license.

Preprints.org (www.preprints.org) | NOT PEER-REVIEWED | Posted: 9 June 2026 doi:10.20944/preprints202606.0589.v1

Therefore, neither c_0 nor $\hbar$ are declared fictitious: they are projection anchors, not independent ontological parameters of the graph. From this follow the electronic units of length, time, and energy:

$$\lambda_e = \frac{\hbar}{m_e c_0}, \qquad \tau_e = \frac{\hbar}{m_e c_0^2}, \qquad E_e = m_e c_0^2.$$

The microscopic UV resolution of the graph is given by the dimensionless number

$$\boxed{\epsilon_0 = \frac{l_0}{\lambda_e} = \frac{\tau_0}{\tau_e}}.$$

Therefore,

$$l_0 = \epsilon_0 \frac{\hbar}{m_e c_0}, \qquad \tau_0 = \epsilon_0 \frac{\hbar}{m_e c_0^2}, \qquad \frac{l_0}{\tau_0} = c_0.$$

In this notation, l_0 and τ_0 are not two independent universal constants. These are the dimensional shadows of a single dimensionless UV resolution ϵ_0. The bare step of graph adjacency differs from the metric step:

$$a_0 = \frac{l_0}{\sqrt{\lambda_{\text{wave}}}}, \qquad c_* = \frac{a_0}{\tau_0} = \frac{c_0}{\sqrt{\lambda_{\text{wave}}}}.$$

Physical metrics and the PPN limit use c_0 and l_0, whereas the exact bare-dispersion of the finite difference is more conveniently written in terms of a_0.

Planck scales as a consequence of gravitational matching

Planck scales in this formulation are not postulated as fundamental quanta of space and time. Following an independent topological derivation or empirical matching of the value of G, they arise as SI projections of the same dimensionless UV resolution:

$$\tau_0 = \epsilon_0 \tau_e, \qquad l_0 = \epsilon_0 \lambda_e.$$

If the gravitational normalization is written as

$$\epsilon_0^2 = \alpha_G^{(e)} = \frac{G m_e^2}{\hbar c_0},$$

then these same formulas take on the familiar Planckian form

$$\tau_0 = \sqrt{\frac{\hbar G}{c_0^5}}, \qquad l_0 = \sqrt{\frac{\hbar G}{c_0^3}}, \qquad M_0 = \sqrt{\frac{\hbar c_0}{G}}.$$

Therefore, the Planck length, time, and mass are not primary axioms, but rather the result of a chosen dimensional projection following the fixing of the dimensionless gravitational coupling.

Appendix F.1.3. Parameter Classes After Dimensionless Formulation

After transitioning to the dimensionless form, it is convenient to distinguish four classes of quantities:

1. **Topological dimensionless anchors:** α_{top}, $\alpha_{s,\text{top}}$, m_p/m_e, $(m_n - m_p)/m_e$, m_μ/m_e.
2. **Projection coefficients:** c_0, $\hbar$, m_e, ε_0 in the SI normalization of charge.
3. **Configurational gravitational normalization:** $N_e^{\text{top}} = |\Omega_e|_{\text{eff}}$, $\epsilon_0 = 1/|\Omega_e|_{\text{eff}}$, and $\alpha_G^{(e)} = 1/|\Omega_e|_{\text{eff}}^2$. They relate the volume of the electron path to the observed gravity, and the discrete-topological derivation program reduces $|\Omega_e|_{\text{eff}}$ to the counting of 4π-equipped stochastic graph paths.
4. **Coarse-graining dynamic functions:** polarization, cosmological, and sector functions, for example

$$\Pi_{\text{IKT}}, \quad \Pi_{\text{IKT}}^{\text{col}}, \quad \lambda_{\text{noise}}^{\text{valve}}, \quad \lambda_{\text{valve}}, \quad \hat{\sigma}_{\text{col}}, \quad f_{4_1}, \quad \lambda_K.$$

© 2026 by the author(s). Distributed under a Creative Commons CC BY license.

Preprints.org (www.preprints.org) | NOT PEER-REVIEWED | Posted: 9 June 2026 doi:10.20944/preprints202606.0589.v1

This division does not artificially reduce the number of open problems, but makes their physical status transparent: IKT must derive dimensionless relations, and dimensional quantities are projections of these relations onto selected laboratory standards.

Appendix F.1.4. Global Dependency Matrix and Status of Results

Due to the wide range of IKT—from local micro-operators to cosmological growth—it is important to explicitly distinguish proven consequences from conditional interfaces, matching layers, and roadmap hypotheses. A working map of result dependencies is provided below.

Dependency	**Result**	**Status**
Background independence, local causality, $\mathcal{H}_m^{\mathrm{edge}}$, $U_m^{(0)} = S_m C_m$	Local unitary routing on a stochastic graph	derived from postulates
$d_H = d_s = 3$, statistical isotropy, prethermal ballistic condition, $\epsilon_{\mathrm{pt}} \ll 1$	Weyl/wave IR-envelope	conditionally derived
$U(1)$-link covariance, Ward identity	Covariant current j^μ and electromagnetic TTC vertex	conditionally derived
Information channel measure, admissibility of strata, spectral equipartition $\rho_s = 1$	$\alpha_{\mathrm{top}}^{-1} = 4\pi^3 + \pi^2 + \pi$	conditional no-fit channel anchor
Closed route K, W_K^{eff}, Θ_K	Mass M_K as Floquet/monodromy gap	conditional derived
K_e, Θ_e, $\lvert\Omega_e\rvert_{\mathrm{eff}}$	$G_{\mathrm{IKT}} = \hbar c_0/(m_e^2 \lvert\Omega_e\rvert_{\mathrm{eff}}^2)$	reduction; prediction after enumeration
M_K-action, universal throughput $d\tau = e^{-\chi_G} dt$	Weak form of the equivalence principle	conditional derived
$SU(3)_{\mathrm{route}}$ hypothesis, singlet-routing constraint	color current and confinement interface	conditional interface
Ξ_{vac}, singlet-routing constraint	shielding of cosmological chirality in strong singlets	conditional protection lemma
$\Xi_{\mathrm{vac}} \neq 0$ from cosmological chiral percolation	P_L weak gateway / P-violation	conditional interface
χ_G plus reciprocal impedance	PPN $\beta = 1$, $\gamma = 1$ weak-field metric interface	conditional derived
Scalar capacity fluctuation, F_h^{obs}	Observed 125 GeV scalar-channel matching	observational matching
$\chi_{\mathrm{vort}}^{\mathrm{prim}}$, $\chi_{\mathrm{vort}}^{\mathrm{gal}}$	Dark-sector lensing/dynamics interface	phenomenological test layer
$A_4 = \eta_4 - \lambda_{\mathrm{wave}}/12$, vortex fluid matching	Coldness of the primary vortex component	conditional fluid-interface matching
$\mathcal{I}_m$ plus $\mathrm{Tr}_{\mathrm{hidden}}$	Reduced arrow of time	conditional derived
$\mathcal{I}_m$, Cheeger bottleneck, neck decoherence	Black-hole drainage / daughter-sector factorization	speculative extension
Graph-growth cascade, external phase-flow balance	Multiverse/homeostasis	speculative extension

Throughout the text, the terms "strict conclusion," "follows," and "predicts" should be understood in accordance with this table. If a result depends on a specific boundary condition or a spectral invariant that has not yet been computed, it is not considered a complete microdynamic conclusion, but rather defines a verifiable mathematical problem.

Appendix F.1.5. What Is Not Considered a Final Result of This Work

For correct scientific communication, it is important to explicitly indicate which elements of IKT in this version are unfinished results and which are programs for further calculation:

- the complete derivation of $SU(3)_{\mathrm{route}}$ as the unique automorphism group of color routing;
- the complete graph β-function of the strong sector and the derivation of running-$\alpha_s(Q^2)$;

© 2026 by the author(s). Distributed under a Creative Commons CC BY license.

Preprints.org (www.preprints.org) | NOT PEER-REVIEWED | Posted: 9 June 2026 doi:10.20944/preprints202606.0589.v1

- the derivation of CKM/PMNS, hypercharges, and electroweak mixing from the topology of the weak gateway;
- independent calculation of M_{K_e}, Γ_e, and Ξ_e, necessary for a complete prediction of G_{IKT};
- spectral derivation of the observed 125 GeV scalar channel;
- a full CMB/LSS/BAO/SN fit for dark energy and the primary vortex dark sector;
- a quantitative verification of the Bullet-like lensing-forward model;
- a rigorous derivation of the equality of spectral weights $\rho_s = 1$ in the formula α_{top};
- complete TTC benchmarks beyond minimal EM/weak examples;
- homeostatic and migration scenarios for the multiverse, which have the status of speculative cosmological extensions.

These open issues are not hidden parameters of the main micro-operator; they define a testable program for further spectral, automorphism, and observational calculations.

Appendix G. Supplement: Summary of IKT Fundamental Equations

Below is a matrix of the mathematical architecture of IKT, demonstrating the connection between microdynamics and phenomenology. Table A1 provides a summary of the basic equations and invariants, documenting the transition from a discrete graph to a continuum.

Table A1. Summary of Basic Equations and Invariants of Information-Kinetic Theory.

No.	Formula	Role	What it shows
1	$G_m = (V_m, E_m)$	Core	dynamic causal graph instead of the primary continuum
2	$\mathcal{H}_m^{\mathrm{edge}} = \ell^2(\vec{E}_m) \otimes \mathbb{C}^2_{\mathrm{spin}}$	Core	fundamental space of the local U_m
3	$U_{\mathrm{cyc}} \simeq e^{-iH_{\mathrm{pre}}T_{\mathrm{cyc}}/\hbar}$	Core	prethermal coherent vacuum branch
4	$i\hbar\partial_t\psi = -i\hbar c_0 \vec{\sigma}\cdot\nabla\psi$	Core	Weyl/wave sector as an infrared envelope
5	$\omega^2 = c_0^2k^2 - c_0^2a_0^2A_4k^4 + \cdots$	Prediction	isotropic DSR correction to massless dispersion
6	$M_K c_0^2 = \hbar\lvert\Theta_K\rvert/T_K$	Anchor	mass as the monodromic phase gap of the route
7	$\alpha_{\mathrm{ch}}^{-1} = \sum_s \rho_s\mu_s \to_{\rho_s=1} 4\pi^3 + \pi^2 + \pi$	Anchor	α_{top} as a channel no-fit anchor
8	$n_e^{(0)} = 2\dim_{\mathbb{R}}(S^2_{\mathrm{dir}} \times S^2_{\mathrm{spin}} \times S^1_{\mathrm{hol}}) = 10$	Anchor	the factorized parameter-rank of the electron path
9	$(m_p/m_e)_{\mathrm{top}} \simeq 6\pi^5$	Anchor	leading proton spectral-channel anchor
10	$m_n - m_p \simeq m_e \ln(4\pi)$	Anchor	logarithmic work of the internal $U(1)$ compactification
11	$G_{\mathrm{IKT}} = \dfrac{\hbar c_0}{M_{K_e}^2(\Gamma_e\mathcal{N}_\alpha^{10}\Xi_e)^2}$	Anchor	reduction of G to K_e, Γ_e, Ξ_e, and α_{top}
12	$j^\mu = \bar{\Psi}\gamma^\mu\Psi$	Interface	electromagnetic current from the $U(1)$-link phase
13	$Q_A^{\mathrm{col}}\lvert\Psi_{\mathrm{phys}}\rangle = 0$	Interface	color singlet constraint and confinement selection
14	$P_\Xi = \frac{1}{2}(1 - s_\Xi\gamma^5)$	Interface	chiral weak-gateway from Ξ_{vac}
15	$ds^2 = -e^{-2\chi_G}c_0^2dt^2 + e^{2\chi_G}d\mathbf{R}^2$	Interface	gravity as phase refraction
16	$\chi_{\mathrm{lens}} = \chi_G + \chi_{\mathrm{vort}}^{\mathrm{prim}} + \chi_{\mathrm{vort}}^{\mathrm{gal}}$	Prediction	total dark-sector lensing potential
17	$v_f^4 = GM_{\mathrm{bar}}a_{\mathrm{vort}}$	Prediction	BTFR hook of the vortex waveguide
18	$\Lambda^{\mathrm{IKT}}_{\mathrm{DE},time} = \Lambda_{\mathrm{par},time} + \Lambda^{\mathrm{valve}}_{\mathrm{noise},time}$	Prediction	IKT dark-energy component only; it is compared with the residual obtained after subtracting matter, radiation, neutrinos, the vortex/dark-matter sector, curvature, and corrections from $3H^2$.
19	$\mathcal{M}^{\mathrm{TTC}}_{\beta\alpha} = \sum_{\mathfrak{C}} \mathcal{A}[\mathfrak{C}]$	TTC	amplitude as a sum over graph cobordisms

$$\Lambda^{\mathrm{valve}}_{\mathrm{noise,time}}(t) = \frac{1}{\tau_0^2}\frac{\lambda_{\max}}{d_0^2 + (t/\tau_0)^2}, \qquad d_0^2 = \frac{\lambda_{\max}}{\lambda_{\mathrm{valve}}} = \frac{\lambda_{\max}}{\tau_0^2\Lambda_{\mathrm{valve}}}.$$

The equations above illustrate the fundamental conceptual basis of IKT. Rigorous mathematical derivations, proofs of lemmas, conditions of applicability, and methods for calculating residual polarization corrections are presented in detail in the relevant sections of the appendices.

© 2026 by the author(s). Distributed under a Creative Commons CC BY license.

Preprints.org (www.preprints.org) | NOT PEER-REVIEWED | Posted: 9 June 2026 doi:10.20944/preprints202606.0589.v1

Appendix H. Supplement: Glossary of Symbols

The main notation used in the article is listed below. The glossary establishes the current IKT formalism following the transition from a single transition matrix to the graph-based quantum walk operator U_m, the classical probability matrix W_{ij}^{cl}, and the separate delay fields p_j, χ_G, and χ_{vort}. For dark matter, a distinction is additionally made between the primary pre-galactic component $\chi_{\mathrm{vort}}^{\mathrm{prim}}$ and the late galactic component $\chi_{\mathrm{vort}}^{\mathrm{gal}}$.

Symbol	Short explanation	Comment / area of application
1. Graph Kinematics and Discrete Updates		
m	Discrete update index / causal layer	Not a set; used in G_m, U_m, ψ_m, N_m.
G_m	Basic directed graph at step m	Fundamental IKT object: $G_m = (V_m, E_m, A_m)$.
V_m	Set of vertices of graph G_m	Nodes / topological dipoles at step m; the insertion isometry is now denoted by $\mathcal{I}_m$.
$\mathcal{H}_m^{\mathrm{edge}}$	Fundamental Hilbert space of micro-dynamics	$\ell^2(\vec{E}_m) \otimes \mathbb{C}^2_{\mathrm{spin}}$; it is precisely on this space that the minimal U_m acts unitarily.
$\mathcal{H}_m^{\mathrm{vert}}$	Node infrared envelope	$\ell^2(V_m) \otimes \mathbb{C}^2_{\mathrm{env}}$; obtained from $\mathcal{H}_m^{\mathrm{edge}}$ via $\mathcal{P}_{\mathrm{vert}}$.
$\mathcal{H}_K^{\mathrm{eff}}$	Effective particle/cycle space	$\mathcal{H}_K^{\mathrm{chir}} \otimes \mathbb{C}^2_{\mathrm{spin}}$; Floquet/homogenized sector of the closed path K.
$\mathcal{I}_m$, $\mathcal{I}_{m,a}$	Isometry and Kraus components of insertion	$\mathcal{I}_m : \mathcal{H}_m \to \mathcal{H}_{m+1}$; the stochastic insertion is given by the CP channel $\rho_{m+1} = \sum_a \mathcal{I}_{m,a} \rho_m \mathcal{I}_{m,a}^\dagger$.
E_m	Set of directed edges of the graph	Defines the oriented connectivity between dipoles.
A_m, A_{ij}	Adjacency matrix and its element	Describes the presence / weight of the connection $j \to i$ at the graph level. Not to be confused with the electromagnetic potential $\mathbf{A}$.
i, j	Vertex indices	Are not coordinates in the space prior to effective embedding.
$j \sim i$	Adjacency in the graph	Indicates the presence of a local connection, not metric proximity in a predefined space.
$d_G(i, j)$	Graph metric	The minimum number of edges between vertices i and j.
ι_m	Effective embedding of the graph	A mapping $\iota_m : V_m \to M_{\mathrm{eff}}$, after which coordinates appear.
M_{eff}	Effective manifold	The macroscopic space that emerges after coarse-graining.
$\mathbf{r}_i$, $\mathbf{r}$, $\mathbf{r}'$	Emergent coordinates	Used only in the continuous / large-scale limit.
$d^3\mathbf{r}$	Volume element	Appears only after transitioning to the effective three-dimensional description.
c_{graph}	Dimensionless causal limit of the graph	In natural graph units, $c_{\mathrm{graph}} = 1$: no more than one local edge is available per causal layer.

© 2026 by the author(s). Distributed under a Creative Commons CC BY license.

Preprints.org (www.preprints.org) | NOT PEER-REVIEWED | Posted: 9 June 2026 doi:10.20944/preprints202606.0589.v1

Symbol	Short explanation	Comment / area of application
c_0	SI projection of the causal cone	Observed speed of light in a weak-field vacuum; not derived as a ratio of independent entities, but defines a dimensional projection $c_{\text{graph}} = 1 \mapsto c_0$.
c	Observed speed of light	In the low-energy limit, it is identified with c_0.
a_0	Bare step of graph adjacency	The length of a single local edge prior to metric calibration of the massless branch; $c_* = a_0/\tau_0$ is not the observed speed of light.
l_0	Metric UV step of the graph	$l_0 = \epsilon_0 \lambda_e = c_0 \tau_0 = \sqrt{\lambda_{\text{wave}} a_0}$; used in the physical coordinate projection.
τ_0	Metric cycle of the graph	$\tau_0 = \epsilon_0 \tau_e$, where $\tau_e = \hbar/(m_e c_0^2)$; dimensional shadow of the dimensionless UV resolution ϵ_0.
ϵ_0	Dimensionless UV resolution of the graph	$\epsilon_0 = l_0/\lambda_e = \tau_0/\tau_e = 1/N_e^{\text{top}} = 1/\lvert\Omega_e\rvert_{\text{eff}}$; the dimensional shadow of the configuration sparsity of the electronic path.
$\alpha_G^{(e)}$	Electronic gravitational coupling	$\alpha_G^{(e)} = G m_e^2/(\hbar c_0) = 1/\lvert\Omega_e\rvert_{\text{eff}}^2$; dimensionless form of gravitational normalization.
N_e^{top}	Configuration index of the electronic path	$N_e^{\text{top}} = \lvert\Omega_e\rvert_{\text{eff}}$; volume of participation of the minimal electronic 4π-spinor path.
Ω_e	Configuration space of the electronic route	Class of microroutes preserving the macroscopic topology of the electronic 4π-spinor frame.
$\lvert\Omega_e\rvert_{\text{eff}}$	Effective size of the electronic configuration space	Volume of participation: $\lvert\Omega_e\rvert_{\text{eff}} = 1/\sum_\omega \lvert a_\omega\rvert^4$; determines N_e^{top}.
$\mathcal{N}_\alpha$	Phase volume of a single electromagnetic routing channel	$\mathcal{N}_\alpha = \alpha_{\text{top}}^{-1} = 4\pi^3 + \pi^2 + \pi$; a channel measure of phase strata, not a literal integer number of states.
$n_e^{(0)}$	Factorized parameter-rank of the electronic 4π-path	The conditional result $n_e^{(0)} = 10$ follows from $S^2_{\text{dir}} \times S^2_{\text{spin}} \times S^1_{\text{hol}}$ and the Dirac/Floquet doubling; the complete prediction of G requires M_{K_e}, Γ_e, Ξ_e, and verification of equal channel normalization.
Γ_e	Frame factor of the electron path	Final factor of Möbius closure and embedding constraints: $N_e^{\text{top}} = \Gamma_e \mathcal{N}_\alpha^{n_e^{(0)}} \Xi_e$.
$\text{SAC}_N(\mathfrak{G}_{\text{vac}})$	Self-avoiding closed paths of length N	Graph-invariant closed paths on the vacuum stochastic ensemble; replace the cubic proxy $\text{SAP}_N(\mathbb{Z}^3)$ in the program for checking $n_e^{(0)}$ and computing Γ_e, Ξ_e.
ν	Discrete path equipment	Non-degenerate transverse frame of a lattice polygon; allows one to determine the band and the linking number $Lk(p, p+\nu)$.

© 2026 by the author(s). Distributed under a Creative Commons CC BY license.

Preprints.org (www.preprints.org) | NOT PEER-REVIEWED | Posted: 9 June 2026 doi:10.20944/preprints202606.0589.v1

Symbol	Short explanation	Comment / area of application
$\mathcal{F}_N^{4\pi}$	Set of 4π-equipped electronic routes	Classes (G,p,ν) with $G \sim \mathfrak{G}_{\mathrm{vac}}$, $p \in \mathrm{SAC}_N(G)$, and $Lk_G(p,p+\nu) = \pm 2$; a key object in the graph-topological program for deriving G.
G_{sym}	The symmetry group of equipped paths	The group of lattice, cyclic, and orientation equivalences; used in Burnside's formula for the exact calculation of Γ_e.
$\mathrm{Aut}(G,p,\nu)$	Automorphisms of an equipped path	Graph-internal group of path stabilizers; replaces the cubic group O_h in the symmetry normalization.
$\mathcal{S}_e$	Topological sparsity of the electron	$\mathcal{S}_e = 1/\lvert\Omega_e\rvert_{\mathrm{eff}}$; the average hardware share of the electron path and its gravitational charge in hardware units.
$\eta_e(v,m)$	Local apparatus fraction of the electron path	The fraction of the bandwidth of the saturated node v in layer m available to the gravitational sector; $\langle \eta_e \rangle = \mathcal{S}_e$.
$\mathcal{M}_0$	Hardware saturated mass in electron units	$\mathcal{M}_0 = M_0/m_e = N_e^{\mathrm{top}} = \lvert\Omega_e\rvert_{\mathrm{eff}}$.
ζ_G	Normalization of the hardware gravitational source	Dimensionless coefficient of the measure of the hardware gravitational charge; the minimum IKT normalization sets $\zeta_G = 1$.
$\mathcal{H}_m^{\mathrm{vert}}$	Coarse-grained nodal envelope	$\ell^2(V_m) \otimes \mathbb{C}^2_{\mathrm{env}}$; interface fibers are added as $\mathcal{F}_{\mathrm{int}}$ on top of the fundamental edge space.
$\ell^2(V_m)$	Space of quadratically summable amplitudes at vertices	The nodal part of the Hilbert space.
q_{int}	Number of internal components in $\mathbb{C}^{q_{\mathrm{int}}}$	Dimension of the internal space; separated from the gauge charge q_{em}.
ψ_m	Microscopic state on the graph	State vector at step m.
Ψ	Smoothed / continuous field	Macroscopic representation of the graph amplitude after coarse-graining.
μ,ν,ρ	Internal component indices	In the component representation $\psi(i,\mu)$; not to be confused with the fine-structure parameters α and the PPN parameters β,γ.
U_m	Fundamental unitary operator of quantum walk	Defines the evolution on a fixed graph: $\psi_{m+1} = U_m \psi_m$.
$U_m(i,\mu;j,\nu)$	Matrix element of the operator U_m	Amplitude of the transition from (j,ν) to (i,μ).
S_m	Shift operator	Unitary permutation of oriented edges in a coined quantum walk.
C_m, C_j	Local "coin"	Unitary routing of internal channels; $C_m = \oplus_j C_j$.
$K(\mathbf{r},\mathbf{r}')$	Macroscopic coordinate kernel	Non-fundamental matrix; appears only after effective graph embedding.

© 2026 by the author(s). Distributed under a Creative Commons CC BY license.

Preprints.org (www.preprints.org) | NOT PEER-REVIEWED | Posted: 9 June 2026 doi:10.20944/preprints202606.0589.v1

Symbol	Short explanation	Comment / area of application
W_{ij}^{cl}	Classical transition probability matrix	Arises after loss of phase information; for uniform averaging of internal input channels $W_{ij}^{\mathrm{cl}} = q_{\mathrm{int}}^{-1} \sum_{\mu,\nu} \lvert U_m(i,\mu;j,\nu)\rvert^2$.
W_{ij}	Historical notation for transition weight	Not used as a fundamental operator in the formalism: the probability is written as W_{ij}^{cl}, the amplitude via U_m.
L_G	Dimensionless graph Laplacian	$(L_G\psi)_i = \sum_{j\sim i}(\psi_j - \psi_i)$; coordinate derivatives appear after the projection $K_a = k_a a_0$.
Ω, K_a	Dimensionless frequency and momentum	$\Omega = \omega\tau_0$, $K_a = k_a a_0$; natural variables of bare-lattice dispersion.
λ_{wave}	Symmetric wave update coefficient	In stochastic dispersion $\omega^2 = c_0^2 k^2 - c_0^2 a_0^2(\eta_4 - \lambda_{\mathrm{wave}}/12)k^4 + \cdots$; the normalization $c_0 = \sqrt{\lambda_{\mathrm{wave}}} a_0/\tau_0$ is fixed after coarse-graining.
ρ_m	Density matrix	Used in describing stochastic insertion as a quantum channel.
$\mathcal{I}_{m,a}$	Insertion channel operators	Kraus operators of stochastic insertion; do not mix with the vertex set V_m.
$\dim \mathcal{H}_m$	Dimension of the state space	Does not decrease upon insertion of nodes.
2. Phase, delay, probability, and operators		
E_j	Node energy in SI projection	Dimensionless energy $\varepsilon_j = E_j/(m_e c_0^2)$; phase delay $\theta_j = \varepsilon_j \epsilon_0$.
E_{loc}	Equivalent local energy	In dimensionless form $\Delta\phi_j = \epsilon_0 E_{\mathrm{loc}}/(m_e c_0^2)$.
E	Energy	Used in predictive formulas via the relation $\varepsilon = E/(m_e c_0^2)$.
E_{Pl}	Planck energy	Appears as an SI projection when $\epsilon_0 = 1/\lvert\Omega_e\rvert_{\mathrm{eff}}$ and $\alpha_G^{(e)} = 1/\lvert\Omega_e\rvert_{\mathrm{eff}}^2$, rather than as the graph's base unit.
M	Mass / mass scale	General symbol for mass; the relations M/m_e are fundamental.
M_0	Hardware saturated mass of the graph projection	$M_0 = m_e/\epsilon_0 = m_e N_e^{\mathrm{top}} = \hbar/(c_0^2\tau_0)$; SI projection of saturated 3D capacity.
M_K	Mass of the topological cycle K	$M_K = m_e \mathcal{M}(K)$; $\mathcal{M}(K)$ is the dimensionless topological mass.
ω_c	Compton frequency	In the dimensionless local mass phase: $\theta_{\mathrm{loc}} = \epsilon_0 M_{\mathrm{loc}}/m_e$.
ω	Angular frequency of the wave	Appears via $\Omega = \omega\tau_0$.
θ_j	Node phase delay	$\theta_j = \epsilon_0 E_j/(m_e c_0^2)$; is not a probability.
θ_{loc}	Local mass phase delay	$\theta_{\mathrm{loc}} = \epsilon_0(M_{\mathrm{loc}}/m_e) = M_{\mathrm{loc}}/M_0$; for a single compact cycle, it can be denoted by θ_M.
$\theta(s)$	Local phase delay density along the cycle	Integrates fundamentally over the number of graph steps; the coordinate form $\Theta_K = \oint_K \theta(s)dl/l_0$ is a projection.
θ_{ij}	Edge $U(1)$ phase	In the factor $U_{ij}^{(q_{\mathrm{em}})} = e^{iq_{\mathrm{em}}\theta_{ij}}$.

© 2026 by the author(s). Distributed under a Creative Commons CC BY license.

Preprints.org (www.preprints.org) | NOT PEER-REVIEWED | Posted: 9 June 2026 doi:10.20944/preprints202606.0589.v1

Symbol	Short explanation	Comment / area of application
θ_a	Longitudinal phase coordinates of proton confinement	$a = 1,2,3$, $\theta_a \in [0,\pi]$; delay phases of the three fermionic arcs.
η_b	Color holonomies of the singlet coupling	$b = 1,2$, $\eta_b \in [0,\pi]$; two neutral phases associated with rank $SU(3) = 2$.
Θ_K	Total delay of the topological cycle K	Integral phase cost of maintaining the knot.
Θ_e	Normalization of the electronic cycle	It is assumed that $\Theta_e \equiv 1$.
Θ_{knot}	Resonant delay of the W/Z gate	Integral of the dwell rate within the resonance.
p_j	Probability of delay / self-loop of the knot	$p_j = 1 - e^{-\theta_j}$, therefore $0 \leq p_j < 1$.
p_{stay}	Probability of local phase retention	$p_{\text{stay}}(v) = 1 - e^{-\theta_{\text{loc}}(v)}$; saturates at large local mass, not total macroscopic mass.
$p_G(r)$	Probability of delay associated with the gravitational potential	$p_G = 1 - e^{-\chi_G}$; distinct from the potential itself χ_G.
p_{trans}	Probability of unretarded translation	$p_{\text{trans}} = 1 - p_G = e^{-\chi_G}$; determines the rate of the local clock in a weak field.
p_{str}	Delay in the color tube	$p_{\text{str}}(\mathbf{A}) \simeq 1 - e^{-\kappa_{\text{str}}\lvert\mathbf{A}\rvert^2}$.
p_{res}	Probability of retention in a weak resonant gate	$p_{\text{res}} = 1 - e^{-\Theta_{\text{knot}}}$.
$p_{\text{threshold}}$	Empty knot threshold delay	In the inflationary exit, $p_{\text{threshold}} \equiv 0$ as $k \to 6$.
χ_G	Weak-field gravitational potential of IKT	Not a probability; normalized as $\chi_G = -\Phi_N/c_0^2 = GM/(c_0^2 r)$ for an isolated mass and enters $\mathbf{g} = c_0^2 \nabla \chi_G$.
χ_{vort}	Macroscopic vortical potential	Sum of the primary and galactic components: $\chi_{\text{vort}} = \chi_{\text{vort}}^{\text{prim}} + \chi_{\text{vort}}^{\text{gal}}$.
$\chi_{\text{vort}}^{\text{prim}}$	Primary vorticity potential	Pre-galactic cold refraction component responsible for the CMB/LSS.
$\chi_{\text{vort}}^{\text{gal}}$	Galactic vortex potential	Late waveguide component induced by the rotating baryonic disk.
$\chi_{\text{2D}}(r)$	Radial waveguide component of the vorticity potential	Gives a logarithmic profile in the disk plane.
χ_{leak}	Vertical leakage of the vorticity potential	A correction of order $O(\epsilon_z)$ to the quasi-two-dimensional regime.
χ_{algo}	Nonlinear topological response coefficient	In the modified speed $c_{\text{eff}} = c_0(1 - \chi_{\text{algo}}\lvert\mathbf{\Omega}\rvert^2)$.
χ_i, χ	Local calibration phase	In the transformation $A_\mu \to A_\mu + \partial_\mu \chi$; not to be confused with χ_G and $\hat{\chi}$.
$\hat{\chi}$	Chirality / helicity operator	$\hat{\chi} = \vec{\sigma} \cdot \vec{n}$.
$\Delta\phi_j$	Elementary phase shift at a node	$\Delta\phi_j = \delta S/\hbar = E_{\text{loc}}\tau_0/\hbar$.
δS	Local algorithmic action quantum	Cost of a single translation step.

© 2026 by the author(s). Distributed under a Creative Commons CC BY license.

Preprints.org (www.preprints.org) | NOT PEER-REVIEWED | Posted: 9 June 2026 doi:10.20944/preprints202606.0589.v1

Symbol	Short explanation	Comment / area of application
$\hbar_{\text{graph}}, h_{\text{graph}}$	Dimensionless phase normalization of the graph	$\hbar_{\text{graph}} = 1$, $h_{\text{graph}} = 2\pi$; the laboratory $\hbar$ is the SI projection of this phase unit.
ρ_{obs}	Reduced density matrix of the local observer	$\rho_{\text{obs}} = \text{Tr}_{\text{hidden}} \lvert\Psi\rangle\langle\Psi\rvert$; the local arrow of time is related to the trace of the hidden graph degrees of freedom.
$\mathcal{H}_K^{\text{eff}}$	Effective space of a stable closed path	$\mathcal{H}_K^{\text{chir}} \otimes \mathbb{C}^2_{\text{spin}}$; Floquet/homogenized particle sector.
$[E_{12}]$	Class of exchange paths of two identical fermionic cycles	Under the FR condition $\rho([E_{12}]) = -1$; defines the exchange antisymmetry of 4π-cycles.
$A^{(m)}_{j\sigma\to a\sigma'}$	Amplitude of the isometric insertion	In $\mathcal{I}_m\lvert j,\sigma\rangle = \sum_{a,\sigma'} A^{(m)}_{j\sigma\to a\sigma'} \lvert j,\sigma\rangle\lvert a,\sigma'\rangle$; a rank greater than one generates entanglement between the old and new sectors.
$\phi_i, \langle\phi\rangle$	Node phase and average phase density	Used in explaining the redshift upon insertion.
$\phi_C(t_{\text{birth}})$	Initial phase of the new vacuum node	Normalized as $\phi_C(t_{\text{birth}}) = 0$.
$\rho_N, \overline{\rho_N}$	Probability density and smoothed density after N steps	The Gaussian envelope refers to $\overline{\rho_N}$, not to the fundamental amplitude.
σ_N	Width of the smoothed envelope after N steps	In bare-graph coordinates, diffusively $\sigma_N^2 \sim Na_0^2$, ballistically $\sigma_N \sim Na_0$; metrically $l_0 = \sqrt{\lambda_{\text{wave}}}a_0$.
$\nabla^2, \sum_a \partial_a^4$	Laplacian and first-order grid correction	Arise in the continuous expansion of the graph Laplacian; the notation ∇^4 is valid only after isotropic averaging.
$\Box$	D'Alembert wave operator	$\Box = \nabla^2 - c_0^{-2}\partial_t^2$ in the adopted notation.
$P_{ab}(\vec{n})$	Transverse projector	$P_{ab} = \delta_{ab} - n_a n_b$.
$\mathbf{P}^{(\text{grav})}_{ijkl}$	Gravitational TT projector	Leaves two transverse trace-free modes.
$\delta\mathbf{\Gamma}_{ij}$	Tensor fluctuation of the density of states	Gravitational analogue of h_{ij} in graph language.
Γ_0	Total computational power of the vacuum	Preserved under free TT transport.
$\vec{n}_{ij}, \vec{n}$	Internal orientation of a directed edge	Not necessarily a coordinate vector prior to coarse-graining.
$\sigma_x, \sigma_y, \sigma_z$	Pauli matrices	Used in the chiral operator and the spinor phase factor.
$\mathcal{Q}_{\text{F}}$	Single-particle configuration space of a fermionic loop	Space of positions, frames, and topological labels of a Möbius-like fermionic path.
$\mathcal{Q}_{\text{F}}^{(2)}$	Configuration space of two identical fermionic cycles	$\mathcal{Q}_{\text{F}}^{(2)} = ((\mathcal{Q}_{\text{F}} \times \mathcal{Q}_{\text{F}}) \setminus \Delta)/S_2$; used in the FR condition for the exchange phase.
Δ	Diagonal of coincident complete states	Excluded when constructing the configuration space of identical fermionic cycles.
$E_{12}, R(2\pi)$	Exchange loop and local 2π-rotation of the frame	In the Finkelstein–Rubinstein condition, $[E_{12}] = [R(2\pi)]$.

© 2026 by the author(s). Distributed under a Creative Commons CC BY license.

Preprints.org (www.preprints.org) | NOT PEER-REVIEWED | Posted: 9 June 2026 doi:10.20944/preprints202606.0589.v1

Symbol	Short explanation	Comment / area of application
$\rho([\cdot])$	One-dimensional representation of the loop class	For a fermionic loop, $\rho([R(2\pi)]) = -1$, $\rho([R(4\pi)]) = +1$.
3. Electromagnetism and gauge notations		
$\mathbf{A}(\mathbf{r}, t)$	Smoothed vector potential / transverse component of the graph state	Electromagnetic macrolimit; not to be confused with the adjacency matrix A_m.
A_μ	Four-potential	Appears in the continuous representation of the loop phase.
$U_{ij}^{(q_{\text{em}})}$	$U(1)$-phase factor on an edge	$U_{ij}^{(q_{\text{em}})} = e^{iq_{\text{em}}\theta_{ij}}$.
$W(\mathcal{C}_{\text{loop}})$	Loop phase / Wilson loop	$W(\mathcal{C}_{\text{loop}}) = \prod_{(ij)\in\mathcal{C}_{\text{loop}}} U_{ij}^{(q_{\text{em}})}$.
$\mathcal{C}_{\text{loop}}$	Closed loop in $W(\mathcal{C}_{\text{loop}})$	Loop phase; not to be confused with the topological complexity C_K.
q_{em}	Calibration charge / phase coefficient	In $e^{iq_{\text{em}}\theta_{ij}}$; distinct from the dimension q_{int}. The minimum value of the channel is given by g_{em}.
g_{em}	Dimensionless minimum electromagnetic channel	$g_{\text{em}}^2 = 4\pi\alpha_{\text{top}}$; fundamental dimensionless $U(1)$ connection of IKT.
e, e_{top}	Elementary electric charge	Not an independent IKT parameter; in SI notation $e_{\text{top}} = \sqrt{4\pi\varepsilon_0\hbar c_0\alpha_{\text{top}}}$.
$e_{\text{eff}}(\mathcal{Q}^2)$	Effective running charge	$e_{\text{eff}} = \sqrt{4\pi\varepsilon_0\hbar c_0\alpha_{\text{eff}}(\mathcal{Q}^2)}$.
ε_0	Dielectric permittivity of vacuum in SI	Macroscopic electromagnetic normalization coefficient, converting the dimensionless coupling g_{em} into coulombs; is not a microscopic axiom of QCD.
q_e, q_m	Electric and magnetic charges	Used in the Dirac quantization condition; the minimum electric charge corresponds to e_{top}.
Q	Total electric charge of an object	Defined by the Hermitian integral of the edge phase current through a closed boundary; this current is obtained from the anti-Hermitian part of the complex kernel.
$\mathbf{B}$	Magnetic induction	In the magnetic flux integral of a monopole.
$d\mathbf{S}$	Element of an oriented surface	In the flux $\oint \mathbf{B}\cdot d\mathbf{S}$.
n	Topological integer of a monopole	In the Dirac condition $q_e q_m/(2\pi\hbar c_0) \in \mathbb{Z}$ in the Heaviside–Lorentz normalization; not to be confused with the generation n in the multiverse.
k	Wavenumber	In the dispersion relation; also used as the mean connectivity in cosmology.
v_{phase}	Phase velocity	$v_{\text{phase}} = \omega/k$.
μ_0	Electromagnetic coefficient in the summary notation	In the equation $\Box\mathbf{A} = \mu_0\mathbf{J}_{\text{phase}}$.
$\mathbf{J}_{\text{phase}}$	Phase current	Source of the electromagnetic macrofield in the summary table.
4. Gravity, Metrics, and Orbital Parameters		

© 2026 by the author(s). Distributed under a Creative Commons CC BY license.

Preprints.org (www.preprints.org) | NOT PEER-REVIEWED | Posted: 9 June 2026 doi:10.20944/preprints202606.0589.v1

Symbol	Short explanation	Comment / area of application
G	Newtonian gravitational constant	SI projection of the configuration volume of the electron path: $G = \hbar c_0/[m_e^2 \lvert\Omega_e\rvert_{\mathrm{eff}}^2]$.
G_{eff}	Effective weak-field matching coefficient	Appears in the transition from the graph Poisson equation to the Newtonian form.
κ_G	Graph coefficient of the Poisson equation	In $\Delta_G \chi_G = -\kappa_G \rho_\theta$ under the convention $\chi_G = -\Phi_N/c_0^2$.
Δ_G	Graph Poisson operator / Laplacian	In the gravitational section; similar in meaning to L_G.
ρ_θ	Phase delay density	Source of the graph equation for χ_G.
ρ	Mass density	In the continuum equation $\nabla^2 \chi_G = -(4\pi G_{\mathrm{eff}}/c_0^2)\rho$ under the convention $\chi_G = -\Phi_N/c_0^2$.
$\mathbf{g}$	Acceleration	$\mathbf{g} = c_0^2 \nabla(\chi_G + \chi_{\mathrm{vort}})$ under the convention $\chi = -\Phi/c_0^2$.
$n_{\mathrm{eff}}(\mathbf{r})$	Effective refractive index of vacuum	$n_{\mathrm{eff}} = e^{2\chi_G} = 1 + 2\chi_G + \mathcal{O}(\chi_G^2)$ in the PPN limit.
v_{eff}	Effective propagation velocity in the potential	$v_{\mathrm{eff}} = c_0/n_{\mathrm{eff}}(\mathbf{r})$.
Φ_N	The standard Newtonian potential	For an attracting mass, $\Phi_N = -GM/r$, and $\chi_G = -\Phi_N/c_0^2 > 0$; does not mix with the quantum walk operator U_m.
ds^2	Effective metric interval	In the PPN limit, $ds^2 = -e^{-2\chi_G} c_0^2 dt^2 + e^{2\chi_G} d\mathbf{r}^2$.
g_{00}	Time component of the effective metric	$g_{00} = -e^{-2\chi_G} = -1 + 2\chi_G - 2\chi_G^2 + \cdots$.
γ, β	Post-Newtonian parameters	In IKT, $\beta = 1$ follows from the exponential delay of local clocks, and $\gamma = 1$ follows from the conditional lemma of inverse phase impedance under isotropic 3D coarse-graining.
Π_G	Local phase throughput	$\Pi_G = e^{-\chi_G}$; this is the phase-throughput factor, not the literal probability of a photon's coordinate jump.
$d\ell_{\mathrm{ph}}$	Phase impedance length	By the conditional lemma of inverse impedance, $d\ell_{\mathrm{ph}} = \Pi_G^{-1} d\ell = e^{\chi_G} d\ell$.
r_s	Schwarzschild radius	$r_s = 2GM/c_0^2$.
M_g	Gravitational length of a mass	$M_g = GM/c_0^2$; used in the B3 exponential exterior.
r_{ph}	B3 photon-capture radius	$r_{\mathrm{ph}} = 2M_g$ for the static exponential exterior.
b_{ph}	B3 capture impact parameter	$b_{\mathrm{ph}} = 2eM_g$; the B3 optical capture area is πb_{ph}^2.
$r_{\mathrm{gate}}, A_{\mathrm{gate}}$	B3 phase-gate throat	$r_{\mathrm{gate}} = M_g$, $A_{\mathrm{gate}} = 4\pi e^2 M_g^2$; this replaces the Schwarzschild horizon area in B3 neck counting.
λ_0	Center regularization length	In the regularized potential $\chi_G(r)$.

© 2026 by the author(s). Distributed under a Creative Commons CC BY license.

Preprints.org (www.preprints.org) | NOT PEER-REVIEWED | Posted: 9 June 2026 doi:10.20944/preprints202606.0589.v1

Symbol	Short explanation	Comment / area of application
Δt	Radar delay	In a weak field $\Delta t \simeq (2/c_0)\int \chi_G dl$.
L_{path}	Optical path length	Used in the radar delay; distinct from the soliton width L_{sol}.
b	Beam direction parameter	In the formula for the gravitational deflection of light.
θ_{light}	Angle of light deflection	$\theta_{\text{light}} = (1+\gamma)2GM/(c_0^2 b)$.
u	Inverse orbital radius	In Binet's equation.
h	Specific orbital moment / also Planck's constant in the equation	In Binet's equation, ℓ_{orb} is used—the specific orbital moment.
a_{orb}	Semi-major axis of the orbit	Used in the precession formula; distinct from the cosmological scale factor $a_{\cos}(t)$.
e_{orb}	Orbital eccentricity	Used in the precession formula; distinct from the elementary charge e.
$\delta\chi_{ij}^{TT}$	Transverse-transverse tensor fluctuation of the gravitational potential	Gravitational wave in the IKT.
$\oplus, \otimes$	Two polarizations of the gravitational wave	Preserved by the TT-projector.
5. Strong and weak interactions		
$V(r)$	String/interaction energy potential	In the strong interaction, $V(r) = \sigma_{\text{str}} r$.
$\hat{\sigma}_{\text{col}}$	Dimensionless value of the color tube	Algorithmic value of the confinement tube elongation by one coarse-grained color step.
σ_{str}	SI projection of the string tension	$\sigma_{\text{str}} = \hat{\sigma}_{\text{col}} m_e^2 c_0^3/\hbar$ or $\eta_{\text{col}} M_0 c_0^2/l_0$; absolute QCD renormalization requires color coarse-graining.
η_{col}	Color coarse-graining factor	Suppresses the bare-Planck string tension to the hadronic scale.
J_x, $\mathbf{J}$, $\mathbf{J}_{\text{quarks}}$	Fluxes / source currents	J_x — 1D flux in the string; $\mathbf{J}_{\text{quarks}}$ — color tube source.
κ_{str}	Color delay saturation coefficient	In $p_{\text{str}}(\mathbf{A})$.
g	Nonlinear coupling constant	In the equation $\Box\mathbf{A} + g^2|\mathbf{A}|^2\mathbf{A} = \mathbf{J}$.
$\mathcal{H}_{\text{col}} \simeq \mathbb{C}^3$	Color inner space	Three-dimensional inner space of color channels; not to be confused with the phase cell $\mathcal{C}_{\text{col}} = [0,\pi]^2_{\text{col}}$.
$G_c \in SU(3)$	Element of the color group	The notation G_c distinguishes the color transformation from the gravitational constant G.
ϵ_{abc}	A fully antisymmetric tensor	Defines the baryon singlet $\epsilon_{abc} q_1^a q_2^b q_3^c/\sqrt{6}$; for the proton — $\epsilon_{abc} u^a u^b d^c/\sqrt{6}$ taking into account the complete spin-flavor-space sector.
T_a	$SU(3)$ generators	$T_a = \lambda_a/2$, $a = 1,\ldots,8$.
λ_a	Gell-Mann matrices	Not to be confused with the coefficients λ in other sections.
P_L, P_R	Chiral projectors	Distinguish the left and right sectors of the fermion route.

© 2026 by the author(s). Distributed under a Creative Commons CC BY license.

Preprints.org (www.preprints.org) | NOT PEER-REVIEWED | Posted: 9 June 2026 doi:10.20944/preprints202606.0589.v1

Symbol	Short explanation	Comment / area of application
Ψ_L, Ψ_R	Left and right chiral components	The left sector forms $SU(2)_L$ doublets; the right sector is an $SU(2)_L$ singlet.
$\mathcal{G}_W$	Charged weak gate	Resonant charged-current coupling: $\mathcal{G}_W P_L = \mathcal{G}_W$, $\mathcal{G}_W P_R = 0$.
$L_{\ell L}, Q_{iL}$	Lepton and quark weak doublets	$L_{\ell L} = (\nu_\ell, \ell^-)^T_L$, $Q_{iL} = (u_i, d_i)^T_L$.
$T_a^{(L)}, T_\pm^{(L)}$	$SU(2)_L$ generators	$T_\pm^{(L)} = T_1^{(L)} \pm i T_2^{(L)}$ define the charged weak transitions within the doublet.
Y	Weak hypercharge	Background edge phase channel $U(1)_Y$; enters into $Q_{\text{em}} = T_3^{(L)} + Y/2$.
Q_{em}	Electromagnetic charge operator	$Q_{\text{em}} = T_3^{(L)} + Y/2$.
W_μ^a, B_μ	Neutral and charged electroweak channels	W_μ^a — $SU(2)_L$ vertex coupling; B_μ — hypercharge edge phase channel.
g_L, g_Y	$SU(2)_L$ and $U(1)_Y$ couplings	Algorithmic capacitances of the nodal weak-gluing channel and edge hypercharge translation.
θ_W	Weinberg angle	Geometric angle of neutral channels: $\tan\theta_W = g_Y/g_L$.
A_μ, Z_μ	Electromagnetic and neutral weak modes	Orthogonal combinations of B_μ and W_μ^3.
M_{EW}	Electroweak matching half-scale	$M_{\text{EW}} = F_h/2$; therefore $M_W = g_L M_{\text{EW}} = g_L F_h/2$ and $M_Z = M_{\text{EW}}\sqrt{g_L^2 + g_Y^2}$.
$\Theta_{\text{knot}}, p_{\text{res}}$	Resonance delay and phase retention	$p_{\text{res}} = 1 - e^{-\Theta_{\text{knot}}}$ for W/Z gates.
$\mathcal{R}_W^{(q)}$	Quark weak re-gluing operator	Projected matrix elements define the CKM block: $V_{ij}^{\text{CKM}} = \langle \widetilde{K}_{u_i} \vert P_u \mathcal{R}_W^{(q)} P_d \vert \widetilde{K}_{d_j} \rangle$.
$V^{\text{CKM}}, U^{\text{PMNS}}$	Flavor mixing matrices	Projected weak-gluing blocks; exact unitarity requires closure of the observed flavour subspace, otherwise leakage operators Δ_d or Δ_ν appear.
$d_{\text{knot}}, \lambda_q, \lambda_\nu$	Topological distance and mixing stiffness	Determine raw weak-overlap kernels whose projected unitary parts give CKM/PMNS; $\lambda_\nu \ll \lambda_q$ is expected.
G_F	Fermi constant	Low-energy limit: $G_F/\sqrt{2} = g_L^2/(8M_W^2)$ for $\hbar = c_0 = 1$.
6. Particles, knots, masses, and topological measures		
K	Topological cycle / knot	Indexes a closed path, interpreted as a particle.
$\mathcal{M}(K)$	Dimensionless topological measure of a knot	Specifies the ratio of the knot's mass to m_e.
m_e	Mass of an electron	Fundamental topological invariant of the mass scale.
m_p	Proton mass	Leading spectral-channel formula: $(m_p/m_e)_{\text{top}} = 6\pi^5$; the physical mass is written as $m_p^{\text{phys}}/m_e = 6\pi^5\rho_p$.

© 2026 by the author(s). Distributed under a Creative Commons CC BY license.

Preprints.org (www.preprints.org) | NOT PEER-REVIEWED | Posted: 9 June 2026 doi:10.20944/preprints202606.0589.v1

Symbol	Short explanation	Comment / area of application
m_μ, m_τ	Masses of the muon and tau lepton	Described by the leading formula $m_K/m_e = 6^{c(K)} H_K(1 - 6\alpha_{\text{top}} f_K + \delta_K^{\text{pol}})$.
m_ν^{eff}	Effective neutrino mass	The neutrino is not a stable local massive node; small masses enter as spectral parameters of the 1D correction, mixing, and cosmological memory of the birth mass.
m_h, m_H	Mass of the observable scalar channel	Spectral gap of the collective longitudinal mode of the graph capacitance; 125 GeV — laboratory projection of the resonance, not the bare mass of the fundamental point field.
$\Phi(x), \Phi_0$	Local phase capacitance of the graph and its equilibrium value	The longitudinal deformation is written as $\Phi(x) = \Phi_0 e^{\varphi(x)}$.
$h(x), F_h$	Phenomenological coordinate of the scalar channel and elastic scale	$h = F_h\varphi$ is used as the detector projection coordinate; $F_h \simeq v_{\text{EW}}$ is expected in the observable electroweak layer.
λ_K	Elastic susceptibility of the node class	$\lambda_K = \partial \ln M_K / \partial \ln \Phi$; the universal hypothesis of the observed scalar response gives $\lambda_K \simeq 1$.
g_{hKK}, g_{hVV}	Observed scalar response coefficients	Phenomenological amplitude coordinates: $g_{hKK} = \lambda_K M_K/F_h$, $g_{hVV} = 2m_V^2/F_h$; non-fundamental interaction carriers.
m_{WIMP}, M_{WIMP}	Mass of hypothetical dark matter particles	Excluded as a fundamental entity in IKT.
$C_K, c(K)$	Topological complexity / minimum number of crossings of the K-node diagram	Defines the crossing-framework of the lepton hierarchy via the factor $6^{c(K)}$.
D	Emergent dimension	Under the condition $k_{\text{crit}} = 2D = 6$.
k_{crit}	Critical average connectivity of a three-dimensional graph	In the current model, $k_{\text{crit}} = 6$.
ρ_K	Normalized electromagnetic correction of a node	In the lepton sector, $\rho_K = 1 - 6\alpha_{\text{top}} f_K + \delta_K^{\text{pol}}$; f_K and δ_K^{pol} must be derived from the node geometry and graph polarization.
δ_μ^{pol}	Polarization correction to the muon mass	Residual correction of the order of 10^{-3} to the leading-order term $6^3(1 - 6\alpha_{\text{top}})$.
V_H	Hyperbolic volume of the octet knot complement	Enters the internal factor $H_{4_1} = \kappa_{\text{emb}} V_H(4_1)$.
H_K, H_{4_1}	Internal topological factor of the lepton knot	For the trefoil, $H_{3_1} = 1$; for the figure-eight $H_{4_1} = \kappa_{\text{emb}} V_H(4_1)$, where κ_{emb} is the spectral invariant of the embedding of the stochastic graph.
f_K, f_{4_1}	Electromagnetic susceptibility of the node	The fraction of phase capacity available to external $U(1)$ traffic; for the trefoil $f_{3_1} = 1$, for the tau the target value $f_{4_1} \simeq 0.20$.

© 2026 by the author(s). Distributed under a Creative Commons CC BY license.

Preprints.org (www.preprints.org) | NOT PEER-REVIEWED | Posted: 9 June 2026 doi:10.20944/preprints202606.0589.v1

Symbol	Short explanation	Comment / area of application
κ_{emb}, δ_K^{pol}	Embedding spectral density and polarization correction	κ_{emb} must be calculated from the spectrum of U_m on the stochastic complement ensemble 4_1; δ_K^{pol} denotes the small graphite/IR polarization.
Γ	Decay width / decay rate	In the decay law, $\Gamma \propto M^5$.
τ_μ, τ_τ	Muon and tau lifetimes	The ratio $\tau_\tau/\tau_\mu \approx (m_\mu/m_\tau)^5$.
$\mathcal{C}_p$	Minimal spectral-channel cell of proton confinement	$\mathcal{C}_p = \mathcal{C}_{\mathrm{arc}} \times \mathcal{C}_{\mathrm{col}}$; is not a complete Haar measure on $SU(3)$.
$\mathcal{C}_{\mathrm{arc}}$	Longitudinal part of the proton confinement cell	$[0,\pi]^3_{\mathrm{arc}}$; the three canonical phase coordinates of the leading Dirichlet modes of the fermionic arcs.
$\mathcal{C}_{\mathrm{col}}^{\mathrm{ch}}$	Color Cartan part of the proton confinement cell	$[0,\pi]^2_{\mathrm{col}}$; two neutral Cartan holonomies of the minimal singlet coupling, associated with rank $SU(3) = 2$; a non-complete Haar measure on $SU(3)$.
μ_{arc}, $\mu_{\mathrm{col}}^{\mathrm{ch}}$	Channel measures of the longitudinal and color parts	$\mu_{\mathrm{arc}} = \pi^3$, $\mu_{\mathrm{col}}^{\mathrm{ch}} = \pi^2$; their ratio is given by $\alpha_{s,\mathrm{top}} = 1/\pi$.
$\mathcal{Q}_{\mathrm{conf}}$	Scale of the confinement gauge	The scale at which the topological anchor of the strong coupling is defined.
$\Pi_{\mathrm{IKT}}^{\mathrm{col}}$	Color graph polarization	Must generate a running $\alpha_s(\mathcal{Q}^2)$, asymptotic freedom, graph analogs $C_A = 3$, $T_R = 1/2$, and a matching to $\alpha_s(M_Z)$.
$\mathcal{C}_{ij}$	Color routing factor on an edge	An element of $SU(3)_{\mathrm{route}}$ that extends the edge transporter in the strong-interface block.
T_A, $A = 1,\ldots,8$	$SU(3)$ generators	Act on the inner space of color routes $\mathcal{H}_{\mathrm{col}} = \mathrm{span}\{\lvert r\rangle, \lvert g\rangle, \lvert b\rangle\}$.
J_A^μ	Color current	$J_A^\mu = \bar{\Psi}\gamma^\mu T_A \Psi$; arises as the Dirac-envelope limit of a non-Abelian color-routing perturbation.
Q_A^{col}	Total color charge generator	Physical asymptotic states satisfy the singlet-routing constraint $Q_A^{\mathrm{col}}\lvert\Psi_{\mathrm{phys}}\rangle = 0$.
$d\mu_{p,\mathrm{ch}}$	Channel measure of proton phase capacitance	$d\mu_{p,\mathrm{ch}} = d\varphi_1 d\varphi_2 d\varphi_3 d\eta_1 d\eta_2$.
$\mu_p(\mathcal{C}_p)$	Internal phase capacitance of the proton cell	$\mu_p(\mathcal{C}_p) = \pi^5$.
$\mathcal{E}_{\mathrm{ext}}$, k_{ext}	External routing sectors of the proton cell	$\mathcal{E}_{\mathrm{ext}} = \{+x,-x,+y,-y,+z,-z\}$, $k_{\mathrm{ext}} = \lvert\mathcal{E}_{\mathrm{ext}}\rvert = 2D = 6$.
$\Theta_p^{(0)}$	Leading dimensionless proton confinement delay	$\Theta_p^{(0)} = 6\pi^5$.
ρ_p	Residual correction to the proton mass	$m_p^{\mathrm{phys}}/m_e = 6\pi^5\rho_p$, $\rho_p \simeq 1.0000188$.
β_i	Neutrino mode topological factor	Dimensionless flavor/topology factor of weak renormalization in the formula $m_{\nu,i}^{\mathrm{birth}}c_0^2 = \beta_i[\rho_{\mathrm{gen}}(t_b)(\hbar c_0)^3]^{1/4}$.

© 2026 by the author(s). Distributed under a Creative Commons CC BY license.

Preprints.org (www.preprints.org) | NOT PEER-REVIEWED | Posted: 9 June 2026 doi:10.20944/preprints202606.0589.v1

Symbol	Short explanation	Comment / area of application
ρ_{gen}	Graph generation density	$\rho_{\mathrm{gen}} = \rho_{\mathrm{par}} + \rho_{\mathrm{noise}}^{\mathrm{valve}}$; sets the dark energy scale for neutrino mass generation.
E_Λ	Dark-energy scale	$E_\Lambda = [\rho_\Lambda (\hbar c_0)^3]^{1/4}$; current value of the order of several meV.
t_b	Neutrino birth time	In the neutrino mass birth-imprint model.
t_{obs}	Neutrino observation time	Used in the imprint conservation condition: $m_{\nu,i}^{\mathrm{eff}}(t_{\mathrm{obs}}; t_b) \simeq m_{\nu,i}^{\mathrm{birth}}(t_b)$.
t_0	Present age / current epoch	Used when comparing $m_\nu^{C\nu B}$ and present-day neutrinos via $[\rho_{\mathrm{gen}}(t_{\mathrm{dec}})/\rho_{\mathrm{gen}}(t_0)]^{1/4}$.
Λ_{valve}	Throughput of the parent throat channel	Physical limit on the initial insertion noise; in dimensionless form $\lambda_{\mathrm{valve}} = \tau_0^2 \Lambda_{\mathrm{valve}}$ and $d_0^2 = \lambda_{\max}/\lambda_{\mathrm{valve}}$.
M_{ign}	Critical mass of the initial parent valve	A scale of the order of $0.6 M_{\mathrm{Moon}}$, limiting the initial energy and channel budget of graph generation.
$\mathcal{U}_{ij}^{\mathrm{eff}}$	Effective edge kernel after coarse-graining	Used for charge, color, and vortex drag.
$\mathcal{U}_{ij}^{(0)}$	Unperturbed effective edge kernel	Base kernel before vortex correction.
$\mathcal{U}_{ij}^{\mathrm{H}}, \mathcal{U}_{ij}^{\mathrm{AH}}$	Hermitian and anti-Hermitian parts of the effective kernel	$\mathcal{U}_{ij}^{\mathrm{H}} = \frac{1}{2}(\mathcal{U}_{ij}^{\mathrm{eff}} + (\mathcal{U}_{ji}^{\mathrm{eff}})^\dagger)$, $\mathcal{U}_{ij}^{\mathrm{AH}} = \frac{1}{2}(\mathcal{U}_{ij}^{\mathrm{eff}} - (\mathcal{U}_{ji}^{\mathrm{eff}})^\dagger)$; the charge flux is given by $F_{ij} = \mathcal{U}_{ij}^{\mathrm{AH}}/i$.
∂V	Volume boundary	In the surface charge integral.
7. Cosmology, Black Holes, and the Multiverse		
N	Number of nodes / effective volume of the graph	In cosmology, $N \propto a_{\mathrm{cos}}^3$ after geometrization.
N_m	Number of vertices at step m	In the general inflationary recursion $N_m = N_0 B_{\mathrm{eff}}^m$; for the saturated 3D regime $B_{\mathrm{eff}} = 8$.
N_0	Initial number of vertices in a clique	Initial state of the daughter universe in the local limit $N_{\mathrm{gate}} = 1$.
$\mathcal{A}_0$	Topological Archipelago	Initial system of saturated subgraphs of the daughter universe: $\mathcal{A}_0 = \{G_{\mathrm{sat}}^{(a)}\}_{a=1}^{N_{\mathrm{gate}}}$.
N_{gate}	Number of parent phase gates	Number of distributed injection points of the daughter graph.
$G_{\mathrm{sat}}^{(a)}$	Saturated subgraph of the Archipelago	Local over-stressed region with $p_{\mathrm{stay}}^{(a)} \to 1$.
B_{eff}	Effective volumetric branching coefficient	$N_{m+1} = B_{\mathrm{eff}} N_m$; for maximum isotropic binary geometrization $B_{\mathrm{eff}} = 2^{D_{\mathrm{eff}}}$.
D_{eff}	Effective dimension of the geometrized expansion	For the observed macroscopic regime, $D_{\mathrm{eff}} = 3$.
$N_{\mathrm{exp}}^{\mathrm{IKT}}(m)$	Graph number of e-folds	$N_{\mathrm{exp}}^{\mathrm{IKT}} = m \ln 2$ for $B_{\mathrm{eff}} = 8$ and $a_{\mathrm{cos},m} = a_{\mathrm{cos},0} 2^m$.
N_{obs}	Observed benchmark for early expansion	Phenomenological measure of sufficient scale factor growth; for example, $N_{\mathrm{obs}} \simeq 60$.

© 2026 by the author(s). Distributed under a Creative Commons CC BY license.

Preprints.org (www.preprints.org) | NOT PEER-REVIEWED | Posted: 9 June 2026 doi:10.20944/preprints202606.0589.v1

Symbol	Short explanation	Comment / area of application
m_{inf}	Number of inflationary cycles of the graph	$m_{\text{inf}} = N_{\text{obs}}/\ln 2$; for $N_{\text{obs}} = 60$ this gives $m_{\text{inf}} \simeq 87$.
$H_{\text{alg,max}}$	Maximum rate of graph geometrization	$H_{\text{alg,max}} = (3\tau_0)^{-1} \ln B_{\text{eff}}$; does not automatically coincide with the Hubble slow-roll parameter.
q	Komov wave number of the CMB mode	Used for the spectrum of primary perturbations to avoid confusion with the graph's degree of connectivity k.
$\mathcal{P}_\zeta(q)$, A_s, n_s	Spectrum of CMB curvature perturbations, amplitude, and scalar slope	Observational parameterization $\mathcal{P}_\zeta = A_s(q/q_*)^{n_s-1}$; in IKT, these are coordinates for comparison with the CMB, not a slow-roll ontology.
$\mathcal{D}_{\text{ins}}(m)$	Power of avalanche insertion noise	Decays as $\mathcal{D}_* \exp[-\gamma_{\text{cool}}(m - m_*)]$ in a window projected onto observable CMB scales.
γ_{cool}	Avalanche noise cooling parameter	In a first approximation, $n_s - 1 \simeq -\gamma_{\text{cool}}/\ln 2$; for $n_s \simeq 0.965$, this gives $\gamma_{\text{cool}} \simeq 2.4 \times 10^{-2}$.
ζ_{lav}, ζ_{arch}	Avalanche and archipelago components of primary curvature	$\zeta = \zeta_{\text{lav}} + \zeta_{\text{arch}}$; the former should dominate in the acoustic CMB range, while the latter is allowed as a small low-multipole residual.
$\Delta_{\text{arch}}(\mathbf{q})$	Directional archipelago residue in the CMB spectrum	Requires $\lvert\Delta_{\text{arch}}\rvert \ll 1$ for $q \gg q_{\text{arch}}$ to avoid violating statistical isotropy.
$N_{\text{corr}}(q)$	Number of independent coarse-grained insertion domains	For $N_{\text{corr}} \gg 1$, central-limit averaging suppresses the primary non-Gaussianity: $f_{\text{NL}}^{\text{IKT}} \sim N_{\text{corr}}^{-1/2}$.
ΔN_m	Increment in the number of nodes per clock cycle	In general form, $\Delta N_m = (B_{\text{eff}} - 1)N_m$.
d_0	Dimensionless valve-depth variable	Non-independent empirical regularization; compact notation for the finite throughput of the parent valve: $d_0^2 = \lambda_{\max}/\lambda_{\text{valve}} = \lambda_{\max}/(\tau_0^2 \Lambda_{\text{valve}})$.
ℓ_{ab}, w_a	Delays and weights of the Archipelago gates	ℓ_{ab} — internal graph delay between saturated gates; w_a — normalized phase injection weight, $\sum_a w_a = 1$.
$\lambda_{\text{noise}}^{\text{valve}}(m)$	Dimensionless valve-limited cosmological noise density	Realizable density: $\lambda_{\text{noise}}^{\text{valve}} = \lambda_{\text{raw}}\lambda_{\text{valve}}/(\lambda_{\text{raw}} + \lambda_{\text{valve}})$; for an almost constant valve, $\lambda_{\text{noise}}^{\text{valve}} = \lambda_{\max}/(d_0^2 + m^2)$.
$\lambda_{\max}$	Dimensionless amplitude of the bare noise asymptotics	In the minimal 3D binary calibration $\lambda_{\max} = \xi = 3(\ln 2)^2$; the physical initial density is further constrained by λ_{valve}.
$\langle k \rangle$	Average graph connectivity	At the singularity $\langle k \rangle = N_0 - 1$, then decreases.
k	Degree / average node connectivity	In $p_{\text{stay}}(k) = 1 - k_{\text{crit}}/k$; not to be confused with the wave number.
ϵ, $\epsilon(t)$	Low probability / false insertion	$1 - \epsilon$ is used in the trigger; in dark energy, $\epsilon(t)$ determines the residual insertion.

© 2026 by the author(s). Distributed under a Creative Commons CC BY license.

Preprints.org (www.preprints.org) | NOT PEER-REVIEWED | Posted: 9 June 2026 doi:10.20944/preprints202606.0589.v1

Symbol	Short explanation	Comment / area of application
P_E	Energy power	Laboratory energy power measured in joules per second; not a graph-channel or node flux.
$\varepsilon_{\mathrm{ch}}^{B3}$	B3 channel energy	Energy per unwound graph-gate channel, $\varepsilon_{\mathrm{ch}}^{B3} = A_0 c_0^6/(8\pi e^2 G^2 M)$.
Φ_{ch}	Phase-channel flux	Graph phase-channel flux measured in channels per unit time; an energy benchmark is converted by $\Phi_{\mathrm{ch}}^{(E)} = P_E/\varepsilon_{\mathrm{ch}}^{B3}$.
$\Phi_{\mathcal{N}}$	Node flux	Effective node-production or node-drainage flux measured in nodes per unit time, $\Phi_{\mathcal{N}} = \nu_{\mathcal{N}}\Phi_{\mathrm{ch}}$.
Φ_{cap}^{B3}	B3 gate capacity	Maximum graph-gate channel capacity, $\Phi_{\mathrm{cap}}^{B3} = N_{\mathrm{gate}}\nu_{\mathrm{gate}}/\tau_0$; not an energy power.
$\Phi_{\mathcal{N},\mathrm{in}}$	Incoming node flux	Node supply from the parent network after energy-to-channel conversion or topological throughput normalization.
$\Phi_{\mathcal{N},\mathrm{out}}$	Outgoing / drain node flux	Black-hole node drainage through B3 graph necks.
$\Phi_{\mathcal{N},\mathrm{noise}}$	Cosmological node noise of residual insertion	Endogenous growth source in dN/dt; measured in nodes per unit time.
$\nu_{\mathcal{N}}$, f_{occ}	Node yield and occupation factor	$\nu_{\mathcal{N}}$ converts phase-channel flux to node flux; f_{occ} is the neck occupation/saturation factor.
σ_{SB}	Stefan–Boltzmann constant	In the estimate of the CMB energy-power benchmark near a graph neck.
T_{CMB}	Cosmic microwave background temperature of the parent universe	In the energy benchmark $P_{\mathrm{in}}^{B3,\mathrm{bench}}$.
M_{ign}	Ignition mass of the daughter universe	Benchmark threshold at which the converted source and unwinding channel fluxes balance.
M_{crit}	Upper limit on the black hole mass	Determined by the loss of coherence of the accretion vortex.
M_{Moon}, $M_{\odot}$	Masses of the Moon and the Sun	Units of comparison for astrophysical masses.
M_{SMBH}	Mass of a supermassive black hole	In sums / integrals of black hole drainage.
M_{parent}	Mass parameter of the parent gateway	In the parent node-throughput balance equation.
R	Reproduction coefficient of daughter universes	In the topological degeneracy hypothesis, $R = 1$.
S_∞	Unified saturated phase flow	Equivalence class of regions with $p_{\mathrm{stay}} \to 1$.
R_{ISCO}	Radius of the last stable orbit / capture radius	For an extreme gate, $R_{ISCO} \approx GM/c_0^2$.
R_{frag}	Fragmentation radius of the accretion disk	Scale of coherence loss of the 2D vortex.
R_0	Normalization radius of fragmentation	In the formula $R_{\mathrm{frag}} = R_0(M/M_{\mathrm{ref}})^{1/27}$.

© 2026 by the author(s). Distributed under a Creative Commons CC BY license.

Preprints.org (www.preprints.org) | NOT PEER-REVIEWED | Posted: 9 June 2026 doi:10.20944/preprints202606.0589.v1

Symbol	Short explanation	Comment / area of application
Q_T	Tumlay stability parameter	In astrophysics, $Q_T = 1$ is the fragmentation threshold; distinct from the electric charge Q.
t_p	Coordinate time of the parent network	In the synchronization of times between the daughter and parent universes.
Δt_p	Interval of parent time per internal cycle	$\Delta t_p = \Delta N_m / \Phi^{\mathrm{cap}}_{\mathcal{N},\mathrm{in}}$ after dimensional separation of node and energy flux.
dm/dt_p	Rate of internal time relative to the parent	Slows down as B_{eff}^{-m}.
$\lambda_N(t)$	Normalized growth rate of the number of nodes	$\lambda_N = (1/N)dN/dt$, dimension T^{-1}.
$H(t)$, $H_{\mathrm{IKT}}(t)$	Hubble parameter in IKT	$H = (1/3N)dN/dt = \lambda_N/3$ for $N \propto a_{\mathrm{cos}}^3$.
H_0	The current value of the Hubble parameter	In the discussion of the Hubble tension.
$a_{\mathrm{cos}}(t)$	The cosmological scale factor	Distinct from the orbital semi-major axis a_{orb} and the vortical acceleration a_{vort}.
$a_{\mathrm{cos},0}$	Normalization of the cosmological scale factor	In the solution $a_{\mathrm{cos}}(t) = a_{\mathrm{cos},0} e^{\lambda_N t/3}$.
$\mathcal{E}_{\mathrm{exp}}(t)$	Total expansion scalar	$\mathcal{E}_{\mathrm{exp}} = 3H^2$; this is the total expansion bookkeeping term and must not be identified with dark energy alone.
$\Lambda^{\mathrm{IKT}}_{\mathrm{DE,time}}(t)$	IKT dark-energy component	$\Lambda^{\mathrm{IKT}}_{\mathrm{DE,time}} = \Lambda_{\mathrm{par},time} + \Lambda^{\mathrm{valve}}_{\mathrm{noise},time}$. It has dimension T^{-2} and denotes only the parent-throughput plus valve-limited noise source, not the full $3H^2$ budget.
$\Lambda^{\mathrm{obs}}_{\mathrm{DE,time}}(t)$	Reconstructed dark-energy residual	Observational residual obtained from $3H^2$ after subtracting baryons, radiation, neutrinos, the IKT vortex/dark-matter component, curvature, and coarse-graining corrections.
$\Lambda^{\mathrm{valve}}_{\mathrm{noise},time}(t)$	Valve-limited noise component of dark energy	In the late epoch, it decays as $\lambda_{\mathrm{max}}/t^2$, and as $t \to 0$ it reaches a finite plateau $\Lambda_{\mathrm{valve}} = \lambda_{\mathrm{max}}/(d_0^2\tau_0^2)$.
$\Lambda_{\mathrm{valve},time}$, λ_{valve}	Parent valve bandwidth	Physical ceiling for early insertion noise. Relationship between dimensional and dimensionless forms: $\lambda_{\mathrm{valve}} = \tau_0^2 \Lambda_{\mathrm{valve},time}$; $d_0^2 = \lambda_{\mathrm{max}}/\lambda_{\mathrm{valve}}$.
ξ	Dimensionless noise relaxation coefficient	In the late tail, $\Lambda_{\mathrm{noise}} = \xi/t^2$; coincides with λ_{max}. For the saturated 3D regime, $\xi = 3(\ln 2)^2$.
κ_{holo}	Legacy holographic horizon capacity	Used only as a comparison notation; in the B3 branch it is replaced by κ_{B3}.
κ_{B3}	B3 graph-gate phase-channel capacity	$\Phi^{B3}_{\mathrm{cap}}(M) = \kappa_{\mathrm{B3}} M^2$, with $\kappa_{\mathrm{B3}} = 4\pi e^2 G^2 \nu_{\mathrm{gate}}/(c_0^4 A_0 \tau_0)$; this is not an energy power.
dn/dM	Black hole mass distribution function	In the black hole drain integral.

© 2026 by the author(s). Distributed under a Creative Commons CC BY license.

Preprints.org (www.preprints.org) | NOT PEER-REVIEWED | Posted: 9 June 2026 doi:10.20944/preprints202606.0589.v1

Symbol	Short explanation	Comment / area of application
$V_n(t)$	Phase volume of the nth-generation universe	In the cascade model of the multiverse.
V_0	Initial phase volume	Normalization of the Erlang distribution.
n	Generation number in the cascade / integer monopole number	Distinguish contextually from $n_{\text{eff}}(\mathbf{r})$ and the monopole charge.
λ_{drain}	Cascade drain rate	In $dV_n/dt = \lambda_{\text{drain}} V_{n-1} - \lambda_{\text{drain}} V_n$.
τ_{life}	Estimate of the universe's lifetime	Of the order of $\lambda_{\text{drain}}^{-1}$ or 10^{33} years in the eschatological section.
8. Dark Matter, Vortices, and Solitons		
$\boldsymbol{\Omega}$, Ω_z	The macroscopic graph curl field and its z-component	The source of the vortex potential χ_{vort}.
$\boldsymbol{\Omega}_{\text{prim}}$	Primary graph torsion	Relic field of the initial topological injection of the Archipelago.
$\boldsymbol{\Omega}_{\text{bar}}$	Baryon-induced vorticity	Late component associated with the rotation of the baryonic disk.
S_{arch}	Archipelago source	Effective initial-boundary condition of the parent injection.
$\mathcal{I}_\Omega$	Invariant amplitude of the primary vorticity	$\mathcal{I}_\Omega = \langle \lvert\boldsymbol{\Omega}_{\text{prim}}\rvert^2 \rangle_L$ after coarse-graining on the scale L.
$n_{\text{vort}}^{\text{prim}}$, δ_{vort}	Density and contrast of the primary vorticity component	$n_{\text{vort}}^{\text{prim}} = \overline{n}_{\text{vort}}(1+\delta_{\text{vort}})$; scalar CMB/LSS projection of the vorticity.
μ_{vort}	Delay per coarse-grained vortical cell	Not the particle mass; coefficient in $\rho_{\text{vort}} = \mu_{\text{vort}} n + K_{\text{vort}} n^2/2$.
K_{vort}	Elastic compressibility of the primary vortical medium	Determines small $w_{\text{vort}}^{\text{prim}}$ and $c_{s,\text{vort}}^2$.
ϵ_{comp}	Compressibility parameter of the primary vortex component	Interface quantity; in the long-wavelength limit, it is related to $\mathcal{C}_{\text{vort}} A_4 (k a_0)^2$.
$w_{\text{vort}}^{\text{prim}}$, $c_{s,\text{vort}}^2$	Effective equation of state and sound speed of the primary vortex	In the long-wavelength limit, $c_{s,\text{vort}}^2/c_0^2 = O((ka_0)^2)$; the coldness follows from the stochastic DSR dispersion.
Σ_{ij}, ϵ_Σ	Residual orientation anisotropy of primary vorticity	In $\langle \Omega_i \Omega_j \rangle_L = \delta_{ij} \mathcal{I}_\Omega/3 + \Sigma_{ij}$; suppresses Π_{vort}.
ϵ_V	Residual vector mode of the Archipelago	Requires $\epsilon_V \ll 1$ to suppress CMB vector modes.
ϵ_H	Residual helicity of the primary vorticity	Controls possible parity-odd TB/EB signals.
$\boldsymbol{\Omega}_0$	Amplitude of the soliton-like vortex packet	In the ansatz $\boldsymbol{\Omega} = \boldsymbol{\Omega}_0 \operatorname{sech}((x - v_c t)/L_{\text{sol}})$.
$\mathbf{J}_{\text{bar}}$	Baryon mass current	$\mathbf{J}_{\text{bar}} = \rho_B \mathbf{v}_B$.
ρ_B	Baryon mass density	In the current $\mathbf{J}_{\text{bar}}$.
$\mathbf{v}_B$	Baryon matter velocity	In the baryon current.
μ_{algo}	Coefficient of coupling between the vortex field and the baryon current	In the equation for $\boldsymbol{\Omega}$.

© 2026 by the author(s). Distributed under a Creative Commons CC BY license.

Preprints.org (www.preprints.org) | NOT PEER-REVIEWED | Posted: 9 June 2026 doi:10.20944/preprints202606.0589.v1

Symbol	Short explanation	Comment / area of application
c_{eff}	Effective translational velocity in a nonlinear vortex vacuum	$c_{\text{eff}} = c_0(1 - \chi_{\text{algo}}\lvert\mathbf{\Omega}\rvert^2)$.
n_{vort}	Vortical graph refractive index	$n_{\text{vort}} = c_0/c_{\text{eff}} \simeq 1 + \chi_{\text{algo}}\lvert\mathbf{\Omega}\rvert^2$.
$\mathbf{D}_{\text{vort}}$	Vorticity phase conductivity tensor	$\text{diag}(D_r, D_\phi, D_z)$.
D_r, D_ϕ, D_z	Components of anisotropic vorticity conductivity	Describe the quasi-2D waveguide reduction of the vortex.
ϵ_z	Relative vertical leakage	$\epsilon_z = D_z/D_\phi \ll 1$; as $\epsilon_z \to 0$, the ideal 2D limit is restored.
$Z_0(z;r)$	Lowest transverse mode of the topological waveguide	Determines the vertical profile $\chi_{\text{vort}}(r,z)$.
$\kappa_z(r)$	Inverse vertical attenuation length	Eigenvalue of the transverse waveguide mode.
$h_{\text{vort}}(r)$	Vertical scale of the vortex halo	$h_{\text{vort}} = \kappa_z^{-1}$; determines the finite thickness of the waveguide halo and is related to the coherent height h_{coh}.
h_{coh}	Effective height of the coherent vortex waveguide	In the saturated BTFR mode, $h_{\text{coh}} = 2\sqrt{GM_{\text{bar}}/a_{\text{vort}}}$.
$R_\perp$	Radius of transverse coherence of the waveguide	$R_\perp^2 = GM_{\text{bar}}/a_{\text{vort}}$; $A_\perp = \pi R_\perp^2$.
V_{guide}	Confinement potential of the topological waveguide	Arises from the gradient of the vortex refractive index n_{vort}.
S_{vort}	Source of the vortex potential	Right-hand side of the anisotropic conduction equation.
χ_{leak}	Small three-dimensional leakage of the vorticity potential	A correction of order $O(\epsilon_z)$ to the leading quasi-2D mode.
a_{vort}	Acceleration scale of saturation of the galactic vortex waveguide	In the minimal calibration $a_{\text{vort}} = c_0 H_{\text{bg}}/(2\pi)$; determines the BTFR $v_f^4 = GM_{\text{bar}}a_{\text{vort}}$.
r_0	Radial normalization of the logarithmic profile	In $\ln(r/r_0)$.
g_{vort}	Vortical contribution to acceleration	$g_{\text{vort}} = -\sqrt{GM_{\text{bar}}a_{\text{vort}}}/r$ in the saturated waveguide region.
v_f	Asymptotic orbital velocity of a star / test mass	In the Tull–Fisher baryon relation $v_f^4 = GM_{\text{bar}}a_{\text{vort}}$.
M_{bar}	Baryonic mass of the galaxy	Source of the late galactic vortex waveguide and BTFR.
H_{bg}	Background cosmological dephasing velocity	In today's SI projection $H_{\text{bg}} \simeq H_0$; sets $a_{\text{bg}} = c_0 H_{\text{bg}}$.
η_{circ}	Geometric factor of the circular waveguide mode	In the minimal cylindrical calibration, $\eta_{\text{circ}} = 1/(2\pi)$.
x	Coordinate along the cluster collision axis	In the soliton-like ansatz for the Bullet Cluster.
v_c	Velocity of the cluster / soliton-like packet	In the expression $\text{sech}((x - v_c t)/L_{\text{sol}})$.

© 2026 by the author(s). Distributed under a Creative Commons CC BY license.

Preprints.org (www.preprints.org) | NOT PEER-REVIEWED | Posted: 9 June 2026 doi:10.20944/preprints202606.0589.v1

Symbol	Short explanation	Comment / area of application
$\boldsymbol{\theta}, \theta_1, \theta_2$	Angular coordinates on the lens plane	Used in $\nabla^2_{\boldsymbol{\theta}}\psi_{\mathrm{IKT}}$, κ, and shear.
ψ_{IKT}	Two-dimensional IKT lens potential	Constructed from $\Phi^{\mathrm{IKT}}_{\mathrm{lens}}$ or from Σ_{eff} in the thin-lens approximation.
$\Phi^{\mathrm{IKT}}_{\mathrm{lens}}$	Three-dimensional lensing potential	$\Phi^{\mathrm{IKT}}_{\mathrm{lens}} = \Phi_{\mathrm{bar}} + \Phi_\Omega$; Φ_Ω is the refractive projection of the vortex, not the potential of a new particle.
$\Sigma_{\mathrm{eff}}, \Sigma_\Omega$	Effective and vortex surface densities of the lens	$\Sigma_{\mathrm{eff}} = \Sigma_{\mathrm{gal}} + \Sigma_{\mathrm{gas}} + \Sigma_\Omega$; used to calculate κ and shear.
Σ_{crit}	Critical surface density of the lens	$\Sigma_{\mathrm{crit}} = c_0^2 D_s/(4\pi G D_l D_{ls})$.
$\kappa, \gamma_1, \gamma_2$	Convergence and shear components	Derivatives of ψ_{IKT}; main observational interface for Bullet-like tests.
$L_{\parallel,a}, L_{\perp,a}, H_{\Omega,a}$	Longitudinal, transverse, and radial widths of the vortex soliton	Ansatz parameters for $\mathcal{I}_{\Omega,a} = \lvert\boldsymbol{\Omega}_a\rvert^2$ in cluster collisions.
$X_{\Omega,a}, Y_{\Omega,a}, Z_{\Omega,a}$	Center of the subcluster vortex soliton	Defines the position of Σ_Ω relative to the X-ray gas and galaxies.
$\rho^{\mathrm{lens}}_\Omega, \rho_{\Omega*}, \rho_{\mathrm{bridge}}$	Volumetric lensing density of the vortex component, normalization, and bridge contribution	Closure relation $\rho^{\mathrm{lens}}_\Omega = \rho_{\Omega*}\sum_a \mathcal{I}_{\Omega,a} + \rho_{\mathrm{bridge}}$.
$\mathbf{R}_{\kappa,a}, \mathbf{R}_{\mathrm{gas},a}, \mathbf{R}_{\mathrm{gal},a}$	Lensing, gas, and galaxy peaks in the cluster	Used for offset profiles of Bullet-like systems.
$\Delta_{\mathrm{gas}\to\kappa,a}, \Delta_{\mathrm{gal}\to\kappa,a}$	Offsets of the lensing peaks relative to the gas and galaxies	The Bullet-like regime requires $\lvert\Delta_{\mathrm{gas}\to\kappa,a}\rvert \gg \lvert\Delta_{\mathrm{gal}\to\kappa,a}\rvert$.
9. Fine-structure constant and stratified measures		
α	Fine-structure constant	In the low-energy context, it is identified with α_{top}; should not be used as an arbitrary flux coefficient.
α_{top}	Topologically normalized infrared anchor	$\alpha^{-1}_{\mathrm{top}} = 4\pi^3 + \pi^2 + \pi$; channel anchor of the electromagnetic coupling and source of $g^2_{\mathrm{em}} = 4\pi\alpha_{\mathrm{top}}$.
$\alpha_{\mathrm{eff}}(\mathcal{Q}^2)$	Effective running coupling constant	Scale-dependent constant after polarization of additional graph channels.
$\alpha_s, \alpha_{s,\mathrm{top}}$	Strong interaction constant and its topological anchor	$\alpha_{s,\mathrm{top}}(\mathcal{Q}_{\mathrm{conf}}) = \mu_{\mathrm{col}}/\mu_{\mathrm{arc}} = 1/\pi$; running to $\alpha_s(M_Z)$ must arise via color graph polarization.
$\mu_{\mathrm{open}}, \mu_{\mathrm{closed}}$	Open and closed measures of the neutron $U(1)$ flux	$\mu_{\mathrm{open}} = \mathrm{Vol}_\Omega(S^2) = 4\pi$, $\mu_{\mathrm{closed}} = 1$; determine the entropy cost of the internal compactification.
$\Delta m_{\mathrm{closure}}$	Cost of internal $U(1)$ closure	$\Delta m^{\mathrm{top}}_{\mathrm{closure}} = m_e \ln(4\pi)$; sets the topological anchor of the $n-p$ splitting.
$\delta^{\mathrm{IR}}_{np}$	Residual correction to the $n-p$ splitting	Small difference between the physical $m_n - m_p$ and the topological $m_e \ln(4\pi)$; the natural scale is given by the inner product of the order $E^{\mathrm{top}}_R = \alpha^2_{\mathrm{top}} m_e/2$.

© 2026 by the author(s). Distributed under a Creative Commons CC BY license.

Preprints.org (www.preprints.org) | NOT PEER-REVIEWED | Posted: 9 June 2026 doi:10.20944/preprints202606.0589.v1

Symbol	Short explanation	Comment / area of application
E_R^{top}	Rydberg scale of the inner loop	$E_R^{\mathrm{top}} = \alpha_{\mathrm{top}}^2 m_e/2 \approx 13.6\,\mathrm{eV}$; a benchmark for the neutron deformation correction.
$\mathcal{G}_W$	Weak beta-relaxation gate	Effective graph operator for the neutron's internal charge closure.
q_β	Dimensionless beta decay energy	$q_\beta = Q_\beta/m_e \simeq \ln(4\pi) - 1 + \delta_{np}^{\mathrm{IR}}/m_e$; defines the phase volume of decay together with the weak gate.
$g_A^{(0)}$	Geometric anchor of the axial factor	$g_A^{(0)} = 4/\pi$; the full g_A requires a graph correction $\delta_A^{\mathrm{graph}}$.
$\mathcal{C}_\alpha$	Stratified phase space for α	Orbital-type space of electromagnetic recombination: $\mathcal{C}_\alpha = \mathcal{C}_4 \sqcup \mathcal{C}_2 \sqcup \mathcal{C}_1$.
$\mathcal{C}_4, \mathcal{C}_2, \mathcal{C}_1$	Orbital strata of the compact part U_m	Regular sector $U(1) \times SU(2)$, reduced Cartan sector, and phase-locked line; measures $4\pi^3$, π^2, π.
$\mu(\mathcal{C}_\alpha)$	Total information channel measure of the stratified space	Trace of the direct sum of the dimension-normalized capacities of orthogonal phase channels.
μ_4, μ_2, μ_1	Information measures of individual strata	Defined as $\mu_s = \lim_{\delta\varphi\to 0} N_s(\delta\varphi)(\delta\varphi)^{d_s}$ and included in the channel trace.
N_{phase}	Effective information channel capacity	$N_{\mathrm{phase}} = 4\pi^3 + \pi^2 + \pi$; is not the raw number of microstates and does not contain a dominant term $(\delta\varphi)^{-4}$.
μ_{ch}	Measure of a single elementary action channel	Normalized to unity in h-units: $\mu_{\mathrm{ch}} = 1$.
$\mathcal{Q}^2$	External resolution scale / invariant momentum scale	Used in $\alpha_{\mathrm{eff}}(\mathcal{Q}^2)$; chosen instead of q^2 to avoid confusion with q_{em} and q_{int}.
$\Pi_{\mathrm{IKT}}(\mathcal{Q}^2)$	Graph polarization function	Describes the contribution of virtually excited channels to the running electromagnetic coupling.
$\Delta\mu_{\mathrm{pol}}(\mathcal{Q}^2)$	Polarization correction to the inverse channel measure	$\Delta\mu_{\mathrm{pol}} = \mu(\mathcal{C}_\alpha)\Pi_{\mathrm{IKT}}$; reduces the effective inverse channel capacitance.
π	Pi	Used in phase volumes and topological formulas.
$\ln 2$	Logarithm of two	In the maximum rate of inflationary doubling.
$\hbar$	Reduced Planck constant	Defines the relationship between action, energy, and phase.
h	Planck constant	The total action quantum per one closed phase cycle: $h = 2\pi\hbar$.
ξ_{dsr}	DSR correction coefficient	In the table of high-energy kinematics.
η	Baryon asymmetry	Mentioned as an open problem: $\eta \approx 6 \times 10^{-10}$.
$\hat{H}$	Hamiltonian	In the table of quantum dynamics and the anti-Hermitian correction.

© 2026 by the author(s). Distributed under a Creative Commons CC BY license.

Preprints.org (www.preprints.org) | NOT PEER-REVIEWED | Posted: 9 June 2026 doi:10.20944/preprints202606.0589.v1

Symbol	Short explanation	Comment / area of application
ΔE_G	Gravitational self-energy of branch differences	Complete energy functional of the conflict between two mass distributions; the one-scale form $\Delta E_G \sim \mathcal{S}_G\, GM^2/R_{\rm eff}$ is used only as an order-of-magnitude estimate.
$\mathcal{J}_{12}$	Dimensionless geometric functional of two branches	Fully dimensionless form of the self-energy after scaling coordinates by λ_e and masses by m_e; defines $\Delta\varepsilon_G = \mathcal{J}_{12}/(2\|\Omega_e\|^2_{\rm eff})$.
$\mathcal{S}_G$	Shape factor of gravitational conflict	Dimensionless coefficient of shape, density, branch displacement, and coarse-graining; $\mathcal{S}_G = 1$ implies only single-scale normalization of the order of magnitude.
$R_{\rm eff}$	Effective gravitational width	Coarse-graining scale of the object or 1D bridge; in a one-scale audit, one can set $R_{\rm eff} \sim \Delta x$, but the exact value is replaced by the functional $\mathcal{J}_{12}$.
$\Gamma_{\rm IKT}$	Bridge decoherence rate	In the CP version of the anti-Hermitian correction, $\Gamma_{\rm IKT} t = [2\|\Omega_e\|_{\rm eff}]^{-1}(\Delta\varepsilon_G)^2\tilde{t}$; the equivalent SI form uses $\tau_0 = \tau_e/\|\Omega_e\|_{\rm eff}$.
$t_{\rm IKT}$	Lifetime of 1D bridge coherence	$t_{\rm IKT} = 1/\Gamma_{\rm IKT}$; one-scale SI projection $t^{\rm oom}_{\rm IKT} \sim 2\|\Omega_e\|^5_{\rm eff} m_e^5 R^2_{\rm eff}/(\hbar \mathcal{S}_G^2 M^4)$.
$L^{(3D)}_{\rm life}$	Equivalent light-like lifetime	$L^{(3D)}_{\rm life} = c_0 t_{\rm IKT}$; is not the topological length of the 1D bridge itself.
10. The TTC Dynamic Interface		
TTC	Calculation of topological transitions	Minimal computational layer of IKT: the graph-surgery ansatz for transitions, cross-sections, and decay widths.
$\mathcal{M}^{\rm TTC}_{\beta\alpha}$	Observable TTC amplitude	$\mathcal{M}^{\rm TTC}_{\beta\alpha} = \sum_{\mathfrak{C}:\alpha\to\beta} W[\mathfrak{C}]$; sum over admissible graph cobordisms.
$\mathfrak{C}$	Graph cobordism / re-linking history	Class of local adjacency matrix operations connecting the initial state α to the final state β.
$\mathcal{V}_v$	Local graph surgery kernel	Effective TTC vertex; must be derived from the micro-operator U_m and weak/electromagnetic/color gates.
$\mathcal{G}_X(q)$	Graph Green's function of channel X	$\mathcal{G}_X = P_X/[L_X + \mu_X^2 + \Pi_X]$; it replaces the virtual carrier ontology with a phase channel function.
$F_K(q^2)$	Topological form factor of cycle K	Suppresses UV contributions at $qa_0 \sim 1$ and encodes the finite size/internal structure of the topological carrier.
$d\Pi_n$	Observed phase volume of n bodies	Infrared limit of the sum over accessible harmonics of the graph; used in $d\sigma$ and $d\Gamma$.
$\mathcal{F}^{\rm topo}_{\mu e}$, $\mathcal{F}^{\rm topo}_{np}$	Topological overlap factors of weak surgery	Matrix elements of the $3_1 \to 0_1$ decoupling and $n \to p$ baryon surgery; in TTC, these are verifiable inference objects.
11. Frequently Used Auxiliary Notations		

© 2026 by the author(s). Distributed under a Creative Commons CC BY license.

Preprints.org (www.preprints.org) | NOT PEER-REVIEWED | Posted: 9 June 2026 doi:10.20944/preprints202606.0589.v1

Symbol	Short explanation	Comment / area of application
$\partial_t, \partial/\partial t$	Time derivative	Used in wave equations.
$\mathcal{O}(\cdot)$	Order of smallness of the correction	For example, $\mathcal{O}(l_0^4)$ or $\mathcal{O}(\chi_G^2)$.
δ_{ab}	Kronecker delta	In the transverse projector.
ϵ_{abc}	Fully antisymmetric tensor	Defines the baryon singlet $\epsilon_{abc}q_1^a q_2^b q_3^c/\sqrt{6}$; for the proton — $\epsilon_{abc}u^a u^b d^c/\sqrt{6}$ taking into account the complete spin-flavor-space sector.
Tr	Trace of a matrix / tensor	Under the condition of trace-free TT fluctuations.
sech	Hyperbolic secant	Form of the soliton solution of a vortex.
$\prod, \sum, \int, \oint$	Product, sum, integral, line integral	Standard mathematical operations; in this article, they often have a topological interpretation.

Appendix I. Conventions for Distinguishing Symbols

In the text, overloaded symbols are distinguished according to the following scheme. The left column shows a potential conflict, the right column shows the notation adopted in the text:

Potential conflict	Distinguished meanings	Accepted notation
V_m / insertion	V_m — set of vertices; insertion — separate embedding	V_m for vertices, $\mathcal{I}_m$ and $\mathcal{I}_{m,a}$ for isometries and Kraus operators.
α	Fine-structure constant and not a flux coefficient	Use κ_{B3}, $\kappa_{\mathcal{N},\text{in}}$, or κ_{flow} for channel/node throughput; reserve α only for the fine structure.
q-family	Dimension, electromagnetic charge, and color vector are distinguished	q_{int}, q_{em}, $\mathbf{q}_c$.
A_m and $\mathbf{A}$	Adjacency matrix and electromagnetic vector potential	Keep A_m for adjacency, but always write "adjacency matrix A_m" in the text; keep the field in bold as $\mathbf{A}$ or A_μ.
U_m / Newtonian potential	U_m — operator; Φ_N — potential	U_m and $\Phi_N = -GM/r$ refer to different objects.
G / $SU(3)$	G — gravitational constant; G_c — color element of the group	$G_c \in SU(3)$.
C-family	Loop and knot complexity are distinguished	$\mathcal{C}_{\text{loop}}$ for loops, C_K for knot complexity.
e-family	Charge and eccentricity are separated	e or e_{top} for elementary charge, $e_{\text{eff}}(\mathcal{Q}^2)$ for running charge, e_{orb} for orbit.
h	Planck constant and orbital angular momentum are separated	h for the Planck constant, ℓ_{orb} for the orbital angular momentum.
λ-family	Wave coefficient and drain rate are separated	λ_{wave} and λ_{drain}.
a-family	Orbit, scale factor, and vortical acceleration are distinguished	a_{orb}, $a_{\cos}(t)$, $a_{\cos,0}$, a_{vort}.
M_0	The instrumental mass and the astrophysical reference mass are distinguished as	M_0 for the graph, M_{ref} for $10^8 M_\odot$.
Q	The electric charge and the Tömör criterion are distinguished as	Q for the charge, Q_T for the Tömör criterion.
χ	Gravitational / vortex potential, gauge phase, and chirality operator	Use χ_G, χ_{vort}, χ^{gauge}, and $\hat{\chi}$ in that order.
L-family	Optical path and soliton width are distinguished as	L_{path} and L_{sol}.

© 2026 by the author(s). Distributed under a Creative Commons CC BY license.

Preprints.org (www.preprints.org) | NOT PEER-REVIEWED | Posted: 9 June 2026 doi:10.20944/preprints202606.0589.v1

References

1. Penrose, R. (1971). *Angular momentum: an approach to combinatorial space-time*. In *Quantum Theory and Beyond* (pp. 151–180). Cambridge University Press.
2. Rovelli, C., and Smolin, L. (1995). *Spin networks and quantum gravity*. *Physical Review D*, 52(10), 5743.
3. Bilson-Thompson, S. O. (2005). *A topological model of composite preons*. *arXiv preprint hep-ph/0503213*.
4. Wolfram, S. (2020). *A Project to Find the Fundamental Theory of Physics*. Wolfram Media.
5. Aharonov, Y., Davidovich, L., and Zagury, N. (1993). *Quantum random walks*. *Physical Review A*, 48(2), 1687.
6. Clowe, D., Bradač, M., Gonzalez, A. H., Markevitch, M., Randall, S. W., Jones, C., and Zaritsky, D. (2006). *A direct empirical proof of the existence of dark matter* (Bullet Cluster 1E 0657-56). *The Astrophysical Journal Letters*, 648(2), L109.
7. Planck Collaboration. (2020). *Planck 2018 results. VI. Cosmological parameters*. *Astronomy and Astrophysics*, 641, A6.
8. Kauffman, L. H. (1987). *State models and the Jones polynomial*. *Topology*, 26(3), 395-407.
9. Finkelstein, D., and Rubinstein, J. (1968). *Connection between spin, statistics, and kinks*. *Journal of Mathematical Physics*, 9(11), 1762–1779.
10. Krusch, S. (2006). *Finkelstein–Rubinstein constraints for the Skyrme model with pion masses*. *Proceedings of the Royal Society A*, 462, 2001–2016.
11. Diósi, L. (1987). *A universal master equation for the gravitational violation of quantum mechanics*. *Physics Letters A*, 120(8), 377–381.
12. Penrose, R. (1996). *On gravity's role in quantum state reduction*. *General Relativity and Gravitation*, 28, 581–600.
13. Donadi, S., Piscicchia, K., Curceanu, C., Diósi, L., Laubenstein, M., and Bassi, A. (2021). *Underground test of gravity-related wave function collapse*. *Nature Physics*, 17, 74–78.
14. NIST/CODATA. (2024). *CODATA recommended values of the fundamental physical constants: 2022*. National Institute of Standards and Technology.
15. Borsanyi, S. et al. (2015). *Ab initio calculation of the neutron-proton mass difference*. *Science*, 347(6229), 1452–1455.
16. Particle Data Group. (2025). *Neutron mean life and neutron decay parameters*. In *Review of Particle Physics*.
17. Particle Data Group, Huston, J., Rabbertz, K., and Zanderighi, G. (2025). *Quantum Chromodynamics*. In *Review of Particle Physics*.
18. Boito, D., Golterman, M., Maltman, K., Peris, S., Rodrigues, M. V., and Schaaf, W. (2025). *Strong coupling at the τ-mass scale from an improved vector isovector spectral function*. *SciPost Physics Proceedings*, 16, 004.
19. N. Afshordi et al., *Big Mysteries Survey: Physicists' views on cosmology, black holes, quantum mechanics, and quantum gravity*, *arXiv:2605.11058. 2026*
20. T. Palmer, *Solving the Mysteries of Quantum Mechanics: Why Nature Abhors a Continuum*, *arXiv:2602.16382. 2026*
21. A. Vikram, L. Shou, Victor Galitski, *Proof of a Universal Speed Limit on Fast Scrambling in Quantum Systems*. *Phys. Rev. Lett.*. 136, 150401. 2026
22. Recent experimental reports on photon scattering dwell-time and effective negative delay phenomena; included as a placeholder for the specific source cited in the introduction.
23. G. Sorci, J. Foo, D. Leibfried, C. Sanner, I. Pikovski, *Quantum Signatures of Proper Time in Optical Ion Clocks*. *Phys. Rev. Lett*. 136, 163602. 2026
24. *Out of Time. A Philosophical Study of Timelessness*. S. Baron, K. Miller, and J. Tallant. *Oxford University Press*. 2022. ISBN: 9780192864888
25. A. Heinesen, T. Clifton. *Observational Tests for Distinguishing Classes of Cosmological Models*. *arXiv:2604.07244. 2026*
26. E. Aprile, J. Aalbers, K. Abe, S. A. Maouloud, L. Althueser, B. Andrieu, E. Angelino, D. A. Martin, S. R. Armbruster, et al. (XENON Collaboration). *WIMP Dark Matter Search Using a 3.1 Tonne-Year Exposure of the XENONnT Experiment*. *Phys. Rev. Lett.*. 135, 221003
27. Hai-Bo Yu. *Three Birds with One Stone: Core-Collapsed SIDM Halos as the Common Origin of Dense Perturbers in Lenses, Streams, and Satellites*. *arXiv:2510.11006. 2026*
28. Juodžbalis, I., Marconcini, C., D'Eugenio, F. et al. A direct black-hole mass measurement in a little red dot at high redshift. Nature 653, 1017–1021 (2026). https://doi.org/10.1038/s41586-026-10579-4
29. Maiolino, R., Übler, H., D'Eugenio, F. et al. A black hole in a near-pristine galaxy 700 Myr after the Big Bang, Monthly Notices of the Royal Astronomical Society, Volume 548, Issue 1, May 2026, staf2109, https://doi.org/10.1093/mnras/staf2109

© 2026 by the author(s). Distributed under a Creative Commons CC BY license.

Preprints.org (www.preprints.org) | NOT PEER-REVIEWED | Posted: 9 June 2026 doi:10.20944/preprints202606.0589.v1

30. O. Adriani et al. Blazars as a potential origin of the KM3-230213A event. JCAP03(2026)033. DOI 10.1088/1475-7516/2026/03/033

Disclaimer/Publisher's Note: The statements, opinions and data contained in all publications are solely those of the individual author(s) and contributor(s) and not of MDPI and/or the editor(s). MDPI and/or the editor(s) disclaim responsibility for any injury to people or property resulting from any ideas, methods, instructions or products referred to in the content.

© 2026 by the author(s). Distributed under a Creative Commons CC BY license.